# WELL-CENTERED MESHING

BY

EVAN B. VANDERZEE

DISSERTATION

Submitted in partial fulfillment of the requirements
for the degree of Doctor of Philosophy in Mathematics
in the Graduate College of the
University of Illinois at Urbana-Champaign, 2010

Urbana, Illinois

Doctoral Committee:

Associate Professor Jeff Erickson, Chair
Assistant Professor Anil N. Hirani, Director of Research
Associate Professor Vadim Zharnitsky, Co-Director of Research
Professor Rob Ghrist, University of Pennsylvania
Doctor Damrong Guoy, Synopsis, Inc.

# Abstract

A well-centered simplex is a simplex whose circumcenter lies in its interior, and a well-centered mesh is a simplicial mesh in which every simplex is well-centered. We examine properties of the well-centered simplex and well-centered meshes, present experimental results from an optimization method designed to make meshes well-centered, and give examples of well-centered tetrahedral meshes of a variety of three-dimensional regions.

*Dedicated to the LORD, the author of knowledge.*

# Acknowledgments

I probably would not have attended the University of Illinois at Urbana-Champaign if I hadn't been able to get financial support during my first year. That support came from Michael Heath through a project creating Java applets to help students understand scientific computing. I am very grateful to Mike for supporting me three academic years under that project, for teaching me about scientific computing and parallel numerical algorithms, and for encouraging me throughout my graduate studies.

If I remember correctly, I first heard about the concept of a well-centered simplex from Isaac Dooley, who was taking a course from Anil Hirani. I am grateful that Anil was willing to ask his students difficult questions and that Isaac was willing to mention the well-centered simplex to me.

All of my committee members have contributed to my academic well-being in significant ways. I thank my advisers Anil Hirani and Vadim Zharnitsky for encouraging me in my work and asking lots of questions. I thank Rob Ghrist for taking an interest in my work and helping me find an advisor in the math department. I thank Jeff Erickson for teaching me some things about computational geometry and computational topology and for advertising the question of whether the cube has an acute triangulation. I thank Damrong Guoy for his advice, for creating many of the meshes I used in my research, and for creating a few of the figures in this dissertation.

Edgar Ramos drafted several of the figures in this dissertation and contributed in other ways as a coauthor and collaborator on some of my work in graduate school. I thank Edgar for helping me understand the material better and for sticking with the research group after moving to Colombia.

I also thank Hale Erten and Alper Üngör, who were kind enough to send us several of their meshes. A mesh of Lake Superior that they created appears in Section 7.5.

I also thank my family, particularly my parents, for their support throughout my graduate studies. My parents accepted me as a gracious gift from God, the seventh and last of their children. They taught me about Jesus and raised me to understand the importance of diligence. They have helped guide me through life and have offered many prayers on my behalf.

There are many others without whom this dissertation would never have been written. I cannot thank all of them here, but I am grateful to God for putting those people into my life and for giving me strength each day to continue the work.

Financial support for my work on this dissertation comes from a number of sources. Some of the work was supported by a fellowship jointly funded by the Computational Science and Engineering Program and the Applied Mathematics Program at the University of Illinois at Urbana-Champaign. Through research assistantship support from my advisers, some of the work was also funded by NSF CAREER Award, Grant No. DMS-0645604 and by NSF Grant DMS 08-07897.

# Table of Contents

List of Notation . . . . . vii

Chapter 1 Introduction . . . . . 1
1.1 Motivation and Previous Results . . . . . 1
1.2 Definitions . . . . . 4
1.3 Overview . . . . . 6

Chapter 2 Distinguishing the Well-Centered Tetrahedron . . . . . 9
2.1 2-Well-Centered, 3-Well-Centered, or Acute . . . . . 10
2.2 Vertex Angle and Angles Associated to Facets . . . . . 13
2.3 Solid Angle . . . . . 15

Chapter 3 Characterizing the Well-Centered Simplex . . . . . 21
3.1 Equatorial Balls . . . . . 21
3.2 Other Geometric Properties . . . . . 23
3.3 Cubic Polynomial Inequalities . . . . . 30

Chapter 4 Combinatorics of Well-Centered Meshes . . . . . 34
4.1 A Quick Introduction to Simplicial Complexes . . . . . 34
4.2 Triangle Meshes in the Plane . . . . . 36
4.3 3-Well-Centered Tetrahedral Meshes in Space . . . . . 38
4.4 2-Well-Centered Tetrahedral Meshes in Space . . . . . 51

Chapter 5 Mesh Improvement . . . . . 59
5.1 Optimization Energy . . . . . 60
5.2 Preprocessing Triangle Meshes in the Plane . . . . . 64
5.2.1 Edge Flip . . . . . 64
5.2.2 Edge Split . . . . . 65
5.2.3 Triangle Subdivision . . . . . 65
5.2.4 The Algorithm . . . . . 67

Chapter 6 Optimal Triangulations . . . . . 69
6.1 Triangulation of 2-Dimensional Point Sets . . . . . 69
6.2 Relationship to the Delaunay Triangulation . . . . . 73

Chapter 7 Experimental Results . . . . . 81
7.1 Mesh of a Disk . . . . . 82
7.2 A Larger Mesh . . . . . 83
7.3 Some More Difficult Tests . . . . . 85
7.4 A Graded Mesh . . . . . 87
7.5 Mesh of Lake Superior . . . . . 88
7.6 Colombia, India, and Thailand . . . . . 91

7.7 A 3-D Mesh . . . . . 91

Chapter 8 Quality Meshes of Particular Domains . . . . . 94
8.1 3-Space, Slabs, and Infinite Rectangular Prisms . . . . . 94
8.2 The Cube . . . . . 98
8.2.1 A Completely Well-Centered Triangulation . . . . . 98
8.2.2 Bounds on Number of Tetrahedra . . . . . 100
8.2.3 Acute Triangulation . . . . . 102
8.3 The Standard Tetrahedron and the Regular Tetrahedron . . . . . 103
8.4 Tetrahedral One-Ring Neighborhoods . . . . . 106
8.5 The Square . . . . . 113

Chapter 9 Conclusions . . . . . 121

References . . . . . 125

Index . . . . . 130

# List of Notation

| | |
|---|---|
| $\lvert\cdot\rvert$ | the absolute value of a real number |
| $\lVert v\rVert$ | the Euclidean norm of a vector $v \in \mathbb{R}^n$ |
| $\langle v, w\rangle$ | the dot product of vectors $v, w \in \mathbb{R}^n$ |
| $u * K$ | the cone of a vertex $u$ to the simplicial complex $K$ |
| $\mathrm{aff}(X)$ | the affine hull of a point set $X$ |
| $B(\sigma^n)$ | the equatorial ball of simplex $\sigma^n$ |
| $\mathrm{Bd}(\sigma^n)$ | the boundary of a simplex $\sigma^n$ |
| $\mathrm{Bd}(K)$ | the boundary of a manifold simplicial complex $K$ |
| $c(\sigma^n)$ | the circumcenter of simplex $\sigma^n$ |
| $C(\sigma^n)$ | the circumsphere of simplex $\sigma^n$ |
| $\mathrm{Cl}(K)$ | the closure of a subcomplex $K$ |
| $d(v)$ | the number of edges incident to vertex $v$ in a triangulation |
| $\mathrm{Int}(\sigma^n)$ | the interior of simplex $\sigma^n$ |
| Lk $\sigma$ | the link of a simplex $\sigma$ in a simplicial complex |
| $\mathbb{R}$ | the set of real numbers |
| $R(\sigma^n)$ | the circumradius of simplex $\sigma^n$ |
| St $\sigma$ | the star of a simplex $\sigma$ in a simplicial complex |
| $\mathbb{Z}$ | the set of integers |

# Chapter 1

# Introduction

A well-centered simplex is a simplex that contains its circumcenter, and a well-centered mesh is a simplicial mesh, i.e., a triangulation, in which every simplex is well-centered. This dissertation is an investigation of the well-centered simplex and well-centered meshes, a body of research begun in the hope of discovering efficient methods for obtaining well-centered meshes. As we shall see, the path of research has led to many interesting and some unexpected results. Before turning to a careful consideration of these results, however, we examine some of the motivations for this research and review important prior contributions.

## 1.1 Motivation and Previous Results

A 2-well-centered triangulation in $\mathbb{R}^2$ is a triangulation in which every triangle is acute. Some examples in Chapter 2 imply that in $\mathbb{R}^n$ for $n \geq 3$, an $n$-dimensional well-centered triangulation is not the same thing as an acute triangulation. However, most applications that have mentioned acute triangulations have considered primarily 2-dimensional triangulations, and are potential application areas for well-centered meshes.

A primary application area for meshes is the finite element solution of problems arising in the physical world. For the finite element method, so-called round elements that have neither small nor large angles are popular [6], but to guarantee convergence of the method, bounding the angles away from $\pi$ is sufficient. Bounding the angles away from 0 is not needed [3]. Bounding the angles away from zero is usually still desirable, since for many partial differential equations small angles in the mesh will lead to a large condition number for the stiffness matrix associated with the finite element method [56]. When putting a bound on how large the angles can be, a bound of $\pi/2$ is not generally needed, but does arise in some circumstances. For example, it has been shown that a finite element solution to a reaction-diffusion problem satisfies a discrete maximum principle when computed on a triangulation that satisfies some geometric conditions. In particular, the triangulation must be acute [17, 12].

Other applications that have made mention of acute triangulations include the computation of geodesic paths on triangulated surfaces and the meshing of a space-time domain. Kimmel and Sethian described an algorithm for numerically solving the Eikonal equation on triangulated domains [35]. Their algorithm, which can be used to compute geodesic paths on triangulated surfaces, is described first for acute triangulations and requires additional work for triangulations that are nonacute. When the tent-pitching algorithm for space-time meshing was first introduced by Üngör and Sheffer, the spatial mesh that the algorithm is based on was required to be an acute triangula-

tion [61]. Later this requirement was removed, at the expense of a possible increase in the number of elements in the generated mesh [27].

In addition to applications that have mentioned acute triangulations, there are some applications that have explicitly mentioned well-centered meshes, though not always by that name. Nicolaides [46] and Sazonov et al. [50, 53, 51, 52] have discussed well-centered meshes in the context of the covolume method and its application in electromagnetics simulations. Well-centered meshes also find application within Discrete Exterior Calculus (DEC), a framework for designing numerical methods for partial differential equations [33, 18]. In DEC, a sufficient condition to discretize the Hodge star operator so that it is represented by a diagonal matrix is that the underlying mesh be well-centered. The diagonal matrix leads to efficient numerical solution. In this context, well-centered meshes coming out of our research have been used for computing solutions to the Darcy flow problem with a stable mixed method derived using DEC [34]. These applications do not strictly require well-centered meshes, but well-centered meshes make the computations easier, more efficient, or more accurate.

The specific subject of well-centered meshes had not been extensively studied prior to this dissertation. Sazonov et al. attempted to construct well-centered meshes using a method of stitching an ideal mesh to a mesh of the region near the boundary [50, 53, 51]. The method was largely unsuccessful for three-dimensional domains, but by avoiding the step of stitching to an ideal mesh and repeating their construction for the near boundary part of the mesh, they did manage to construct a well-centered mesh of one specific domain [52].

Outside of the results of Sazonov et al. there are really no results on well-centered meshes worth mentioning. There are, however, some prior results about the related concept of self-centered meshes. The difference between the definition of a self-centered mesh and the definition of a well-centered mesh, which is made more precise in Sec. 1.2, is like the difference between the definition of a nonobtuse mesh and the definition of an acute mesh. It is the difference between a strict and a nonstrict inequality, a closed set and an open set. Though this distinction may seem small, it is very important. For instance, for the $n$-cube in $\mathbb{R}^n$ a collection of $n!$ path-simplices (also called orthoschemes) fit around a main diagonal of the cube to form a nonobtuse fully self-centered triangulation of the $n$-cube [6], but it was recently shown that for $n \geq 4$ there is no acute triangulation of the $n$-cube and for $n \geq 5$ there is no acute triangulation tiling space [37]. For $n \geq 4$ it is not yet known whether there is a completely well-centered triangulation of the $n$-cube or a completely well-centered triangulation that tiles $\mathbb{R}^n$.

The first mention of self-centered meshes may be a conference paper of Rajan in 1991 [48]. Rajan showed that a self-centered triangulation in any dimension $\mathbb{R}^n$ is a Delaunay triangulation. He later published a journal paper with the same result [47] Bern and Eppstein cite Rajan's result in a survey about mesh generation and optimal triangulations, pointing out that a stronger condition called fully self-centered is needed to guarantee that a closed primal mesh element and its orthogonal closed circumcentric dual element have nonempty intersection [8]. Along with Chew and Eppstein, they solve the problem of fully self-centered nonobtuse triangulation of point sets in $\mathbb{R}^n$ [6]. In 1999, Schmitt and Spehner reprove Rajan's result in a slightly different context and relate the result to a concept of angle [54]. Chapter 2 discusses the results of Schmitt and Spehner in more detail.

The problem of acute triangulation of polygons has received much more attention in the literature. Burago and Zalgaller proved in 1960 that any polygon has an acute triangulation [15].

Their argument was not constructive, but it applies to nonconvex polygons with polygonal holes and is a small part of their proof that abstract polyhedra built by gluing together polygons can be geometrically realized.

In the late 1980s and early to mid 1990s, a variety of authors looked at the problem of explicitly constructing nonobtuse and acute triangulations of polygons. Initially nonobtuse triangulations were constructed and later methods were developed for transforming the nonobtuse triangulations into acute triangulations. We refer to [37] and [11] for the majority of these references, but mention that Maehara [41] and Yuan [68] developed the algorithms for transforming a nonobtuse triangulation into an acute one.

The algorithms of Maehara and Yuan are quite complicated, and the author knows of no implementations of their algorithms. Moreover, since both are concerned with maintaining the linear bound on the number of triangles in the triangulation, their algorithms can produce angles that are arbitrarily close to $\pi/2$; for any bound less than $\pi/2$ the required number of triangles may depend on the geometry of the input, even if the input is a point set [7, 9]. (An input polygon with an arbitrarily small angle could make any bound less than $\pi/2$ impossible, but the dependence on geometry here is related to aspect ratios of the elements.) A more recent method that Erten and Üngör propose for acute triangulation [28] is more promising from a practical point of view. Their heuristic, based on a variant of Delaunay refinement, is easy to implement, and they present experimental results in their paper. The initial experimental results have some angles very close to $\pi/2$, but with some modifications their method can generate triangle meshes of sufficiently nice input polygons that meet an angle bound strictly less than $\pi/2$ but use a relatively small number of triangles [60].

There has also been attention given to acute triangulation of particular polygonal regions. Burago and Zalgaller proved that any triangle could be triangulated with at most 7 acute triangles [15]. Lindgren showed that there is no acute triangulation (acute dissection, in fact) of the square with fewer than 8 triangles and gave an acute triangulation of the square with exactly 8 triangles [40]. Cassidy and Lord showed that there exists an acute triangulation of the square with $m = 8$ triangles and with $m$ triangles for any $m \geq 10, m \in \mathbb{Z}$, but not with $m = 9$ or $m < 8$ triangles [16]. Liping Yuan considered acute triangulation of pentagons, proving in her thesis an upper bound of 54 on the number of triangles needed to construct such a triangulation [69]. Yuan gives a more extensive bibliography of results related to particular domains, crediting Manheimer with an independent solution for triangles; Hangan, Itoh, and Zamfirescu with extending the solution for the square to rectangles; and Maehara with a variety of results related to triangles and both convex and nonconvex quadrilaterals.

Nonobtuse and acute triangulation of objects of dimension higher than two and triangulation of surfaces of polyhedra have also been studied. Some of these results are discussed in Chapter 8 of this dissertation. The recent review of the subject by Brandts et al. [11] and the paper by Kopczyński et al. [37] give many other excellent references. The acute triangulation of polyhedral surfaces can be treated with techniques similar to those for polygons. Acute triangulation of three-dimensional objects is still largely an open problem except for some specific regions such as the Platonic solids.

## 1.2 Definitions

In the discussion of motivation and background material we have assumed that readers have some familiarity with the notion of acute and we have defined the term well-centered with only a general concept. This section more carefully defines these concepts and introduces some other concepts, terminology, and notation that are important in this dissertation.

A set of $n$ points in $\mathbb{R}^m$, labeled $v_0, v_1, \ldots v_n$ is *affinely independent* if the two conditions $\sum_{i=0}^{n} c_i v_i = 0$ and $\sum_{i=0}^{n} c_i = 0$ together imply that $c_i = 0$ for each $i = 1, \ldots, n$. A single point is always affinely independent, and any greater number of points is affinely independent if and only if the set of vectors $\{v_1 - v_0, v_2 - v_0, \ldots, v_n - v_0\}$ is linearly independent. A *simplex* of *dimension* $n$, also called an $n$-simplex, is the convex hull of $n+1$ affinely independent points, called the *vertices* of the simplex. A simplex may be denoted by a Greek letter, usually $\sigma$, $\tau$, or $\rho$, or it may be denoted by explicitly listing it's vertices. When denoted by a Greek letter, the dimension of the simplex is often given as a superscript. For example, $\sigma^3 = v_0 v_1 v_2 v_3$ refers to a tetrahedron that is the convex hull of the four points $v_0$, $v_1$, $v_2$, and $v_3$.

From a computational point of view, a simplex is usually represented by a list of its vertices, and there is no way guarantee that the vertices are, in fact, affinely independent. In most of this dissertation we have assumed, often implicitly, that when we speak of a simplex, even if it is computationally represented, its points are affinely independent. This kind of general position assumption is common and is made with little, if any, loss of generality.

An *affine space* in $\mathbb{R}^n$ is a set of points $A$ such that the set of points $\{x - v_0 : x \in A\}$ is a linear subspace of $\mathbb{R}^n$ for some $n$-vector $v_0$. (It is possible that $v_0 = 0$.) The *affine hull* of a set $X$ of points in $\mathbb{R}^n$, denoted $\mathrm{aff}(X)$, is the smallest affine space in $\mathbb{R}^n$ that contains $X$. We frequently consider the affine hull of a simplex $\sigma^n = v_0 v_1 \ldots v_n$ in $\mathbb{R}^m$, $m \geq n$. In that case the following is an equivalent definition.

$$\mathrm{aff}(v_0 \ldots v_n) = \left\{ \sum_{i=0}^{n} \lambda_i v_i : \sum_{i=0}^{n} \lambda_i = 1,\ -\infty < \lambda_i < \infty \quad \text{for } i = 0, \ldots, n \right\}.$$

Frequently the affine hull is used in discussing the affine hull of a triangle that is a face of a tetrahedron. The three vertices of the triangle define a plane, i.e., a 2-dimensional affine space, and that plane is the affine hull of the triangle. For this reason, the affine hull of a simplex has sometimes been called the plane of the simplex.

For each $n$-simplex $\sigma^n$ in $\mathbb{R}^n$ with $n \geq 1$, there is a unique point that is equidistant from the vertices of the simplex. This point is called the *circumcenter* of the simplex, and is denoted $c(\sigma^n)$. For an $n$-simplex $\sigma^n$ in $\mathbb{R}^m$ with $m > n$, there are multiple points that are equidistant from the vertices of $\sigma^n$, and we take the circumcenter to be the point among these that has the minimum distance to the vertices of $\sigma^n$. It is equivalent to define the circumcenter as the unique point in $\mathrm{aff}(\sigma^n)$ that is equidistant from the vertices of $\sigma^n$. The *circumradius* of a simplex is the distance from the circumcenter to one of its vertices. We often use $R(\sigma^n)$ to denote the circumradius of simplex $\sigma^n$. For a 0-dimensional simplex, that is, a vertex, we take the circumcenter to be the vertex itself, and the circumradius is 0.

The *circumsphere* of a simplex $\sigma^n$, which we sometimes denote by $C(\sigma^n)$, we define to be a sphere in $\mathrm{aff}(\sigma^n)$ of radius $R(\sigma^n)$ centered at $c(\sigma^n)$. It is important to note that this sphere is a

subset of $\text{aff}(\sigma^n)$; later we will distinguish this from a sphere that has the same center and radius but extends beyond $\text{aff}(\sigma^n)$. We also distinguish the sphere from a "solid" object in $\text{aff}(\sigma^n)$. The *circumball* of a simplex $\sigma^n$ is a ball in $\text{aff}(\sigma^n)$ of radius $R(\sigma^n)$. The circumball of a simplex is the convex hull of the circumsphere of the simplex.

A *face* of a simplex $\sigma^n = v_0 v_1 \dots v_n$ is a simplex $\tau^k = u_0 u_1 \dots u_k$ such that $u_i$ is a vertex of $\sigma^n$ for each $i = 0, \dots, k$. This includes the possibility that $k = n$, so $\sigma^n$ is a face of itself. We write $\tau^k \prec \sigma^n$ to indicate that $\tau^k$ is a face of $\sigma^n$. A face $\tau^k \prec \sigma^n$ that has dimension $k$ may also be called a $k$-face of $\sigma^n$. A *proper face* of a simplex $\sigma$ is a $k$-face for which $0 \leq k < n$. A *facet* of an $n$-simplex is a face of dimension $n-1$. An *edge* of a simplex is a face of dimension 1.

An $n$-simplex $\sigma^n$ is *$n$-well-centered* if $c(\sigma^n)$ is in the interior of $\sigma^n$. More generally, an $n$-simplex $\sigma^n$ is *$k$-well-centered* if each of its $k$-faces is $k$-well-centered in the sense of the first definition. This could be combined for several different $k$ with parentheses. For example, $(k_1, k_2)$-well-centered is interpreted as both $k_1$-well-centered and $k_2$-well-centered. An $n$-simplex that is $k$-well-centered for each $k$, $1 \leq k \leq n$ is *completely well-centered*. (The reader's intuition about what is meant by the boundary and interior of a simplex is probably correct. More formal definitions of these terms are given in Chapter 4 in the quick introduction to simplicial complexes included there.) In many cases the term well-centered is explicitly qualified with a dimension, but when the mean is obvious from context or the particular dimension is unimportant, e.g., because the concept well-centered is being discussed without reference to a particular situation, the term well-centered may be used without a specific dimension mentioned.

The definition of completely well-centered has ignored the question of whether a 0-simplex can be 0-well-centered. Given our definition of the circumcenter of a 0-simplex and the definition of the interior of a simplex, a 0-simplex is 0-well-centered, but the question is mostly pedantic, and every simplex is 0-well-centered by these definitions. Any (nondegenerate) simplex is also 1-well-centered, since the circumcenter of a segment is the midpoint of the segment, which is in the interior of the segment.

A *self-centered* simplex is a simplex $\sigma^n$ that contains $c(\sigma^n)$, possibly on its boundary. A *fully self-centered* simplex is a simplex for which every $k$-face is self-centered. (See [8, 6].) Some constructions in higher-dimensional spaces use the path simplex, which is also called an orthoscheme. Such a simplex is fully self-centered [6], but many of the circumcenters of faces lie on edges of the simplex, and it is not well-centered.

The definitions of well-centered simplex and self-centered simplex have an obvious extension to simplicial meshes. For instance, a simplicial mesh is $k$-well-centered if each $k$-simplex in the mesh is $k$-well-centered.

There are a variety of ways to measure angles in a simplex. Many of these concepts of angle are equivalent for the 2-simplex, but there are differences in higher dimensions. We discuss some more of these concepts of angle in Chapter 2, but define here those we consider most important. A *dihedral angle* of a simplex is an angle measured between two facets of the simplex. Two $(n-1)$-dimensional facets of an $n$-simplex meet in an $(n-2)$-dimensional face $\rho^{n-2}$. There is a 2-dimensional affine space $A$ orthogonal to $\rho^{n-2}$, and projecting the two facets into $A$ produces two segments that meet at a point. The angle between these two segments, measured in the usual manner of an angle of a triangle, is the dihedral angle between the two facets.

We say that a simplex is *dihedral acute* if each of its dihedral angles has measure strictly less

than $\pi/2$. Throughout this dissertation we say that a simplex is *acute* if it is dihedral acute. The same terminology is adopted in [26] and elsewhere. This definition of an acute 2-simplex agrees with the common notion of an acute triangle.

For a tetrahedron we define a solid angle in analogy to a 2-dimensional angle as follows. In $\mathbb{R}^2$ an angle between two rays, measured in radians, is the length of an arc intercepted by the two rays on a unit circle centered at the origin of the rays, i.e., the *apex* of the angle. For any generalized cone In $\mathbb{R}^3$, the *solid angle*, measured in steradians, is the surface area intercepted by the cone on a unit sphere centered at the apex of the cone. Thus the solid angle at a vertex $v$ of a tetrahedron is the solid angle for the cone whose apex is $v$ and whose bounding rays are the infinite extension of the three facets incident to $v$. This definition of the solid angle of a tetrahedron is equivalent to the definition in [6], where the definition is extended to higher-dimensional simplices as well. They also define the dihedral angle as we have here and discuss an entire family of angles of a simplex defined with the same geometric concept of an intercepted portion of a sphere.

For a tetrahedron we are also interested in what are called face angles of the tetrahedron. A *face angle* is an angle of one of the triangle facets $\tau^2$ of the tetrahedron, measured in $\text{aff}(\tau^2)$ as an angle of a triangle is normally measured in $\mathbb{R}^2$. A tetrahedron has twelve face angles and is 2-well-centered if and only if each of its twelve face angles has measure strictly less than $\pi/2$.

As a final definition we note that for a simplex $\sigma^n = v_0 v_1 \dots v_n$ any point $x$ in $\text{aff}(\sigma^n)$ can be written uniquely as a linear combination of the vertices of $\sigma^n$ with

$$x = \alpha_0 v_0 + \alpha_1 v_1 + \cdots + \alpha_n v_n = \sum_{i=0}^{n} \alpha_i v_i \qquad \text{and} \qquad \sum_{i=0}^{n} \alpha_i = 1\,.$$

The coefficients $\alpha_i$ in this linear combination are called the *barycentric coordinates* of the point $x$. A point is in the interior of the simplex if and only if each barycentric coordinate $\alpha_i > 0$. Thus an $n$-simplex $\sigma^n$ is $n$-well-centered if and only if each barycentric coordinate of $c(\sigma^n)$ is strictly positive. In Chapter 3 we will briefly discuss a way to compute the barycentric coordinates.

## 1.3 Overview

The results of this dissertation are organized beginning with a focus on the simplex and moving out to a broader viewpoint of simplicial meshes. The first two chapters are results specific to the simplex itself. Chapter 2 considers a variety of specific examples of simplices and, focusing particularly on the tetrahedron, shows that a well-centered simplex is not the same thing as an acute simplex in $\mathbb{R}^3$ and higher dimensions. The chapter also introduces several other generalizations of the angle into higher dimensions and relates some of these concepts to an $h/R$ quantity related to well-centered simplices. The chapter closes by examining the relationship of the solid angle of a tetrahedron to whether the tetrahedron is well-centered. It is shown that in a 3-well-centered tetrahedron every solid angle is less than $\pi$, in a 2-well-centered tetrahedron or completely well-centered tetrahedron every solid angle is less than $\pi/2$, and both of these bounds are sharp.

Chapter 3 continues the focus on the simplex, but turns the attention to alternate characterizations of the well-centered simplex and tools for proving that a simplex is is not well-centered. We define the equatorial ball and characterize the $n$-well-centered $n$-simplex in terms of the relationship

of the vertices of the simplex to equatorial balls. We prove the Cylinder Condition, a necessary geometric property of the $n$-well-centered $n$-simplex, and the Prism Condition, a sufficient geometric condition to prove that an $n$-simplex is $n$-well-centered. We show that given a fixed facet $\tau^{n-1}$ of an $n$-simplex, the simplex will be $n$-well-centered if and only if the coordinates of the vertex $u$ opposite $\tau^{n-1}$ satisfy some cubic (or lower degree) polynomial inequalities depending on $\tau^{n-1}$.

The focus shifts in Chapter 4 to simplicial meshes, but remains mostly local in considering the combinatorial properties of the neighborhood of a vertex in a well-centered mesh. The chapter opens with a consideration of the combinatorics of 2-well-centered meshes in $\mathbb{R}^2$. The local combinatorial properties are obvious but help set the stage for analogous questions in higher dimensions and motivate an algorithm presented later. We also prove a somewhat more global property for triangle meshes in $\mathbb{R}^2$, i.e., we show that a 2-well-centered mesh in $\mathbb{R}^2$ has no enclosing cycle of length less than 5.

In higher dimensions, specifically $\mathbb{R}^3$, we consider only local combinatorial properties of well-centered meshes that can be expressed in terms of the neighborhood of an interior vertex in the mesh. We prove a variety of combinatorial properties of well-centered meshes in $\mathbb{R}^3$ and give examples of infinite families of vertex neighborhoods that cannot appear and can appear in well-centered tetrahedral meshes in $\mathbb{R}^3$. In corollaries to the main results it is shown that an interior vertex of a 3-well-centered tetrahedral mesh in $\mathbb{R}^3$ must have at least 7 incident edges and an interior vertex of a 2-well-centered tetrahedral mesh in $\mathbb{R}^3$ must have at least 9 incident edges. Small example meshes show that both of these results are sharp.

In Chapter 5 the subject is simplicial meshes considered as a whole. We present an optimization method that seeks to transform a given input mesh into a well-centered mesh. The method uses the quantity $h/R$ and is motivated in part by observations about the geometry of the well-centered simplex discussed earlier. The chapter closes with an algorithm that deals with the possible combinatorial problems of input meshes for triangles meshes in $\mathbb{R}^2$.

The algorithm of Chapter 5 for addressing combinatorial problems of input meshes is an algorithm that makes local changes to the mesh. This approach is contrasted in Chapter 6 with the idea of treating the mesh connectivity as a global combinatorial optimization problem. We show that relative to the optimization energy $E_\infty$ defined in Chapter 5 a globally optimal triangulation of a point set in $\mathbb{R}^2$ is a triangulation that minimizes the maximum angle. Along the way we reprove the results of Rajan [47] and Schmitt and Spehner [54] relating well-centered meshes to Delaunay triangulations. In $\mathbb{R}^2$ this result yields a nice double optimality relating well-centered meshes, Delaunay triangulations, and the quantity $h/R$. We show that the nice relationship between Delaunay triangulations and the quantity $h/R$ in $\mathbb{R}^2$ does not extend to higher dimensions except for a limited result in $\mathbb{R}^3$.

Chapter 7 discusses our implementation of the optimization method described in Chapter 5 and presents a variety of experimental results. The experimental results demonstrate that the method can find 2-well-centered meshes in $\mathbb{R}^2$ with a large number of elements (up to 60000) and complicated geometry. The method also appears to preserve grading well when possible and can be successful in finding well-centered meshes in $\mathbb{R}^3$ if the input mesh has sufficiently nice combinatorial properties.

Since constructing meshes in $\mathbb{R}^3$ with sufficiently nice combinatorial properties is a nontrivial task, much of the work on well-centered meshes in $\mathbb{R}^3$ has made use of hand constructions. In many cases these hand construction were combined with some form of the optimization discussed in Chapters 5 and 7. Chapter 8 discusses a variety of well-centered meshes in $\mathbb{R}^3$ and $\mathbb{R}^2$ that have

been constructed as part of the research on well-centered meshes. Meshes presented in Chapter 8 include completely well-centered meshes of $\mathbb{R}^3$, slabs in $\mathbb{R}^3$, infinite rectangular prisms in $\mathbb{R}^3$, the cube in $\mathbb{R}^3$, and subtriangulations of several tetrahedra. Although well-centered tetrahedral meshes in $\mathbb{R}^3$ may be relatively rare, they seem to be easier to construct and more common than acute tetrahedral meshes in $\mathbb{R}^3$.

# Chapter 2

# Distinguishing the Well-Centered Tetrahedron

Several authors have discussed self-centered or well-centered simplices since they were defined by Rajan around 1991 [48], and many of these authors have considered the relationship of the well-centered simplex—especially the well-centered tetrahedron—to other properties. Bern et al. observed that a well-centered tetrahedron need not be dihedral nonobtuse [6], and that a nonobtuse tetrahedron need not be 3-well-centered [6]. Eppstein et al. demonstrated that any dihedral acute tetrahedron has acute facets [26]. Later Brandts et al. generalized this, proving that any acute simplex has acute facets [10]. Thus any acute simplex is 2-well-centered. Brandts also noted that there are simplices with acute facets that are not themselves acute.

Schmitt and Spehner related well-centered simplices to a condition on two different types of angles that they defined, one a linear angle and the other a solid angle, each said to be *associated to a facet* [54]. Finally, Sazonov et al. discussed the connection of well-centered tetrahedra with an angle they defined as the *vertex angle*, which turns out to be exactly the same as the linear angle associated to the facet opposite the vertex [50]. In the same paper Sazonov et al. claimed incorrectly that a tetrahedron must be 2-well-centered in order to be 3-well-centered, citing the work of Bern et al. They also claimed that their vertex angle and the solid angle for the same vertex have a particular relationship, but this is not correct unless the solid angle referred to is the solid angle associated to the facet opposite the vertex as defined by Schmitt and Spehner, and Sazonov et al. do not appear to be aware of that work.

The purpose of this chapter is to bring together all of these different ideas about the relationship of well-centered tetrahedra to other tetrahedral angles and show that there are important distinctions between the properties 2-well-centered and 3-well-centered. It is also hoped that this chapter will clarify some of the confusion that could be caused by the claims of Sazonov et al. In particular, we show which combinations of the properties 2-well-centered, 3-well-centered, and dihedral acute are possible and give specific examples of tetrahedra that satisfy each of the different possible combinations. We also discuss bounds on the solid angle at the vertex of a tetrahedron for tetrahedra that are 3-well-centered or 2-well-centered. [1]

[1] Table 2.1 and slightly different versions of Figs. 2.1, 2.2, 2.3, 2.4, 2.5, and 2.6 appeared as Table 1 and Figs. 2, 3, 4, 5, 6, and 7 in the article "Triangulation of Simple 3D Shapes with Well-Centered Tetrahedra" on pages 19–35 of the *Proceedings of the 17th International Meshing Roundtable*, published in 2008 [62]. The article was written by the author Evan VanderZee and his coauthors Anil N. Hirani and Damrong Guoy. Some of the text of Sec. 2.1 is also drawn from that publication. That publication is 

| Figure | 3-WC | 2-WC | Acute |
|---|---|---|---|
| 2.1 | Y | Y | Y |
| 2.2 | Y | Y | N |
| 2.3 | N | N | N |
| 2.4 | N | Y | Y |
| 2.5 | N | Y | N |
| 2.6 | Y | N | N |

Table 2.1: A tetrahedron may have any of six different possible combinations of the properties 2-well-centered (2-WC), 3-well-centered (3-WC), and dihedral acute. Each combination of properties is represented by a row in this table, with a Y (resp. N) indicating that the tetrahedron does (resp. does not) have the property. The table refers to Figs. 2.1 through 2.6, which show examples of the different possible combinations.

## 2.1 2-Well-Centered, 3-Well-Centered, or Acute

In this section we show that it is important to distinguish between the properties 2-well-centered, 3-well-centered, and acute as they relate to tetrahedra. No one of the three properties is equivalent to any of the other properties, and in only one case does one property imply another—the property acute for a tetrahedron implies the property 2-well-centered [26, 10]. This leaves six different ways to combine the properties 2-well-centered, 3-well-centered, and acute for a tetrahedron. All six such combinations can be realized by tetrahedra, as summarized in Table 2.1, which refers to Figs. 2.1 through 2.6.

Each figure shows a picture of a tetrahedron inside of its circumsphere. The circumcenter is marked by a small, unlabeled axes indicator, and the tetrahedron is rotated so that it is not hard to see whether the circumcenter is interior to the tetrahedron. The exact coordinates of the vertices of each tetrahedron are given.

Some statistics concerning the quality of each tetrahedron are also included. We briefly discuss these statistics here. The face angle and dihedral angle are defined in Chapter 1. It should be clear that a tetrahedron is 2-well-centered if and only if the maximum face angle is less than $\pi/2$ radians, and a tetrahedron is acute if and only if the maximum dihedral angle is less than $\pi/2$ radians. The quantity $R/\ell$ is known as the circumradius to shortest edge ratio, because $R$ stands for the circumradius and $\ell$ stands for the length of the shortest edge of the tetrahedron. The circumradius to shortest edge ratio, which has a range of $[\sqrt{3/8} \approx 0.612, \infty)$, is a familiar quantity in the context of Delaunay refinement and has been used in a variety of contexts to assess the quality of tetrahedral meshes.

The quantity $h/R$, which we will come back to in Chapter 5, is a means of quantifying the 3-well-centeredness of the tetrahedron. It is computed with respect to each facet of the tetrahedron. The $R$ of the quantity stands for the circumradius of the tetrahedron, and the $h$ stands for height. To be precise, $h$ is the signed height of the circumcenter of the tetrahedron above the facet, where above (i.e., $h > 0$) is in the direction towards the remaining vertex of the tetrahedron. Thus $h/R$ is positive with respect to every facet if and only if the circumcenter is inside of the tetrahedron, and the minimum $h/R$ is positive if and only if the tetrahedron is 3-well-centered. The range of values



Some material from this article also appears in Chapter 8. The specific material reused in that chapter is enumerated in the footnote beginning on page 94.

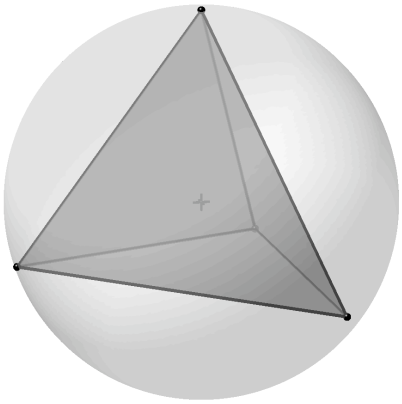

| Vertex Coordinates | | |
|---|---|---|
| $x$ | $y$ | $z$ |
| 0.6 | $-0.64$ | $-0.48$ |
| 0.48 | 0.8 | $-0.36$ |
| $-0.96$ | 0 | $-0.28$ |
| 0 | 0 | 1 |

| Quality Statistics | | |
|---|---|---|
| Quantity | Min | Max |
| $h/R$ | 0.254 | 0.371 |
| Face Angle | 50.92° | 67.08° |
| Dihedral Angle | 58.76° | 76.98° |
| $R/\ell$ | 0.690 | |

Figure 2.1: A tetrahedron that is completely well-centered and dihedral acute.

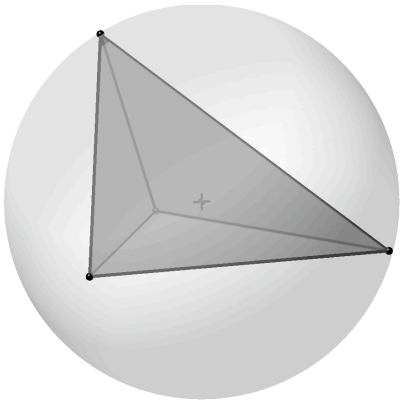

| Vertex Coordinates | | |
|---|---|---|
| $x$ | $y$ | $z$ |
| 0 | 0.96 | $-0.28$ |
| $-0.744$ | $-0.64$ | $-0.192$ |
| 0.856 | $-0.48$ | $-0.192$ |
| $-0.48$ | 0.192 | 0.856 |

| Quality Statistics | | |
|---|---|---|
| Quantity | Min | Max |
| $h/R$ | 0.224 | 0.427 |
| Face Angle | 46.26° | 77.62° |
| Dihedral Angle | 52.71° | 94.15° |
| $R/\ell$ | 0.733 | |

Figure 2.2: A completely well-centered tetrahedron that is not dihedral acute.

| Vertex Coordinates | | |
|---|---|---|
| $x$ | $y$ | $z$ |
| 0.224 | $-0.768$ | $-0.6$ |
| 0.8 | 0 | $-0.6$ |
| 0.224 | 0.768 | $-0.6$ |
| $-0.28$ | 0 | 0.96 |

| Quality Statistics | | |
|---|---|---|
| Quantity | Min | Max |
| $h/R$ | $-0.029$ | 0.600 |
| Face Angle | 29.89° | 106.26° |
| Dihedral Angle | 35.42° | 116.68° |
| $R/\ell$ | 1.042 | |

Figure 2.3: A tetrahedron that is not dihedral acute, 2-well-centered, or 3-well-centered.

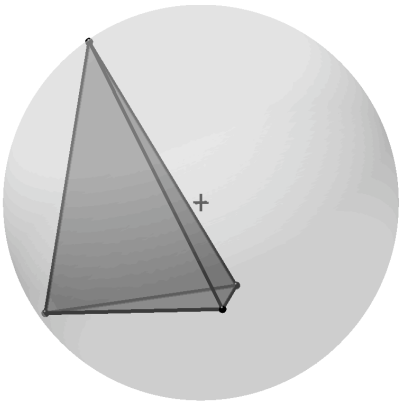

| Vertex Coordinates | | |
|---|---|---|
| $x$ | $y$ | $z$ |
| 0.36 | $-0.8$ | $-0.48$ |
| 0.768 | 0.28 | $-0.576$ |
| $-0.6$ | 0.64 | $-0.48$ |
| 0.576 | 0.168 | 0.8 |

| Quality Statistics | | |
|---|---|---|
| Quantity | Min | Max |
| $h/R$ | $-0.109$ | 0.562 |
| Face Angle | 41.71° | 83.76° |
| Dihedral Angle | 53.33° | 85.72° |
| $R/\ell$ | 0.863 | |

Figure 2.4: A tetrahedron that is dihedral acute and 2-well-centered, but not 3-well-centered.

| Vertex Coordinates | | |
|---|---|---|
| $x$ | $y$ | $z$ |
| $-0.152$ | 0.864 | $-0.48$ |
| $-0.64$ | $-0.6$ | $-0.48$ |
| 0.6 | $-0.64$ | $-0.48$ |
| $-0.192$ | $-0.64$ | 0.744 |

| Quality Statistics | | |
|---|---|---|
| Quantity | Min | Max |
| $h/R$ | $-0.024$ | 0.630 |
| Face Angle | 42.08° | 85.44° |
| Dihedral Angle | 59.94° | 91.20° |
| $R/\ell$ | 0.806 | |

Figure 2.5: A tetrahedron that is not dihedral acute or 3-well-centered, but is 2-well-centered.

| Vertex Coordinates | | |
|---|---|---|
| $x$ | $y$ | $z$ |
| 0 | $-0.6$ | $-0.8$ |
| 0.64 | $-0.024$ | $-0.768$ |
| $-0.64$ | $-0.024$ | $-0.768$ |
| 0 | 0.352 | 0.936 |

| Quality Statistics | | |
|---|---|---|
| Quantity | Min | Max |
| $h/R$ | 0.112 | 0.765 |
| Face Angle | 25.69° | 95.94° |
| Dihedral Angle | 40.33° | 105.62° |
| $R/\ell$ | 1.161 | |

Figure 2.6: A tetrahedron that is not dihedral acute or 2-well-centered, but is 3-well-centered.

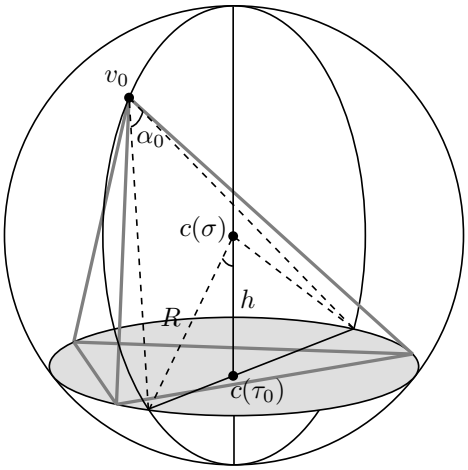


Figure 2.7: In a tetrahedron $\sigma$, the vertex angle $\alpha_0$ at a vertex $v_0$ is the angle subtended by the circumball of the facet $\tau_0$ opposite $v_0$, as measured in the plane defined by the three points $v_0$, $c(\sigma)$, and $c(\tau_0)$. The cosine of this angle is $h/R$. The figure shows edges of $\sigma$ in a medium gray and the circumball of $\tau_0$ in a lighter gray.

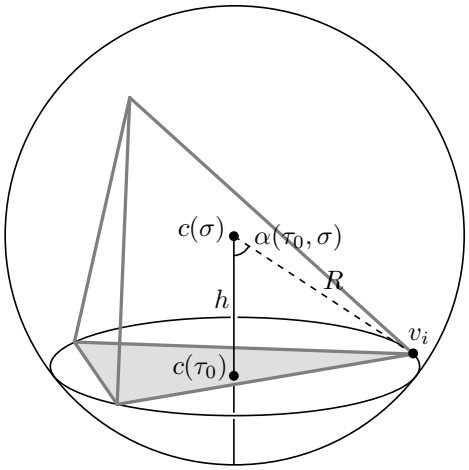


Figure 2.8: The linear angle $\alpha(\tau_0, \sigma)$ associated to the facet $\tau_0$ of a tetrahedron $\sigma$ is the angle at $c(\sigma)$ between the external normal to $\tau_0$ (external with respect to $\sigma$) and the vector from $c(\sigma)$ to some vertex $v_i$ of $\tau_0$. Clearly $\cos(\alpha(\tau_0, \sigma)) = h/R$, and $\alpha(\tau_0, \sigma)$ is the same as the vertex angle $\alpha_0$. The tetrahedron in this figure is the same as in Fig. 2.7, but here facet $\tau_0$ is shown light gray.

of $h/R$ is $(-1, 1)$, and $h/R = 1/3$ relative to each facet of the regular tetrahedron.

## 2.2 Vertex Angle and Angles Associated to Facets

In this section we introduce the vertex angle defined by Sazonov et al. and the angles associated to facets as defined by Schmitt and Spehner, and we show that these are closely tied to each other and to the quantity $h/R$ discussed at the end of Sec. 2.1.

First we define the vertex angle that Sazonov et al. discuss in [50]. Figure 2.7, similar to a figure in [50], gives a graphical representation of the vertex angle of a tetrahedron. In a tetrahedron $\sigma$ we consider a particular vertex $v_0$ and the facet $\tau_0$ opposite $v_0$. A plane containing the points $v_0$, $c(\sigma)$, and $c(\tau_0)$ intersects the circumball of $\tau$ in a segment whose midpoint is $c(\tau_0)$. The angle under which $v_0$ sees this segment is the vertex angle $\alpha_0$. Observe that $\alpha_0$ is an inscribed angle in a circle with center $c(\sigma)$. Dividing the corresponding central angle in half, we obtain a new angle congruent to $\alpha_0$, and it should be clear from Fig. 2.7 that with the appropriate sign for $h$, $h/R = \cos(\alpha_0)$. Sazonov et al. were aware of this and, in fact, use the quantity $h/R$ in measuring the quality of their meshes.

In [54], on the other hand, Schmitt and Spehner do not comment on the cosine of their angle associated to a facet. Their *linear angle associated to a facet* $\tau_0$ of an inscribable polyhedron $\sigma$ with circumcenter $c(\sigma)$, e.g., a tetrahedron, is the angle $\alpha(\tau_0, \sigma)$ between a vector normal to $\tau_0$ pointing outward from $\sigma$ and the vector from $c(\sigma)$ to a vertex of $\tau_0$. (See Fig. 2.8.) In a tetrahedron $\sigma$, the linear angle associated to a facet $\tau_0$ is just a different definition for the vertex angle at the vertex $v_0$ opposite $\tau_0$, and $\cos(\alpha(\tau_0, \sigma)) = h/R$ in any inscribable polyhedron $\sigma$.

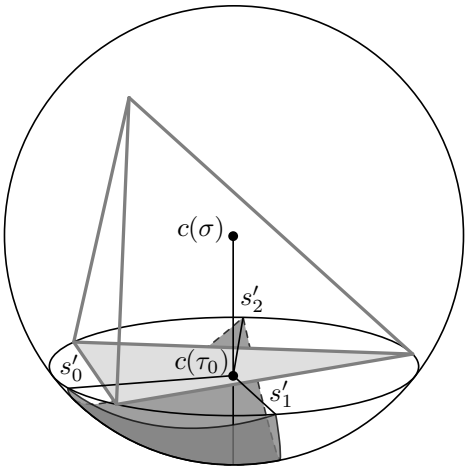


Figure 2.9: The solid angle $\alpha_s(\tau_0, \sigma)$ associated to the facet $\tau_0$ of a tetrahedron $\sigma$ is the solid angle at $c(\sigma)$ that intersects the external normal to $\tau_0$ and is bounded by the vectors from $c(\sigma)$ to $s'_i$. Here each $s'_i$ is the intersection of the circumsphere of $\sigma$ with an external normal to a facet of $\tau_0$. In the figure, facet $\tau_0$ is shown in light gray. The area of the dark gray region is $\alpha_s(\tau_0, \sigma)$ scaled by $R(\sigma)$.

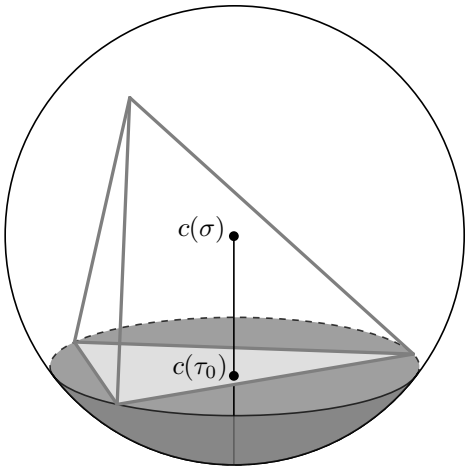


Figure 2.10: The alternative solid angle associated to a facet $\tau_0$, which we denote $\widetilde{\alpha}_s(\tau_0, \sigma)$, is the solid angle at $c(\sigma)$ that intersects the external normal to $\tau_0$ and is bounded by a cone from $c(\sigma)$ through the circumcircle of $\tau_0$. Facet $\tau_0$ appears in light gray, and the area of the dark gray region is the measure of $\widetilde{\alpha}_s(\tau_0, \sigma)$ scaled by $R(\sigma)$. The angle $\widetilde{\alpha}_s(\tau_0, \sigma)$ is a function of $h/R$.

Schmitt and Spehner also define in [54] a solid angle associated to a facet of an inscribable polyhedron. Figure 2.9 depicts their solid angle associated to a facet of a tetrahedron. Because they wanted to define a solid angle that had a monotone relationship to the quantity $h/R$, Schmitt and Spehner could not use the solid angle from $c(\sigma)$ to the facet $\tau_0$; if $\tau_0$ is not 2-well-centered, then this relationship does not hold. Instead they define the solid angle associated to a facet as follows. Consider the facet $\tau_0$. For each facet $\upsilon_i$ of $\tau_0$ (which is an edge of a tetrahedron in our case), let $s'_i$ be the point of intersection of the circumsphere of $\sigma$ with the normal to $\upsilon_i$, where the normal is external with respect to $\tau_0$. The *solid angle associated to a facet* $\tau_0$ is the solid angle $\alpha_s(\tau_0, \sigma)$ bounded by the vectors from $c(\sigma)$ to $s'_i$ that intersects the vector normal to $\tau_0$ pointing outward from $\sigma$.

The key element of the solid angle associated to a facet as defined by Schmitt and Spehner is that it has a monotone relationship to the quantity $h/R$. They could also have used the angle $\widetilde{\alpha}_s(\tau_0, \sigma)$ shown in Fig. 2.10, which we call the *alternative solid angle associated to facet* $\tau_0$. This alternative is easier to define; it is the solid angle at $c(\sigma)$ that intersects the external normal to $\tau_0$ and is bounded by the cone from $c(\sigma)$ to the circumsphere of $\tau_0$. All of the results in [54] related to the angle $\alpha_s(\tau_0, \sigma)$ also hold for $\widetilde{\alpha}_s(\tau_0, \sigma)$. An important difference between these alternatives is that $\alpha_s(\tau_0, \sigma)$ depends on the shape of the facet $\tau_0$, and $\widetilde{\alpha}_s(\tau_0, \sigma)$ is a function of $h/R$ that depends on only the dimension. In a tetrahedron, for instance, one can show that $\widetilde{\alpha}_s(\tau_0, \sigma) = 2\pi(1 - h/R)$.

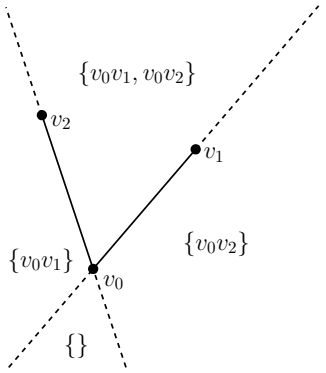


Figure 2.11: Consider a tetrahedron $v_0v_1v_2v_3$. The lines through $v_0v_1$ and $v_0v_2$ divide the plane $\text{aff}(v_0v_1v_2)$ into four regions. One can determine whether the dihedral angles along $v_0v_1$ and $v_0v_2$ are acute by looking at which of the four region contains the orthogonal projection of $v_3$ into $\text{aff}(v_0v_1v_2)$. This figure lists the dihedral angles that are acute in each region.

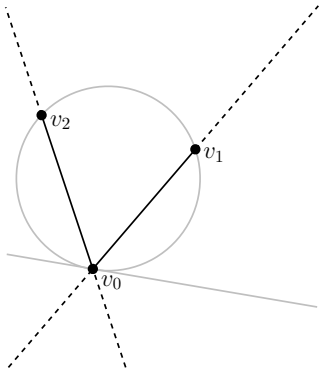


Figure 2.12: The tangent line to $C(v_0v_1v_2)$ at $v_0$ separates the interior of the circumball of $v_0v_1v_2$ from the region where neither $v_0v_1$ nor $v_0v_2$ has an acute dihedral angle. By Proposition 3.2.1 we conclude that if $v_0v_1v_2v_3$ is 3-well-centered, then either the dihedral angle along $v_0v_1$, the dihedral angle along $v_0v_2$, or both dihedral angles are acute.

## 2.3 Solid Angle

Recall that a *solid angle* at the apex $v$ of a cone in $\mathbb{R}^3$, defined in Chapter 1, refers to the area subtended by the cone on a unit sphere centered at $v$. In an arbitrary tetrahedron the solid angle at a vertex may approach $2\pi$. In a tetrahedron $\sigma = v_0v_1v_2v_3$, for example, if vertex $v_0$ is pushed arbitrarily close to a fixed point in the interior of the facet $v_1v_2v_3$, the solid angle in $\sigma$ at $v_0$ will approach $2\pi$.

There are some bounds that relate the solid angle at a vertex of a tetrahedron to whether the tetrahedron is well-centered, but the relationship is not a characterization. We start with a result about dihedral angles of a 3-well-centered tetrahedron that will lead us to bounds for the solid angles of a 3-well-centered tetrahedron.

**Lemma 2.3.1.** *For any two incident edges of a 3-well-centered tetrahedron, at least one of the dihedral angles along the two edges is acute.*

*Proof.* Let $\sigma = v_0v_1v_2v_3$ be a 3-well-centered tetrahedron. It suffices to show that at least one of the dihedral angles along edges $v_0v_1$ and $v_0v_2$ is acute.

Let $w_3$ be the orthogonal projection of $v_3$ into $\text{aff}(v_0v_1v_2)$. Then the dihedral angle along $v_0v_1$ is acute if and only if $w_3$ and $v_2$ lie on the same side of the line through $v_0$ and $v_1$. (See Fig. 2.11.) The angle is a right angle if $w_3$ lies on $v_0v_1$.

Proposition 3.2.1, which we prove in chapter 3, states that because $\sigma$ is 3-well-centered, $w_3$ must lie in the interior of the circumball of $v_0v_1v_2$. The region in which neither dihedral angle is acute lies outside of the circumball (see Fig. 2.12), so $w_3$ must lie in a region where at least one of the dihedral angles is acute. □

**Proposition 2.3.2.** *Let $v$ be a vertex of a 3-well-centered tetrahedron $\sigma$. The solid angle of the tetrahedron at $v$ is less than $\pi$.*

*Proof.* Choose an edge $e$ incident to $v$ that has a dihedral acute angle. (By Lemma 2.3.1, this can be done.) The acute dihedral angle is defined by two halfplanes that meet at edge $e$. In a unit sphere centered at $v$, these two halfplanes subtend an area less than $\pi$. Since the tetrahedron $\sigma$ lies in the region bounded by the two halfplanes, the solid angle in $\sigma$ at $v$ subtends an even smaller area, also less than $\pi$. □

**Remark.** The bound of Proposition 2.3.2 is sharp. For some $1 > \varepsilon > 0$, consider the tetrahedron $\sigma_\varepsilon$ with vertices

$$v_0 = (0,0,0) \qquad v_1 = (1,0,0) \qquad v_2 = \left(\frac{\varepsilon^2}{2} - 1, \varepsilon, 0\right) \qquad v_3 = \left(1, \frac{2}{\varepsilon} - \frac{3\varepsilon}{4}, \frac{4}{\varepsilon^2}\right).$$

Tedious computation shows that the barycentric coordinates of the circumcenter of $\sigma_\varepsilon$ are

$$\begin{aligned}
\mu_0 &= \frac{1}{4096}\left(1024 - 1024\varepsilon^2 + 256\varepsilon^4 + 172\varepsilon^6 - 75\varepsilon^8 + 9\varepsilon^{10}\right) \\
\mu_1 &= \frac{1}{4096}\left(512 + 384\varepsilon^2 - 224\varepsilon^4 - 54\varepsilon^6 + 33\varepsilon^8 - 9\varepsilon^{10}\right) \\
\mu_2 &= \frac{1}{2048}\left(256 + 320\varepsilon^2 + 16\varepsilon^4 - 39\varepsilon^6 + 9\varepsilon^8\right) \\
\mu_3 &= \frac{1}{512}\left(256 - 8\varepsilon^4 - 5\varepsilon^6 + 3\varepsilon^8\right).
\end{aligned}$$

Since each barycentric coordinate of the circumcenter is positive, $\sigma_\varepsilon$ is 3-well-centered. Moreover, the solid angle at vertex $v_0$ turns out to be

$$2\,\mathrm{atan}\left(16\varepsilon \Big/ \left[4\varepsilon^2 - \varepsilon^4 + 2\varepsilon^2\sqrt{4+\varepsilon^4} + 2\varepsilon^2\sqrt{16 + 4\varepsilon^2 - 2\varepsilon^2 + (9/16)\varepsilon^6}\right.\right.$$
$$\left.\left. + \sqrt{256 + 64\varepsilon^2 + 32\varepsilon^4 + 25\varepsilon^6 - 8\varepsilon^8 + (9/4)\varepsilon^{10}} + \sqrt{256 + 64\varepsilon^2 - 32\varepsilon^4 + 9\varepsilon^6}\right]\right),$$

which reduces to $2\,\mathrm{atan}(1/(\varepsilon + O(\varepsilon^3)))$ for $0 < \varepsilon < 1$. Thus as $\varepsilon \to 0$, the solid angle approaches $\pi$. Figure 2.13 shows four of the tetrahedra $\sigma_\varepsilon$, with $\varepsilon$ decreasing from left to right. In the drawing of each tetrahedron the positive $x$-axis points into the page and the positive $y$-axis points to the left.

Considering the result stated in Proposition 2.3.2, one might wonder whether there is any statement about the converse. Is there some upper bound on the solid angle that would guarantee that a tetrahedron is 3-well-centered? We shall see later that the answer to this question is no, but first we discuss the situation for 2-well-centered tetrahedra.

**Proposition 2.3.3.** *Let $v$ be a vertex of a 2-well-centered tetrahedron $\sigma$. The solid angle of the tetrahedron at $v$ is less than $\pi/2$.*

*Proof.* Let $\sigma = v_0v_1v_2v_3$ be a 2-well-centered tetrahedron and consider the solid angle at $v = v_0$. Let $\widetilde{v}_0 = (0,0,0)$, and for $i = 1,2,3$ let $\widetilde{v}_i = \widehat{v_i - v_0}$ be a unit vector in the direction $v_i - v_0$. The solid angle at $v_0$ in $\sigma$ is the same as the solid angle at $\widetilde{v}_0$ in $\widetilde{\sigma} = \widetilde{v}_0\widetilde{v}_1\widetilde{v}_2\widetilde{v}_3$, though $\widetilde{\sigma}$ might not be 2-well-centered.

For each $i = 1,2,3$, $j = 1,2,3$, $i \neq j$, the dot product $\langle \widetilde{v}_i, \widetilde{v}_j \rangle > 0$ because the face angles at $v_0$ are acute. In addition, Hadamard's inequality states that for a square $n \times n$ matrix $A = (a_{ij})$ with entries in $\mathbb{R}$, the determinant is bounded by $|\det(A)| \leq \prod_{j=1}^{n} \sqrt{(\sum_{i=1}^{n} a_{ij}^2)}$, so taking the unit vectors

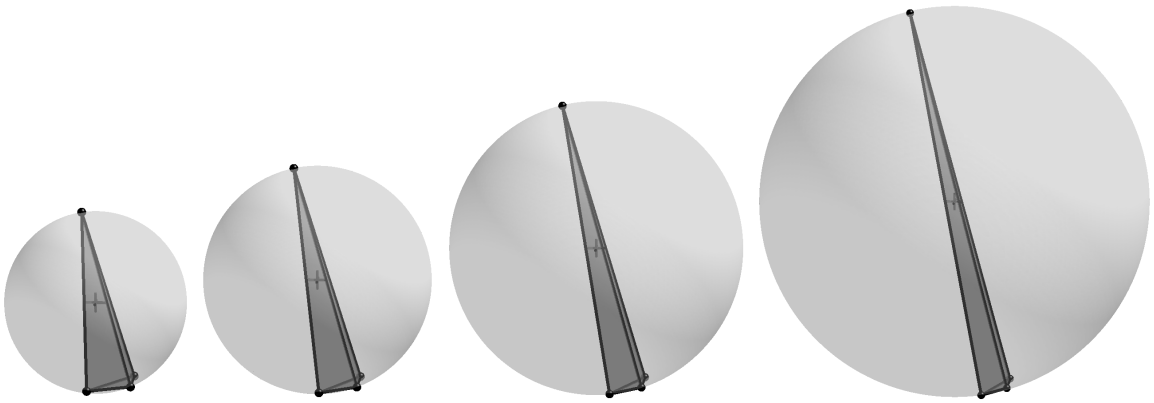

Figure 2.13: The solid angle at a vertex of a 3-well-centered tetrahedron may be arbitrarily close to $\pi$. These four tetrahedra are from a family of 3-well-centered tetrahedra with a parameter $\varepsilon$ such that as $\varepsilon \to 0$, the solid angle at one of the vertices approaches $\pi$. From left to right these are the tetrahedra $\sigma_\varepsilon$ for $\varepsilon = 1, 7/8, 3/4, 5/8$ and the largest solid angles are approximately $0.4604\pi$, $0.5120\pi$, $0.5685\pi$, $0.6302\pi$.

$\widetilde{v}_i$ as columns of a matrix, we have $0 \leq \det([\,\widetilde{v}_1 \;\; \widetilde{v}_2 \;\; \widetilde{v}_3\,]) \leq 1$. (We can assume the determinant is nonnegative by choosing the proper orientation of $\sigma$.) Using these observations we bound the solid angle at $\widetilde{v}_0$ in $\widetilde{\sigma}$ by

$$2\,\mathrm{atan}\left(\frac{\det([\,\widetilde{v}_1 \;\; \widetilde{v}_2 \;\; \widetilde{v}_3\,])}{\|\widetilde{v}_1\|\,\|\widetilde{v}_2\|\,\|\widetilde{v}_3\| + \langle\widetilde{v}_1,\widetilde{v}_2\rangle\,\|\widetilde{v}_3\| + \langle\widetilde{v}_1,\widetilde{v}_3\rangle\,\|\widetilde{v}_2\| + \langle\widetilde{v}_2,\widetilde{v}_3\rangle\,\|\widetilde{v}_1\|}\right)$$
$$= 2\,\mathrm{atan}\left(\frac{\det([\,\widetilde{v}_1 \;\; \widetilde{v}_2 \;\; \widetilde{v}_3\,])}{1 + \langle\widetilde{v}_1,\widetilde{v}_2\rangle + \langle\widetilde{v}_1,\widetilde{v}_3\rangle + \langle\widetilde{v}_2,\widetilde{v}_3\rangle}\right) < 2\,\mathrm{atan}(1) = \frac{\pi}{2}\,.$$

□

Proposition 2.3.3 could also be proved using more geometric arguments. The bound on the face angle is a bound on the length of the arcs that bound the subtended area on the unit sphere. One can show that the subtended area lies in 1/8th of the sphere by placing the two endpoints of the longest arc on the equator and arguing that the third point must lie in the region swept out as the arc on the equator contracts to a pole along longitudinal lines.

**Remark.** The bound of Proposition 2.3.3, like the bound of Proposition 2.3.2, is sharp. We again consider a one-parameter family of tetrahedra for a parameter $\varepsilon$. The tetrahedron $\sigma_\varepsilon$ with vertices

$$v_0 = (0,0,0) \qquad v_1 = (1,\varepsilon,0) \qquad v_2 = (\varepsilon,1,0) \qquad v_3 = (1/2,1/2,1/\varepsilon)$$

for some $0 < \varepsilon < 1$. Computing the barycentric coordinates of the circumcenter of each face shows that $\sigma_\varepsilon$ is 2-well-centered for each $\varepsilon$ in the range. The solid angle at $v_0$ is

$$2\,\mathrm{atan}\left(\frac{2-2\varepsilon}{\sqrt{4+2\varepsilon^2}+\varepsilon\left(\sqrt{4+4\varepsilon^2}+\sqrt{4+2\varepsilon^2}\right)}\right) = 2\,\mathrm{atan}\left(\frac{2-2\varepsilon}{2+O(\varepsilon)}\right),$$

which approaches $\pi/2$ from below as $\varepsilon \to 0$. Figure 2.14 shows four of these tetrahedra $\sigma_\varepsilon$, with $\varepsilon$ decreasing from left to right. In the drawing of each tetrahedron the positive $x$-axis points towards

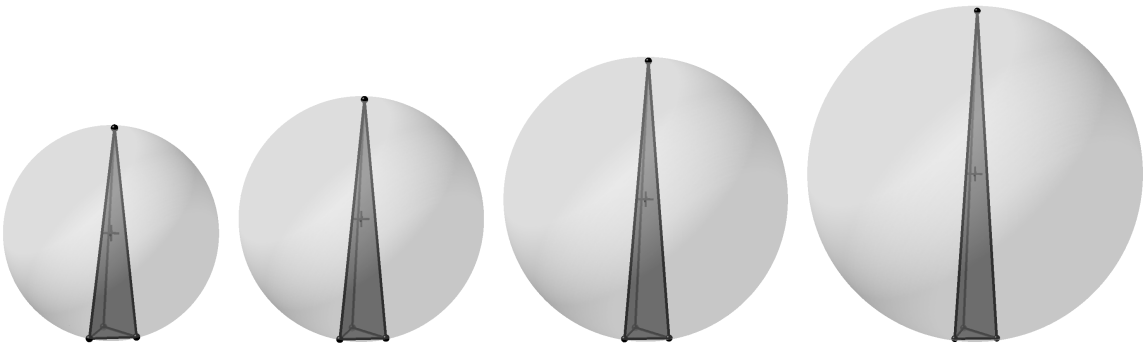

Figure 2.14: The solid angle at a vertex of a completely well-centered tetrahedron may be arbitrarily close to $\pi/2$. These four tetrahedra are from a family of completely well-centered tetrahedra with a parameter $\varepsilon$ such that as $\varepsilon \to 0$, the solid angle at one of the vertices approaches $\pi/2$. From left to right these are the tetrahedra $\sigma_\varepsilon$ for $\varepsilon = 7/32, 3/16, 5/32, 1/8$ and the largest solid angles are approximately $0.3133\pi$, $0.3370\pi$, $0.3618\pi$, $0.3875\pi$.

the right and the positive $y$-axis points into the page.

In addition to being 2-well-centered, the tetrahedron $\sigma_\varepsilon$ is 3-well-centered for any $0 < \varepsilon < 1$, so the bound of Proposition 2.3.3 is sharp for completely well-centered tetrahedra as well as for 2-well-centered tetrahedra.

We see that a tetrahedron that is 3-well-centered or 2-well-centered has guaranteed quality in the sense of no large solid angles. This is the easiest quality to guarantee of the no large angle problems [6], and it is natural to ask whether being well-centered implies any other large angle or any small angle bounds. To answer this question we consider a tetrahedron with vertices

$$v_0 = \left(-\frac{1}{2}, 0, -\frac{\varepsilon}{2}\right) \qquad v_1 = \left(\frac{1}{2}, 0, -\frac{\varepsilon}{2}\right) \qquad v_2 = \left(0, \frac{1}{2}, \frac{\varepsilon}{2}\right) \qquad v_3 = \left(0, -\frac{1}{2}, -\frac{\varepsilon}{2}\right).$$

As $\varepsilon \to 0$, this tetrahedron becomes a sliver, with solid angles approaching 0, some dihedral angles approaching $\pi$, and other dihedral angles approaching 0. Yet for any $\varepsilon > 0$, the tetrahedron is completely well-centered. Figure 2.15 shows an example tetrahedron from this family. We conclude that in terms of small and large angle bounds, being well-centered does not guarantee anything except a bound on the largest solid angle.

Another natural question is whether anything can be said about the converse of Propositions 2.3.2 and 2.3.3. Does there exist some upper bound $\theta > 0$ such that a tetrahedron with all solid angles smaller than $\theta$ must be well-centered? The answer is no. The tetrahedron with vertices

$$v_0 = \left(-0.96, 0.28, -\frac{\varepsilon}{2}\right) \qquad v_1 = \left(0.96, 0.28, \frac{\varepsilon}{2}\right) \qquad v_2 = \left(0.6, 0.8, -\frac{\varepsilon}{2}\right) \qquad v_3 = \left(-0.6, 0.8, \frac{\varepsilon}{2}\right)$$

is a tetrahedron that is neither 2-well-centered nor 3-well-centered for $\varepsilon > 0$, yet all of the solid angles of the tetrahedron are $O(\varepsilon)$. (See Fig. 2.16.) Thus a tetrahedron with solid angles approaching 0 need not be well-centered.

On the other hand, the strongest quality condition among the no small/large angle conditions is the requirement that no solid angles are small [6]. Indeed, bounding the solid angle away from 0 implies a bound on the solid angle away from $2\pi$. It is possible that some lower bound on the solid

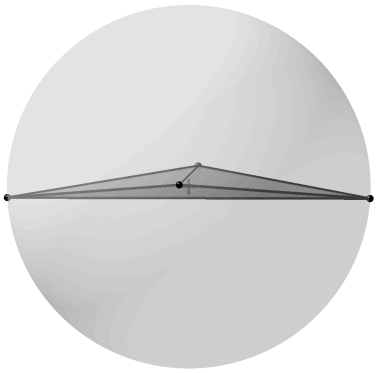

Figure 2.15: Except for the upper bounds on the largest dihedral angle, there are no small or large angle bounds for well-centered tetrahedra. This tetrahedron is from a one-parameter family of completely well-centered tetrahedra with parameter $\varepsilon$. As $\varepsilon \to 0$, all solid angles of the tetrahedron approach 0, two of the dihedral angles approach $\pi$, and the remaining dihedral angles approach 0. This particular tetrahedron has parameter $\varepsilon = 1/16$.

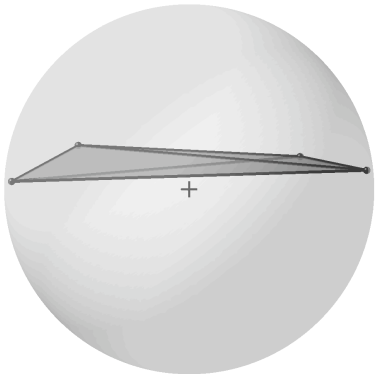

Figure 2.16: No upper bound on the solid angle can guarantee that a tetrahedron is well-centered. This tetrahedron comes from a one-parameter family of tetrahedra that are neither 2-well-centered nor 3-well-centered. As the parameter $\varepsilon$ goes to 0, all solid angles of the tetrahedron approach 0. The tetrahedron shown in the figure is the member of the family with parameter $\varepsilon = 1/16$.

angle of a tetrahedron would guarantee that the tetrahedron is well-centered. We leave this as an open question.

# Chapter 3

# Characterizing the Well-Centered Simplex

In Chapter 2 we considered some examples of well-centered tetrahedra and saw that there are differences between 3-well-centered tetrahedra, 2-well-centered tetrahedra, and dihedral acute tetrahedra. We also looked at several concepts of angle in a tetrahedron, and saw that some of these concepts are related to the quantity $h/R$.

In this chapter we move from our focus on the tetrahedron to the more general setting of the $n$-simplex. The focus is on the $n$-well-centered $n$-simplex in particular. We introduce some theoretical tools for working with the $n$-well-centered $n$-simplex and develop intuition along the way by discussing geometric properties and how they generalize from the familiar two-dimensional case. The opening discussion of equatorial balls is related to the quantity $h/R$, though it might not be obvious here, and we will return to $h/R$ in Chapter 5 in the discussion of our cost function for mesh optimization. [1]

## 3.1 Equatorial Balls

We begin with an alternate characterization of the $n$-well-centered $n$-simplex in terms of equatorial balls, which we now define.

**Definition.** Let $\sigma^n$ be a simplex embedded in a hyperplane $P^m$ with $m > n$. The *equatorial ball* of $\sigma^n$ in $P^m$ is the closed ball $\{x \in P^m : \|x - c(\sigma^n)\| \leq R(\sigma^n)\}$. Recall that $c(\sigma^n)$ is the circumcenter of $\sigma^n$ and $R(\sigma^n)$ its circumradius. The notation $\|\cdot\|$ denotes the standard Euclidean norm. We use the notation $B(\sigma^n)$ for the equatorial ball of a simplex $\sigma^n$.

In this dissertation the term *equatorial ball* is used almost exclusively in the context of $\sigma^n \prec \sigma^{n+1}$, and the hyperplane $P^m$ is understood to be $\text{aff}(\sigma^{n+1})$. Thus the notation $B(\sigma^n)$ need not indicate which hyperplane $P^m$ is the containing hyperplane for the equatorial ball. The text explicitly discusses what is intended if the equatorial ball lies in some other hyperplane.

**Theorem 3.1.1** (Equatorial Balls Characterization)**.** *The $n$-simplex $\sigma^n = v_0v_1 \ldots v_n$ is $n$-well-centered if and only if for each $i = 0, 1, \ldots, n$, vertex $v_i$ lies strictly outside the equatorial ball*

[1] Theorem 3.1.1, Fig. 3.1, and Fig. 3.2 are scheduled to appear as Theorem 4.1, Fig. 4.1, and Fig. 4.2 in the article "Well-Centered Triangulation" in the SIAM Journal of Scientific Computing [64]. The article was written by the author Evan VanderZee and his coauthors Anil N. Hirani, Damrong Guoy, and Edgar A. Ramos. A significant portion of the text of Sec. 3.1 is also based on that article. The copyright for that article belongs to the Society for Industrial and Applied Mathematics (SIAM). The copyrighted material that is used here is reprinted with kind permission of SIAM.

Much of the text and many of the other figures from this chapter are from an article that is being prepared by the author and his colleagues. In particular, Figure 3.3 and its explanation are based on contributions of Edgar Ramos towards that article ([65]).

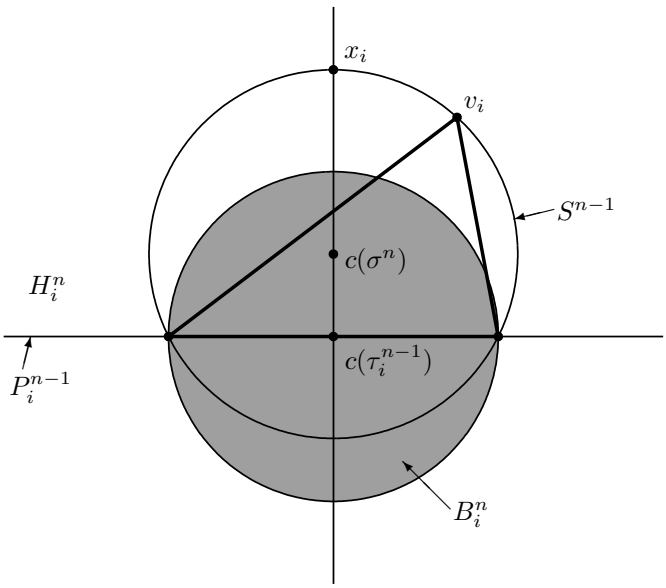


Figure 3.1: An illustration of the proof of Theorem 3.1.1 in two dimensions. In an $n$-well-centered simplex $\sigma^n$, vertex $v_i$ and circumcenter $c(\sigma^n)$ lie in the same open half-space $H_i^n$, the region where circumsphere $S^{n-1}$ lies outside equatorial ball $B_i^n$.

$B_i^n := B(v_0 v_1 \dots v_{i-1} v_{i+1} \dots v_n)$ *of the facet opposite* $v_i$.

*Proof.* Figure 3.1 provides a pictorial sketch of the proof for the case $n = 2$. The notation is the same as in the general case.

Let $S^{n-1}$ be the circumsphere of $\sigma^n$. For a particular vertex $v_i$ of $\sigma^n$, we denote the facet of $\sigma^n$ opposite $v_i$ by $\tau_i^{n-1} = v_0 v_1 \dots v_{i-1} v_{i+1} \dots v_n$. We use $P_i^{n-1}$ as a shorthand notation for the affine hull of $\tau_i^{n-1}$.

Now $\text{aff}(\sigma^n)$ is a copy of $\mathbb{R}^n$, and each $P_i^{n-1}$ divides $\text{aff}(\sigma^n)$ into two half-spaces. One of these half-spaces contains the interior of $\sigma^n$. We call this half-space $H_i^n$, taking it to be an open set that does not include its boundary $P_i^{n-1}$. Notice that $v_i \in H_i^n$.

First we suppose that $\sigma^n$ is $n$-well-centered. Choose some $i \in \{0, \dots, n\}$. Since $\sigma^n$ is $n$-well-centered, $c(\sigma^n)$ lies in $H_i^n$. Consider, then, the line through $c(\sigma^n)$ and $c(\tau_i^{n-1})$. Within $H_i^n$, this line intersects $S^{n-1}$ at a point $x_i$ such that $\|x_i - c(\sigma^n)\| = R(\sigma^n)$. Moreover, $\left\|x_i - c(\tau_i^{n-1})\right\| > R(\sigma^n) > R(\tau_i^{n-1})$. We see that $x_i$ lies outside $B_i^n$ and conclude that $S^{n-1} \cap H_i^n$ lies outside $B_i^n$. In particular, since $v_i \in S^{n-1} \cap H_i^n$, we know that $v_i$ lies outside $B_i^n$. This statement holds for each $i = 0, 1, \dots, n$, so necessity is proved.

For sufficiency we consider an $n$-simplex $\sigma^n$ such that $v_i$ lies outside $B_i^n$ for each $i = 0, 1, \dots, n$. Choose some $i \in \{0, \dots, n\}$. The hyperplane $P_i^{n-1}$ cuts $S^{n-1}$ into two parts, one lying inside $B_i^n$, and one lying outside $B_i^n$. As we saw in the preceding paragraph, $c(\sigma^n)$ lies on the same side of $P_i^{n-1}$ as the part of $S^{n-1}$ that lies outside $B_i^n$. Since $v_i \in S^{n-1}$ is outside $B_i^n$, $c(\sigma^n)$ and $v_i$ lie on the same side of $P_i^{n-1}$. We conclude that $c(\sigma^n) \in H_i^n$. This holds for each $i = 0, 1, \dots, n$, so $c(\sigma^n) \in \bigcap_{i=0}^n H_i$. In words, the circumcenter of $\sigma^n$ lies in the interior of $\sigma^n$. □

Figure 3.2 illustrates Theorem 3.1.1 as it applies to a tetrahedron. For each vertex $v_i$ of the tetrahedron, Fig. 3.2 shows the equatorial ball $B(\tau_i)$ of the facet $\tau_i$ opposite $v_i$, emphasizing in a

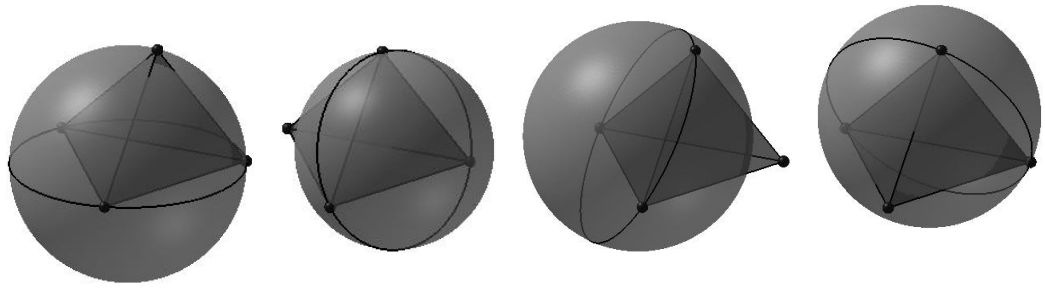

Figure 3.2: Four views of the same 3-well-centered tetrahedron $\sigma^3$ in the same orientation. From left to right the views show $\sigma^3$ with the equatorial balls of its bottom, right, left, and rear facets. For each facet $\tau_i^2$ of $\sigma^3$, the circumsphere (i.e., circumcircle) of $\tau_i^2$, which is an equator of the equatorial ball $B(\tau_i^2)$, is shown. Because the tetrahedron is 3-well-centered, the vertex $v_i$ opposite facet $\tau_i^2$ lies outside $B(\tau_i^2)$; Theorem 3.1.1 states that an $n$-simplex is $n$-well-centered if and only if for each vertex $v_i$, $v_i$ lies outside of the equatorial ball of the facet $\tau_i^{n-1}$ opposite $v_i$. For the bottom facet and rear facet views in the figure, the reader may need to look closely to see that the edges incident to $v_i$ do pierce $B(\tau_i^2)$, and $v_i$ does lie outside $B(\tau_i^2)$.

darker color the circumcircle of $\tau_i$, which is a great circle on $B(\tau_i)$. The figure shows that in each case $v_i$ is outside the equatorial ball of $\tau_i$, so we can conclude that the tetrahedron is 3-well-centered. Moreover, this same condition is satisfied by every 3-well-centered tetrahedron.

Theorem 3.1.1 is a complete characterization of the $n$-well-centered simplex in terms of equatorial balls. It uses the equatorial ball of every facet of the $n$-simplex. Focusing on the equatorial ball of just one facet $\tau_i^{n-1}$ of an $n$-simplex $\sigma^n$, Theorem 3.1.1 has an obvious implication.

**Corollary 3.1.2** (One-Facet Equatorial Ball Condition)**.** *Let $\sigma^n = u * \tau^{n-1}$. If the simplex $\sigma^n$ is $n$-well-centered, then $u$ lies strictly outside of $B(\tau^{n-1})$.*

Corollary 3.1.2 uses the notation $\sigma^n = u * \tau^{n-1}$, meaning that $\sigma^n$ is the convex hull of vertex $u$ and the vertices of $\tau^{n-1}$. The notation, which is used frequently in this chapter, denotes the cone operation of simplicial complexes, and is defined in that setting in Chapter 4.

Notice that Corollary 3.1.2 is not a characterization. It is, however, a geometric property of the $n$-well-centered $n$-simplex. The corollary applies in the situation of a fixed facet $\tau^{n-1}$ with a free vertex $u$ opposite the fixed facet. Most of the remaining results in this chapter are discussed in that setting, and the next section will relate Corollary 3.1.2 to some other geometric properties of the $n$-well-centered $n$-simplex in that setting.

## 3.2 Other Geometric Properties

There are many interesting and theoretically useful geometric properties of the $n$-well-centered $n$-simplex. Chapter 2 already made use of one of these properties, and they will appear again in Chapter 4. This section formally proves several of these geometric properties. Before turning to the proofs, though, we develop some intuition and informally introduce the results by examining Fig. 3.3.

In the sketches we are given a triangle $\tau$ embedded in $\mathbb{R}^3$. Triangle $\tau$ represents a facet of a

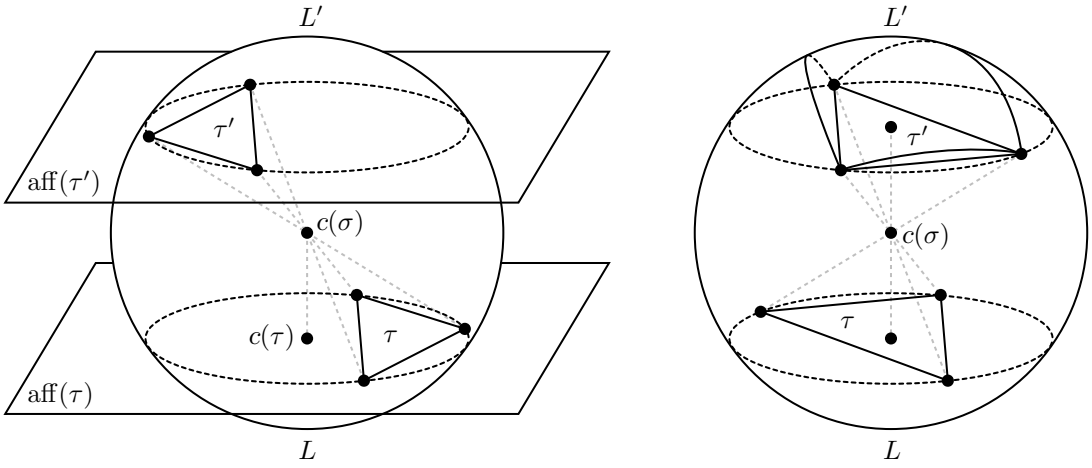


Figure 3.3: Consider constructing a tetrahedron $\sigma$ given a fixed facet $\tau$ of the tetrahedron and the circumcenter $c(\sigma)$ of the tetrahedron. These sketches show the reflection $\tau'$ of $\tau$ through $c(\sigma)$. In the case on the left $\tau$ is not 2-well-centered; on the right $\tau$ is 2-well-centered. The constructed tetrahedron $\sigma$ will be 3-well-centered if and only if its vertex $u$ opposite $\tau$ lies in the spherical triangle determined by the intersection of $C(\sigma)$ and a (geometric) cone on $\tau'$ with apex $c(\sigma)$. The graphic on the right shows the outline of this spherical triangle.

tetrahedron $\sigma$. The vertices of $\tau$ are fixed, but the fourth vertex of $\sigma$, which we call $u$, is not yet determined. (Thus tetrahedron $\sigma$ does not appear in Fig. 3.3.) For the sketches in Fig. 3.3 we suppose that the circumcenter $c(\sigma)$ of the tetrahedron is given. Thus $u$ is constrained to lie on a particular sphere, the circumsphere of $\sigma$. The left side of Fig. 3.3 considers the case in which $\tau$ is not 2-well-centered. On the right, $\tau$ is 2-well-centered.

The left side of Fig. 3.3 shows $\tau$ lying in the plane $\mathrm{aff}(\tau)$. It also shows $\tau'$ and $\mathrm{aff}(\tau')$, the reflections of $\tau$ and $\mathrm{aff}(\tau)$ through $c(\sigma)$. The plane $\mathrm{aff}(\tau)$ intersects $C(\sigma)$, the circumsphere of $\sigma$, to determine a lower spherical cup $L$, and $\mathrm{aff}(\tau')$ determines an upper spherical cup $L'$. From intuition about the geometry, one can see that in order to construct a 3-well-centered simplex $\sigma$, the vertex $u$ must lie strictly inside the spherical triangle determined by the intersection of $L'$, the upper cup of $C(\sigma^n)$, with a geometric cone from apex $c(\sigma^n)$ through $\tau'$. (The right side of Fig. 3.3 shows the outline of this spherical triangle, but the spherical triangle is not shown on the left side.)

In particular, notice that there is a necessary condition that $u$ must lie strictly in the upper cup $L'$ of the circumsphere. A somewhat weaker necessary condition states that $u$ must lie either in $L$ or in $L'$, i.e., that the orthogonal projection of $u$ into $\mathrm{aff}(\tau)$ (vertical projection in Fig. 3.3) must be interior to the circumball of $\tau$. The One-Facet Equatorial Ball Condition of Corollary 3.1.2, restated in the notation of Fig. 3.3 is the necessary condition that $u$ must not lie in the lower cup $L$. Thus combining Corollary 3.1.2 with the statement about the orthogonal projection of $u$ recovers the condition that $u$ must lie in $L'$.

In case $\tau$ is 2-well-centered, as it is on the right side of Fig. 3.3, we see that the orthogonal projection of the spherical triangle on $L'$ into $\mathrm{aff}(\tau)$ contains the orthogonal projection of $\tau'$ into $\mathrm{aff}(\tau)$. Hence if $u$ is placed somewhere outside $L$ such that the orthogonal projection of $u$ into $\mathrm{aff}(\tau)$ lies strictly inside the orthogonal projection of $\tau'$ into $\mathrm{aff}(\tau)$, then $u$ must lie strictly inside the spherical triangle on $L'$. This geometric reasoning provides a sufficient condition that can be used

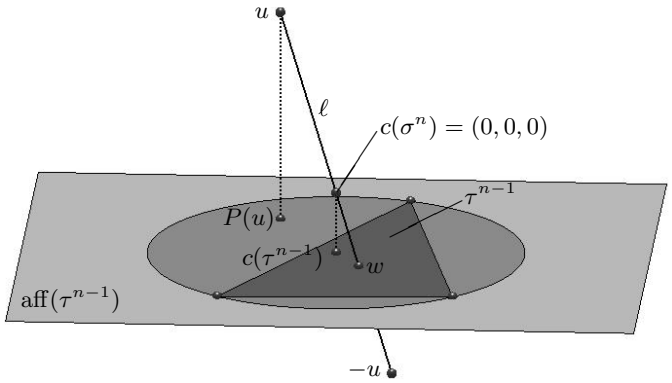


Figure 3.4: Because the tetrahedron $\sigma^n = u * \tau^{n-1}$ is 3-well-centered, $P(u)$ lies inside the circumball of $\tau^{n-1}$.

to prove a tetrahedron $\sigma$ is 3-well-centered. The two geometric conditions introduced in this and the previous paragraph form the basis of this section. They are generalized to higher dimensions and proved formally in Propositions 3.2.1 and 3.2.2.

Before leaving the informal introduction of the remaining results in this chapter, we consider varying the position of $c(\sigma)$, moving it along the line through $c(\tau)$ orthogonal to $\text{aff}(\tau)$. For each position of $c(\sigma)$ there is some spherical triangle of locations for $u$ that will produce a 3-well-centered tetrahedron with circumcenter $c(\sigma)$ and facet $\tau$. As $c(\sigma)$ varies, these spherical triangles sweep out a solid 3-dimensional region. Given the fixed facet $\tau$, the constructed tetrahedron $\sigma$ will be 3-well-centered if and only if vertex $u$ lies in this region. Section 3.3 shows that in arbitrary dimensions this region can be described in terms of cubic polynomial inequalities in the coordinates of $u$. (See Fig. 3.10.)

Now we turn to a formal statement and proof of the necessary condition that vertex $u$ must lie either in the upper or lower cup on the circumsphere of an $n$-well-centered $n$-simplex $\sigma$. Figure 3.4 is a sketch in $\mathbb{R}^3$ that accompanies the proof of this proposition.

**Proposition 3.2.1** (Cylinder Condition)**.** *Let $\sigma^n$ be an $n$-well-centered $n$-simplex in $\mathbb{R}^n$ with $u$ a vertex of $\sigma^n$ and $\tau^{n-1}$ the facet of $\sigma^n$ opposite $u$. That is, let $\sigma^n = u * \tau^{n-1}$. Let $P$ be the orthogonal projection $P : \mathbb{R}^n \to \text{aff}(\tau^{n-1})$. Then $\left\|P(u) - c(\tau^{n-1})\right\| < R(\tau^{n-1})$, i.e., vertex $u$ projects to the interior of the circumball of $\tau^{n-1}$.*

*Proof.* Consider the coordinate system on $\mathbb{R}^n$ such that $c(\sigma^n)$ is the origin and $\text{aff}(\tau^{n-1}) = \{x \in \mathbb{R}^n : x_n = k\}$ for some constant $k \leq 0$. In this coordinate system, $P$ is the projection map

$$P : (x_1, \ldots, x_{n-1}, x_n) \mapsto (x_1, \ldots, x_{n-1}, k).$$

Let $u = (x_1, \ldots, x_n)$ in this coordinate system. We have assumed that $\sigma^n$ is $n$-well-centered, so $c(\sigma^n)$ (the origin) is strictly interior to $\sigma^n$. It follows that $k < 0$ and $x_n > 0$.

Consider the line segment $\ell$ from $u$ to $-u$, a diameter of $C(\sigma^n)$. Moreover, $\ell \cap \text{Int}(\tau^{n-1}) \neq \emptyset$. This follows from the fact that $\sigma^n$ is $n$-well-centered; we have $\sigma^n = u * \tau^{n-1}$ and $c(\sigma^n) \in \text{Int}(\sigma^n)$, so there must be some point $w \in \text{Int}(\tau^{n-1})$ such that $c(\sigma^n)$ lies on $uw$, a proper subsegment of $\ell$. We notice, then, that the point $-u$ lies below $\text{aff}(\tau^{n-1})$ and conclude that $x_n > -k$.

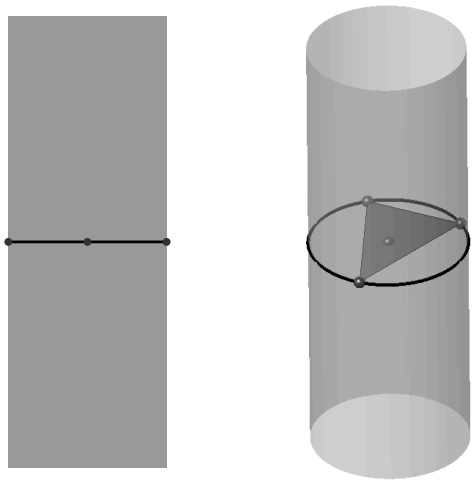

Figure 3.5: If a simplex $u * \tau^{n-1}$ is $n$-well-centered, then $u$ is interior to a solid right spherical cylinder over the circumsphere of $\tau^{n-1}$.

By the Pythagorean theorem, $R(\tau^{n-1})^2 + k^2 = R(\sigma^n)^2$. We also have

$$\sum_{i=1}^{n} x_i^2 = R(\sigma^n)^2,$$

since $u$ lies on the circumsphere of $\sigma^n$. It follows that

$$\left\|P(u) - c(\tau^{n-1})\right\|^2 = \sum_{i=1}^{n-1} x_i^2 = R(\sigma^n)^2 - x_n^2 < R(\sigma^n)^2 - k^2 = R(\tau^{n-1})^2.$$

□

The generalization for an $n$-well-centered $n$-simplex embedded in $\mathbb{R}^m$ for $m > n$ is immediate. The proof is very similar, but begins by choosing a coordinate system on $\mathbb{R}^m$ that satisfies

$$\text{aff}(\sigma^n) = \{x \in \mathbb{R}^m : x_i = 0 \text{ for } i = n+1, \ldots, m\}$$

as well as the other specifications given in the proof.

**Remark.** Given a particular simplex $\tau^{n-1} \subset \mathbb{R}^n$ and the circumcenter of $\sigma^n$, the Cylinder Condition says, in the notation of Fig. 3.3, that if $\sigma^n$ is $n$-well-centered, then vertex $u$ must lie either in the upper cup $L'$ or the lower cup $L$. Proposition 3.2.1 also has a geometric interpretation given a particular simplex $\tau^{n-1} \subset \mathbb{R}^n$ without a fixed circumcenter. If $\sigma^n = u * \tau^{n-1}$ is $n$-well-centered, then vertex $u$ lies within a solid right spherical cylinder over $C(\tau^{n-1})$. Figure 3.5 illustrates the condition in 2D and 3D, making it clear how this condition generalizes from the familiar 2-D case into higher dimensions. In each of the sketches in Fig. 3.5 the vertices of the base simplex $\tau^{n-1}$, as well as the circumcenter $c(\tau^{n-1})$, are marked by small dark-colored balls. If $u * \tau^{n-1}$ is $n$-well-centered, then the vertex $u$ must lie inside the gray cylinder over the circumsphere of $\tau^{n-1}$.

**Remark.** We have seen two necessary conditions for an $n$-simplex to be $n$-well-centered — the One-Facet Equatorial Ball Condition (Corollary 3.1.2) and the Cylinder Condition (Proposition 3.2.1).

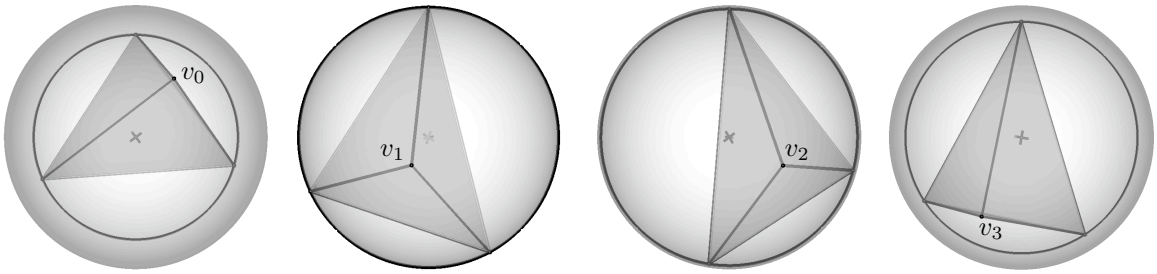


Figure 3.6: Four different views of the tetrahedron $\sigma^3$ from Fig. 2.5. Each view looks directly down onto a facet $\tau_i^2$ opposite a vertex $v_i$ of the tetrahedron. It can be seen from the pictures that each vertex $v_i$ projects to the interior of the circumball of $\tau_i^2$, since in each case vertex $v_i$ looks like its inside the circumcircle of $\tau_i$, drawn in a darker shade. Thus $\sigma^3$ satisfies the Cylinder Condition at each of its vertices. It is also the case that $\sigma^3$ satisfies the One-Facet Equatorial Ball at three of its four vertices. The vertex that does not satisfy the condition of Corollary 3.1.2 is vertex $v_1$. For this vertex only, the picture shows $c(\sigma^3)$ lying behind $\tau_1^2$ and $C(\tau_1^2)$ (just barely) on the closer hemisphere of the circumsphere of $\sigma^3$.

In $\mathbb{R}^2$ satisfying these two necessary conditions at a single vertex $u$ opposite a segment $\tau^1$ is sufficient to guarantee that the 2-simplex $u * \tau^1$ is 2-well-centered. In $\mathbb{R}^n$ for $n \geq 3$, however, an $n$-simplex $\sigma^n$ that is not $n$-well-centered may have one or more vertices $u$ such that $\sigma^n = u * \tau^{n-1}$ and $u$ satisfies both the One-Facet Equatorial Ball Condition and the Cylinder Condition with respect to $\tau^{n-1}$.

**Example.** For example, consider the tetrahedron $\sigma = \sigma^3$ from Fig. 2.5. Its vertices are

$$\begin{aligned} v_0 &= (-0.152, 0.864, -0.48), \\ v_1 &= (-0.64, -0.6, -0.48), \\ v_2 &= (0.6, -0.64, -0.48), \text{ and} \\ v_3 &= (-0.192, -0.64, 0.744), \end{aligned}$$

and its circumcenter lies at the origin. Figure 3.6 shows that for each $i \in \{0, 1, 2, 3\}$, vertex $v_i$ of $\sigma^3$ satisfies the Cylinder Condition with respect to $\tau^{n-1}$. For $i \in \{0, 2, 3\}$, $v_i$ also satisfies the One-Facet Equatorial Ball Condition. Nonetheless, as can be clearly seen in Fig. 2.5 and concluded from the fact that $v_1$ does not satisfy the One-Facet Equatorial Ball Condition, $\sigma^3$ is not 3-well-centered. Thus satisfying the Cylinder Condition at every vertex does not guarantee that a tetrahedron will be 3-well-centered. Similarly, satisfying both the Cylinder Condition and the One-Facet Equatorial Ball Condition at three of the four vertices of a tetrahedron does not guarantee that a tetrahedron will be well-centered.

**Example.** The tetrahedron from Fig. 2.5 is not dihedral acute. The tetrahedron with vertices at $(-0.01, -0.01, -0.01)$, $(1, 0, 0)$, $(0, 1, 0)$, and $(0, 0, 1)$ is an acute tetrahedron that is in other ways very similar to the previous example. It is not 3-well-centered, but all of its vertices satisfy the Cylinder Condition and three of them satisfy the One-Facet Equatorial Ball Condition.

**Remark.** Any tetrahedron that is dihedral acute satisfies the Cylinder Condition at each of its vertices. The orthogonal projection of a vertex $v_i$ of an acute tetrahedron into $\text{aff}(\tau_i)$ lies strictly inside facet $\tau_i$ (see Lemma 2 in [26]), so it must lie strictly inside the circumball of $\tau_i$.

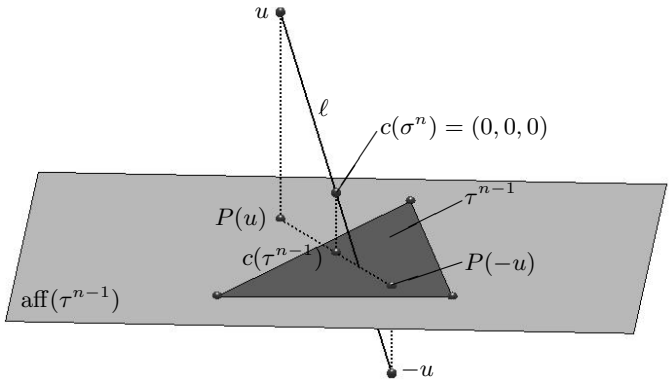


Figure 3.7: Because $P(-u)$ and $c(\tau^{n-1}) = P(c(\sigma^n))$ are both interior to $\tau^{n-1}$ and $c(\sigma^n)$ is above $\text{aff}(\tau^{n-1})$, we know that the tetrahedron $\sigma^n = u * \tau^{n-1}$ is 3-well-centered.

We have seen evidence that the combined Cylinder Condition and One-Facet Equatorial Ball Condition are not strong enough to prove that an $n$-simplex is $n$-well-centered if $n \geq 3$. There is, however, a stronger set of conditions that can be used to prove a simplex $u * \tau^{n-1}$ is $n$-well-centered just by looking at $\tau^{n-1}$ and the position of $u$ relative to $\tau^{n-1}$. Proposition 3.2.2 states these conditions, making use again of the map $P$ from Proposition 3.2.1, the orthogonal projection from $\mathbb{R}^n$ to $\text{aff}(\tau^{n-1})$. Figure 3.7 is a sketch in $\mathbb{R}^3$ that accompanies the proof of Proposition 3.2.2.

**Proposition 3.2.2** (Prism Condition)**.** *Let $\tau^{n-1}$ be an $(n-1)$-well-centered simplex in $\mathbb{R}^n$ and $\sigma^n = u * \tau^{n-1}$. If $u$ lies outside the equatorial ball $B(\tau^{n-1})$ and the reflection of $P(u)$ through $c(\tau^{n-1})$ is interior to $\tau^{n-1}$, then $\sigma^n$ is $n$-well-centered.*

*Proof.* We assume the stated hypothesis and take the coordinate system with $c(\sigma^n)$ at the origin and $\text{aff}(\tau^{n-1}) = \{x \in \mathbb{R}^n : x_n = k\}$ for some constant $k \leq 0$, the same coordinate system that was used in the proof of Proposition 3.2.1. As we saw in the proof of Theorem 3.1.1, the fact that $u$ lies outside the equatorial ball of $\tau^{n-1}$ implies that $c(\sigma^n)$ and vertex $u$ lie interior to the same open halfspace with respect to $\text{aff}(\tau^{n-1})$. It follows that $k < 0$ and $x_n > k$.

Observe that, as shown in Fig. 3.7, the reflection of $P(u)$ through $c(\tau^{n-1})$ is $P(-u)$. By the hypothesis, $P(-u)$ lies in the interior of $\tau^{n-1}$. Thus $P(-u)$ is interior to the circumball of $\sigma^n$. In terms of coordinates, this means

$$\|P(u)\|^2 = \|P(-u)\|^2 = k^2 + \sum_{i=1}^{n-1} x_i^2 < R(\sigma^n)^2 = \sum_{i=1}^{n} x_i^2$$

It follows that $|x_n| > |k| = -k$. Since we know that $x_n > k$, we conclude that $x_n > -k > 0$.

Let $\ell$ be the line segment from $u$ to $-u$. We will show that $\ell$ intersects the interior of $\tau^{n-1}$. Then, because $\sigma^n = u * \tau^{n-1}$ and $k < 0 < x_n$ (so that $c(\sigma^n) \in \ell$ is above $\tau^{n-1}$ and below $u$), we will be able to conclude that $c(\sigma^n)$ is interior to $\sigma^n$. We know that $P(c(\sigma^n)) = c(\tau^{n-1})$ is interior to $\tau^{n-1}$ because $\tau^{n-1}$ is $(n-1)$-well-centered. Since $P(-u)$ and $P(c(\sigma^n))$ are both interior to $\tau^{n-1}$, the line segment from $c(\sigma^n)$ to $-u$, which is a subsegment of $\ell$, is interior to the (convex) infinite prism $\tau^{n-1} \times \mathbb{R} = \{x \in \mathbb{R}^n : P(x) \in \tau^{n-1}\}$. Moreover, $0 > k > -x_n$ (i.e., $c(\sigma^n)$ is above $\tau^{n-1}$ and $-u$ is below $\tau^{n-1}$), so this subsegment intersects the interior of $\tau^{n-1}$. □

Figure 3.8: In this tetrahedron the top vertex $v_3$ and the facet $\tau_3^2$ opposite $v_3$ satisfy all of the conditions of Proposition 3.2.2 except the requirement that $\tau_3^2$ should be 2-well-centered. This tetrahedron is not 3-well-centered, demonstrating that we cannot remove from the Prism Condition the requirement for $\tau^{n-1}$ to be $(n-1)$-well-centered.

The generalization for an $n$-well-centered $n$-simplex embedded in $\mathbb{R}^m$ with $m > n$, as for Proposition 3.2.1, is immediate. Again the only significant change in the proof is starting with a coordinate system on $\mathbb{R}^m$ that satisfies

$$\text{aff}(\sigma^n) = \{x \in \mathbb{R}^m : x_i = 0 \text{ for } i = n+1, \ldots, m\}$$

as well as the other specifications in the proof.

It is worth pointing out that the requirement that facet $\tau^{n-1}$ be $(n-1)$-well-centered cannot be removed from Proposition 3.2.2. This may already be clear from the discussion of Fig. 3.3 that introduced the results in this chapter, but we include an explicit example to emphasize the point.

**Example.** The tetrahedron in Fig. 3.8, which we saw earlier in Fig. 2.3 is the convex hull of vertices

$$\begin{aligned} v_0 &= (0.224, -0.768, -0.6), \\ v_1 &= (0.8, 0, -0.6), \\ v_2 &= (0.224, 0.768, -0.6), \text{ and} \\ v_3 &= (-0.28, 0, 0.96)\,. \end{aligned}$$

The bottom facet in Fig. 3.8, which is the triangle $\tau_3^2 = [v_0 v_1 v_2]$, lies in the plane $x_3 = -0.6$ and is an obtuse triangle. (The obtuse angle is at vertex $v_2$, the rightmost vertex in Fig. 3.8.) Considering this tetrahedron relative to the Prism Condition, we satisfy the requirements that $v_3$ lie outside $B(\tau_3^2)$ and that the reflection of $P(u)$ through $c(\tau_3^2)$ be interior to $\tau_3^2$. Indeed, $c(\tau_3^2) = (0, 0, -0.6)$ and $R(\tau_3^2) = 0.8$, with $\left\|v_3 - c(\tau_3^2)\right\| = \sqrt{2.512} \approx 1.58$, so $v_3$ is outside $B(\tau_3^2)$, and $P(-u) = (0.28, 0, -0.6)$, which is inside $\tau^2$. Thus we satisfy all of the requirements of Proposition 3.2.2 except the requirement that $\tau_3^2$ be 2-well-centered. It is clear from Fig. 3.8 that this is not sufficient; the circumcenter of $v_3 * \tau_3^2$, marked by the usual small axis directions indicator, lies outside the tetrahedron.

**Remark.** Like the condition of Proposition 3.2.1, the condition of Proposition 3.2.2 has a nice geometric interpretation in the setting of a fixed facet $\tau^{n-1} \subset \mathbb{R}^n$ with $c(u * \tau^{n-1})$ not given,

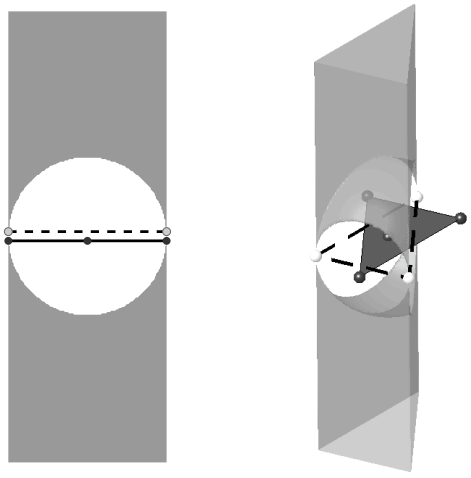

Figure 3.9: If the base simplex $\tau^{n-1}$ is $(n-1)$-well-centered, then when the vertex $u$ lies outside $B(\tau^{n-1})$ but interior to an infinite prism over the reflection of $\tau^{n-1}$ through $c(\tau^{n-1})$, simplex $u*\tau^{n-1}$ is $n$-well-centered. The left side of this figure portrays the 2-dimensional case, and the right side the 3-dimensional case. In each case the base simplex $\tau^{n-1}$, which is $(n-1)$-well-centered, is shown in dark colors and solid lines, and its reflection is outlined with lighter colors and dashed lines. A vertex $u$ lying in the gray region is guaranteed to construct an $n$-well-centered $n$-simplex $u * \tau^{n-1}$. In the picture on the left, the base simplex $\tau^1$ and its reflection through $c(\tau^1)$ should actually lie on top of each other, but are set slightly apart in the drawing so that the reader can distinguish them from each other.

provided that $\tau^{n-1}$ is $(n-1)$-well-centered. For a given $(n-1)$-well-centered facet $\tau^{n-1}$, if the vertex $u$ opposite $\tau^{n-1}$ lies outside $B(\tau^{n-1})$ and inside an infinite prism (a right cylinder) over the reflection of $\tau^{n-1}$ through $c(\tau^{n-1})$, then $\sigma^n = u * \tau^{n-1}$ is $n$-well-centered. Figure 3.9 portrays this region for specific examples in 2 and 3 dimensions.

## 3.3 Cubic Polynomial Inequalities

In Sec. 3.2 we considered the situation of a fixed facet $\tau^{n-1}$ and a vertex $u$ opposite $\tau^{n-1}$ used to construct an $n$-simplex $\sigma^n = u * \tau^{n-1}$. We proved two geometric propositions related to whether $\sigma^n$ is $n$-well-centered, one a necessary condition, and the other a sufficient condition. The regions defined by those two propositions are fairly intuitive geometrically, but may be quite different from each other. For example, in the 3-D pictures on the right hand sides of Figs. 3.5 and 3.9, the same base simplex $\tau^{n-1}$ yields rather different regions. This section closes the gap between the necessary condition region and the sufficient condition region by developing a precise algebraic description of the set of positions of $u$ that will produce an $n$-well-centered $n$-simplex $u * \tau^{n-1}$. The algebraic description takes the form of a system of cubic polynomial inequalities in the coordinates of $u$.

The inequalities are derived from a linear system of equations discussed in [5]. This linear system, which provides one way to compute the circumcenter of a simplex $\sigma^n$ embedded in $\mathbb{R}^m$ for $m \geq n$, is briefly reviewed here. We may write the circumcenter $c$ of a simplex $\sigma^n = v_0 v_1 \dots v_n$ as a linear combination of the vertices $v_i \in \mathbb{R}^m$,

$$c = \alpha_0 v_0 + \alpha_1 v_1 + \cdots + \alpha_n v_n,$$

with the coefficients $\alpha_i$ satisfying $\sum_{i=0}^{n} \alpha_i = 1$. The coefficients $\alpha_i$ are known as the *barycentric coordinates* of the circumcenter. The condition that $\sigma^n$ be $n$-well-centered is the same as the condition that $0 < \alpha_i$ for every $\alpha_i$, i.e., the condition that the circumcenter be a convex combination of the vertices of $\sigma^n$ with strictly positive coefficients.

Suppose we are given the coordinates of the vertices $v_i$ of $\sigma^n$. We know that

$$\langle c - v_i, c - v_i \rangle = \|c - v_i\|^2 = R^2$$

for each vertex $v_i$. Introducing the variable $\lambda = R^2 - \|c\|^2$, we obtain the $n+1$ equations $2\langle c, v_i \rangle + \lambda = \|v_i\|^2$. Since the vertices $v_i$ are known, each equation is a linear equation in the $n+2$ unknowns $\alpha_0, \alpha_1, \ldots, \alpha_n, \lambda$. The final equation of the system is $\sum_{i=0}^{n} \alpha_i = 1$, which forces the $\alpha_i$ to be barycentric coordinates. As long as this linear system of $n+2$ equations in $n+2$ unknowns is nonsingular, we can solve it to find the barycentric coordinates of the circumcenter. If the simplex is nondegenerate, i.e., if the $n+1$ vertices are affinely independent, then the simplex has a unique, finite circumcenter, which, like every point in $\mathrm{aff}(\sigma^n)$, has unique barycentric coordinates. It follows that the linear system has a unique solution; hence the matrix is nonsingular.

Let $A$ be the matrix of this linear system and $b$ the right-hand side,

$$A = \begin{pmatrix} 2\langle v_0, v_0 \rangle & 2\langle v_0, v_1 \rangle & \cdots & 2\langle v_0, v_n \rangle & 1 \\ 2\langle v_1, v_0 \rangle & 2\langle v_1, v_1 \rangle & \cdots & 2\langle v_1, v_n \rangle & 1 \\ \vdots & \vdots & \ddots & \vdots & \vdots \\ 2\langle v_n, v_0 \rangle & 2\langle v_n, v_1 \rangle & \cdots & 2\langle v_n, v_n \rangle & 1 \\ 1 & 1 & \cdots & 1 & 0 \end{pmatrix}, \qquad b = \begin{pmatrix} \langle v_0, v_0 \rangle \\ \langle v_1, v_1 \rangle \\ \vdots \\ \langle v_n, v_n \rangle \\ 1 \end{pmatrix}.$$

For $i = 0, 1, \ldots, n$ we let $A_i$ be the matrix $A$ with column $i+1$ replaced by $b$. Cramer's rule tells us that $\alpha_i = \det(A_i)/\det(A)$. If we consider vertices $v_0, \ldots, v_{n-1}$ to be the vertices of some given $\tau^{n-1}$ and $v_n$ to be a free vertex $u$, then we see already that the barycentric coordinates $\alpha_i$ are rational functions of the coordinates of $u$. Thus the conditions $\alpha_i > 0$ are algebraic inequalities in the coordinates of $u$.

To simplify matrix $A$ a little, we translate each vertex of the simplex by $-v_0$. The translation may change the value of $\lambda$ in the solution vector — in fact, $\lambda = 0$ always holds for the translated system — but the barycentric coordinates of the circumcenter are not changed by translating the vertices of the simplex. If $m > n$ we make one further simplification. In the translated coordinate system, we rotate the simplex about the origin (now at $v_0$) to obtain a simplex for which vector $v_i - v_0 \in \{x : x_{n+1} = \cdots = x_m = 0\}$ for each $i = 1, \ldots, n$. Rotation about the origin is an orthogonal transformation, so it does not change any of the entries of the linear system or the right hand side vector (which are dot products) and does not change the barycentric coordinates of the circumcenter. We denote this orthogonal rotation matrix by $Q$, with $Q$ the identity if no rotation is needed.

If we restrict our attention to one of the open halfspaces bounded by $\mathrm{aff}(\tau^{n-1})$ and assume that $\tau^{n-1}$ is not degenerate, then we have either $\det(A) > 0$ or $\det(A) < 0$ throughout the halfspace, because $\det(A)$ is a continuous function of the entries in $A$ and $A$ is singular only when $u \in \mathrm{aff}(\tau^{n-1})$, i.e., when $\sigma^n = u * \tau^{n-1}$ is degenerate. We will see that, in fact, $\det(A) \leq 0$ holds everywhere, so

$\det(A) < 0$ throughout the halfspace.

The first row and the first column of $A$ in the simplified linear system are all zeroes except for the last entry, which is 1 in both cases. Computing the determinant of $A$ by first expanding across the first row and then expanding down the first column (one with an odd number of entries and the other with an even number of entries) we find that $\det(A) = -\det(B)$ where $B$ is the submatrix of $A$ spanning rows 2 to $n+1$ and columns 2 to $n+1$. The $n \times n$ submatrix $B$ has the form $2V^{\mathrm{T}}V$, where $V$ is the $m \times n$ matrix

$$V = \begin{pmatrix} Q(v_1 - v_0) & Q(v_2 - v_0) & \cdots & Q(v_n - v_0) \end{pmatrix}.$$

By construction of $Q$, the last $m - n$ coordinates of each vector $Q(v_i - v_0)$ are zeroes. Thus if we take $\widetilde{V}$ to be the first $n$ rows of $V$, then $\widetilde{V}$ is an $n \times n$ matrix that satisfies $B = 2V^{\mathrm{T}}V = 2\widetilde{V}^{\mathrm{T}}\widetilde{V}$. We see that $\det(B) = 2^n \det(\widetilde{V})^2 \geq 0$. Observing that $\det(\widetilde{V})$ is the signed volume of the parallelepiped spanned by the vectors that form the columns of $\widetilde{V}$, we note that $\det(B) > 0$ holds when the columns of $\widetilde{V}$ are linearly independent, i.e. when the vertices of the original simplex are affinely independent.

Thus with the assumption that $\tau^{n-1}$ is a fully $(n-1)$-dimensional simplex, we know that $\det(A) < 0$ when the vertex $u$ lies in either of the open halfspaces bounded by $\mathrm{aff}(\tau^{n-1})$. For $u$ outside $\mathrm{aff}(\tau^{n-1})$, then, we conclude that $\alpha_i = \det(A_i)/\det(A) > 0$ if and only if $\det(A_i) < 0$. Hence the simplex $u * \tau^{n-1}$ will be $n$-well-centered if and only if the coordinates of $u$ satisfy the polynomial inequality $\det(A_i) < 0$.

It remains to show that the equation $\det(A_i) = 0$ is a polynomial in the coordinates of $u$ of degree at most 3. To do this we examine the entries of $A_i$ that depend on $u$. All of these entries appear in row $n+1$ or in column $n+1$. At most two of these entries, the entry at position $(n+1, n+1)$ and the entry at $(n+1, i+1)$, are quadratic in the coordinates of $u$. (Only one entry is quadratic in the coordinates of $u$ when $i = n$. The case $i = n$ is, in fact, a quadratic polynomial inequality that corresponds to the One-Facet Equatorial Ball Condition.) Every other entry that depends on $u$ is linear in the coordinates of $u$. Using $S_n$ to denote the group of permutations on $n$ letters, the determinant of an $n \times n$ matrix $M$ can be written as

$$\det(M) = \sum_{\pi \in S_n} \mathrm{sgn}(\pi) \prod_{j=1}^{n} M_{j\pi(j)},$$

where $M_{jk}$ stands for the entry in row $j$, column $k$ of matrix $M$, and $\mathrm{sgn}(\pi)$ is the sign of the permutation. Considering the structure of matrix $A_i$, we observe that each product in this definition of $\det(A_i)$ involves at most two terms that depend on $u$, and at most one of these, the entry selected from row $n+1$, is quadratic in the coordinates of $u$. Thus the determinant is a summation of terms that are polynomial in the coordinates of $u$ and have degree at most 3.

We state the conclusions of the foregoing discussion as a formal proposition.

**Proposition 3.3.1.** *Let $\sigma^n = u * \tau^{n-1}$ for a fixed facet $\tau^{n-1}$. The $n$-simplex $\sigma^n$ is $n$-well-centered if and only if the coordinates of vertex $u$ satisfy the inequalities $\det(A_i) < 0$, which are cubic polynomial inequalities in the coordinates of $u$.*

Figure 3.10 gives a graphical representation for a particular $\tau^{n-1}$ of the precise region where the vertex $u$ may be placed to produce a 3-well-centered tetrahedron $u * \tau^{n-1}$. The facet $\tau^{n-1}$ used in

Figure 3.10: An $n$-simplex $\sigma^n = u * \tau^{n-1}$ is $n$-well-centered if and only if the coordinates of vertex $u$ satisfy inequality $\det(A_i) < 0$ for each $i = 0, 1, \ldots, n$. When $\tau^{n-1}$ is a fixed nondegenerate simplex, each inequality $\det(A_i) < 0$ is a polynomial inequality in the coordinates of $u$ with degree at most 3. This figure gives a graphical representation for a particular $\tau^2$ of the region where a vertex $u$ will produce a 3-well-centered tetrahedron $u * \tau^2$. The figure was generated using MATLAB's isosurface function and evaluations of the polynomial inequalities on a finite grid, so the picture has some imperfections. For instance, the entire circumcircle of $\tau^2$ should lie in the boundary of the permissible region, but in the figure it appears that there is a small gap above and below $\text{aff}(\tau^2)$.

Fig. 3.10 is the same facet used to illustrate the necessary condition for a tetrahedron in Fig. 3.5 and the sufficient condition for a tetrahedron in Fig. 3.9, so readers can see for this facet $\tau^{n-1}$ how the precise necessary and sufficient condition region compares to the regions defined by the Cylinder Condition and the Prism Condition. The facet $\tau^{n-1}$ along with its circumcircle and the reflection of $\tau^{n-1}$ through $c(\tau^{n-1})$ are shown in Fig. 3.10 to aid this comparison.

# Chapter 4

# Combinatorics of Well-Centered Meshes

In Chapter 2 and Chapter 3, we studied properties of well-centered simplices. In this chapter we shift from our focus on the simplex itself to the broader context of simplicial meshes. A mesh composed of triangles or tetrahedra is a simplicial mesh, and as such, is a particular kind of simplicial complex. We find the language of simplicial complexes to be particularly helpful in the study of well-centered meshes. We assume that most readers are already somewhat familiar with simplicial complexes, but we have included Sec. 4.1 as a brief introduction to simplicial complexes defining some of the key terms we have adopted. Readers familiar with simplicial complexes can skip Sec. 4.1, but should see the discussion of our definition of a geometric realization of an abstract simplicial complex on page 35 and read the definition of an interior vertex on page 35. Those less familiar with simplicial complexes may wish to consult [43] for a more extensive introduction.

Section 4.2 discusses the combinatorial properties of 2-well-centered triangle meshes embedded in $\mathbb{R}^2$. This includes some observations regarding the neighborhood of a vertex in a 2-well-centered triangle mesh in $\mathbb{R}^2$. Most of these comments about local combinatorial properties are obvious, but they provide a background for later sections in the chapter and motivate an algorithm discussed in Chapter 5. Section 4.2 closes by proving a statement about global combinatorial properties of 2-well-centered triangle meshes in $\mathbb{R}^2$.

In Sec. 4.3 and Sec. 4.4 we analyze the local combinatorial properties of well-centered tetrahedral meshes embedded in $\mathbb{R}^3$. The results are the analog in $\mathbb{R}^3$ of the obvious local combinatorial properties of well-centered triangle meshes in $\mathbb{R}^2$. In $\mathbb{R}^3$, however, the results are not at all obvious. Indeed, some of the results are unexpected, and there is still no complete characterization of the local combinatorial properties of well-centered tetrahedral meshes in $\mathbb{R}^3$. Section 4.3, which discusses the situation for 3-well-centered tetrahedral meshes, proves two results that apply to the general case of $n$-well-centered $n$-simplicial meshes embedded in $\mathbb{R}^n$. The results in Sec. 4.4 are all stated for the specific case of 2-well-centered tetrahedral meshes in $\mathbb{R}^3$, though at least some of them could also be extended to 2-well-centered $n$-simplicial meshes in $\mathbb{R}^n$. [1]

## 4.1 A Quick Introduction to Simplicial Complexes

Recall that an $n$-simplex $\sigma^n$, i.e., a simplex of *dimension* $n$ is the convex hull of $n+1$ affinely independent vertices. A *simplicial complex* $K$ is a collection of simplices such that

1. for each $\sigma \in K$, for each $\tau \prec \sigma$, $\tau \in K$

[1] Much of the material in this chapter, both text and figures, is drawn from an article that is being prepared by the author and his colleagues [65]. In particular, in the proof of Theorem 4.3.2, the argument that there is a simplex of $K$ containing the point $u$ is largely due to Edgar Ramos.

2. for each $\sigma, \tau \in K$, $\sigma \cap \tau$ is a face of both $\sigma$ and $\tau$

The second condition allows for the possibility that $\sigma$ and $\tau$ do not intersect. Then $\sigma \cap \tau = \emptyset$ is the $-1$-simplex, which is a face of every simplex. A simplicial complex is *finite* if the collection $K$ is finite. We will work exclusively with finite simplicial complexes. The *dimension* of the simplicial complex $K$ is the dimension $n$ of a highest-dimensional simplex $\sigma^n \in K$.

The *underlying space* of a simplicial complex $K$ is a topological space whose points are the union of all the simplices of $K$. For a finite simplicial complex, the topology on the underlying space of $K$ is the subspace topology of the point set as a subset of Euclidean space. A simplicial complex $K$ is a *manifold complex* if the underlying space of $K$ is a manifold (with or without boundary).

An *abstract simplicial complex* is like a simplicial complex except that the vertices are not assigned any coordinates, so the intersection property of the definition cannot be checked. A *geometric realization* of an abstract simplicial complex in Euclidean space $\mathbb{R}^n$ is an assignment of coordinates in $\mathbb{R}^n$ to the vertices. We use this term somewhat differently than it is has sometimes been used, since we do not require a geometric realization to be a simplicial complex. (It may fail the intersection property in the definition of a simplicial complex.) If a geometric realization of an abstract simplicial complex is, in fact, a simplicial complex, then we call it an *embedding* of the abstract simplicial complex. An abstract simplicial complex is said to be a manifold complex if it has an embedding as a manifold complex.

The *boundary* of a simplex $\sigma$, denoted $\mathrm{Bd}(\sigma)$, is the union of all proper faces of $\sigma$. The *interior* of a simplex $\sigma$, denoted $\mathrm{Int}(\sigma)$, is defined as $\sigma - \mathrm{Bd}(\sigma)$. We also use $\mathrm{Bd}(K)$ to denote the boundary of a manifold simplicial complex, by which we mean the set of simplices that lie in $\partial M$, where $M$ is the (manifold) underlying space of $K$ and $\partial$ is the usual operator denoting the boundary of a manifold.

The *star* of a vertex $v$ in a simplicial complex is the union of the interiors of all simplices incident to $v$, including $v$ itself, which is the interior of the 0-simplex $v$ incident to $v$. We denote the star of $v$ as $\mathrm{St}\ v$. In symbols, then, we have $\mathrm{St}\ v = \bigcup_{v \prec \sigma} \mathrm{Int}(\sigma)$. This definition extends to any simplex $\tau$ in a simplicial complex as $\mathrm{St}\ \tau = \bigcup_{\tau \prec \sigma} \mathrm{Int}(\sigma)$. The *closure* of a simplicial subcomplex $K$ is defined as $\mathrm{Cl}(K) = K \cup \bigcup_{\sigma \in K} \mathrm{Bd}(\sigma)$, i.e., the union of $K$ with all of the faces of simplices in $K$. The closure of a star is sometimes called the closed star. The *link* of a simplex $\tau$, denoted $\mathrm{Lk}\ \tau$ is the union of all simplices in the closed star of $\tau$ that are disjoint from $\tau$. For a vertex $v$, this can be written as $\mathrm{Lk}\ v = \mathrm{Cl}(\mathrm{St}\ v) - \mathrm{St}\ v$.

The *cone* of a vertex $u$ and a simplex $\sigma^n = v_0 v_1 \dots v_n$ is the simplex $u * \sigma^n = \tau^{n+1} = u v_0 v_1 \dots v_n$. The cone of a vertex $u$ with a simplicial complex $K$ is $u * K = \bigcup_{\sigma \in K} u * \sigma$, the union of the cone of $u$ with each simplex in $K$.

As a final definition in our quick introduction to simplicial complexes, we discuss the meaning of an *interior vertex* in a simplicial complex. We speak of an interior vertex in the context of an $n$-dimensional simplicial complex embedded in $\mathbb{R}^n$. In this context a vertex $v$ is an interior vertex if (the underlying space of) $\mathrm{Lk}\ v$ is homeomorphic to $S^{n-1}$, the sphere of dimension $n-1$. Thus the closed star of $v$ is homeomorphic to an $n$-dimensional ball in $\mathbb{R}^n$, and the point $v$ lies in the interior of the ball in the standard topology on $\mathbb{R}^n$.

## 4.2 Triangle Meshes in the Plane

The local combinatorial properties of an interior vertex $v$ of a 2-well-centered triangle mesh $M$ in $\mathbb{R}^2$ are easy to analyze. We know that the triangles incident to $v$ form a disk around $v$. Thus the sum of the angles incident to $v$ is $2\pi$. If there are 4 or fewer triangles incident to $v$, then for any embedding in the plane some angle incident to $v$ measures $\pi/2$ or larger, and the neighborhood of $v$ is not 2-well-centered. On the other hand, if there are $m \geq 5$ triangles incident to $v$, then placing $v$ at the center of a regular $m$-gon creates a neighborhood for $v$ consisting of $m$ congruent acute isosceles triangles. Thus there are no combinatorial barriers to embedding $M$ such that all triangles incident to $v$ are 2-well-centered. To say it another way, if $M$ is a 2-well-centered triangle mesh embedded in $\mathbb{R}^2$, then every interior vertex of $M$ has at least 5 neighbors, and for any $m \geq 5$ there exists a 2-well-centered triangle mesh $M$ in $\mathbb{R}^2$ containing an interior vertex with exactly $m$ neighbors.

Another way to think about this condition is to talk about the link of an interior vertex $v$. For a triangle mesh in $\mathbb{R}^2$, the link of an interior vertex $v$ is a triangulation isomorphic to $S^1$. As a graph, then, the link of $v$ is a cycle $C_m$, where $m$ is the number of triangles incident to $v$. If $M$ is a 2-well-centered triangle mesh in the plane, then for every interior vertex $v$, Lk $v$ is a copy of $C_m$ for some $m \geq 5$. We will see later in this chapter that it is useful to talk about the local combinatorial properties of well-centered meshes in terms of the link of an interior vertex. We will also see that cycles $C_m$ for $m \geq 5$ are important in defining global combinatorial properties for 2-well-centered triangle meshes in the plane.

For a 2-well-centered triangle mesh $M$ in $\mathbb{R}^2$ we can also say something about a vertex $v$ on the boundary of the mesh. If $M$ is embedded such that the sum of angles at $v$ is $\geq (k-1)\pi/2$, then at least $k$ triangles and at least $k+1$ edges are incident to $v$. In particular, suppose we are embedding $M$ conforming to a fixed geometric boundary, and consider a fixed vertex $v$ on the boundary. In this case we know the sum of angles at $v$, and if there are $k$ or more triangles incident to $v$, then there are no combinatorial barriers to obtaining a 2-well-centered neighborhood of $v$.

For both the interior vertex and the boundary vertex, the combinatorial restrictions on the neighborhood of a vertex boil down to the number of triangles incident to the vertex. If a vertex has enough neighbors, then the combinatorics allow a well-centered neighborhood. In this setting we say that a vertex that does not have enough neighbors is a *lonely vertex*. In Sec. 5.2 we give an algorithm that takes a triangle mesh with lonely vertices and produces a similar mesh without lonely vertices by making local modifications to the mesh connectivity, such as edge flips and limited vertex insertions.

For many of the triangle meshes encountered in practice, getting rid of lonely vertices with the algorithm of Sec. 5.2 is sufficient to create a mesh that can be embedded in $\mathbb{R}^2$ as a 2-well-centered mesh. There are, however, some triangle meshes that do not have a 2-well-centered embedding in $\mathbb{R}^2$ even though they satisfy all of the local combinatorial requirements.

To aid the discussion of these meshes, we introduce the concept of an enclosing cycle. By the Jordan curve theorem, a closed curve in $\mathbb{R}^2$ separates $\mathbb{R}^2$ into two parts, one bounded and one unbounded. When we speak of a triangle mesh in $\mathbb{R}^2$, we assume that the unbounded face is identified, so we can speak in a meaningful way about the part of the mesh bounded by a cycle. A cycle $C_m$ in a triangle mesh embeddable in the plane is said to be an *enclosing cycle* if the part of the mesh bounded by $C_m$ contains at least one vertex not on $C_m$ and the underlying space of the

part of the mesh bounded by $C_m$ is homeomorphic to a disk. Any vertex $v \notin C_m$ in the part of the mesh bounded by $C_m$ is *enclosed* by $C_m$. The easiest example of an enclosing cycle is the link of an interior vertex.

Edelsbrunner, Tan, and Waupotitsch observed in Lemma 2.1 of [23] that if $\sigma^1$ is an edge in a triangulation $M$ of a point set in $\mathbb{R}^2$, then the largest angle in $M$ is at least as large as the maximum over vertices $v$ not incident to $\sigma^1$ of the angle at $v$ in $v * \sigma^1$. (This is true even though $v * \sigma^1$ may not be a triangle of $M$.) We now adapt their lemma and its proof to a slightly more general context that is more appropriate to the subject of enclosing cycles.

**Lemma 4.2.1.** *Let $\sigma^1$ be an edge in a triangulation $M$ in $\mathbb{R}^2$ with the underlying space of $M$ homeomorphic to a disk. Then the largest angle in $M$ is at least as large as the maximum of the angle at $v$ in $v * \sigma^1$ where the maximum is taken over vertices $v$ such that the intersection of $v * \sigma^1$ with the underlying space of $M$ is homeomorphic to a disk.*

*Proof.* The proof is essentially the same as in [23]. We consider an edge $\sigma^1 \in M$ and a vertex $v$ not on $\sigma^1$ such that $v * \sigma^1$ intersects $M$ in a disk, and we choose $\sigma^1$ and $v$ to maximize the angle at $v$ in $v * \sigma^1$ among all such edge-vertex pairs. Then no vertex of $M$ lies inside $v * \sigma^1$.

If $v * \sigma^1$ is a triangle of $M$, we are done. Otherwise, since $v * \sigma^1$ intersects the underlying space of $M$ in a disk, there must be some edge $\tau^1 \in M$ that either crosses both of the (nonexistent) edges of $v * \sigma^1$ or crosses one of the edges of $v * \sigma^1$ and shares an endpoint with $\sigma^1$. If there is more than one possible choice for $\tau^1$, then we choose $\tau^1$ to maximize the angle at $v$ in $v * \tau^1$. It is clear that the angle at $v$ in $v * \tau^1$ is larger than the angle at $v$ in $v * \sigma^1$.

If $v * \tau^1$ intersects $M$ in a disk, then we have found a contradiction to the maximality of the angle at $v$ in $v * \sigma^1$, and we are done. On the other hand, if $v * \tau^1$ does not intersect $M$ in a disk, we can argue as follows. We know that there is a triangle $\rho^2 \in M$ with $\tau^1 \prec \rho^2$ such that $\rho^2$ is in the same closed halfspace as vertex $v$ with respect to $\mathrm{aff}(\tau^1)$. (This follows because the triangles of $M$ must cover the disk $M \cap v * \sigma^1$.) Let $u$ be the vertex of $\rho^2$ opposite $\tau^1$, so that $\rho^2 = u * \tau^1$. If $u$ is in $v * \tau^1$, then the angle at $u$ in $u * \tau^1 = \rho^2 \in M$ is larger than the angle at $v$ in $v * \sigma^1$, and we have a contradiction. If $u$ is outside $v * \tau^1$, then some edge $\omega^1 \prec \rho^2$ intersects a (nonexistent) edge of $v * \tau^1$, and the angle at $v$ in $v * \omega^1$ is larger than the angle at $v$ in $v * \tau^1$, contradicting the maximality of $\tau^1$. □

**Theorem 4.2.2.** *A triangle mesh $M$ in $\mathbb{R}^2$ that has an enclosing cycle $C_m$ of length $m < 5$ (i.e., $m = 3$ or $m = 4$) cannot be embedded in the plane as a 2-well-centered triangle mesh.*

*Proof.* Suppose towards contradiction that $M$ is embedded in $\mathbb{R}^2$ as a 2-well-centered mesh. We first consider the case that the vertices of $C_m$ are in convex position. Choose some vertex $v \notin C_m$ in the part of the mesh bounded by $C_m$. Label the edges of $C_m$ as $\tau_1^1, \ldots, \tau_m^1$. Since $m \leq 4$ we can assume without loss of generality that the angle at $v$ in triangle $v * \tau_1^1$ has measure $\geq \pi/2$. By Lemma 4.2.1, $M$ is not 2-well-centered.

If the vertices of $C_m$ are not in convex position, then $m = 4$ and the interior angle at some vertex $u$ on $C_m$ is greater than $\pi$. Thus for some $\tau_1^1$ not incident to $u$, the angle at $u$ in $u * \tau_1^1$ has measure $> \pi/2$, and the intersection of $u * \tau_1^1$ with the underlying space of $M$ is homeomorphic to a disk. Again Lemma 4.2.1 applies, and $M$ is not 2-well-centered. □

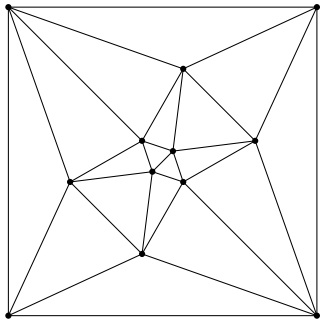

Figure 4.1: A triangle mesh that contains an enclosing cycle $C_m$ of length $m < 5$ cannot be embedded in the plane as a 2-well-centered mesh. This mesh has an enclosing cycle of length $m = 4$, and even though it has no lonely vertex, it cannot be embedded in the plane as a 2-well-centered mesh. Four of the triangles in this embedding are nonacute.

Clearly Theorem 4.2.2 includes in it the earlier statement about local combinatorial properties of 2-well-centered meshes in the plane, but it also captures combinatorial requirements on a global scale. For example, the mesh of a square in Fig. 4.1 satisfies all of the local combinatorial properties of a 2-well-centered mesh, but there is no way to embed it in $\mathbb{R}^2$ as a 2-well-centered mesh of some quadrilateral.

There are other ways to think about Theorem 4.2.2 and other ways to prove it. In particular, it is clear from Lemma 4.2.1 that a mesh with an enclosing cycle of length 5 must have a maximum angle of at least $2\pi/5$, at least if the vertices on the cycle are in convex position. It is possible to use some ideas about optimizing nonsmooth functions and some ideas from Springborn's thesis [59] to prove this in a different way and find some other combinatorial constraints that give a lower bound on the maximum angle in an embedding of a triangle mesh in $\mathbb{R}^2$. In all cases known to the author, though, these lower bounds are strictly less than $\pi/2$. Thus we ask the following question. If $M$ is a triangle mesh that is homeomorphic to a disk and has no enclosing cycle of length less than 5, does this imply that $M$ can be embedded in $\mathbb{R}^2$ as a 2-well-centered mesh?

## 4.3 3-Well-Centered Tetrahedral Meshes in Space

The combinatorial properties of tetrahedral meshes in $\mathbb{R}^3$ are more complex than the analogous properties for triangle meshes in $\mathbb{R}^2$. We have already seen that in a triangle mesh in $\mathbb{R}^2$, the link of an interior vertex is a set of edges that form a cycle $C_m$ around the vertex, i.e., a triangulation of a topological circle ($S^1$). The number of edges incident to the interior vertex, which is the number $m$ of vertices on the cycle, completely characterizes the neighborhood of the vertex. In tetrahedral meshes in $\mathbb{R}^3$, on the other hand, the link of an interior vertex is a triangulation of a topological sphere $S^2$. Thus the number of edges incident to the vertex does not completely characterize the neighborhood of the vertex.

In this section we will prove a lower bound on the number of edges that must be incident to an interior vertex in a 3-well-centered tetrahedral mesh in $\mathbb{R}^3$. We will also show that for any $m \geq 4$ there is a triangulation of $S^2$ with $m$ vertices that cannot appear as the link of a vertex in a 3-well-centered tetrahedral mesh in $\mathbb{R}^3$. Thus it is not possible to use the number of edges incident

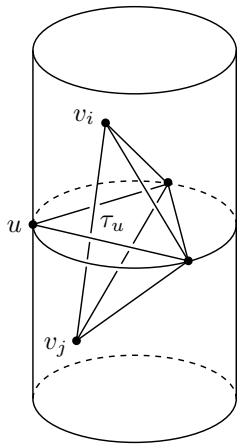


Figure 4.2: If vertices $v_i$ and $v_j$ are both contained in the interior of the solid right spherical cylinder over the circumcircle of $\tau_u$, then $u$ lies outside the simplex formed from $v_i$, $v_j$, and the vertices of $\tau_u$ other than $u$ itself.

to an interior vertex to express a sufficient local combinatorial condition for the neighborhood of an interior vertex in a 3-well-centered mesh in $\mathbb{R}^3$. We do develop some alternative sufficient conditions.

In graph theory the term *planar triangulation* refers to a triangulation that can be embedded cellularly on $S^2$. Such a graph can also be embedded cellularly in the plane. In order to prevent possible confusion with triangle meshes embedded in the plane, we try to avoid these terms when we refer to the link of a vertex in a tetrahedral mesh in $\mathbb{R}^3$. Instead, we stick with the terminology a *triangulation of* $S^2$. Many of the results in this section and the next apply specifically to tetrahedral meshes in $\mathbb{R}^3$ and are stated in terms of triangulations of $S^2$.

We begin, however, with some results that apply to $n$-simplicial meshes embedded in $\mathbb{R}^n$. The first is a lemma that generalizes the following statement about triangle meshes, using the Cylinder Condition (Proposition 3.2.1) to relate geometry to combinatorics. If a planar triangle $\sigma^2 = v_0v_1v_2$ is subdivided into three triangles by adding a vertex $u$ interior to $\sigma^2$, adding edges $uv_0$, $uv_1$, and $uv_2$ to obtain $u * \mathrm{Bd}(\sigma^2)$, then at most one of the three triangles $uv_0v_1$, $uv_0v_2$, and $uv_1v_2$ in $u * \mathrm{Bd}(\sigma^2)$ is an acute triangle. The main idea of the proof of Lemma 4.3.1 is illustrated by Fig. 4.2.

**Lemma 4.3.1.** *For $n \geq 2$, let $\sigma^n = v_0v_1 \dots v_n$ have facets $\tau_0^{n-1}, \tau_1^{n-1}, \dots, \tau_n^{n-1}$, with vertex $v_i$ opposite facet $\tau_i^{n-1}$. If $u$ is a point lying in $\sigma^n$, then at most one of the $n$-simplices of $u * \mathrm{Bd}(\sigma^n)$, i.e., at most one of the simplices $u * \tau_0^{n-1}, u * \tau_1^{n-1}, \dots, u * \tau_n^{n-1}$, is an $n$-well-centered $n$-simplex.*

*Proof.* For the statement we consider $u$ to be a point lying in $\sigma^n$, including the possibility that $u \in \mathrm{Bd}(\sigma^n)$. It suffices, however, to prove the statement for $u \in \mathrm{Int}(\sigma^n)$. Indeed, if $u$ is on the boundary of $\sigma^n$ and two or more of the simplices $u * \tau_i^{n-1}$ are $n$-well-centered, then we can slightly perturb $u$ into the interior and obtain a point $u \in \mathrm{Int}(\sigma^n)$ with at least two $n$-well-centered $n$-simplices. Thus we assume that $u$ is a point in the interior of $\sigma^n$.

Let $\tau_i^{n-1}$ and $\tau_j^{n-1}$ be distinct facets of $\sigma^n$. Then $u * \tau_i^{n-1}$ and $u * \tau_j^{n-1}$ are $n$-simplices, and $\tau_i^{n-1} \cap \tau_j^{n-1}$ is an $(n-2)$-dimensional face of $\sigma^n$. The face $\tau_i^{n-1} \cap \tau_j^{n-1}$ is incident to all but two of the vertices of $\sigma^n$, the two vertices $v_i$ and $v_j$. Notice that $u * \tau_i^{n-1}$ and $u * \tau_j^{n-1}$ have a common facet, the $(n-1)$-simplex $u * (\tau_i^{n-1} \cap \tau_j^{n-1})$, which we name $\tau_u^{n-1}$. We let $T \subset \mathrm{aff}(\sigma^n)$ be the solid right spherical cylinder over the circumball of $\tau_u^{n-1}$.

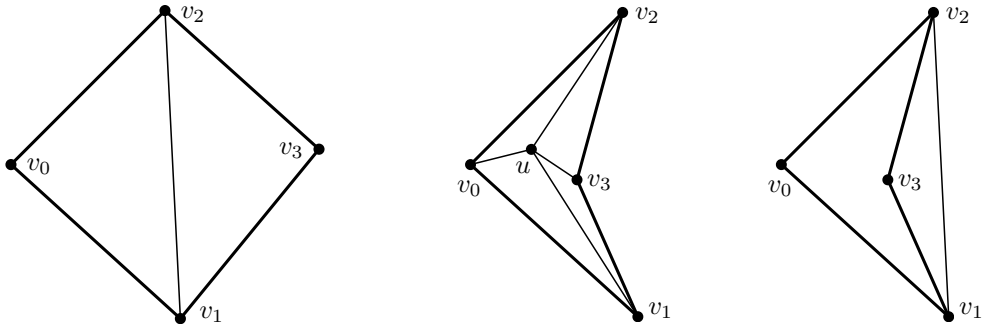


Abstract Complex $K$, $\mathrm{Bd}(K) = L$ | Embedding of $M = u * L$ | Induced Geometric Realization of $K$

Figure 4.3: In $\mathbb{R}^2$ the simplicial complex $K$ consisting of two triangles $v_0v_1v_2$ and $v_1v_3v_2$ and their faces (left) satisfies the hypothesis of Theorem 4.3.2 for the mesh $M = u*L$ embedded in $\mathbb{R}^2$ (center), so $M$ is not 2-well-centered. The embedding of $M$ in $\mathbb{R}^2$ induces a geometric realization of $K$ into $\mathbb{R}^2$ (right). The geometric realization of $K$ is not an embedding in this case, since $v_1v_3v_2$ is inverted here. The particular embedding of $M$ does not affect the existence of the abstract complex $K$ in Theorem 4.3.2; there is no embedding of $M$ that is 2-well-centered.

Assume towards contradiction that $u * \tau_i^{n-1}$ and $u * \tau_j^{n-1}$ are both $n$-well-centered. By the Cylinder Condition, both $v_i$ and $v_j$ lie in the interior of $T$. Now $T$ is a convex set, and all the vertices of $\sigma^n$ lie in $T$, so $\sigma^n \subset T$. On the other hand, $u$ lies on the circumsphere of $\tau_u^{n-1}$, so $u$ lies on the boundary of $T$. Thus $u \notin \mathrm{Int}(\sigma^n)$, since $\mathrm{Int}(\sigma^n)$ is a subset of the interior of $T$. But this contradicts the assumption that $u \in \mathrm{Int}(\sigma^n)$, which we made in the first paragraph of the proof. We conclude that at most one of $u * \tau_i^{n-1}$, $u * \tau_j^{n-1}$ is $n$-well-centered. □

The next theorem applies Lemma 4.3.1 in the context of simplicial complexes. Recall that the geometric realization of an abstract simplicial complex designates any assignment of coordinates to the vertices of the abstract simplicial complex, and a geometric realization might not be an embedding (or even an immersion).

**Theorem 4.3.2.** *Let $u$ be an interior vertex of an $n$-dimensional simplicial complex $M$ (e.g., a mesh) embedded in $\mathbb{R}^n$, and set $L = \mathrm{Lk}\ u$. If there exists an abstract finite $n$-dimensional simplicial complex $K$ such that*

*(i) $K$ is an $n$-manifold complex (with boundary)*

*(ii) $\mathrm{Bd}(K)$ is isomorphic to $L$, and*

*(iii) for every $n$-simplex $\sigma^n \in K$, there are at least two $(n-1)$-simplices in $\mathrm{Bd}(\sigma^n) \cap L$,*

*then $u * L$ is not $n$-well-centered.*

*Proof.* We first observe that every vertex of $K$ must also be a vertex of $L$. By assumption (i), every simplex of $K$ is a face of some $n$-simplex of $K$, so if $K$ had a vertex $v$ not in $L$, then there would be some $n$-dimensional simplex $\sigma^n \in K$ incident to $v$, and $\sigma^n$ would have only one $(n-1)$-dimensional face not incident to $v$. Since $v \notin L$, it follows that $\mathrm{Bd}(\sigma^n) \cap L$ would contain at most one $(n-1)$-simplex, and (iii) would not be satisfied.

The embedding of $M$ in $\mathbb{R}^n$ includes an embedding of $u * L$ in $\mathbb{R}^n$. Since every vertex of $K$ is a vertex of $L$, this embedding of $u * L$ in $\mathbb{R}^n$ induces a geometric realization of $K$ into $\mathbb{R}^n$. (As shown in Fig. 4.3, the geometric realization might not be an embedding.)

We have an embedding of the simplicial complex $u * L$ in $\mathbb{R}^n$. Since it is an embedding, each $n$-dimensional simplex is a fully $n$-dimensional geometric object, and we have consistent orientation. Moreover, $L$ is star-shaped with respect to $u$. We claim that by (i) and (ii) this implies that there is some simplex in the induced geometric realization of $K$ that contains the point $u$ (possibly on its boundary). We return to this claim in a moment, but first we show how this completes the proof.

Fix a simplex $\sigma^n \in K$ that contains $u$. Now consider the $n$-simplices of $u * \mathrm{Bd}(\sigma^n)$. By assumption (iii) of the hypothesis, at least two of these simplices have a facet in $L$. Each simplex of $u * \mathrm{Bd}(\sigma^n)$ with a facet in $L$ is a member of $u * L$, and by Lemma 4.3.1 at most one of these simplices is $n$-well-centered. We conclude that at least one of the simplices of $u * L \subseteq M$ is not $n$-well-centered.

Now we prove the claim that there is a simplex of the geometric realization of $K$ that contains the point $u$. Choose a line $\ell$ through $u$ in general position. General position here means that $\ell$ does not intersect any face of $K$ of dimension less than $n-1$. Such an $\ell$ can be chosen unless $u$ itself lies on a simplex $\rho^k$ of $K$ of dimension $k < n-1$, and in that case we are done, since there is some $\sigma^n \succ \rho^k$ that contains $u$.

Since $u * L$ is a simplicial complex and $L$ is star-shaped with respect to $u$, $\ell$ intersects exactly two simplices of $L$, each of dimension $n-1$, and the intersection points are in opposite directions from $u$ along $\ell$. For reference, we designate a $+$ and a $-$ direction and name facet $\tau_+^{n-1}$ (resp. $\tau_-^{n-1}$) as the facet of $L$ intersected by $\ell$ in the $+$ ($-$) direction from $u$. Starting from $\tau_+^{n-1}$ we describe a walk along $\ell$ through $n$-simplices and $(n-1)$-simplices of the geometric realization of $K$ that ends at $\tau_-^{n-1}$. By continuity of this walk and $\tau_+^{n-1}$, $\tau_-^{n-1}$ in opposite directions from $u$, there must be some $n$-simplex in the geometric realization of $K$ that contains $u$.

The walk is as follows. Since $K$ is a manifold with a boundary and $\tau_+^{n-1}$ is on the boundary, there is a unique $\sigma_1^n$ incident to $\tau_0^{n-1} := \tau_+^{n-1}$. Then for a given $\sigma_i^n$ the walk is on $\ell$ at $\tau_{i-1}^{n-1}$, and $\ell$ intersects some unique second facet of $\sigma_i^n$, which we name $\tau_i^{n-1}$. As long as $\tau_i^{n-1} \neq \tau_-^{n-1}$, we are not on the boundary of $K$, so (since $K$ is manifold) there are exactly two $n$-dimensional simplices incident to $\tau_i^{n-1}$. One of these is $\sigma_i^n$, and the other we name $\sigma_{i+1}^n$. Since $K$ is a manifold complex, the sequence $\tau_i^{n-1}$ has no repetitions and must eventually end at $\tau_-^{n-1}$. (The $\sigma_i^n$ in the sequence may flip back and forth in orientation, which corresponds to the walk going back and forth along $\ell$.) □

It is worth noting that the existence of the abstract simplicial complex $K$ has no dependence on the particular embedding of $M$ in $\mathbb{R}^n$. Theorem 4.3.2 is really a combinatorial statement, and we can use it to show that a particular *abstract* simplicial complex $L = \mathrm{Bd}(K)$ cannot appear as the link of an interior vertex in an $n$-well-centered mesh embedded in $\mathbb{R}^n$.

The case $n = 3$ is of particular interest. Using the One-Ring Necessary Condition of Theorem 4.3.2 it is fairly easy to establish a tight lower bound on the number of edges incident to a vertex in a 3-well-centered tetrahedral mesh embedded in $\mathbb{R}^3$.

**Corollary 4.3.3.** *Let $M$ be a 3-well-centered tetrahedral mesh embedded in $\mathbb{R}^3$. For every interior vertex $u$ of $M$, at least 7 edges of $M$ are incident to $u$.*

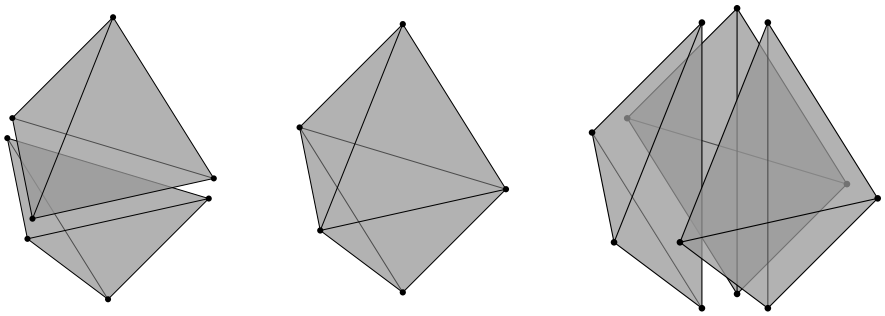

Figure 4.4: There is only one triangulation of $S^2$ with 5 vertices, and it has two corresponding tetrahedral complexes such that each tetrahedron has at least two facets in common with the triangulation.

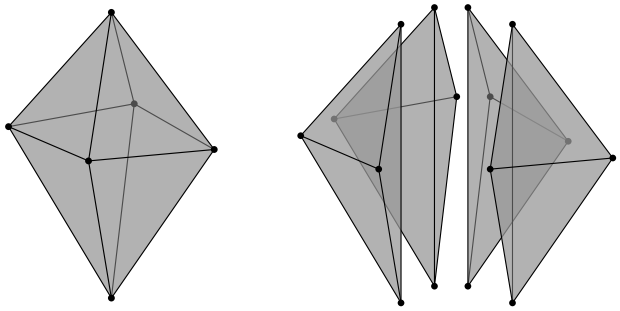

Figure 4.5: For one of the triangulations of $S^2$ with 6 vertices, each vertex has exactly four neighbors. There is a tetrahedral complex consisting of four tetrahedra such that each tetrahedron has two facets in common with this triangulation of $S^2$.

*Proof.* Britton and Dunitz have assembled a catalog of all polyhedra with at most 8 vertices, which includes all the triangulations of $S^2$ with at most 8 vertices [14]. By Theorem 4.3.2 it suffices to show that each such triangulation $L$ of $S^2$ with at most 6 vertices has a corresponding manifold tetrahedral complex $K$ such that $\mathrm{Bd}(K)$ is isomorphic to $L$ and each tetrahedron of $K$ has at least two facets in common with $L$.

There is only one triangulation of $S^2$ with 4 vertices—the boundary of a tetrahedron. The corresponding tetrahedral complex is that single tetrahedron.

There is also only one triangulation of $S^2$ with 5 vertices. This triangulation is shown in Fig. 4.4 along with two corresponding tetrahedral complexes. Either complex certifies that the triangulation cannot be the link of any vertex in a 3-well-centered mesh.

For six vertices there are two nonisomorphic triangulations of $S^2$. The first is shown in Fig. 4.5 along with its corresponding tetrahedral complex. The second is drawn in Fig. 4.6 along with its corresponding tetrahedral complex. □

When there are $m \geq 7$ vertices, there exist triangulations $L$ of $S^2$ with $m$ vertices such that there is no tetrahedral complex $K$ satisfying the conditions specified in Theorem 4.3.2. In particular, the triangulations of $S^2$ with 7 vertices and degree lists $(5, 5, 5, 4, 4, 4, 3)$ and $(6, 5, 5, 5, 3, 3, 3)$, i.e., polyhedra 7–1 and 7–4 in the catalog of Britton and Dunitz, both can appear as the link of a vertex in a 3-well-centered mesh. Figure 4.7 shows an example of a 3-well-centered mesh in $\mathbb{R}^3$ consisting of a single vertex $u$ and its neighborhood $\mathrm{Cl}(\mathrm{St}\ u)$ such that $\mathrm{Lk}\ u$ is a triangulation with

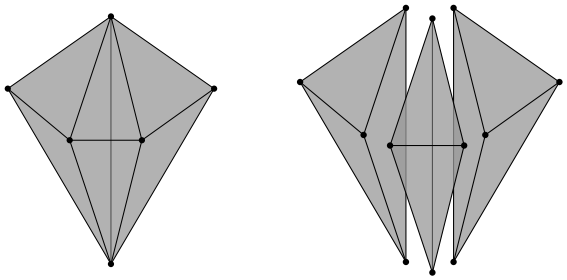

Figure 4.6: In the other triangulation of $S^2$ with 6 vertices, the degree list is $(5, 5, 4, 4, 3, 3)$. This triangulation of $S^2$ also has a corresponding tetrahedral complex such that each tetrahedron has at least two facets in common with the triangulation.

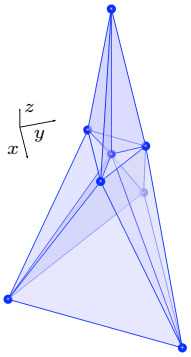


| $x$ | $y$ | $z$ |
|---|---|---|
| 0 | 0 | 0 |
| 0 | 0 | 1 |
| −0.1041 | −0.0601 | 0.0117 |
| 0.1041 | −0.0601 | 0.0117 |
| 0 | 0.1202 | 0.0117 |
| 0 | −0.3622 | −0.8656 |
| 0.3137 | 0.1811 | −0.8656 |
| −0.3137 | 0.1811 | −0.8656 |

Figure 4.7: A 3-well-centered mesh with an interior vertex $u$ such that Lk $u$ has seven vertices and degree list $(5, 5, 5, 4, 4, 4, 3)$. The vertex coordinates are listed in the table at right; vertex $u$ is at the origin.

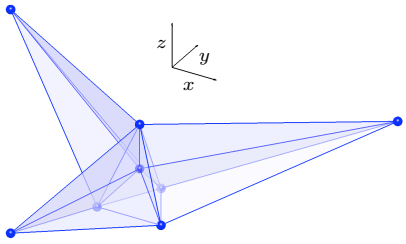


| $x$ | $y$ | $z$ |
|---|---|---|
| 0 | 0 | 0 |
| 0 | 0 | 1 |
| 0 | 0.8334 | −0.8588 |
| −0.7217 | −0.4167 | −0.8588 |
| 0.7217 | −0.4167 | −0.8588 |
| 0 | −5.0494 | 1.0696 |
| 4.3729 | 2.5247 | 1.0696 |
| −4.3729 | 2.5247 | 1.0696 |

Figure 4.8: A 3-well-centered mesh with an interior vertex $u$ such that Lk $u$ has seven vertices and degree list $(6, 5, 5, 5, 3, 3, 3)$. The vertex coordinates are listed in the table at right; vertex $u$ is at the origin.

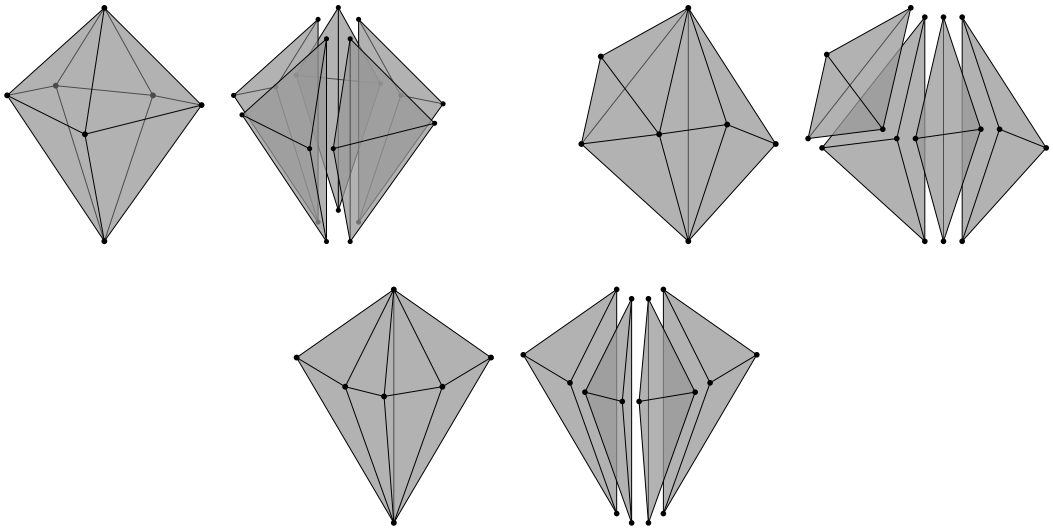

Figure 4.9: There are five triangulations of $S^2$ with seven vertices. Two of these can appear as the link of a vertex in a 3-well-centered mesh, as demonstrated in Fig. 4.7 and Fig. 4.8. The other three cannot appear as the link of a vertex in a 3-well-centered mesh. They are each shown here along with a tetrahedral complex $K$ that certifies this (by Theorem 4.3.2). These triangulations of $S^2$ are polyhedra 7–5 (top left), 7–3 (top right), and 7–2 (bottom center) from the catalog of Britton and Dunitz [14].

degree list $(5, 5, 5, 4, 4, 4, 3)$. Figure 4.8 shows a similar example for the degree list $(6, 5, 5, 5, 3, 3, 3)$. There are three other triangulations of $S^2$ with 7 vertices. As shown in Fig. 4.9, each of these three triangulations of $S^2$ has a corresponding tetrahedral complex $K$ satisfying the requirements of Theorem 4.3.2, so none of these can appear as the link of a vertex in a 3-well-centered mesh.

There are 14 nonisomorphic triangulations of $S^2$ with 8 vertices. Of these, 5 have tetrahedral complexes $K$ that certify they cannot be the link of a vertex in a 3-well-centered tetrahedral mesh in $\mathbb{R}^3$. Figure 4.10 shows these five triangulations of $S^2$, which are polyhedra 8–4, 8–5, 8–6, 8–7, and 8–13 in the catalog of Britton and Dunitz, along with tetrahedral complexes certifying that they cannot appear as the link of an interior vertex in a 3-well-centered mesh. Each of the other 9 triangulations of $S^2$ with 8 vertices can appear as the link of a vertex in a 3-well-centered tetrahedral mesh in $\mathbb{R}^3$. (Meshes that establish this claim appear in Chapter 8.) For $m \leq 8$ vertices, then, Theorem 4.3.2 completely characterizes which triangulations of $S^2$ can and cannot appear in a 3-well-centered embedded in $\mathbb{R}^3$. In fact, as we discuss later in this section, we have shown that the theorem is also a characterization for $m = 9$.

It is interesting to note that the degree list of polyhedron 8–7 from the catalog of Britton and Dunitz, which cannot be the link of an interior vertex in a 3-well-centered mesh in $\mathbb{R}^3$, is the same as the degree list of polyhedron 8–8 from their catalog, which can be the link of a an interior vertex in a 3-well-centered mesh. (See Fig. 8.14 on page 107.) *Thus the degree list of a triangulation does not provide enough information to determine whether the triangulation can be the link of a vertex in a* 3*-well-centered tetrahedral mesh in* $\mathbb{R}^3$. There are 50 nonisomorphic triangulations of $S^2$ with 9 vertices, 233 nonisomorphic triangulations of $S^2$ with 10 vertices, and an exponentially growing number of triangulations of $S^2$ with more vertices [42], so although attempting a direct construction of a 3-well-centered mesh for each triangulation of $S^2$ with 9 or 10 vertices is possible,

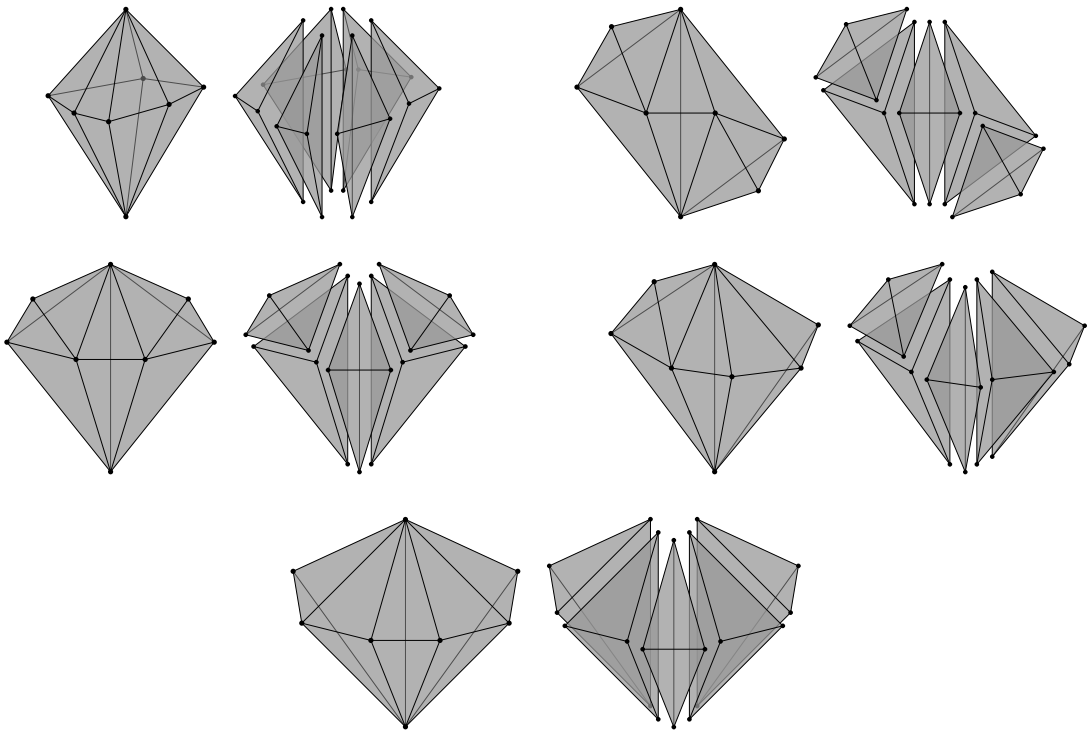

Figure 4.10: There are fourteen triangulations of $S^2$ with eight vertices. Of these, five cannot appear as the link of a vertex in a 3-well-centered mesh. Each of these five is shown here along with a tetrahedral complex $K$ that certifies it cannot be the link of an interior vertex in a 3-well-centered mesh. These triangulations are polyhedra 8–13 (top left), 8–7 (top right), 8–6 (middle left), 8–5 (middle right), and 8–4 (bottom center) from the catalog of Britton and Dunitz.

something more abstract will be needed to definitively characterize which triangulations can be made 3-well-centered.

In the rest of this section we discuss some results that move in the direction of characterizing which triangulations of $S^2$ can appear as the link of a vertex in a 3-well-centered mesh in $\mathbb{R}^3$. The results fall short of a complete characterization, but do show that the set of triangulations of $S^2$ that cannot appear as the link of a vertex in a 3-well-centered mesh and the set of triangulations that can appear as the link of a vertex are both infinite sets.

**Corollary 4.3.4.** *For any integer $m \geq 4$ there is a triangulation of $S^2$ with $m$ vertices that cannot appear as the link of a vertex in a 3-well-centered tetrahedral mesh in $\mathbb{R}^3$.*

*Proof.* We have already proved that this holds for $4 \leq m \leq 8$.

For $m \geq 9$ we note that the tetrahedral complexes shown on the right hand sides of Figs. 4.4 and 4.5 and on the top left in Fig. 4.9 and in Fig. 4.10 belong to an infinite family. Consider a tetrahedral complex $K$ consisting of a set of $m-2$ tetrahedra that close around a common edge. The complex $K$ satisfies the conditions of Theorem 4.3.2, so $\mathrm{Bd}(K)$ cannot appear as the link of a vertex in a 3-well-centered mesh. $\mathrm{Bd}(K)$ is a triangulation of $S^2$ on $m$ vertices with degree list $(m-2, m-2, 4, \ldots, 4)$. □

By deleting a single tetrahedron from the complex $K$ described in the proof of Corollary 4.3.4, we obtain another infinite family of triangulations of $S^2$ that cannot appear as the link of a vertex in a 3-well-centered tetrahedral mesh in $\mathbb{R}^3$. Each member of this family is a triangulation on $m$ vertices with degree list $(m-1, m-1, 4, \ldots, 4, 3, 3)$. This family generalizes the tetrahedral complexes shown on the left hand side of Fig. 4.4, the right hand side of Fig. 4.6, the bottom center of Fig. 4.9, and the bottom center of Fig. 4.10. It can be shown that the triangulations of $S^2$ with degree lists $(m-2, m-2, 4, \ldots, 4)$ and $(m-1, m-1, 4, \ldots, 4, 3, 3)$ are unique.

The family of triangulations of $S^2$ described in the proof of Corollary 4.3.4 is a special case among triangulations that cannot be the link of a vertex in a 3-well-centered mesh in $\mathbb{R}^3$, because every member of the family has minimum vertex degree 4. In all of the other examples we have seen for $m \geq 5$, the triangulation of $S^2$ has exactly two vertices of degree 3, and in the complex $K$ these two vertices are each a vertex of a tetrahedron $\sigma^n$ with three facets in $\sigma^n \cap L$. By gluing another tetrahedron onto one of the three facets of one of these tetrahedra, we obtain a new tetrahedral complex $K$ that has the same property. Thus $L = \mathrm{Bd}(K)$ has exactly two vertices of degree 3 and cannot be the link of an interior vertex in a 3-well-centered mesh in $\mathbb{R}^3$. We conjecture that every tetrahedral complex $K$ satisfying the conditions of Theorem 4.3.2 is either from the family described in the proof of Corollary 4.3.4 or can be constructed by successively gluing tetrahedra onto the boundary of a smaller complex as described, starting from a single tetrahedron. (Indeed, it should be relatively straightforward to prove this, but we omit the details of a proof.)

For the triangulations of $S^2$ with $m = 9$ vertices, these constructions of tetrahedral complexes satisfying Theorem 4.3.2 produces 11 nonisomorphic triangulations that cannot appear as the link of a vertex in a 3-well-centered mesh in $\mathbb{R}^3$. This leaves 39 triangulations of $S^2$ on 9 vertices that may or may not appear as the link of a vertex in a 3-well-centered mesh.

Corollary 4.3.4 shows that there is a substantial difference between 2-well-centered meshes in $\mathbb{R}^2$ and 3-well-centered meshes in $\mathbb{R}^3$. In the case of triangle meshes in $\mathbb{R}^2$, where we consider

triangulations of $S^1$ as the link of a vertex, the only two triangulations that cannot appear as the link of a vertex are the 3-cycle and the 4-cycle. In contrast, there are infinitely many triangulations of $S^2$ that cannot be the link of a vertex in a 3-well-centered mesh in $\mathbb{R}^3$. We claimed earlier that there are also infinitely many triangulations of $S^2$ that can appear as the link of a vertex in a 3-well-centered mesh in $\mathbb{R}^3$. One way to prove this is to explicitly construct an infinite family of 3-well-centered meshes with different vertex links. We will do exactly that in a moment, with the help of the following lemma, which we prove using the Prism Condition (Proposition 3.2.2).

**Lemma 4.3.5.** *Let $S_0^{n-1}$ be a unit $(n-1)$-sphere centered at a point $u$. If $\tau^{n-1}$ is an $(n-1)$-well-centered $(n-1)$-simplex whose vertices lie on $S^{n-1}$, and the distance from $u$ to $\mathrm{aff}(\tau^{n-1})$ is greater than $1/\sqrt{2}$, then $\sigma^n := u * \tau^{n-1}$ is an $n$-well-centered $n$-simplex.*

*Proof.* Suppose that $\tau^{n-1}$ is an $(n-1)$-well-centered simplex meeting the conditions specified in the hypothesis. Let $S_0^{n-2}$ be the circumsphere of $\tau^{n-1}$. $S_0^{n-2}$ is the intersection of $\mathrm{aff}(\tau^{n-1})$ with $S_0^{n-1}$, i.e., an $(n-2)$-sphere lying in $S_0^{n-1}$. The orthogonal projection of $u$ into $\mathrm{aff}(\tau^{n-1})$, which we denote by $P(u)$, is the center of $S_0^{n-2}$, i.e., the circumcenter $c(\tau^{n-1})$ of $\tau^{n-1}$.

Since $\tau^{n-1}$ is $(n-1)$-well-centered, it contains the point $c(\tau^{n-1})$. Thus $\tau^{n-1}$ contains the reflection of $P(u)$ through $c(\tau^{n-1})$. The circumradius of $\tau^{n-1}$ satisfies $R(\tau^{n-1})^2 + z^2 = 1$, where $z$ is the distance from $u$ to $\mathrm{aff}(\tau^{n-1})$, so because $z^2 > 1/2$, we have $R(\tau^{n-1}) < 1/\sqrt{2}$, and $u$ lies outside the equatorial ball of $\tau^{n-1}$. By the Prism Condition, $\sigma^n$ is $n$-well-centered. □

It is relatively straightforward to prove the converse as well. For $\sigma^n = u * \tau^{n-1}$ with the vertices of $\tau^{n-1}$ lying on a sphere $S_0^{n-1}$ centered at $u$, if $\tau^{n-1}$ is not $(n-1)$-well-centered or the distance $z$ from $u$ to $\mathrm{aff}(\tau^{n-1})$ satisfies $z \leq 1/\sqrt{2}$, then $\sigma^n$ is not $n$-well-centered. This proof is left to the reader; the result is not needed in this dissertation.

The simplex $\sigma^n = u * \tau^{n-1}$ in Lemma 4.3.5 is an *isosceles simplex* with all vertices of $\tau^{n-1}$ equidistant from the apex vertex $u$. When $n = 2$, Lemma 4.3.5 reduces to the statement that an isosceles triangle is acute if the apex angle is acute. In higher dimensions Lemma 4.3.5 tells us when an isosceles simplex is $n$-well-centered. Note that in an isosceles simplex all of the faces incident to the apex vertex $u$ are isosceles; the plane of each such face intersects the sphere $S^{n-1}$ in some lower-dimensional sphere centered at $u$, and Lemma 4.3.5 can be applied to these isosceles faces. It follows that $\sigma^n$ will be completely well-centered if $\tau^{n-1}$ is completely well-centered and $z > 1/\sqrt{2}$. In particular, for the case $n = 3$, an isosceles tetrahedron with an acute triangle facet opposite the apex vertex is a completely well-centered tetrahedron.

Thus from any triangulation of a unit sphere $S^2$ with sufficiently small acute triangles we can create a completely well-centered tetrahedral mesh in $\mathbb{R}^3$ by taking the cone $u * \tau^2$ of each acute triangle $\tau^2$ with the center $u$ of the sphere $S^2$. Figure 4.11 shows a completely well-centered tetrahedral mesh constructed in this fashion. The boundary of the mesh in Fig. 4.11 is an acute triangulation of $S^2$ selected from an infinite family of acute triangulations of $S^2$. The next two paragraphs describe this family.

Consider the set of vertices consisting of the north pole $(0, 0, 1)$, the south pole $(0, 0, -1)$, and the vertices of two regular $k$-gons, one in the plane $z = 0.352$ and the other in the plane $z = -0.352$. We set the polygons exactly off phase from each other. For instance, let the coordinates of the polygon

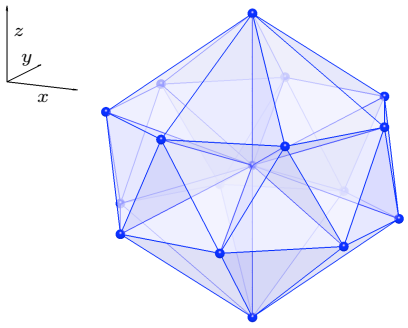


Figure 4.11: For $k \geq 4$ we can create an acute triangulation of the unit sphere from a set of vertices consisting of the north and south poles and two out-of-phase regular $k$-gons. Coning such a triangulation to the origin produces a completely well-centered tetrahedral mesh. The figure shows the tetrahedral mesh obtained for $k = 7$.

vertices be

$$(0.936\cos\left(\frac{2i\pi}{k}\right), 0.936\sin\left(\frac{2i\pi}{k}\right), 0.352), \quad i = 0, 1, \ldots, k-1\,,$$

$$(0.936\cos\left(\frac{(2i+1)\pi}{k}\right), 0.936\sin\left(\frac{(2i+1)\pi}{k}\right), -0.352), \quad i = 0, 1, \ldots, k-1\,.$$

Let each pole vertex be adjacent to all of the vertices of the closer regular polygon. This constructs $k$ isosceles triangles incident to each pole. We take each vertex of a regular polygon to be adjacent to the closer pole, the two neighbors on its own regular polygon, and two vertices from the other regular polygon. Because the regular polygons are exactly out of phase, triangles formed entirely from vertices of the two regular polygons are also isosceles. The example in Fig. 4.11 creates a completely well-centered tetrahedral mesh based on this construction for the case $k = 7$.

We claim that if $k \geq 4$, then each triangle $\tau^2$ of this construction is acute and satisfies the condition that the distance from the origin to $\tau^2$ is greater than $1/\sqrt{2}$. Since $k \geq 4$ it is clear that the apex angles of the isosceles triangles incident to the poles are acute angles. Verifying that the other triangles are acute and that the triangles are far enough from the origin is straightforward and we omit the details. Lemma 4.3.5 applies, and as an immediate consequence we have the following.

**Proposition 4.3.6.** *There are infinitely many triangulations of $S^2$ that can appear as the link of a vertex in a completely well-centered mesh.*

For large enough $k$, this construction of acute triangulations of a unit sphere $S^2$ can be generalized. One can use more than two regular $k$-gons, alternating the phase between each successive $k$-gon. For example, when $k \geq 5$, a construction with the pole vertices and the vertices of 3 alternating-phase regular polygons in the planes $z = -0.6$, $z = 0$, and $z = 0.6$ creates an acute triangulation of $S^2$. Similarly, for $k \geq 5$ one can use 4 regular polygons in the planes $z = -0.8432$, $z = -0.352$, $z = 0.352$, and $z = 0.8432$. For a construction alternating phases with 5 regular polygons, $k \geq 6$ suffices if the polygons are in the planes $z = -0.936$, $z = -0.5376$, $z = 0$, $z = 0.5376$, and $z = 0.936$. Figure 4.12 shows an example of a completely well-centered mesh creating using the generalized construction with 5 regular polygons.

The author suspects that for $m \geq 8$ vertices the majority of triangulations of $S^2$ on $m$ vertices are triangulations that can appear as a link of a vertex in a 3-well-centered mesh. We do not

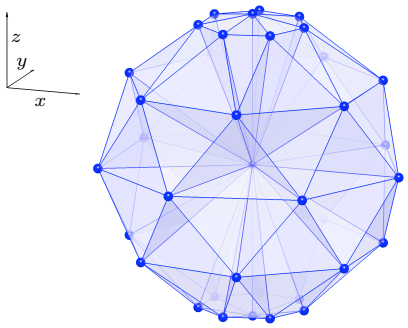


Figure 4.12: The construction of acute triangulations of a unit sphere $S^2$ that uses 2 out-of-phase regular polygons can be generalized to use a greater number of regular polygons, alternating phase between each polygon. This completely well-centered mesh was constructed using five regular 7-gons in the planes $z = \pm 0.936$, $z = \pm 0.5376$, and $z = 0$.

formally prove that conjecture here, but in light of the the next proposition, it is highly likely. The proposition provides a method for constructing a large family of triangulations that can appear as the link of a vertex in a 3-well-centered tetrahedral mesh in $\mathbb{R}^3$. In this proposition and throughout the dissertation, the notation $\measuredangle abc$ refers to the (smaller) angle at $b$ between rays $ba$ and $bc$.

**Proposition 4.3.7.** *Let $G$ be a triangulation of $S^2$ with face $v_2v_3v_4$, and let $\widetilde{G}$ be the triangulation obtained from $G$ by replacing the face $v_2v_3v_4$ with a new vertex $v_1$ and the three faces $v_1v_2v_3$, $v_1v_2v_4$, $v_1v_3v_4$. Let $M$ be an abstract tetrahedral mesh consisting of a single vertex $u$ together with its closed neighborhood* $\mathrm{Cl}(\mathrm{St}\ u)$ *such that* $\mathrm{Lk}\ u$ *is isomorphic to $G$, and let $\widetilde{M}$ be the analogous mesh with* $\mathrm{Lk}\ u$ *isomorphic to $\widetilde{G}$. If there exists an embedding of $M$ into $\mathbb{R}^3$ such that*

*(i) $M$ is 3-well-centered*

*(ii) face angle $\measuredangle uv_iv_j$ is acute for each $i, j \in \{2, 3, 4\}, i \neq j$ ,*

*then there exists an embedding of $\widetilde{M}$ into $\mathbb{R}^3$ satisfying*

*(i) $\widetilde{M}$ is 3-well-centered*

*(ii) face angle $\measuredangle uv_iv_j$ is acute for each $i, j \in \{1, 2, 3, 4\}, i \neq j$ .*

*Proof.* Figure 4.13 accompanies this proof and may help the reader visualize the geometric constructions discussed in the proof. Consider a particular tetrahedral mesh that satisfies the conditions of the hypothesis. In this mesh the tetrahedron $\sigma = \sigma^3 = uv_2v_3v_4$ is 3-well-centered, so $c(\sigma)$ is interior to $\sigma$.

Let $\ell$ be the line through $u$ and $c(\sigma)$. Line $\ell$ intersects the circumsphere of $\sigma$ at two points. One of these is $u$, and the other we name $u'$. We define

$$u'_\varepsilon = (1 - \varepsilon)u' + \varepsilon u\,,$$

a point lying on $\ell$. Because $\sigma$ is 3-well-centered, we know that segment $uu'$ intersects triangle $v_2v_3v_4$ at some point $u'_{\varepsilon_0}$, with $1/2 > \varepsilon_0 > 0$. We can cut $\sigma$ into the three tetrahedra $uv_2v_3u'_{\varepsilon_0}$, $uv_2v_4u'_{\varepsilon_0}$, and $uv_3v_4u'_{\varepsilon_0}$.

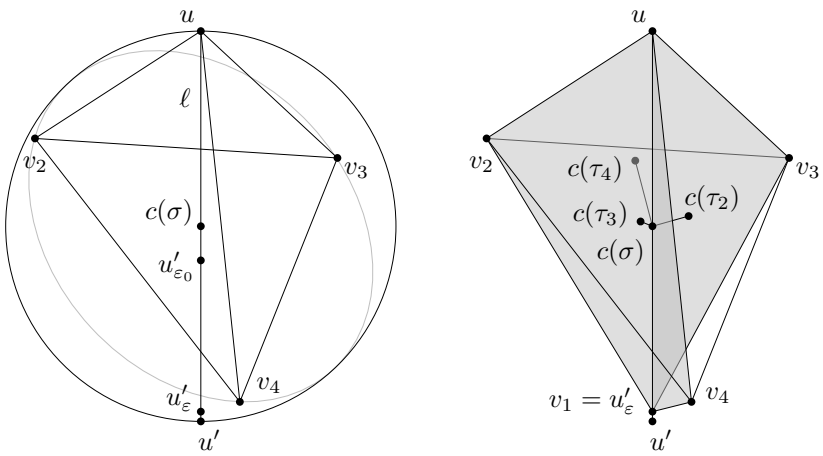


Figure 4.13: Given a 3-well-centered tetrahedron $\sigma = uv_2v_3v_4$ with acute angles $\measuredangle uv_iv_j$, one can construct three tetrahedra $uv_1v_2v_3$, $uv_1v_2v_4]$, and $uv_1v_3v_4$ by adding a new vertex $v_1 = u'_\varepsilon$ along the line $\ell$ through $u$ and $c(\sigma)$. The circumcenters of the constructed tetrahedra lie along lines connecting $c(\sigma)$ to the circumcenters $c(\tau_i)$ of the facets $uv_iv_j$ of $\sigma$. As discussed in Proposition 4.3.7, when $v_1$ is close enough to $u'$—the reflection of $u$ through $c(\sigma)$—the three constructed tetrahedra will be 3-well-centered and the angles $\measuredangle uv_1v_i$, $\measuredangle uv_iv_1$ will be acute. The angles $\measuredangle v_iuv_j$ do not need to be acute for this construction. For instance, $\measuredangle v_2uv_3$ is not an acute angle in this figure.

For $\varepsilon_0 > \varepsilon > 0$ we consider the three tetrahedra $uv_2v_3u'_\varepsilon$, $uv_2v_4u'_\varepsilon$, and $uv_3v_4u'_\varepsilon$. We claim that for sufficiently small $\varepsilon > 0$ these three tetrahedra are 3-well-centered and the face angles $\measuredangle uu'_\varepsilon v_i$, $\measuredangle uv_iu'_\varepsilon$ are acute for each $i = 2, 3, 4$.

Examining the face angles first, we note that at $\varepsilon = 0$ the circumcenters of the facets $uv_iu'_\varepsilon = uv_iu'$ coincide with $c(\sigma)$ and with each other. Indeed, each of these facets is a right triangle with its circumcenter lying on the hypotenuse $uu'_\varepsilon = uu'$. As $\varepsilon$ increases, $\measuredangle v_iuu'_\varepsilon$ does not change, $\measuredangle uv_iu'_\varepsilon$ decreases, becoming smaller than $\pi/2$, and $\measuredangle uu'_\varepsilon v_i$ increases but remains less than $\pi/2$ for sufficiently small $\varepsilon$.

Turning to the tetrahedra, then, we will argue that the specific tetrahedron $uv_2v_3u'_\varepsilon$ is 3-well-centered for sufficiently small $\varepsilon$. The same argument with changed vertex and facet labels applies to the other two tetrahedra, so this will complete the proof. We know that, regardless of the value of $\varepsilon$, the circumcenter of $uv_2v_3u'_\varepsilon$ lies on the line orthogonal to $\operatorname{aff}(uv_2v_3) = \operatorname{aff}(\tau_4)$ passing through $c(\tau_4)$; this line is the locus of points equidistant from $u$, $v_2$, and $v_3$. The precise location of $c(uv_2v_3u'_\varepsilon)$ varies continuously with $\varepsilon$. At $\varepsilon = 0$, $c(uv_2v_3u'_\varepsilon)$ coincides with $c(\sigma)$, and as $\varepsilon$ increases from 0 towards $\varepsilon_0$, $c(uv_2v_3u'_\varepsilon)$ moves in the direction of vector $c(\tau_4) - c(\sigma)$. Because $\measuredangle uv_2v_3$ and $\measuredangle uv_3v_2$ are acute, we know that $c(\tau_4)$ lies in the sector of $\operatorname{aff}(\tau_4)$ bounded by rays $uv_2$ and $uv_3$. Thus segment $c(\sigma)\,c(\tau_4) \cap \sigma$ is contained in tetrahedron $uv_2v_3u'_{\varepsilon_0}$, which is contained in the tetrahedron $uv_2v_3u'_\varepsilon$. We conclude that for sufficiently small $\varepsilon > 0$, tetrahedron $uv_2v_3u'_\varepsilon$ is 3-well-centered. □

Because the face angles $\measuredangle uv_1v_i$, $\measuredangle uv_iv_1$ are acute in the construction described in Proposition 4.3.7, the construction can be iterated. If a triangulation $G$ of $S^2$ satisfies the conditions of Proposition 4.3.7, then a degree 3 vertex $v_1$ can be inserted into face $v_2v_3v_4$. In the new triangulation of $S^2$, the three new faces incident to $v_1$ all satisfy the conditions of Proposition 4.3.7, so a degree 3 vertex can be inserted into any one of those three faces, and so on. In particular, starting from any

link of an interior vertex in a completely well-centered tetrahedral mesh in $\mathbb{R}^3$, one can successively insert vertices of degree 3 into any face to create a large family of triangulations that can appear as the link of a vertex in a 3-well-centered mesh. For example, each completely well-centered neighborhood constructed from an acute triangulation of a unit sphere $S^2$ is the basis of some infinite family of triangulations of $S^2$ that can appear as the link of a vertex in a 3-well-centered mesh in $\mathbb{R}^3$.

It is also worth mentioning that for each of the 9 triangulations of (topological) $S^2$ with 8 vertices $v_1, \ldots, v_8$ that can appear as Lk $u$ for a vertex $u$ in a 3-well-centered mesh $M$ in $\mathbb{R}^3$, there is an embedding of $M$ into $\mathbb{R}^3$ for which the neighborhood of $u$ is 3-well-centered and all of the face angles $\measuredangle uv_iv_j$ are acute in each face $uv_iv_j$. Using Proposition 4.3.7 to add vertices of degree 3 to the various faces of these triangulations, one can show that 34 of the 50 triangulations of $S^2$ with 9 vertices can appear as the link of a vertex in a 3-well-centered tetrahedral mesh embedded in $\mathbb{R}^3$. Recall that 11 of these 50 triangulations cannot be the link of a vertex in a 3-well-centered mesh. This leaves a mere 5 triangulations of $S^2$ with 9 vertices that are not classified, and we have empirically shown that these 5 triangulations of $S^2$ can also appear as the link of a vertex in a 3-well-centered mesh. (See Chapter 8.)

## 4.4 2-Well-Centered Tetrahedral Meshes in Space

Corollary 4.3.3 shows that in a 3-well-centered mesh there are at least 7 edges incident to each vertex. In the following discussion we will see that the combinatorial constraints for a mesh to be 2-well-centered are quite different from the constraints for a mesh to be 3-well-centered, and in terms of the minimum number of edges incident to a vertex, are more stringent. As in Sec. 4.3, the discussion focuses on Lk $u$ where $u$ is a vertex interior to a tetrahedral mesh in $\mathbb{R}^3$.

**Definition.** We say that a particular triangulation $G$ of $S^2$ *permits a 2-well-centered neighborhood* of a vertex $u$ if there exists a tetrahedral mesh $M$ in $\mathbb{R}^3$ such that $u$ is an interior vertex of $M$, Lk $u$ is isomorphic to $G$ (as a simplicial complex), and all facets of $M$ incident to $u$ are 2-well-centered.

It should be noted that this definition does not directly address the question of whether the tetrahedra incident to $u$ are 2-well-centered tetrahedra, since each tetrahedron incident to $u$ has one facet lying on Lk $u$, and that facet is not incident to $u$. We shall see, however, that for tetrahedral meshes in $\mathbb{R}^3$, the smallest triangulation that permits a 2-well-centered neighborhood in the sense of this definition can, in fact, appear as the link of a vertex in a completely well-centered mesh. Finally, note that phrasing the problem in terms of the facets of $M$ incident to $u$ actually reduces the problem to determining whether the face angles at $u$ are acute, because if there is an arrangement of rays at $u$ such that all of the face angles formed at $u$ by these rays are acute, and all the tetrahedra are properly oriented, then we can place the neighbors of $u$ at the points where these rays intersect a unit sphere centered at $u$. This will create a neighborhood of $u$ in which every 2-dimensional face incident to $u$ is an isosceles triangle with an acute apex angle at $u$.

The first result of this section is a simple observation that forms the foundation for the theory developed in the rest of the section.

**Lemma 4.4.1.** *Let $u$ and $v_1$ be adjacent vertices in a tetrahedral mesh $M$ in $\mathbb{R}^3$ and let $v_i$ be a vertex of* Lk $u$ *that is adjacent to $v_1$. The angle $\measuredangle v_1uv_i$ is acute if and only if $v_i \in H_1$, where $H_1$ is*

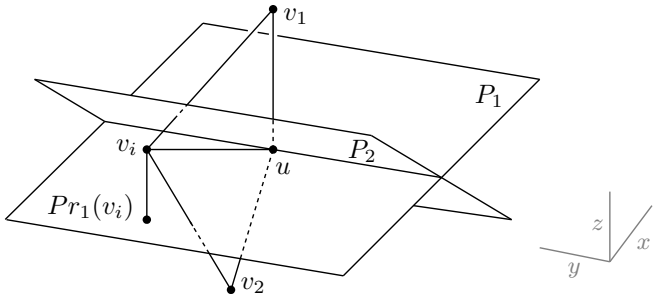


Figure 4.14: If a 2-well-centered mesh contains two vertices $v_1$ and $v_2$ that both lie in Lk $u$, are not adjacent to each other, and have a common neighbor $v_i$ and if $v_2$ lies in $H_1'$, then the orthogonal projection of $v_i$ into $P_1$, i.e., the point $Pr_1(v_i)$, must lie in $P_1 \cap H_2$.

*the open halfspace that contains $v_1$ and is bounded by the plane through $u$ orthogonal to the vector $v_1 - u$.*

*Proof.* The angle $\measuredangle v_1uv_i$ is acute if and only if $\langle v_1 - u, v_i - u\rangle > 0$, where $\langle\cdot,\cdot\rangle$ is the standard inner product on $\mathbb{R}^3$, and this holds if and only if $v_i$ lies in $H_1$. □

The next two technical lemmas are based on Lemma 4.4.1. They lead to the proof of the main result of this section. In both lemmas and in the subsequent theorem we use the following notation. We denote by $u$ a vertex in a tetrahedral mesh in $\mathbb{R}^3$, and the $m$ vertices of Lk $u$ are labeled $v_1, \ldots, v_m$. For each vertex $v_i$, the plane through $u$ orthogonal to $v_i - u$ is denoted $P_i$, and the open halfspace bounded by $P_i$ that contains $v_i$ is denoted $H_i$. The other halfspace bounded by $P_i$ will be called $H_i'$, and we take this to be a closed halfspace, which contains its boundary $P_i$. The orthogonal projection of a vertex $v_j$ into $P_i$ will be denoted $Pr_i(v_j)$.

**Lemma 4.4.2.** *Let $v_1$ and $v_2$ be nonadjacent vertices of* Lk *$u$, with $v_2 \in H_1'$. If $v_i$ is a vertex adjacent to both $v_1$ and $v_2$ such that $\measuredangle v_1uv_i$ and $\measuredangle v_2uv_i$ are both acute angles, then the orthogonal projection of $v_i$ into $P_1$ lies in $P_1 \cap H_2$.*

*Proof.* The sketch in Fig. 4.14 illustrates this result. For an algebraic proof we assign a coordinate system with $u$ as the origin and $v_1$ lying on the positive $z$ axis. Using coordinates $(x_i, y_i, z_i)$ for vertex $v_i$, the condition $v_2 \in H_1'$ means that $z_2 \leq 0$. Since the angle $\measuredangle v_1uv_i$ is acute, Lemma 4.4.1 implies that $v_i$ must lie in $H_1$, and since the angle $\measuredangle v_2uv_i$ is acute, Lemma 4.4.1 implies that $v_i$ must lie in $H_2$. Thus $v_i$ lies in $H_1 \cap H_2$. Since $H_1 \cap H_2$ would be empty if $v_2$ had coordinates $(0, 0, z_2)$, we can conclude that $v_2$ does not lie on the $z$-axis. With the remaining freedom in defining a coordinate system we specify that $v_2$ has coordinates $(x_2, 0, z_2)$ with $x_2 < 0$.

Now since $v_i \in H_1$, we know that $z_i \geq 0$. We also know that $\langle v_i, v_2\rangle = x_ix_2 + z_iz_2 > 0$, because $v_i \in H_2$. We have established that $z_iz_2 \leq 0$ and that $x_2 < 0$. It follows that $x_i < 0$. The projection $Pr_1(v_i)$ has coordinates $(x_i, y_i, 0)$ and is interior to $P_1 \cap H_2 = \{(x, y, 0) : x < 0\}$. □

**Lemma 4.4.3.** *Let $v_1$ and $v_2$ be nonadjacent vertices of* Lk *$u$, with $v_2 \in H_1'$. If $v_iv_2v_j$ is a 2-simplex of* Lk *$u$ such that $v_i, v_j$ are both adjacent to $v_1$ and the face angles $\measuredangle v_1uv_i$, $\measuredangle v_1uv_j$, $\measuredangle v_2uv_i$, $\measuredangle v_2uv_j$, are all acute angles, then $Pr_1(v_iv_2v_j) \subset P_1 \cap H_2$, i.e., the orthogonal projection of the entire facet $v_iv_2v_j$ into $P_1$ lies in $H_2$.*

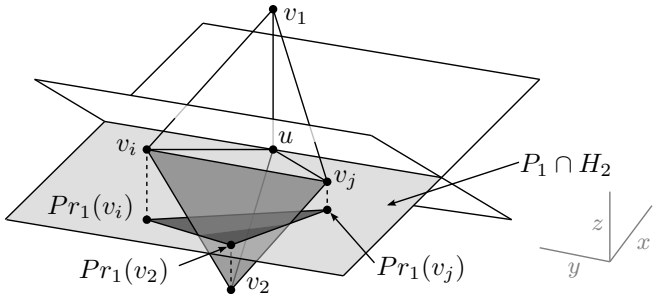


Figure 4.15: Let $u$ be a vertex of a tetrahedral mesh embedded in $\mathbb{R}^3$, and let $v_1$, $v_2$, $v_i$, $v_j$ be vertices of Lk $u$ with adjacencies as shown. If the face angles at $u$ between adjacent vertices of Lk $u$ are all acute angles, but $\measuredangle v_1uv_2$ is nonacute, then the projection of facet $v_iv_2v_j$ into $P_1$ lies in $P_1 \cap H_2$.

*Proof.* See the sketch in Fig. 4.15. From the given hypotheses we can conclude by Lemma 4.4.2 that $Pr_1(v_i)$ and $Pr_1(v_j)$ both lie in $P_1 \cap H_2$. Using the same coordinate system defined in the proof of Lemma 4.4.2, the point $Pr_1(v_2)$ has coordinates $(x_2, 0, 0)$ with $x_2 < 0$, thus it lies in $P_1 \cap H_2$ as well. It follows that the orthogonal projection of the 2-simplex $v_iv_2v_j$ into $P_1$, which is the convex hull of $Pr_1(v_i)$, $Pr_1(v_2)$, and $Pr_1(v_j)$, lies entirely in the convex set $P_1 \cap H_2$. □

Applying the above two lemmas, we obtain a combinatorial necessary condition on the neighborhood of an interior vertex in a 2-well-centered mesh.

**Theorem 4.4.4.** *Let $G$ be a triangulation of $S^2$ with $m$ vertices. If $G$ contains a vertex $v_1$ of degree $d(v_1) \geq m - 3$, then $G$ does not permit a 2-well-centered neighborhood.*

*Proof.* We consider a vertex $u$ such that Lk $u$ is isomorphic to $G$ where $G$ has a vertex of degree at least $m - 3$ and consider a geometric realization of Cl(St $u$) in $\mathbb{R}^3$. Label the vertices of Lk $u$ with the labels $v_1, v_2, \ldots, v_m$ such that $v_1$ is a vertex of maximum degree and the (at most two) vertices not adjacent to $v_1$ are listed immediately after $v_1$ (e.g., labeled $v_2$, $v_3$ if there are two of them). We choose a coordinate system on $\mathbb{R}^3$ such that $u$ is at the origin and $v_1$ lies on the positive $z$ axis.

Assume that all of the face angles $\measuredangle v_iuv_j$ are acute. We claim this implies that for any facet $v_iv_jv_k$ with at least one vertex in $H_1'$, the orthogonal projection of the facet into $P_1$, i.e., $Pr_1(v_iv_jv_k)$, does not contain vertex $u$. Assuming this claim for the moment, we see that $u$ lies outside the (solid) polyhedron bounded by Lk $u$. (See Fig. 4.16.) Since $u$ is outside this polyhedron, some 3-simplex incident to $u$ must be inverted. Thus the geometric realization of Cl(St $u$) is not an embedding, and the claim completes the proof.

We proceed to prove the claim. Noting that $v_1 \in H_1$ by our definition of $H_1$, we observe that for $i \geq 4$, vertex $v_i$ must lie in $H_1$ because $v_i$ is adjacent to $v_1$. (This follows from Lemma 4.4.1.) Thus there are only two types of facets that may have nonempty intersection with $H_1'$. The first type is $v_iv_2v_j$ or $v_iv_3v_j$ where $v_i$ and $v_j$ both are adjacent to $v_1$, and the second type is $v_2v_3v_j$ for $j \geq 4$. Consider, then, the first type of facet, taking the specific notation $v_iv_2v_j$. (The same argument applies to $v_iv_3v_j$.) If $v_2$ lies in $H_1$, we are done; the facet does not intersect $H_1'$. Otherwise $v_2$ lies in $H_1'$. Hence $\measuredangle v_1uv_2$ is nonacute, and $v_2$ is not adjacent to $v_1$. Lemma 4.4.3 applies.

The proof for facets of the second type is more complicated. If both $v_2$ and $v_3$ lie in $H_1$, we are done. If one vertex lies in $H_1 \cup P_1$ and the other lies in $H_1'$, we assume without loss of generality that $z_2 \leq 0$ and $z_3 \geq 0$.

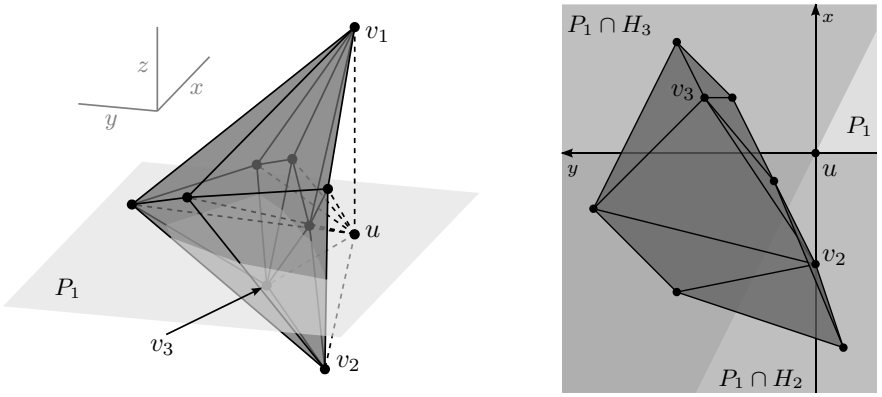


Figure 4.16: When Lk $u$ has $m$ vertices and one of the vertices $v_1$ has degree $d(v_1) \geq m-3$, any geometric realization of Cl(St $u$) in $\mathbb{R}^3$ with all face angles at $u$ acute is not an embedding. Theorem 4.4.4 shows that if we consider such a geometric realization and project every facet that intersects $H_1'$ into $P_1$, then the union of the projected facets does not contain $u$. The sketch at left shows an example of a geometric realization of a tetrahedral mesh Cl(St $u$) in $\mathbb{R}^3$ such that every face angle at vertex $u$ is acute. In the sketch, $v_1$ has degree $d(v_1) = 6 = m-3$ in Lk $u$. The sketch at right shows the result of taking the geometric realization on the left and projecting each facet that intersects $H_1'$ into $P_1$.

Then $v_2$ is not adjacent to $v_1$. If $v_3$ is adjacent to $v_1$, then Lemma 4.4.3 applies directly with $v_3$ functioning as $v_i$. On the other hand, the arguments of Lemmas 4.4.2 and 4.4.3 can be applied with $v_3$ functioning as $v_i$ even if $v_3$ is not adjacent to $v_1$. (In the proofs of Lemmas4.4.2 and 4.4.3 we used $v_i$ adjacent to $v_1$ to establish only that $z_i \geq 0$ and that $v_2$ does not lie on the $z$-axis. The latter holds in this case because $v_2$ and $v_1$ have common neighbor $v_j \neq v_3$.)

This leaves the case $z_2 < 0$ and $z_3 < 0$. As noted above, $v_2$ does not lie on the $z$-axis. We choose the coordinate system with $v_2 = (x_2, 0, z_2)$, $x_2 < 0$. We also assume without loss of generality that $y_3 \geq 0$. (We can reflect through the plane $y = 0$ if $y_3 < 0$.) See Fig. 4.17 for sketches related to this case.

By applying Lemma 4.4.1 three times, we obtain $v_j \in H_1 \cap H_2 \cap H_3$, and by applying Lemma 4.4.2 twice we obtain $Pr_1(v_j) \in P_1 \cap H_2 \cap H_3$. If $x_3 < 0$, then the whole segment $Pr_1(v_2v_3)$ lies in $P_1 \cap H_2$, and since $Pr_1(v_j) \in P_1 \cap H_2$, it follows that $Pr_1(v_2v_3v_j) \subset P_1 \cap H_2$. Thus $Pr_1(v_2v_3v_j)$ does not contain $u$.

So we assume that $x_3 \geq 0$. Now if $x_3 = 0$ we know that $y_3 \neq 0$ because $v_3$, like $v_2$, does not lie on the $z$-axis. Moreover, $x_3 > 0$ also implies $y_3 \neq 0$, since otherwise $P_1 \cap H_3$ would be $\{(x, y, 0) : x > 0\}$, yielding $P_1 \cap H_2 \cap H_3 = \emptyset \ni Pr_1(v_j)$. A point on segment $Pr_1(v_2v_3)$ has the form

$$\lambda Pr_1(v_2) + (1-\lambda)Pr_1(v_3) = \lambda(x_2, 0, 0) + (1-\lambda)(x_3, y_3, 0)\,,$$

with $0 \leq \lambda \leq 1$. Thus for a point $p = (x_p, y_p, 0)$ on $Pr_1(v_2v_3)$, either $x_p < 0$ and the point lies in $P_1 \cap H_2$ or both $x_p \geq 0$ and $y_p > 0$ so that $\langle p, v_3 \rangle = x_p x_3 + y_p y_3 > 0$ and the point lies in $P_1 \cap H_3$. We conclude that $Pr_1(v_2v_3) \subset P_1 \cap (H_2 \cup H_3)$.

Finally we note that there must exist a point $p_0 = (\varepsilon, y_{p_0}, 0)$ with $\varepsilon < 0$ such that $p_0$ lies on segment $Pr_1(v_2v_3)$ and $p_0 \in P_1 \cap H_2 \cap H_3$. Thus we can decompose $Pr_1(v_2v_3v_j)$ into the two pieces $p_0 * Pr_1(v_2v_j)$ and $p_0 * Pr_1(v_3v_j)$, with the first piece lying in $P_1 \cap H_2$ and the second piece lying in

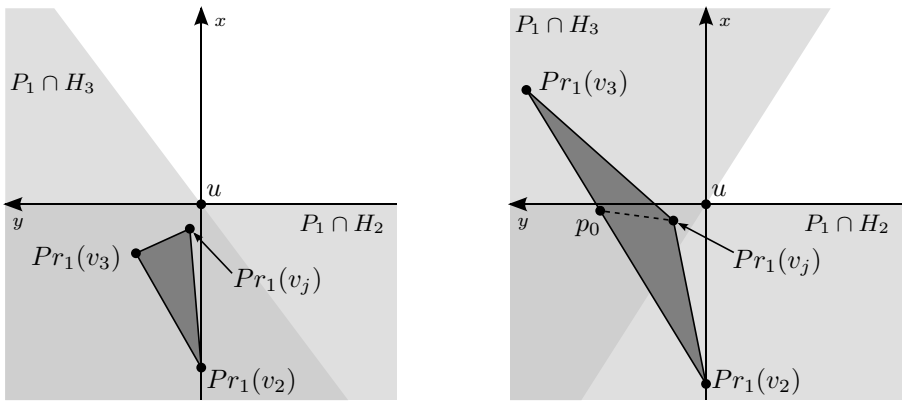


Figure 4.17: In the proof of Theorem 4.4.4, the most difficult case to analyze is a facet of the second type $v_2v_3v_j$ with $z_2 < 0$ and $z_3 < 0$. These sketches illustrate the projection of the facet $v_2v_3v_j$ into $P_1$ for the two subcases $x_3 < 0$ (left) and $x_3 \geq 0$ (right). In both subcases, $Pr_1(v_j)$ lies in $P_1 \cap H_2 \cap H_3$. When $x_3 < 0$, $Pr_1(v_3) \in P_1 \cap H_2$, so the projection of facet $v_2v_3v_j$ into $P_1$ is a subset of $P_1 \cap H_2$. When $x_3 \geq 0$, the projected facet can be decomposed into two pieces meeting along the segment from $p_0$ to $Pr_1(v_j)$. One of these pieces lies in $P_1 \cap H_2$, and the other piece lies in $P_1 \cap H_3$. In both subcases we see that $u \notin Pr_1(v_2v_3v_j)$.

$P_1 \cap H_3$. It follows that $Pr_1(v_2v_3v_j)$ does not contain $u$. □

Recall that Euler's formula specifies a relationship between the number of vertices, edges, and faces in a planar graph, e.g., a triangulation of $S^2$. If $m$, $e$, and $f$ are the number of vertices, edges, and faces respectively, then Euler's formula states that $m - e + f = 2$ for planar graphs. In a triangulation of $S^2$, each face is incident to three edges and each edge is incident to two faces, so $2e = 3f$, and the relationship $f = 2(m-2)$ can be derived. Moreover, in a triangulation of $S^2$ each face is incident to three vertices, and vertex $v_i$ is incident to $d(v_i)$ faces, so $\sum_i d(v_i) = 3f = 6(m-2)$. Combining these consequences of Euler's formula with Theorem 4.4.4, we easily obtain a lower bound on the number of edges incident to an interior vertex in a 2-well-centered tetrahedral mesh in $\mathbb{R}^3$.

**Corollary 4.4.5.** *Let $M$ be a 2-well-centered (or completely well-centered) tetrahedral mesh in $\mathbb{R}^3$. For every vertex $u$ interior to $M$, at least 9 edges of $M$ are incident to $u$.*

*Proof.* Let $G = \text{Lk } u$ for some interior vertex $u$ of a 2-well-centered mesh $M$, and let $m$ be the number of edges incident to $u$, i.e., the number of vertices of $G$. Consider the possibility $m = 8$. Euler's formula shows that for $m = 8$ we have $\sum_i d(v_i) = 36$ so the average vertex degree is 4.5, and there must be at least one vertex of degree at least $5 = m - 3$. By Theorem 4.4.4, this cannot occur, for such a graph $G$ would not permit a 2-well-centered neighborhood of $u$. Similarly, if $m = 7$ the average degree is $30/7 > 4$ and there must be a vertex of degree at least $m - 2$. For $m = 6$ the average degree is 4 and there must be a vertex of degree at least $m - 2$. In each of the cases $m = 5$ and $m = 4$, there is only one triangulation, and this triangulation has a vertex of degree $m - 1$. □

When $m = 9$, the average degree is $4\frac{2}{3}$, and there exists a triangulation of $S^2$ with degree list $(5, 5, 5, 5, 5, 5, 4, 4, 4)$ that can appear as the link of an interior vertex in a completely well-centered mesh. Figure 4.18 shows an example of a completely-well-centered mesh that has a single interior vertex $u$ such that Lk $u$ is a 9-vertex triangulation of $S^2$ with the specified degree list. Up to

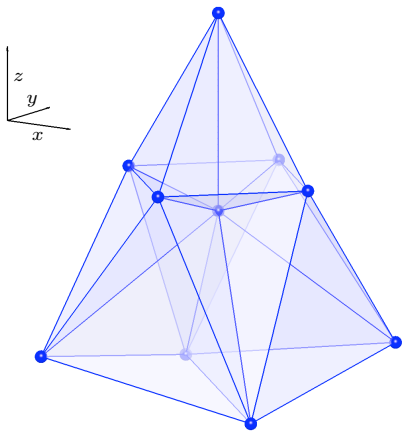


| $x$ | $y$ | $z$ |
|---|---|---|
| 0 | 0 | 0 |
| 0 | 0 | 1 |
| 0 | 0.533 | 0.164 |
| 0.533 | 0 | 0.164 |
| 0 | −0.533 | 0.164 |
| −0.533 | 0 | 0.164 |
| 0.63 | 0.63 | −0.7 |
| −0.63 | −0.63 | −0.7 |
| 0.594 | −0.594 | −0.9 |
| −0.594 | 0.594 | −0.9 |

Figure 4.18: A completely well-centered mesh with an interior vertex $u$ such that Lk $u$ has nine vertices and degree list $(5, 5, 5, 5, 5, 5, 4, 4, 4)$. The vertex coordinates are listed in the table at right; vertex $u$ is at the origin.

isomorphism, this is the only triangulation of $S^2$ with 9 vertices and no vertex of degree 6 or more, so there are no other triangulations of $S^2$ with 9 vertices that can appear as the link of a vertex in a 2-well-centered or completely well-centered tetrahedral mesh in $\mathbb{R}^3$.

It is clear from Theorem 4.4.4 that for each integer $m \geq 4$ there is a triangulation of $S^2$ with $m$ vertices that cannot appear as the link of a vertex in a 2-well-centered tetrahedral mesh in $\mathbb{R}^3$. We have also seen, by Proposition 4.3.6, that there are infinitely many triangulations of $S^2$ that can appear as the link of an interior vertex in a 2-well-centered tetrahedral mesh in $\mathbb{R}^3$. The next two results, in the same spirit as Proposition 4.3.7, show how to modify a triangulation of $S^2$ that permits a 2-well-centered neighborhood and construct other triangulations of $S^2$ that permit a 2-well-centered neighborhood.

In Proposition 4.4.6, we will consider a triangulation $G$ of $S^2$ with a vertex $v_1$ such that $d(v_1) = 3$. In this context, the expression $G - v_1$ means the triangulation of $S^2$ obtained by deleting vertex $v_1$ from triangulation $G$. To be more explicit, suppose that $v_2$, $v_3$, and $v_4$ are the three neighbors of $v_1$ in $G$. Then $G - v_1$ is obtained from $G$ by removing vertex $v_1$ along with the three triangles incident to $v_1$ and adding the triangle $v_2v_3v_4$.

**Proposition 4.4.6.** *A triangulation $G$ of $S^2$ that contains a vertex $v_1$ of degree three permits a 2-well-centered neighborhood if and only if the triangulation $G - v_1$ permits a 2-well-centered neighborhood.*

*Proof.* First we suppose that $G$ permits a 2-well-centered neighborhood. Then consider some tetrahedral mesh embedded in $\mathbb{R}^3$ that consists of a single interior vertex $u$ and Cl(St $u$) such that Lk $u$ is isomorphic to $G$ and each facet incident to vertex $u$ is 2-well-centered. Deleting $v_1$ from Lk $u$ to obtain $G - v_1$ removes the three facets of the mesh that are incident to edge $uv_1$, but has no effect on the other facets of the mesh that are incident to $u$. Thus all facets incident to $u$ after removing $v_1$ are 2-well-centered, and the modified mesh is a tetrahedral mesh in $\mathbb{R}^3$ that certifies that $G - v_1$ permits a 2-well-centered neighborhood.

On the other hand, suppose that $G - v_1$ permits a 2-well-centered neighborhood. Then consider some tetrahedral mesh in $\mathbb{R}^3$ that consists of a single interior vertex $u$ and Cl(St $u$) such that Lk $u$

is isomorphic to $G$ and each facet incident to vertex $u$ is 2-well-centered. We choose a coordinate system on $\mathbb{R}^3$ such that $u$ lies at the origin and identify each vertex $v_i$ of Lk $u$ with the vector originating at the origin and terminating at $v_i$. Let $v_2, v_3$, and $v_4$ be the three vertices of Lk $u$ that are adjacent to $v_1$ in $G$. Then the mesh contains facets $v_2uv_3$, $v_3uv_4$, and $v_4uv_2$. Moreover, since the face angles at $u$ in these facets are acute, we have $\langle v_i, v_j\rangle > 0$ for each $i, j \in \{2, 3, 4\}$. Let vertex $v_1 = \lambda_2 v_2 + \lambda_3 v_3 + \lambda_4 v_4$ with $\lambda_i > 0$ for each $i = 2, 3, 4$. Then for each $i = 2, 3, 4$ we have

$$\langle v_1, v_i\rangle = \lambda_2 \langle v_2, v_i\rangle + \lambda_3 \langle v_3, v_i\rangle + \lambda_4 \langle v_4, v_i\rangle > 0\,.$$

Thus as long as $v_1$ lies interior to the cone at $u$ bounded by vectors $v_2$, $v_3$, and $v_4$, it will make acute face angles with each of $v_2$, $v_3$, and $v_4$. It follows that $G$ permits a 2-well-centered neighborhood. □

Notice that Proposition 4.4.6 also implies that adding or deleting a degree three vertex from a triangulation of $S^2$ that does not permit a 2-well-centered neighborhood creates another triangulation of $S^2$ that does not permit a 2-well-centered neighborhood. In particular, this means that Theorem 4.4.4 does not characterize the triangulations of $S^2$ that cannot appear as the link of a vertex in a 2-well-centered tetrahedral mesh in $\mathbb{R}^3$. The family of triangulations that do not permit a 2-well-centered neighborhood appears to be much larger than the family of triangulations that cannot appear as the link of a vertex in a 3-well-centered tetrahedral mesh in $\mathbb{R}^3$.

In the next proposition, we consider the case of a triangulation $G$ of $S^2$ with a vertex $v_1$ such that $d(v_1) = 4$. To talk about removing vertex $v_1$ from $G$ in this case, we need to specify an edge to add after removing the vertex. Let $v_2$, $v_3$, $v_4$, and $v_5$ be the neighbors of $v_1$, listing in cyclic order. Then $(G - v_1) \cup v_2v_4$ is the triangulation of $S^2$ obtained from $G$ by removing vertex $v_1$ along with the four edges and triangles incident to $v_1$ and adding the edge $v_2v_4$ along with the two triangles $v_2v_3v_4$ and $v_2v_4v_5$.

**Proposition 4.4.7.** *Consider a triangulation $G$ of $S^2$ that contains a vertex $v_1$ of degree four with neighbors $v_2$, $v_3$, $v_4$, $v_5$ (listed in cyclic order). If $(G - v_1) \cup v_2v_4$ or $(G - v_1) \cup v_3v_5$ permits a 2-well-centered neighborhood, then $G$ permits a 2-well-centered neighborhood.*

*Proof.* Suppose without loss of generality that $(G-v_1)\cup v_2v_4$ permits a 2-well-centered neighborhood. Consider some tetrahedral mesh in $\mathbb{R}^3$ that consists of a single interior vertex $u$ and Cl(St $u$) such that Lk $u$ is isomorphic to $(G - v_1) \cup v_2v_4$ and each facet incident to vertex $u$ is 2-well-centered. We choose a coordinate system on $\mathbb{R}^3$ such that $u$ lies at the origin and identify each vertex $v_i$ of Lk $u$ with the vector originating at the origin $u$ and terminating at $v_i$. We know that $\langle v_2, v_3\rangle > 0$, $\langle v_3, v_4\rangle > 0$, $\langle v_4, v_5\rangle > 0$, $\langle v_5, v_2\rangle > 0$, and $\langle v_2, v_4\rangle > 0$, because each of these pairs of vectors bounds a face with an acute face angle at $u$.

Now let $v_1 = (v_2 + v_4)/2$ and, deleting the facet $v_2uv_4$, add the four facets $v_1uv_i$ for $i = 2, 3, 4, 5$. The new facets $v_1uv_2$ and $v_1uv_4$ have face angles at $u$ that are smaller than the angle $\measuredangle v_2uv_4$, so they are acute. The facets $v_1uv_3$ and $v_1uv_5$ also have acute face angles at $u$ because

$$\langle v_1, v_3\rangle = \frac{1}{2}\langle v_2, v_3\rangle + \frac{1}{2}\langle v_4, v_3\rangle > 0$$

and similarly

$$\langle v_1, v_5\rangle = \frac{1}{2}\langle v_2, v_5\rangle + \frac{1}{2}\langle v_4, v_3\rangle > 0\,.$$

We see that adding $v_1 = (v_2 + v_4)/2$ has created a new mesh for which all face angles at $u$ are acute and Lk $u$ is isomorphic to $G$. Thus $G$ permits a 2-well-centered neighborhood. $\square$

# Chapter 5

# Mesh Improvement

In Chapter 2 through Chapter 4 we developed theory related to the well-centered simplex and well-centered meshes. Now in Chapter 5 we introduce a heuristic for obtaining well-centered simplicial meshes. The heuristic is based on mesh optimization and motivated in part by the theory discussed in earlier chapters.

Meshes can be optimized in a variety of ways, so it is important to clarify the assumptions we make in our mesh optimization heuristic. We assume that the input can be represented as a set of vertices with specified coordinates and a connectivity table defining which subsets of vertices bound simplices. Some of the vertices are designated as boundary vertices. We adopt the conventions that the coordinates of boundary vertices cannot be modified during optimization and the connectivity table is fixed. The coordinates of *free vertices*, i.e., vertices that are not designated as boundary vertices, may be modified by the optimization.

We define a cost functional, or *energy*, on meshes that assigns some real number to the set of vertex coordinates and the connectivity table that define the mesh. The optimization energy we use is introduced in Sec. 5.1. The objective of the mesh optimization is to find a minimum of the cost functional by relocating the free vertices. The energy is designed such that the mesh is likely to be well-centered when the optimization has achieved a minimum of the energy.

Because we have adopted the conventions that the connectivity table is fixed and that the boundary vertices cannot move, it is possible to define input meshes for which mesh optimization cannot produce a well-centered mesh. In particular, if the connectivity table is defined such that the mesh does not satisfy the combinatorial requirements of well-centered meshes developed in Chapter 4, then repositioning vertices through mesh optimization will not produce a well-centered mesh. Section 5.2 discusses a preprocessing algorithm that addresses this potential problem for triangle meshes embedded in $\mathbb{R}^2$. The preprocessing algorithm guarantees that the mesh satisfies the local combinatorial requirements of triangle meshes embedded in $\mathbb{R}^2$, i.e., it guarantees that no vertex of the triangle mesh is a lonely vertex.

The mesh improvement methods discussed in [20] and [1] are good mesh improvement techniques based on optimization. Our mesh optimization is similar to those methods in that it is based on an iterative procedure to minimize an energy defined globally on the mesh, but it differs in that the mesh connectivity and the boundary vertices remain fixed as the energy is minimized. The cost function used in our mesh optimization is also different from the energies defined in [20] and [1]; in contrast to those cost functions, our energy was explicitly designed with the goal of finding well-centered meshes. [1]

[1] A large portion of this chapter has been modified from material previously published by the author and his coauthors. Most of the material in Sec. 5.1 is based on [64] and is reprinted here by the permission of the copyright

## 5.1 Optimization Energy

In the proof of Theorem 3.1.1 we showed that in order for a simplex $\sigma^n$ to be $n$-well-centered, the circumcenter $c(\sigma^n)$ and vertex $v_i$ must lie in the same halfspace of $\text{aff}(\sigma^n)$ with respect to hyperplane $\text{aff}(\tau_i^{n-1})$ for each $i = 0, 1, \ldots, n$. This statement could be represented by a set of discrete variables $X_i$ such that $X_i = 1$ if $c(\sigma^n)$ and $v_i$ are in the same halfspace and $X_i = 0$ otherwise. The simplex is $n$-well-centered if and only if $X_i = 1$ for each $i$. In defining an optimization energy, however, we move from this discrete variable to a continuous variable. Instead of asking, "Is the simplex well-centered?", we now ask, "How well-centered is the simplex?"

To answer this quantitative question we introduce the function $h(v_i, \sigma^n)$, the signed distance from $c(\sigma^n)$ to $\text{aff}(\tau_i^{n-1})$. We take the sign of $h(v_i, \sigma^n)$ to be positive if $c(\sigma^n)$ and $v_i$ lie in the same halfspace with respect to $\text{aff}(\tau_i^{n-1})$ and negative if $\text{aff}(\tau_i^{n-1})$ lies between $c(\sigma^n)$ and $v_i$. For purposes of computation, the positions of $c(\sigma^n)$ and $c(\tau_i^{n-1})$ can be found by solving small linear systems as discussed in [5]. (See also Sec. 3.3.) Then the magnitude of $h(v_i, \sigma^n)$ can be calculated as the distance between $c(\sigma^n)$ and $c(\tau_i^{n-1})$, and the sign of $h(v_i, \sigma^n)$ can be calculated by testing whether $c(\sigma^n)$ and $v_i$ have the same orientation with respect to $\text{aff}(\tau_i^{n-1})$. A simplex $\sigma^n$ is well-centered if and only if $h(v_i, \sigma^n) > 0$ for every vertex $v_i$ of $\sigma^n$, and it becomes more well-centered as the minimum $h(v_i, \sigma^n)$ grows. When $h(v_i, \sigma^n)$ is large for each $i = 0, 1, \ldots, n$, there is some flexibility in moving around the vertices of $\sigma^n$ while keeping $\sigma^n$ well-centered.

Intuitively the concept of how well-centered a simplex is should not depend on the scale of the simplex. The quantity $h(v_i, \sigma^n)$ by itself, however, does change as $\sigma^n$ is scaled. Thus we divide $h(v_i, \sigma^n)$ by the circumradius $R(\sigma^n)$ to get a quantity independent of the scaling of $\sigma^n$. The quantity $h(v_i, \sigma^n)/\, R(\sigma^n)$ is the basis of our mesh optimization energy. A mesh optimization energy based directly on $h$ might also be good, but it seems likely that an energy based on $h/R$ will keep the grading (the relative sizes of the elements) of the result mesh more similar to the grading of the initial mesh. Sazonov et al. also noticed that the quantity $h/R$ is helpful in quantifying well-centeredness of a simplex [50].

This $h/R$ is the same $h/R$ mentioned in Chapter 2 as a means to quantify the 3-well-centeredness of a tetrahedron. As mentioned there, $-1 < h(v_i, \sigma^n)/\, R(\sigma^n) < 1$ for finite $\sigma^n$. This follows from $R(\sigma^n)^2 = h(v_i, \sigma^n)^2 + R(\tau_i^{n-1})^2$.

Consider the function

$$f_n(\sigma^n) = \max_{\text{vertices } v \in \sigma^n} \left| \frac{h(v, \sigma^n)}{R(\sigma^n)} - k_n \right|,$$

where $0 < k_n \leq 1$ is some constant that may depend on the dimension $n$ of the simplex. If we

holder.

Much of the rest of the chapter is modified from [63]. In particular, Figs. 5.2, 5.3, 5.4, 5.5, 5.6, and 5.7 appeared in [63] as Figs. 2, 3, 4, 5, 6, and 7. Portions of Figs. 7.2 and 7.8 are also substantially similar to (but not the exactly the same as) portions of Figs. 10 and 12 from [63]. The article [63] is "Well-centered Planar Triangulation — An Iterative Approach," written by the author Evan VanderZee and his coauthors Anil N. Hirani, Damrong Guoy, and Edgar Ramos. It appeared electronically in 2007 and in print in 2008 on pages 121–138 of the *Proceedings of the 16th International Meshing Roundtable*. The publication [63] is 

minimize $f_n$ instead of maximizing $h/R$, and if $k_n$ is chosen properly, we find that we can penalize simplex vertices where $h/R$ approaches 1 (e.g., small angles of triangles and sharp points of needle tetrahedra) as well as vertices where $h/R \leq 0$.

**Proposition 5.1.1.** *Any simplex $\sigma^n$ has a vertex $v_i$ such that $h(v_i, \sigma^n)/\, R(\sigma^n) \leq 1/n$, and equality is achieved if and only if $\sigma^n$ is the regular $n$-simplex.*

*Proof.* If $\sigma^n$ is not $n$-well-centered, then there exists some vertex $v_i$ such that $h(v_i, \sigma^n)/\, R(\sigma^n) \leq 0 < 1/n$, so we assume that $\sigma^n$ is $n$-well-centered. Define $h := \min_i h(v_i, \sigma^n)$ and consider a geometric sphere $S^{n-1} \subset \text{aff}(\sigma^n)$ with center $c(\sigma^n)$ and radius $h$. We claim that $\sigma^n$ contains this sphere $S^{n-1}$. Indeed, for each facet $\tau_i^{n-1}$ of $\sigma^n$, the radius of $S^{n-1}$ is $h \leq h(v_i, \sigma^n)$, so the entire sphere is contained in the same (closed) half space as $c(\sigma^n)$ and $v_i$. Thus the sphere is contained in the intersection of half spaces that defines the simplex.

It follows, then, that $h \leq r(\sigma^n)$, where $r(\sigma^n)$ is the *inradius* of $\sigma^n$, the radius of the largest sphere that can be inscribed in $\sigma^n$. We see that $h/R \leq r/R$, and $r/R \leq 1/n$ with equality achieved for only the regular simplex is a known result. (The inequality $r/R \leq 1/n$ is proved in [36], among others.) □

We see from Proposition 5.1.1 that in terms of the minimum $h/R$, no simplex is more well-centered than the regular simplex. This agrees with our intuition about the concept well-centered, and when choosing $k_n$ in the function $f_n(\sigma^n)$, we would like to keep this property. Specifically, we want $f_n(\sigma^n)$ to be minimized when $\sigma^n$ is the regular $n$-simplex. Taking $k_n = 1/n$ may be a good choice; when $k_n = 1/n$, $f_n(\sigma^n) = 0$ for the regular $n$-simplex $\sigma^n$, and it is obvious that $f_n$ is minimized at the regular $n$-simplex. On the other hand, Proposition 5.1.1 has an easy corollary that the regular simplex minimizes $f_n$ for any $1 \geq k_n \geq 1/n$.

**Corollary 5.1.2.** *For $k_n \geq 1/n$, the function $f_n(\sigma^n)$ is minimized when $\sigma^n$ is a regular simplex.*

*Proof.* Suppose that $k_n \geq 1/n$. For $\sigma^n$ a regular simplex we have $f_n(\sigma^n) = k_n - 1/n$. For an arbitrary simplex $\sigma^n$ there exists some vertex $v_i$ of $\sigma^n$ such that $h(v_i, \sigma^n)/\, R(\sigma^n) \leq 1/n$, and

$$f_n(\sigma^n) \geq \left| \frac{h(v_i, \sigma^n)}{R(\sigma^n)} - k_n \right| = k_n - \frac{h(v_i, \sigma^n)}{R(\sigma^n)} \geq k_n - \frac{1}{n}\,.$$

□

In light of Corollary 5.1.2, we consider $k_n = 1/2$, independent of $n$, to be the best generic choice. For $k_n = 1/2$, cost function $f_n$ assigns a value less than $1/2$ to any simplex that is $n$-well-centered and a value greater than or equal to $1/2$ to any simplex that is not $n$-well-centered. At the same time, the optimal simplex continues to be the regular simplex, and among well-centered simplices $f_n$ penalizes those with $h/R$ value near 0 or 1. We use $k_n = 1/2$ for all of the experimental results of Chapter 7.

For $k_n > 0$ a simplex is guaranteed to be $n$-well-centered when $|h/R - k_n| < k_n$, though this is not a necessary condition if $k_n < 1/2$. For $k_n \geq 1/2$, at least, the goal of obtaining a well-centered mesh is consistent with the goal of minimizing $|h/R - k_n|$ over all vertices and all simplices of the mesh. This motivates the definition of the following cost function defined on a mesh $M$ specified by

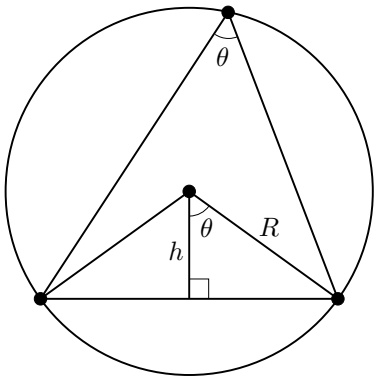


Figure 5.1: For a triangle, $h/R = \cos(\theta)$.

its vertex coordinates $V$ and connectivity table $T$.

$$E_{n,\infty}(M) = E_\infty(M) = E_\infty(V,T) = \max_{\substack{\text{simplices } \sigma^n \in T \\ \text{vertices } v_i \prec \sigma^n}} \left| \frac{h(v_i,\sigma^n)}{R(\sigma^n)} - \frac{1}{2} \right|.$$

We usually suppress the $n$ in the notation for $E_\infty$, since the particular $n$ is either irrelevant or made clear by the context. We will also use the following cost functions defined with parameter $p \geq 1$, which are approximations to $2E_\infty$.

$$E_{n,p}(M) = E_p(M) = E_p(V,T) = \sum_{\substack{\sigma^n \in T \\ v_i \prec \sigma^n}} \left| \frac{2h(v_i,\sigma^n)}{R(\sigma^n)} - 1 \right|^p.$$

The cost functions $E_p$ approximate $2E_\infty$ in the sense that $\lim_{p\to\infty} (E_p(M))^{1/p} = 2E_\infty(M)$. Thus for large $p$, the cost function $E_p$ is very similar to $E_\infty$, and for small $p$ the cost functions are less similar. The parameter $p$ controls the relative importance of each vertex-simplex pair. With $E_\infty$ the cost function looks at the vertex-simplex pair(s) with the absolute worst quality and tries to improve it (them). Away from the worst vertex-simplex pair(s), the gradient of $E_\infty$ is not well-defined. Cost function $E_p$ is similar for large $p$, but does have a well-defined gradient away from the worst vertex-simplex pair(s). For small $p$, on the other hand, the energy $E_p$ takes the quality of all vertex-simplex pairs into account, and $E_p$ might be reduced by degrading the $h/R$ value at the worst vertex-simplex pair and simultaneously improving the $h/R$ value at several other vertex-simplex pairs.

The factor of 2 in the definition of $E_p$ is included for numerical robustness; for any parameter $p$, $|2h/R - 1|^p < 1$ if and only if $|h/R - 1/2| < 1/2$. It is convenient to choose $p$ as a positive even integer, since the absolute value does not need to be explicitly computed in that case. Note also that the energy is not well-defined for a degenerate simplex, which may occur in a computational setting. For a degenerate simplex we define the circumcenter to be the point at infinity and take $h/R = -1$. This definition produces cost functions $E_p$ that are upper semicontinuous.

**Remark.** In the case of a triangle embedded in $\mathbb{R}^2$, the quantity $h/R$ has a simple interpretation. We see from Fig. 5.1 that $h/R = \cos(\theta)$ for a triangle in the plane. Thus the cost functions defined

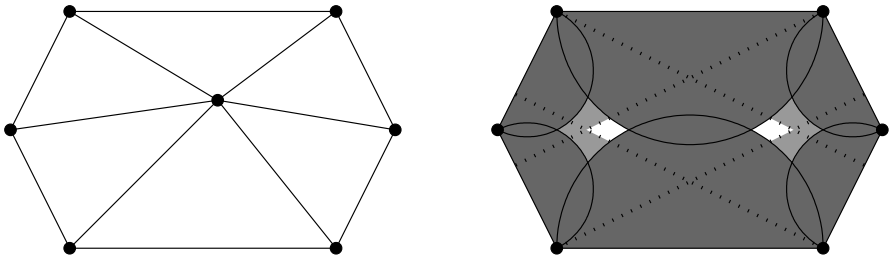

Figure 5.2: A cost function that accurately reflects the goal of creating a 2-well-centered triangle mesh in $\mathbb{R}^2$ cannot guarantee a unique minimum because the set of vertex coordinates that make the mesh well-centered may be a symmetric disconnected set.

over a mesh $M$ as

$$\sum_{\theta \in M} |\cos(\theta) - 1/2|^p \ ,$$

are a constant multiple of the $E_p$ energy defined here. We introduced the cost functions based on $\cos(\theta)$ in [63] and used mesh optimization with the cost functions to find acute triangle meshes in $\mathbb{R}^2$.

For a tetrahedron in three dimensions, there are several different ways to think about the quantity $h/R$. The vertex angle of a tetrahedron, the linear angle associated to a facet of a tetrahedron, and the alternative solid angle associated to a facet of a tetrahedron, which are all defined in Sec. 2.2, are closely related to each other and to the quantity $h/R$.

**Remark.** The cost functions $E_p$ and $E_\infty$ are not convex. When designing a cost function for mesh optimization, one might hope to develop a function that has a unique optimum, preferably one that is convex. We claim, however, that it is not possible to define an energy that accurately reflects the goal of creating a well-centered mesh and also has a unique minimum.

Consider the simple mesh shown on the left in Fig. 5.2. We adopt our usual conventions that the boundary vertices and the mesh connectivity are fixed. Thus the interior vertex of this mesh is the only vertex that is free to move. Optimizing a cost function that accurately reflects the goal of creating a well-centered mesh should move the free interior vertex to a place where the mesh is well-centered. The right side of Fig. 5.2 shows where the free vertex can be placed to produce a well-centered mesh. The light gray regions are prohibited because placing the free vertex in those regions would make some boundary angle nonacute. (The dotted lines indicate how the four most important boundary angles influence the definition of this region.) The darker gray regions, shown overlaying the light gray region, are prohibited because placing the interior vertex in those regions would make some angle at the interior vertex nonacute.

Removing the prohibited gray regions leaves two small white regions. If the interior vertex is placed in either of these white regions, the mesh will be 2-well-centered. These white regions, the locations that will produce a 2-well-centered mesh, form a disconnected set in $\mathbb{R}^2$. Moreover, the mesh is radially symmetric, so there is no reasonable way to design a cost function that has a lower energy value in one white region compared to the other white region. If there were such a cost function, we could rotate the mesh by $\pi$ and find that the energy value had changed for the rotated set of triangles. Any symmetric energy that has minima in both white regions and no minima outside

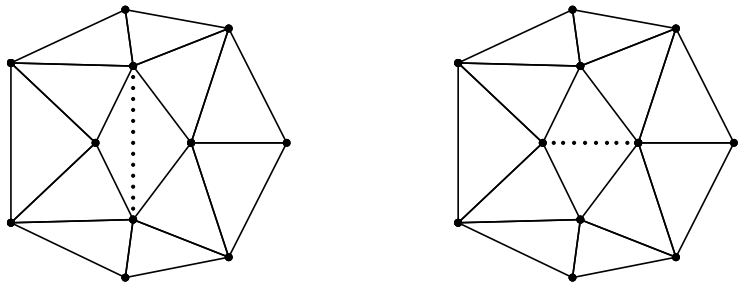

Figure 5.3: The edge flip operation can increase the valence of a lonely vertex. In the initial mesh (left) there is exactly one lonely vertex. Deleting the edge represented by a dotted line segment in the initial and replacing it with the dotted line segment in the final mesh (right) produces a mesh with no lonely vertices.

the white regions must have at least two distinct global minima.

In most triangle meshes embedded in $\mathbb{R}^2$ there is an interior vertex $v$ that has exactly six neighbors, all of which are interior vertices. Since all the interior vertices are free to move, we can arrange the six neighbors of $v$ in a small neighborhood around $v$ such that the closed star of $v$ is a scaling of the mesh shown on the left side of Fig. 5.2. Leaving the neighbors of $v$ in this arrangement of positions and moving around $v$ should exhibit this same nonconvexity for most triangle meshes in $\mathbb{R}^2$ for any cost function that accurately reflects the goal of creating a 2-well-centered triangle mesh.

## 5.2 Preprocessing Triangle Meshes in the Plane

In Sec. 4.2 we defined a lonely vertex in a triangle mesh in the plane as a vertex that, subject to the assumption of fixed boundary vertices, does not satisfy the local combinatorial requirements of being a 2-well-centered mesh. Any triangle mesh in the plane that has a lonely vertex is not 2-well-centered and cannot be made 2-well-centered by any mesh optimization that fixes boundary vertices. In this section we describe an algorithm that takes a general triangle mesh in $\mathbb{R}^2$ as input and creates a similar triangle mesh that has no lonely vertices. The algorithm depends on three operations that locally modify the mesh connectivity. We first discuss the three operations — edge flip, edge split, and triangle subdivision — and later describe how the algorithm uses the operations to increase the valence of lonely vertices.

### 5.2.1 Edge Flip

The simplest local modification to mesh connectivity is the ubiquitous edge flip. Figure 5.3 illustrates the edge flip and shows that the edge flip can be used to increase the valence of a lonely vertex. In the example, the final mesh, shown at right in Fig. 5.3, is a 2-well-centered mesh.

In the edge flip operation there are two vertices whose valence decreases and two vertices whose valence increases. We permit an edge flip only if flipping the edge does not introduce new lonely vertices or degrade existing ones. For example, if the endpoints of the prospective deleted edge are both interior vertices in the mesh, the edge flip is not permitted if either endpoint has valence five or less. We also do not permit an edge flip if flipping the edge would introduce an inverted triangle.

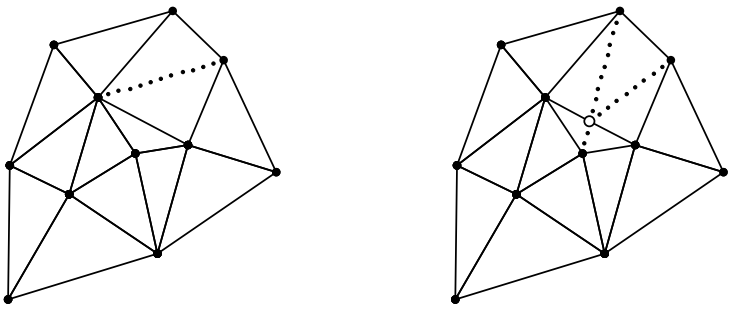

Figure 5.4: When no edge flip can increase the valence of a lonely vertex, the more aggressive edge split operation might be able to increase the valence of the vertex. In this illustration of the edge flip, the initial mesh (left) has exactly one lonely vertex $v$, and no edge on the link of $v$ may be flipped. To perform the edge split, an edge (dotted line segment) in the initial mesh is replaced by one new vertex (the empty circle), one split edge, and three new edges (dotted line segments) in the final mesh.

### 5.2.2 Edge Split

The edge split operation, illustrated in Fig. 5.4, is a more aggressive mesh modification operation than the edge flip. We generally consider the edge split operation as a unit, but it could be broken down as inserting a new degree four vertex followed by an edge flip that increases the valence of the newly inserted vertex. For the example in Fig. 5.4, the final mesh is not 2-well-centered, but it has no lonely vertices, and can be made 2-well-centered by relocating the new vertex. It is also worth pointing out that in this example there is no permissible edge flip that would increase the valence of the lonely vertex.

For the edge split operation we add the new vertex at the midpoint of an existing edge. This *split edge* may not be an edge on the boundary of the triangle mesh. The edge deleted by the edge split operation must also be an interior edge. Analyzing the vertices that appear in the initial mesh, we see that an edge split decreases the valence of one vertex and increases the valence of two vertices. We do not permit the edge split if the vertex whose valence decreases would become (or already is) a lonely vertex. We also do not permit the edge split if it would introduce an inverted triangle. At the end of the edge split operation, the vertex that was inserted is an interior vertex with exactly five neighbors, so it is not a lonely vertex.

### 5.2.3 Triangle Subdivision

The edge split operation is quite versatile, since in the interior of the mesh there is usually a choice of both which edge to split and which endpoint of the edge will decrease in valence. There are some cases, though, when no edge split is permitted, and a more aggressive mesh modification is necessary. In almost all of these cases, the triangle subdivision operation, illustrated in Fig. 5.5, can be used to increase the valence of a lonely vertex in the mesh. The final mesh in Fig. 5.5 has some angles that are significantly larger than the largest angle of the initial mesh, but it has been improved combinatorially. The final mesh has no lonely vertices, and one can obtain a 2-well-centered mesh by relocating its interior vertices.

If the mesh shown in Fig. 5.5 were a submesh of a larger mesh, it might be possible to do an

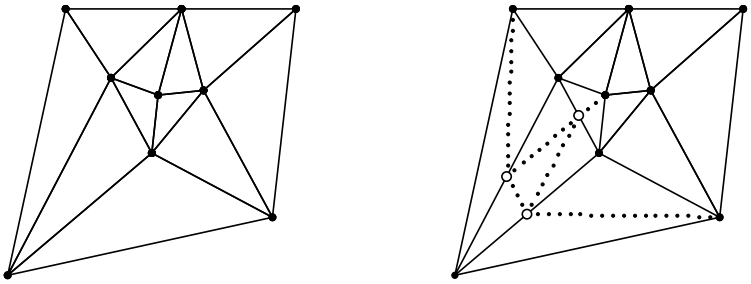

Figure 5.5: The triangle subdivision operation introduces three new vertices to increase the valence of a lonely vertex. In this illustration, the initial mesh (left) has exactly one lonely vertex. The triangle subdivision operation does not delete anything from the initial mesh, but adds three new vertices (empty circles), splits three edges, and adds up to six new edges (dotted line segments) to create the final mesh (right). There will be fewer new line segments if the subdivided triangle has an edge on the boundary of the mesh.

edge split to increase the valence of the lonely vertex, but if this submesh occurs with the two edges at the top along the boundary of the mesh, then there is no permissible edge split that increases the valence of the lonely vertex. Even if the mesh is a submesh of a larger mesh, there is no permissible edge flip that will increase the valence of the lonely vertex. Thus in some cases triangle subdivision is necessary.

The vertices added to the mesh in a triangle subdivision operation are inserted at the midpoints of edges in the initial mesh. Thus a Loop subdivision is applied to the subdivided triangle in both a geometric and a combinatorial sense. The new vertices have valence five if they are interior to the mesh, and are incident to three triangles (four edges) if they are inserted along the boundary of the mesh, so the new vertices are not lonely. (This assumes that new boundary vertices may be inserted at the midpoint of a boundary segment. In the case of meshing a domain with a curved boundary, one might prefer to specify some way to insert a new boundary vertex on the curved boundary. Even in that case the boundary angle at the new vertex should be significantly less than $3\pi/2$ if the curved boundary is resolved well, so a new boundary vertex should not be lonely.)

A triangle subdivision can increase the valence of a lonely vertex $v$ if and only if some edge in Lk $v$ is incident to two triangles. If there is a lonely vertex $v$ with every edge in Lk $v$ on the boundary of the mesh, however, a single triangle subdivision is not sufficient to increase the valence of the lonely vertex. In that case we resort to a double triangle subdivision, as illustrated in Fig. 5.6. Double triangle subdivision can be performed within a single triangle to increase the valence of some vertex of the triangle. Thus we see that through some local mesh modification we can increase the valence of any lonely vertex of a mesh.

A double triangle subdivision adds six vertices to the mesh, splits three of the initial edges of the mesh, and adds between twelve and fourteen new edges to the mesh. Vertices added to the mesh by a double subdivision are like vertices added in a regular triangle subdivision; no added vertex will be a lonely vertex. We see again that in our example (Fig. 5.6) the final mesh has some very large angles. Increasing the valence of lonely vertices is part of preprocessing, though. There is a 2-well-centered mesh with the same mesh connectivity table and boundary vertices as the final mesh in Fig. 5.6.

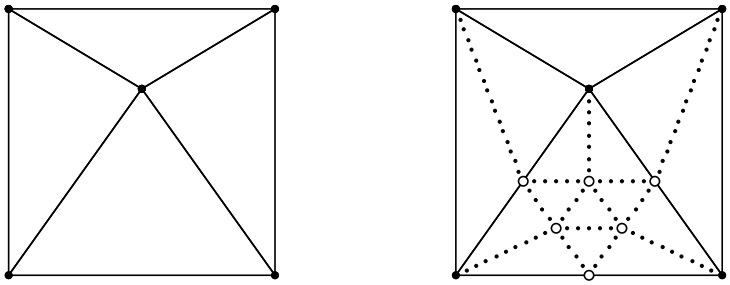

Figure 5.6: In extreme cases a double triangle subdivision may be necessary. If the initial mesh (left) is the entire input mesh, then no single triangle subdivision will increase the valence of the lonely vertex. Subdividing twice, however, does provide a way to increase the valence of the lonely vertex.

```
for each lonely vertex v
    repeat
        perform first permissible operation among:
            edge flip,
            edge split,
            triangle subdivision,
            double triangle subdivision;
    until v is not lonely
end
```

Figure 5.7: Preprocessing Algorithm

### 5.2.4 The Algorithm

There are multiple ways to organize these mesh modification operations into an algorithm that creates a mesh without lonely vertices. The algorithm presented in Fig. 5.7 is a simple algorithm that accomplishes that goal. In the analysis of the mesh modification operations, we saw that each permissible operation increases the valence of some lonely vertex and does not introduce any new lonely vertices or decrease the valence of any lonely vertices. Since the double triangle subdivision is always permissible and there are a finite number of lonely vertices in a finite triangle mesh in the plane, the algorithm of Fig. 5.7 must eventually terminate at a mesh with no lonely vertices. The repeat-until loop of the algorithm is required because there may be lonely vertices in the mesh, e.g. interior vertices that initially have valence three, that need to increase valence more than once.

Each local mesh modification operation increases the valence of at least one vertex other than the target lonely vertex, and some operations decrease the valence of select vertices. Thus performing one local mesh modification can affect whether a nearby mesh modification is permissible. For instance, flipping one edge may make it possible to flip another edge that initially could not be flipped. The order in which we consider lonely vertices can change the final mesh produced by the algorithm.

The fact that some operations may influence whether other operations are permissible also suggests that it may be advantageous to implement an algorithm with stages. Each stage looks like the algorithm in Fig. 5.7, but except for the last stage of the algorithm, a stage will have a shorter list

of operations. For example, one could implement a first stage that allows only edge flips, a second stage that allows edge flips and edge splits, and a final stage that is exactly the algorithm in Fig. 5.7. In the earlier stages the until condition in Fig. 5.7 would need to be modified to detect whether a mesh modification had occurred; the algorithm should move on to the next lonely vertex when no mesh modification is permissible among the shorter list of possible operations.

The preprocessing algorithm used in Chapter 7 for the large majority of experimental results on triangle meshes in $\mathbb{R}^2$ is a four-stage algorithm. The first two stages allow only edge flips, the third stage allows edge flips and edge splits, and the final stage is the algorithm in Fig. 5.7. The idea behind this algorithm is to limit the number of new vertices inserted into the mesh. For each lonely vertex we check three times whether edge flips are permissible before making any more aggressive modification that inserts vertices into the mesh. This idea is merely a heuristic, and there is no reason to believe that it will in general insert the minimum number of new vertices needed to obtain a mesh without lonely vertices.

For several of the experimental results on triangle meshes in $\mathbb{R}^2$ we applied a more complicated preprocessing algorithm. In these cases we ourselves created the initial input mesh using Shewchuk's software Triangle [55], and this allowed us to make some assumptions about the quality of the input mesh. We do not discuss the more complicated preprocessing algorithm in detail, but make a few comments about its features. First, the more complicated algorithm relaxes the definition of lonely vertex for boundary vertices to the idea of a nearly lonely vertex. For example if a boundary vertex is incident to exactly one triangle and the angle at the boundary vertex is less than $\pi/2$ but greater than $\pi/2 - \varepsilon$ for some parameter $\varepsilon > 0$, the vertex will be nearly lonely, and the algorithm will require that there be at least two triangles incident to the vertex. Second, the more complicated algorithm is fussier about creating large angles in the mesh. The basic algorithm allows edge flips if they do not invert triangles, but the more complicated algorithm calculates the largest angle in the new triangles that would be created by edge flips or edge splits, and it rejects some operations that would be allowed by the basic algorithm. Finally, the more complicated algorithm employs some heuristics to find beneficial edge flips in regions where there are no lonely vertices.

The more complicated preprocessing algorithm is more aggressive than the basic algorithm in making changes to the initial mesh. In that sense it moves away from the goal of creating a well-centered mesh that is similar to the initial mesh. On the other hand, since we make use of the more complicated preprocessing algorithm exclusively in cases where we generate the mesh ourselves, it could be considered as a helpful tool for the generation of 2-well-centered triangle meshes of domains in $\mathbb{R}^2$.

# Chapter 6

# Optimal Triangulations

In Chapter 5 we defined the energy $E_\infty$ for a mesh $M$ with vertex coordinates $V$ and mesh connectivity table $T$. In contrast to the mesh optimization methods of [20] and [1], we adopted the convention that the mesh connectivity table is fixed during mesh optimization. We also introduced a preprocessing algorithm for triangle meshes in $\mathbb{R}^2$. In this chapter we consider the option of globally optimizing the mesh connectivity in a fashion similar to that of [20] and [1]. We show that for $E_\infty$ the globally optimal triangulation for triangle meshes in the plane is a *minmax triangulation*, i.e., a triangulation that minimizes the maximum angle. We also discuss some reasons behind our choice to keep the mesh connectivity table fixed during mesh optimization.

As a general rule, the minmax triangulation differs from the Delaunay triangulation, which maximizes the minimum angle [57]. When a point set in $\mathbb{R}^2$ has a 2-well-centered triangulation, however, the Delaunay triangulation and the minmax triangulation are the same. This chapter proves that and discusses some other connections between the Delaunay triangulation and well-centered meshes. [1]

## 6.1 Triangulation of 2-Dimensional Point Sets

Suppose that we are given a fixed set of vertices $V$ in $\mathbb{R}^2$, not all collinear. We want to find a triangulation $T$ of the convex hull of $V$ that minimizes $E_\infty(V, T)$. When we speak about a triangulation $T$ in this section, we assume (often implicitly) that the triangulation $T$ comes from some finite set of admissible triangulations. When not explicitly specified as something else, an admissible triangulation is a triangulation $T$ that is a simplicial complex in $\mathbb{R}^2$ with vertex set $V$ that covers the convex hull of $V$. Thus there are no inverted or overlapping triangles. It is worth noting that many of the results in this section hold even if we change or restrict the set of admissible triangulations. For example, we might change the admissible triangulations to accommodate meshing a nonconvex polygon, or a polygon with a hole, and we might restrict the admissible triangulations to contain only those triangulations that have no lonely vertices.

Since $E_\infty$ can be expressed as a function of the angles of triangles for triangle meshes in $\mathbb{R}^2$, we find it helpful to start with a very general proposition about functions of angles. The proposition defines a function $E_f$ on triangulations and discusses $\arg\min E_f$, the set $\mathcal{T}$ of triangulations $T$ such that $E_f(T) = \min_S E_f(S)$ for every $T \in \mathcal{T}$.

[1] Figure 6.1 is scheduled to appear as Fig. 6.1 in the article "Well-Centered Triangulation" in the SIAM Journal of Scientific Computing [64]. The article was written by the author Evan VanderZee and his coauthors Anil N. Hirani, Damrong Guoy, and Edgar A. Ramos. A significant portion of the text of Sec. 6.1 is also based on that article. The copyright for that article belongs to the Society for Industrial and Applied Mathematics (SIAM). The copyrighted material that is used here is reprinted with kind permission of SIAM.

**Proposition 6.1.1.** *Let $f$ be a strictly increasing function of $\theta$ and $g$ a nondecreasing function of $\theta$ for $\theta \in [0, \pi]$. Define $E_f(T) = \max\{f(\theta_i)\}$ and $E_g(T) = \max\{g(\theta_i)\}$, with angle $\theta_i$ ranging over every angle of every triangle of $T$. Then* $\arg\min E_f \subseteq \arg\min E_g$.

*Proof.* For each triangulation $T$ there exists some angle $\theta_T$ such that $E_f(T) = \max\{f(\theta_i)\} = f(\theta_T)$. For every angle $\theta$ in every triangle of $T$, we have $f(\theta_T) \geq f(\theta)$.

Consider a triangulation $T_0 \in \arg\min E_f$. For any triangulation $T$, $E_f(T_0) \leq E_f(T)$. Thus $f(\theta_{T_0}) \leq f(\theta_T)$. Moreover, since $f$ is a strictly increasing function of $\theta$, we conclude that $\theta_{T_0} \leq \theta_T$. Then since $g$ is nondecreasing, this implies that $g(\theta_{T_0}) \leq g(\theta_T)$.

We claim that for each triangulation $T$ and each angle $\theta$ in each triangle of $T$ we have $g(\theta_T) \geq g(\theta)$. If this were not the case, then there would exist some $T$ and some angle $\widetilde{\theta}$ in some triangle of $T$ such that $g(\widetilde{\theta}) > g(\theta_T)$. Since $g$ is nondecreasing, it would follow that $\widetilde{\theta} > \theta_T$, and since $f$ is strictly increasing, we would conclude that $f(\widetilde{\theta}) > f(\theta_T)$. But this contradicts our definition of $\theta_T$ as an angle for which $f(\theta_T) = \max\{f(\theta_i)\} \geq f(\widetilde{\theta})$. Thus the claim is correct.

We see that $g(\theta_T) = \max\{g(\theta_i)\} = E_g(T)$ for each triangulation $T$. In particular, $g(\theta_{T_0}) \leq g(\theta_T)$ implies that $E_g(T_0) \leq E_g(T)$. This holds for each triangulation $T$, so $T_0 \in \arg\min E_g$. □

Recall that $h/R = \cos(\theta)$ for a triangle in the plane. Thus for a fixed set of vertices $V$ in $\mathbb{R}^2$ we have

$$E_\infty(V,T) = E_\infty(T) = \max_{\substack{\sigma^2 \in T \\ v_i \prec \sigma^2}} \left| \frac{h(v_i, \sigma^2)}{R(\sigma^2)} - \frac{1}{2} \right| = \max_{\theta \in T} \left| \cos(\theta) - \frac{1}{2} \right| .$$

The following simple cost function on triangulations, which picks out the angle measure of the largest angle in the mesh, will also be useful.

$$E_{\max}(V,T) = E_{\max}(T) = \max_{\theta \in T} \theta$$

Now we are prepared to prove the following two corollaries to Proposition 6.1.1.

**Corollary 6.1.2.** *If $f$ is a strictly increasing function of $\theta$ for $\theta \in [0, \pi]$, then* $\arg\min E_f = \arg\min E_{\max}$.

*Proof.* The cost function $E_{\max}$ has the form $E_g$ where $g(\theta) = \theta$ is the identity function on $[0, \pi]$. Since $g$ and $f$ are both strictly increasing functions, Proposition 6.1.1 applies in both directions. Thus $\arg\min E_f \subseteq \arg\min E_{\max}$ and $\arg\min E_{\max} \subseteq \arg\min E_f$. We conclude that $\arg\min E_f = \arg\min E_{\max}$. □

**Corollary 6.1.3.** *Let $V$ be a fixed set of vertices and suppose that all (admissible) triangulations of $V$ have maximum angle at least $\pi/2$. Then a triangulation minimizing $E_{\max}$ minimizes $E_\infty$ and vice versa.*

*Proof.* Define the function $f$ on $[0, \pi]$ by

$$f(\theta) = \begin{cases} \theta/\pi & \text{if } 0 \leq \theta < \pi/2, \\ 1/2 - \cos(\theta) = |\cos(\theta) - 1/2| & \text{if } \pi/2 \leq \theta \leq \pi. \end{cases}$$

Now $E_f$ is a strictly increasing function, and, by the hypothesis, for any triangulation $T$ of $V$ we can choose some $\theta_T \geq \pi/2$ such that $E_f(T) = f(\theta_T) = 1/2 - \cos(\theta_T)$. The function $|\cos(\theta) - 1/2|$

that defines $E_\infty$ is not strictly increasing on $[0, \pi]$, but $|\cos(\theta) - 1/2| \leq 1/2$ on $[0, \pi/2)$, so $E_\infty(T) = E_f(T) = f(\theta_T)$. Thus $\arg\min E_f = \arg\min E_\infty$ and $E_f$ is effectively the same as $E_\infty$. Since $f$ is strictly increasing on $[0, \pi]$, Corollary 6.1.2 applies, and $\arg\min E_\infty = \arg\min E_f = \arg\min E_{\max}$. □

Corollary 6.1.3 says that if $V$ has no 2-well-centered triangulation, then the triangulations that minimize $E_\infty$ are exactly the triangulations that minimize the maximum angle. The proof of Corollary 6.1.3 cannot be extended to the case where there exists a 2-well-centered triangulation $T$ of $V$; in that case we may have $E_\infty(T) = \cos(\theta_T) - 1/2$ for some $\theta_T$ near 0. Theorem 6.1.5, however, which we prove based on the next lemma, shows that the statement of Corollary 6.1.3 does extend to the case of a 2-well-centered triangulation $T$ of $V$. (A somewhat more general version of Thm 6.1.5 appeared in [8], with a different proof.)

**Lemma 6.1.4.** *Let $V$ be a fixed set of vertices in $\mathbb{R}^2$, not all collinear. If the Delaunay complex of $V$ is not a triangulation, i.e., if a Delaunay triangulation of $V$ is not unique, then no Delaunay triangulation of $V$ is 2-well-centered.*

*Proof.* If the Delaunay complex of $V$ has a cell that is not a triangle, then the cell is a convex polygon with $k > 3$ vertices. The vertices of the polygon are cocircular, and the circumball of the polygon contains no vertices except the $k$ vertices of the polygon. A (nonunique) Delaunay triangulation of $V$ is obtained by arbitrarily triangulating each cell of the Delaunay complex that is not a triangle.

We claim that for $k > 3$, any triangulation of a $k$-gon in the Delaunay complex must have a nonacute triangle. Indeed, such a triangulation has at most one acute triangle. The vertices of the $k$-gon are cocircular, so every triangle of the triangulation of the $k$-gon has the same circumcenter, the center of the circle that passes through all the vertices of the $k$-gon. At most one of these $k - 2 \geq 2$ triangles has the circumcenter in its interior, and a triangle is 2-well-centered if and only if its circumcenter is in its interior. □

**Theorem 6.1.5.** *Let $V$ be a fixed set of vertices in $\mathbb{R}^2$, not all collinear. If there exists a triangulation $T$ of $V$ that is 2-well-centered, then $T$ is the unique 2-well-centered triangulation of $V$. Moreover $T$ is the Delaunay triangulation of $V$ and minimizes the maximum angle among triangulations of $V$.*

*Proof.* Suppose that $T_0$ is a 2-well-centered triangulation of $V$. Then $T_0$ is a Delaunay triangulation of $V$. (This result of Rajan [47] can be proved as an easy corollary of Theorem 3.1.1. See Sec. 6.2.) By Lemma 6.1.4, $T_0$ is the unique Delaunay triangulation in this case.

Consider some triangulation $T \neq T_0$ of $V$. If $T$ were a 2-well-centered triangulation, then $T$ would be a Delaunay triangulation. But this would contradict $T \neq T_0$, since $T_0$ is the unique Delaunay triangulation. Thus $T$ is not 2-well-centered, and the maximum angle in $T$ is at least $\pi/2$. We conclude that $T_0$ minimizes the maximum angle and is the unique 2-well-centered triangulation of $V$. □

Putting Theorem 6.1.5 together with Corollary 6.1.3 provides the answer to the question that started this section; given a fixed point set $V$ and considering triangulations that cover the convex hull of $V$, we can now more easily identify triangulations that minimize $E_\infty(V, T)$.

**Corollary 6.1.6.** *Let $V$ be a fixed set of vertices in $\mathbb{R}^2$. A triangulation $T$ minimizes the maximum angle if and only if $T$ minimizes $E_\infty(V, T)$.*

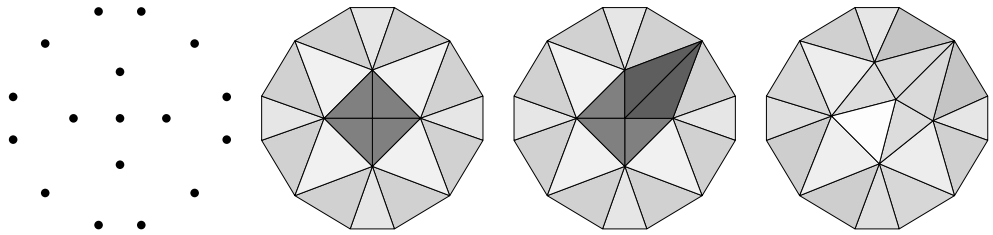

Figure 6.1: The minmax triangulation of a point set $V$ may have a lonely interior vertex even if there is a triangulation of $V$ with no lonely vertices. From left to right, this shows a point set $V$, the minmax triangulation $T_0$ of $V$, a triangulation $T_1$ of $V$ with no lonely vertices, and a 2-well-centered triangulation obtained by relocating vertices to optimize $E_4$ for triangulation $T_1$.

*Proof.* If $V$ has a 2-well-centered triangulation $T_0$, then Theorem 6.1.5 applies, and $T_0$ is the unique triangulation that minimizes the maximum angle. In addition, $E_\infty(V, T_0) < 1/2$, and since no other triangulation is 2-well-centered, $E_\infty(V, T) \geq 1/2$ for any triangulation $T \neq T_0$. Otherwise $V$ has no 2-well-centered triangulation, and Corollary 6.1.3 applies. □

In the early 1990s, Edelsbrunner, Tan, and Waupotitsch studied the problem of minimizing the maximum angle and developed an $O(n^2 \log n)$ time algorithm for computing the minmax triangulation [24]. Now that we know that a triangulation $T$ that minimizes $E_\infty(V, T)$ is a minmax triangulation, their algorithm gives us a reasonably efficient algorithm to compute the triangulation that minimizes $E_\infty(V, T)$.

In the mesh optimization algorithm discussed in Chapter 5, we adopted the convention that the mesh connectivity table remains fixed during optimization, and we developed a preprocessing algorithm that makes local modifications to the mesh. The fixed mesh connectivity table sets our method apart from the methods of [20] and [1], which alternate recalculating the optimal triangulation with relocating vertices. We have now seen that it is possible (in $\mathbb{R}^2$, at least) to compute a triangulation that minimizes $E_\infty$. Considering the effectiveness of [20] and [1], we note that an experimental study to try to minimize $E_\infty$ by alternating between recomputing the optimal triangulation and optimizing vertex locations might be a worthwhile study. There are, however, a number of reasons we have opted to avoid this in our algorithm.

The primary reason we avoid recomputing the optimal triangulation is that the minmax triangulation may have lonely vertices, and we want to prevent the introduction of lonely vertices into the mesh. A simple example in Fig. 6.1 illustrates this point. The minmax triangulation of the point set $V$ in Fig. 6.1 has a lonely vertex. In addition, for the minmax triangulation the vertex locations optimize both $E_\infty$ and $E_4$. Thus it is a fixed point for a method that seeks to optimize $E_\infty$ by alternating between computing the minmax triangulation and relocating vertices.

If we change the triangulation by local preprocessing, though, we obtain a triangulation $T_1$ that has no lonely vertices. For triangulation $T_1$ the vertex locations do not optimize $E_\infty$, and relocating vertices to optimize $E_4$ produces a 2-well-centered mesh.

This objection to computing the minmax triangulation during mesh optimization motivates the problem of computing a minmax triangulation among triangulations that have no lonely vertices. Unfortunately, it is not clear whether this problem has an efficient solution.

A second reason we avoid recomputing the minmax triangulation is efficiency. The computation

takes $O(n^2 \log n)$ time. This running time is polynomial in $n$ but is larger than the $O(n \log n)$ time to compute the Delaunay triangulation, which optimizes the energies defined in [20] and [1]. Furthermore, the Delaunay triangulation is widely used, and there are several good implementations of algorithms to compute the Delaunay triangulation, but the minmax triangulation is not widely used, and the author knows of no good implementations of an algorithm that computes it.

We also note that the minmax triangulation of a point set may bear little resemblance to an input triangulation. If a user has a triangulation that is good in many respects but is not 2-well-centered, then computing the minmax triangulation may make undesired changes to the mesh. The local mesh modifications of the preprocessing algorithm may better preserve the initial mesh.

Finally, we comment that neither the local preprocessing algorithm nor the polynomial time algorithm for computing the minmax angle triangulation of a point set in $\mathbb{R}^2$ has an obvious generalization to higher dimensions.

## 6.2 Relationship to the Delaunay Triangulation

As early as 1991, Rajan showed that if a point set $V$ has an $n$-well-centered triangulation $T$, then $T$ is the Delaunay triangulation of the point set [48]. Indeed, it is not hard to prove this using Theorem 3.1.1.

**Proposition 6.2.1.** *If a simplicial mesh $T$ of a convex subset of $\mathbb{R}^n$ is $n$-well-centered, then the mesh is a Delaunay triangulation of its vertex set $V$.*

*Proof.* Let $\tau^{n-1}$ be a facet in $T$. If $\tau^{n-1}$ lies on the boundary of the convex hull of $V$, then it is automatically a locally Delaunay facet. Otherwise $\tau^{n-1}$ is incident to two $n$-simplices $\sigma_u^n = u * \tau^{n-1}$ and $\sigma_v^n = v * \tau^{n-1}$. Since $\sigma_v^n$ is $n$-well-centered, Theorem 3.1.1 tells us that $v$ lies outside the circumball of $\tau^{n-1}$. Now $\text{aff}(\tau^{n-1})$ cuts $C(\sigma_u^n)$ into two pieces, and the piece that lies in the same halfspace as $v$ is inside the circumball of $\tau^{n-1}$. Thus $v$ lies outside the circumball of $\sigma_u^n$, and $\tau^{n-1}$ is locally Delaunay.

Since every facet of $T$ is locally Delaunay, $T$ is globally Delaunay [22]. □

Since the late 1970's it has been known that in $\mathbb{R}^2$ the Delaunay triangulation maximizes the minimum angle [57]. Thus Theorem 6.1.5 says that a 2-well-centered triangulation in the plane enjoys a sort of double optimality in that it both maximizes the minimum angle and minimizes the maximum angle. Does this double optimality extend to higher dimensions? In particular, does an $n$-well-centered triangulation in $\mathbb{R}^n$ have this double optimality for the $h/R$ generalization of the angle?

We will see that in higher dimensions there is optimality in one direction. Optimality in the other direction is still an open question. We do show, however, that the Delaunay triangulation, which minimizes the maximum $h/R$ in $\mathbb{R}^2$, does not always minimize the maximum $h/R$ in $\mathbb{R}^3$. We also prove that the maximum $h/R$ value occurs at a locally Delaunay facet for triangulations in $\mathbb{R}^2$ and $\mathbb{R}^3$. We show that this result does not extend to higher dimensions and discuss a related local optimality result for Delaunay triangulations. First we show that an $n$-well-centered triangulation in $\mathbb{R}^n$ maximizes the minimum $h/R$. This result is a straightforward generalization of Theorem 6.1.5, which shows that a 2-well-centered triangulation minimizes the maximum angle. (The minmax angle

triangulation is the maxmin $h/R$ triangulation.) The proof of this result is much the same as the proof of Theorem 6.1.5.

**Theorem 6.2.2.** *Let $V$ be a fixed set of $\geq n+1$ vertices in $\mathbb{R}^n$. If there exists an $n$-dimensional triangulation $T$ of $V$ that is $n$-well-centered, then $T$ is the unique $n$-well-centered triangulation of $V$ and maximizes the minimum $h/R$ among triangulations of $V$.*

*Proof.* Let $T_0$ be an $n$-well-centered triangulation of $V$. By Proposition 6.2.1, $T_0$ is a Delaunay triangulation. Uniqueness of the Delaunay triangulation follows from the higher-dimensional analog of Lemma 6.1.4. Any nonunique Delaunay triangulation has some set of $\geq n+2$ cospherical vertices triangulated into $\geq 2$ $n$-simplices. All of these $n$-simplices have the same circumcenter, so they cannot all be $n$-well-centered.

If we consider a triangulation $T \neq T_0$ of vertex set $V$, then $T$ is not $n$-well-centered, since otherwise it would be a Delaunay triangulation and $T_0$ would not be unique. Since $T$ is not $n$-well-centered, $T$ contains some $n$-simplex $\sigma^n$, and a vertex $v \prec \sigma^n$ such that $h(v,\sigma^n)/R(\sigma^n) \leq 0$. For $T_0$, on the other hand, $h(v,\sigma^n)/R(\sigma^n) > 0$ for every $v \prec \sigma^n$ in $T_0$. Thus $T_0$ maximizes the minimum $h/R$. □

Since the Delaunay triangulation minimizes the maximum $h/R$ among triangulations of a fixed point set $V$ in $\mathbb{R}^2$, one might hope to extend this result to higher dimensions and use it to prove double optimality for $n$-well-centered triangulations in $\mathbb{R}^n$. Unfortunately, the result does not extend to even $\mathbb{R}^3$, as we see in the following example.

**Example 6.2.3.** Let $V$ be the set of vertices in $\mathbb{R}^3$ given by

$$\{v_0 = (-1,0,0),\quad v_1 = (1/2,-\sqrt{3}/2,0),\quad v_2 = (1/2,\sqrt{3}/2,0),\quad v_3 = (0,0,-1/2),\quad v_4 = (0,0,1/2)\}\,.$$

Then the (unique) Delaunay triangulation of $V$ consists of three congruent tetrahedra $[v_0v_1v_3v_4]$, $[v_0v_2v_4v_3]$, and $[v_1v_2v_3v_4]$ meeting along edge $v_3v_4$. The $h/R$ values in each of these three tetrahedra are approximately

$$-0.19611614,\quad -0.19611614,\quad 0.72057669,\quad 0.72057669\,.$$

If we flip edge $v_3v_4$ for face $v_0v_1v_2$ we obtain a triangulation consisting of two congruent tetrahedra $[v_0v_1v_3v_2]$ and $[v_0v_1v_2v_4]$. Each of these tetrahedra has $h/R$ values of approximately

$$-0.6,\quad 0.70710678,\quad 0.70710678,\quad 0.70710678\,.$$

We see that the Delaunay triangulation does not minimize the maximum $h/R$ value among triangulations of $V$.

In the example, the Delaunay triangulation of $V$ is not 3-well-centered. Thus $V$ has no 3-well-centered triangulation, and the example does not answer the question of whether an $n$-well-centered triangulation possesses a double optimality. This example has another interesting feature as well. In both triangulations the maximum $h(v_i,\sigma^n)/R(\sigma^n)$ value occurs at some $v_i \prec \sigma^n$ such that the facet $\tau_i^{n-1}$ opposite $v_i$ is a locally Delaunay facet, where a locally Delaunay facet is defined as follows.

**Definition.** A facet $\tau^{n-1}$ in an $n$-dimensional mesh is said to be *locally Delaunay* if either $\tau^{n-1}$ is on the boundary of the mesh or $\tau^{n-1}$ is incident to two $n$-simplices $\sigma_u^n = u * \tau^{n-1}$ and $\sigma_v^n = v * \tau^{n-1}$ such that $v$ lies outside the circumball of $\sigma_u^n$ or on $C(\sigma_u^n)$. (Vertex $v$ lies outside the circumball of $\sigma_u^n$ if and only if vertex $u$ lies outside the circumball of $\sigma_v^n$.)

The fact that the maximum $h/R$ value occurs at a locally Delaunay facet in the example is not accidental. Indeed, we will prove the following proposition later in this chapter.

**Proposition 6.2.4.** *Let $V$ be a fixed set of points in $\mathbb{R}^n$ for $n = 2$ or $n = 3$, and let $T$ be a triangulation of $V$ with $n$-simplices. Wherever the maximum $h(v, \sigma^n)/R(\sigma^n)$ value in $T$ occurs, the facet opposite $v$ in $\sigma^n$ is a locally Delaunay facet.*

We delay the proof of Proposition 6.2.4 temporarily to assemble several related results. The first two lemmas are basically geometric lemmas that apply in any dimension $n \geq 2$. For these two lemmas we adopt the following notation. We consider an $n$-simplex $\sigma^n = v_0 v_1 \dots v_n$ and label its facets $\tau_i^{n-1}$ so that $\tau_i^{n-1}$ is the facet opposite $v_i$. We label the facets of $\tau_n^{n-1}$, which are a subset of the $(n-2)$-dimensional faces of $\sigma^n$, as $\rho_i^{n-2} = \tau_i^{n-1} \cap \tau_n^{n-1}$. See also the left side of Fig. 6.2.

**Lemma 6.2.5.** *$|h(v_i, \sigma^n)| \leq |h(v_n, \sigma^n)|$ if and only if $\left\|c(\tau_i^{n-1}) - c(\rho_i^{n-2})\right\| \geq \left\|c(\tau_n^{n-1}) - c(\rho_i^{n-2})\right\|$.*

*Proof.* Vector $c(\sigma^n) - c(\tau_i^{n-1})$ is orthogonal to $\operatorname{aff}(\tau_i^{n-1})$ for each $i = 0, 1, \dots, n$, so we can apply the Pythagorean theorem to write

$$\begin{aligned}\left\|c(\sigma^n) - c(\rho_i^{n-2})\right\|^2 &= \left\|c(\sigma^n) - c(\tau_i^{n-1})\right\|^2 + \left\|c(\tau_i^{n-1}) - c(\rho_i^{n-2})\right\|^2 \\ &= h(v_i, \sigma^n)^2 + \left\|c(\tau_i^{n-1}) - c(\rho_i^{n-2})\right\|^2\end{aligned}$$

and

$$\begin{aligned}\left\|c(\sigma^n) - c(\rho_i^{n-2})\right\|^2 &= \left\|c(\sigma^n) - c(\tau_n^{n-1})\right\|^2 + \left\|c(\tau_n^{n-1}) - c(\rho_i^{n-2})\right\|^2 \\ &= h(v_n, \sigma^n)^2 + \left\|c(\tau_n^{n-1}) - c(\rho_i^{n-2})\right\|^2 .\end{aligned}$$

□

Another way to think about Lemma 6.2.5 is to consider the relationship of $h(v_i, \sigma^n)$ to $R(\tau_i^{n-1})$. For a fixed $R(\sigma^n)$, as $|h(v_i, \sigma^n)|$ grows, $R(\tau_i^{n-1})$ shrinks. Thus $|h(v_i, \sigma^n)| \leq |h(v_n, \sigma^n)|$ if and only if $R(\tau_i^{n-1}) \geq R(\tau_n^{n-1})$. This observation could be used to write a different proof of Lemma 6.2.5 based on the fact that $R(\tau_i^{n-1})^2 = R(\rho_i^{n-2})^2 + \left\|c(\tau_i^{n-1}) - c(\rho_i^{n-2})\right\|^2$.

**Lemma 6.2.6.** *Let $P$ be the map that sends a point $x$ in $\mathbb{R}^n$ to the orthogonal projection of $x$ into $\operatorname{aff}(\tau_n^{n-1})$. If $|h(v_i, \sigma^n)| \leq |h(v_n, \sigma^n)|$ and $h(v_n, \sigma^n) < 0$, then $P(v_n)$ lies in the interior of the reflection of the circumball of $\tau_n^{n-1}$ across $\operatorname{aff}(\rho_i^{n-2})$.*

*Proof.* Figure 6.2 illustrates Lemma 6.2.6 for a general tetrahedron. We consider a simplex $\sigma^n$ satisfying $|h(v_i, \sigma^n)| \leq |h(v_n, \sigma^n)|$ and $h(v_n, \sigma^n) < 0$. We first prove the lemma for the special case $c(\tau_n^{n-1}) = c(\rho_i^{n-2})$. In this special case, reflection across $\operatorname{aff} \rho_i^{n-2}$ is a symmetry of the circumball of $\tau_n^{n-1}$, so it suffices to prove that $P(v_n)$ lies in the circumball of $\tau_n^{n-1}$.

Since $h(v_n, \sigma^n) < 0$, the hyperplane $\operatorname{aff}(\tau_n^{n-1})$ separates $c(\sigma^n)$ from $v_n$. We say in this proof that points in the same halfspace as $c(\sigma^n)$ (respectively $v_n$) are above (below) $\operatorname{aff}(\tau_n^{n-1})$. Since $v_n$ is

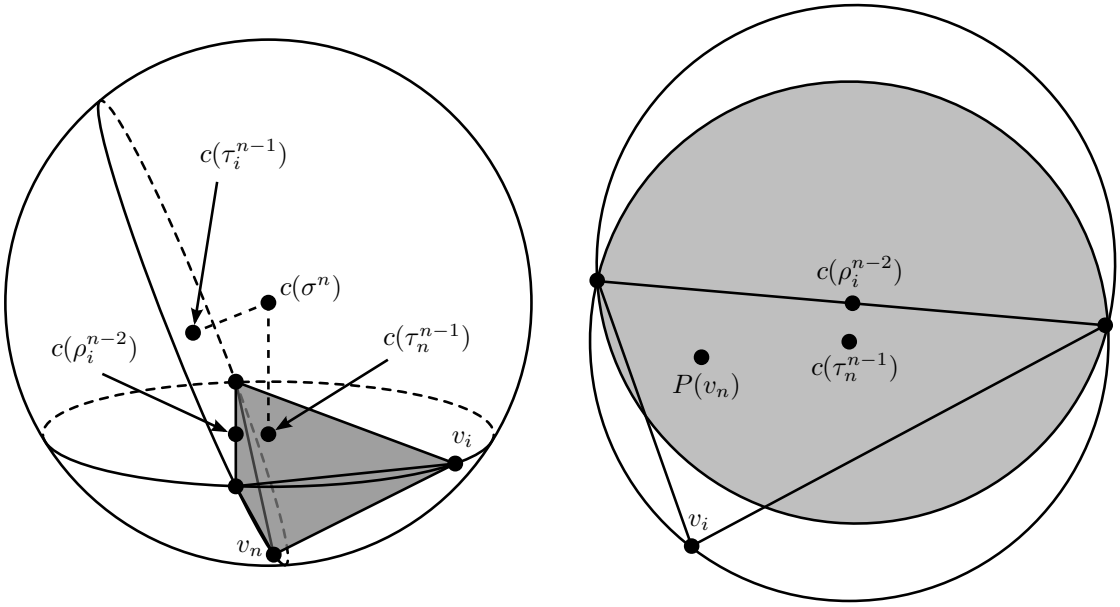


Figure 6.2: Consider a simplex $\sigma^n$ with facets $\tau_n^{n-1}$ and $\tau_i^{n-1}$ such that $|h(v_i, \sigma^n)| \leq |h(v_n, \sigma^n)|$ and $h(v_n, \sigma^n) < 0$ (left). Let $P$ be the orthogonal projection into $\text{aff}(\tau_n^{n-1})$. Because $h(v_n, \sigma^n) < 0$, we know that $P(v_n)$ lies in the circumball of $\tau_n^{n-1}$. Lemma 6.2.6 says that for $\rho_i^{n-2} = \tau_i^{n-1} \cap \tau_n^{n-1}$, $P(v_n)$ also lies in the reflection of the circumball of $\tau_n^{n-1}$ across $\rho_i^{n-2}$. Thus $P(v_n)$ lies in the intersection of two balls in $\text{aff}(\tau_n^{n-1})$, as shown in the sketch on the right.

below $\text{aff}(\tau_n^{n-1})$, it lies in a lower spherical cup of $C(\sigma^n)$. Thus $P(v_n)$ always lies in the circumball of $\tau_n^{n-1}$. In particular, this proves the lemma for the special case $c(\tau_n^{n-1}) = c(\rho_i^{n-2})$.

So we assume that $c(\tau_n^{n-1}) \neq c(\rho_i^{n-2})$. Then $\left\|c(\tau_n^{n-1}) - c(\rho_i^{n-2})\right\| > 0$, and since $|h(v_i, \sigma^n)| \leq |h(v_n, \sigma^n)|$, this implies (by Lemma 6.2.5) that $\left\|c(\tau_i^{n-1}) - c(\rho_i^{n-2})\right\| > 0$ as well. Thus vectors $c(\rho_i^{n-2}) - c(\tau_n^{n-1})$ and $c(\rho_i^{n-2}) - c(\tau_i^{n-1})$ both have well-defined direction.

Now vertex $v_n$ lies on $C(\tau_i^{n-1})$, and we can decompose vector $v_n - c(\tau_i^{n-1})$ into two orthogonal vectors $u_i$ and $w_i$ as shown at left in Fig. 6.3, with $u_i$ pointing in the direction $c(\rho_i^{n-2}) - c(\tau_i^{n-1})$ and $w_i$ in the linear subspace $\text{aff}(\rho_i^{n-2}) - c(\rho_i^{n-2})$. Since $u_i$ and $w_i$ are orthogonal, we can apply the Pythagorean theorem to write

$$\|u_i\|^2 + \|w_i\|^2 = R(\tau_i^{n-1})^2 = R(\rho_i^{n-2})^2 + \left\|c(\rho_i^{n-2}) - c(\tau_i^{n-1})\right\|^2 . \tag{6.1}$$

After $w_i$ is defined we can choose a vector $u_{n,i}$ in the direction of $c(\rho_i^{n-2}) - c(\tau_n^{n-1})$ such that $c(\tau_n^{n-1}) + w_i + u_{n,i}$ lies on $C(\tau_n^{n-1})$. Then $w_i$ is orthogonal to $u_{n,i}$, so

$$\|u_{n,i}\|^2 + \|w_i\|^2 = R(\tau_n^{n-1})^2 = R(\rho_i^{n-2})^2 + \left\|c(\rho_i^{n-2}) - c(\tau_n^{n-1})\right\|^2 . \tag{6.2}$$

Rearranging equations (6.1) and (6.2), we obtain

$$\|u_i\|^2 - \left\|c(\rho_i^{n-2}) - c(\tau_i^{n-1})\right\|^2 = R(\rho_i^{n-2})^2 - \|w_i\|^2 = \|u_{n,i}\|^2 - \left\|c(\rho_i^{n-2}) - c(\tau_n^{n-1})\right\|^2 . \tag{6.3}$$

Notice, then, that $|h(v_i, \sigma^n)| \leq |h(v_n, \sigma^n)|$, so by Lemma 6.2.5 we have $\left\|c(\tau_i^{n-1}) - c(\rho_i^{n-2})\right\| \geq \left\|c(\tau_n^{n-1}) - c(\rho_i^{n-2})\right\|$. Combining this fact with equation (6.3) and observing that $R(\rho_i^{n-2})^2 -$

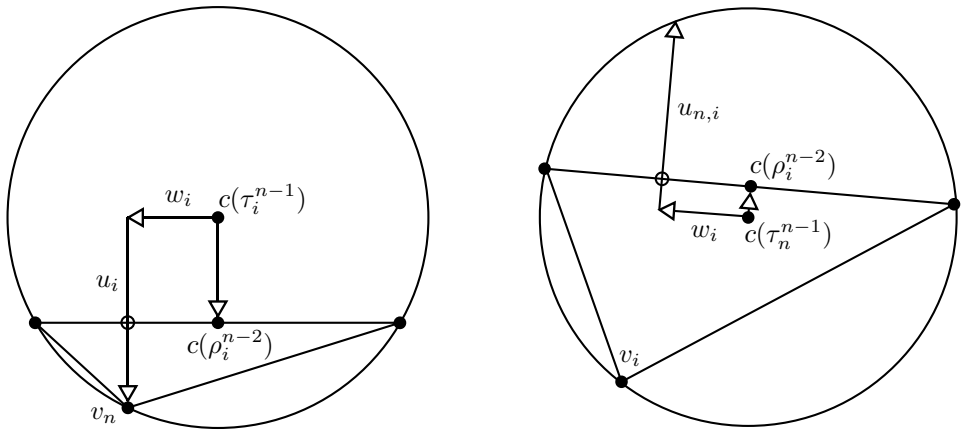


Figure 6.3: In the general case in the proof of Lemma 6.2.6, we decompose vector $v_n - c(\tau_i^{n-1})$ into orthogonal vectors $w_i$ and $u_i$, with $u_i$ pointing in the direction of $c(\rho_i^{n-2}) - c(\tau_i^{n-1})$ (left). Then we define vector $u_{n,i}$ in the direction of $c(\rho_i^{n-2}) - c(\tau_n^{n-1})$ such that $c(\tau_n^{n-1}) + w_i + u_{n,i}$ lies on the circumsphere of $\tau_n^{n-1}$ (right). The proof uses these vectors and the point $c(\rho_i^{n-2}) + w_i$, which is marked by an open circle in each of these sketches.

$\|w_i\|^2 > 0$ holds because $v_n$ is below $\text{aff}(\tau_n^{n-1})$, we can conclude that

$$\|u_{n,i}\| - \left\|c(\rho_i^{n-2}) - c(\tau_n^{n-1})\right\| \geq \|u_i\| - \left\|c(\rho_i^{n-2}) - c(\tau_i^{n-1})\right\| .$$

Now the point in $\rho_i^{n-2}$ closest to vertex $v_n$ is the point $c(\rho_i^{n-2}) + w_i$, and the distance between these two points is $\|u_i\| - \left\|c(\rho_i^{n-2}) - c(\tau_i^{n-1})\right\|$. Moreover, the distance from $P(v_n)$ to $c(\rho_i^{n-2}) + w_i$ is strictly less than the distance from $v_n$ to $c(\rho_i^{n-2}) + w_i$. This completes the proof, for $P(v_n)$ lies in $\tau_n^{n-1}$ on a line through $c(\rho_i^{n-2}) + w_i$ orthogonal to $\text{aff}(\rho_i^{n-2})$, and the distance along that line to the closer point on $C(\tau_n^{n-1})$ is $\|u_{n,i}\| - \left\|c(\rho_i^{n-2}) - c(\tau_n^{n-1})\right\|$. □

Now we can apply Lemma 6.2.6 to prove a result that holds for every simplex $\sigma^n$ in dimensions $n = 2$ and $n = 3$, but does not hold for some simplices $\sigma^n$ if $n \geq 4$. This result is key to proving Proposition 6.2.4, and we will see that Proposition 6.2.4 does not extend to dimensions $n \geq 4$.

**Proposition 6.2.7.** *In a simplex $\sigma^n$ for $n = 2$ or $n = 3$,*

$$\max_{v \prec \sigma^n} \left| \frac{h(v, \sigma^n)}{R(\sigma^n)} \right| = \max_{v \prec \sigma^n} \frac{h(v, \sigma^n)}{R(\sigma^n)}$$

*Proof.* Since $h$ and $R$ scale together, we may assume without loss of generality that $R(\sigma^n) = 1$ and proceed to show that $\max_{v \prec \sigma^n} |h(v, \sigma^n)| = \max_{v \prec \sigma^n} h(v, \sigma^n)$. If $h(v, \sigma^n) \geq 0$ for every $v \prec \sigma^n$, then there is nothing to show, so we assume that there exists some vertex $v$ such that $h(v, \sigma^n) < 0$, and we label the vertices $v_0, v_1, \ldots, v_n$ such that $h(v_n, \sigma^n) = \min_{v \prec \sigma^n} h(v, \sigma^n) < 0$.

We first consider the case $n = 2$. In this case, $\cos(\measuredangle v_2) = h(v_2, \sigma^2) < 0$ implies that $\measuredangle v_2 > \pi/2$. Moreover, since $\measuredangle v_i < (\pi - \measuredangle v_2)$ for $i = 0, 1$, we have $\cos(\measuredangle v_i) = h(v_i, \sigma^2) > \left|h(v_2, \sigma^2)\right|$ for both $i = 0, 1$.

The case $n = 3$ is more difficult. In that case we look at the facet $\tau_3^2 \prec \sigma^3$ and consider the reflection of its circumball through each of its edges. As shown in Fig. 6.4, the reflected circumspheres intersect at the orthocenter of the triangle, and any point in the circumball of the original triangle

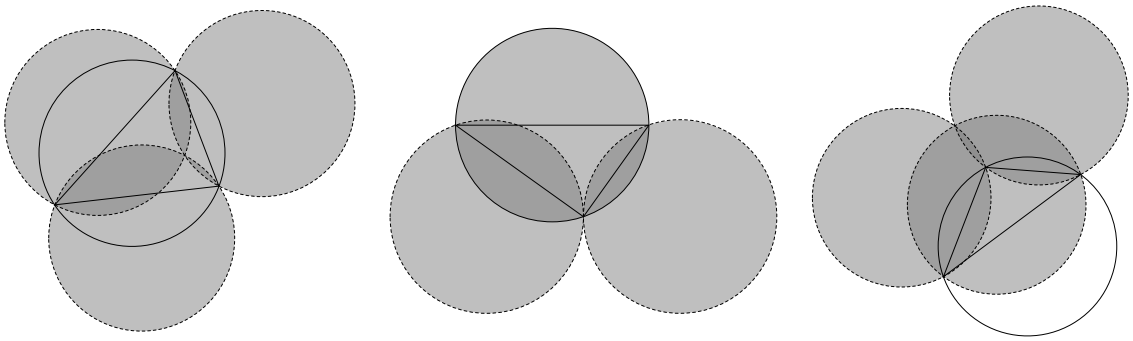

Figure 6.4: Each of these sketches shows a triangle, its circumball, and the reflection of the circumball across each edge of the triangle. The sketches are from left to right for the three different cases acute, right, and obtuse. In each case, a point in the circumball of the original triangle lies is in the interior of at most two of the reflected copies of the circumball.

lies in the interior of at most two of the reflected circumballs. (If the original triangle is obtuse, as in the case at right in Fig. 6.4, there is a nonempty open set where all three reflected circumballs intersect, but that region lies outside the circumball of the triangle.)

In particular, the point $P(v_3)$ lies in at most two of the reflected circumballs. Let $\rho_0^1$ be an edge of $\tau_3^2$ such that $P(v_3)$ is not interior to the reflection of the circumball of $\tau_3^2$ across $\rho_0^1$. By the contrapositive of Lemma 6.2.6, $\left|h(v_0, \sigma^3)\right| > \left|h(v_3, \sigma^3)\right|$. Thus $\max_{v \prec \sigma^3} \left|h(v, \sigma^3)\right| > \left|h(v_3, \sigma^3)\right|$. We chose $v_3$ such that $h(v_3, \sigma^3)$ is minimal, so this completes the proof. □

The next lemma can be proved several different ways. Indeed, some might consider the statement an obvious one. Nonetheless, we state the result for easy later reference, and we include a proof for the sake of completeness.

**Lemma 6.2.8.** *For $n \geq 2$, let $\tau^{n-1}$ be a fixed $(n-1)$-dimensional simplex embedded in $\mathbb{R}^m$, $m > n$ and consider the family of $n$-simplices $v * \tau^{n-1}$ for some vertex $v \in \mathbb{R}^m$. Then $h(v, \sigma^n) / R(\sigma^n)$ is an increasing function of $h(v, \sigma^n)$.*

*Proof.* If $v \in \text{aff}(\tau^{n-1})$, then $h(v, \sigma^n) = -\infty$ and $h(v, \sigma^n)/R(\sigma^n) = -1$ are both minimal, so we assume $v \notin \text{aff}(\tau^{n-1})$. By the Pythagorean theorem, we have

$$R(\sigma^n)^2 = h(v, \sigma^n)^2 + R(\tau^{n-1})^2 \text{ , which implies}$$
$$\left(\frac{h(v, \sigma^n)}{R(\sigma^n)}\right)^2 = 1 - \frac{R(\tau^{n-1})^2}{R(\sigma^n)^2}$$

Since $R(\tau^{n-1})$ is fixed, the first equation shows that $R(\sigma^n)$ increases as $|h(v, \sigma^n)|$ increases. Moreover, the second equation shows that $|h(v, \sigma^n)| \,/\, R(\sigma^n)$ increases as $R(\sigma^n)$ increases.

Thus $|h(v, \sigma^n)| \,/\, R(\sigma^n)$ is an increasing function of $|h(v, \sigma^n)|$. A straightforward case analysis comparing $h(v_1, \sigma^n)$ and $h(v_2, \sigma^n)$ when the terms are negative, zero, and positive completes the proof. □

Finally we are in a position to prove Proposition 6.2.4.

*Proof of Proposition 6.2.4.* It suffices to show that in $\mathbb{R}^n$, $n = 2, 3$, for any facet $\tau^{n-1}$ that is not

locally Delaunay and any vertex $v$ opposite $\tau^{n-1}$ in some $n$-simplex $\sigma^n = v * \tau^{n-1}$, $h(v, \sigma^n)/\, R(\sigma^n)$ is not maximal.

We consider a particular facet $\tau^{n-1}$ that is not locally Delaunay. Facet $\tau^{n-1}$ is not on the boundary of the mesh, so there are exactly two $n$-simplices incident to $\tau^{n-1}$. We denote these by $\sigma_u^n = u * \tau^{n-1}$ and $\sigma_v^n = v * \tau^{n-1}$, and we say that $\sigma_u^n$ is above $\text{aff}(\tau_{n-1})$, which is above $\sigma_v^n$. Now $c(\sigma_u^n)$ and $c(\sigma_v^n)$ both lie on the line through $c(\tau^{n-1})$ orthogonal to $\text{aff}(\tau^{n-1})$, and since $\tau^{n-1}$ is not locally Delaunay, $c(\sigma_v^n)$ is above $c(\sigma_u^n)$.

It follows that at least one of $\sigma_u^n$, $\sigma_v^n$ is not $n$-well-centered because its circumcenter is on the "wrong" side with respect to $\text{aff}(\tau^{n-1})$. Suppose without loss of generality that this is simplex $\sigma_u^n$. Then $c(\sigma_u^n)$ is below $\text{aff}(\tau^{n-1})$, and $h(u, \sigma_u^n)/\, R(\sigma_u^n) < 0$. By Proposition 6.2.7 there exists some vertex $\widetilde{u} \prec \sigma_u^n$, $\widetilde{u} \neq u$, such that $|h(\widetilde{u}, \sigma_u^n)/\, R(\sigma_u^n)|$ is maximal in $\sigma_u^n$, and $h(\widetilde{u}, \sigma_u^n)$ is positive.

There are two cases to consider for $\sigma_v^n$. If $c(\sigma_v^n)$ is above $\text{aff}(\tau^{n-1})$, then $h(v, \sigma_v^n)/\, R(\sigma_v^n) < 0 < h(\widetilde{u}, \sigma_u^n)/\, R(\sigma_u^n)$. Otherwise $c(\sigma_v^n)$ is on or below $\text{aff}(\tau^{n-1})$, but because it is above $c(\sigma_u^n)$ we have $|h(v, \sigma_v^n)| < |h(u, \sigma_u^n)|$. Then by Lemma 6.2.8 we have $|h(v, \sigma_v^n)/\, R(\sigma_v^n)| < |h(u, \sigma_u^n)/\, R(\sigma_u^n)|$. Hence $h(v, \sigma_v^n)/\, R(\sigma_v^n) < h(\widetilde{u}, \sigma_u^n)/\, R(\sigma_u^n)$.

We see that neither $h(u, \sigma_u^n)/\, R(\sigma_u^n)$ nor $h(v, \sigma_v^n)/\, R(\sigma_v^n)$ is maximal. □

Lemma 6.2.8 says that an $n$-dimensional Delaunay triangulation in $\mathbb{R}^n$ is in some sense a locally optimal triangulation for minimizing the maximum $h/R$. Consider a particular facet $\tau^{n-1}$ that is a facet of the Delaunay triangulation. Suppose that $\tau^{n-1}$ appears as a facet in some triangulation $T$, and let $\sigma_u^n = u * \tau^{n-1}$ be a tetrahedron incident to $\tau^{n-1}$. We call the halfspace containing $\sigma_u^n$ the halfspace above $\text{aff}(\tau^{n-1})$. If $\sigma_u^n$ is not a Delaunay tetrahedron, i.e., if the circumball of $\sigma_u^n$ contains some vertex $v$, $v \not\prec \sigma_u^n$, then $v$ is above $\text{aff}(\tau^{n-1})$. (If $v$ were below $\text{aff}(\tau^{n-1})$, then any circumball of any simplex $\sigma^n \succ \tau^{n-1}$ would contain either $u$, $v$, or both, so $\tau^{n-1}$ could not be a facet of the Delaunay triangulation.) Define $\sigma_v^n = v * \tau^{n-1}$. It follows from Lemma 6.2.8 that $h(v, \sigma_v^n)/\, R(\sigma_v^n) < h(u, \sigma_u^n)/\, R(\sigma_u^n)$. In other words, if $\sigma_u^n$ is not a Delaunay tetrahedron, then the $h/R$ value above facet $\tau^{n-1}$ in triangulation $T$ is larger than the $h/R$ value above $\tau^{n-1}$ in the Delaunay triangulation.

The idea behind Proposition 6.2.4 is to strengthen this result. In a triangulation $T$, the maximum $h/R$ occurs at a locally Delaunay facet $\tau^{n-1}$. If the simplex containing the maximum $h/R$ is a Delaunay simplex, then the maximum $h/R$ value in $T$ is the same as the maximum $h/R$ value in the Delaunay triangulation. Otherwise $\sigma_u^n$ incident to $\tau^{n-1}$ is not a Delaunay tetrahedron, but maximizes $h/R$. If $\tau^{n-1}$ is a facet of the Delaunay triangulation as well as locally Delaunay, then by retriangulating to get the Delaunay triangulation, we are guaranteed to improve the maximum $h/R$ value at $\tau^{n-1}$.

In $\mathbb{R}^2$ this idea can be turned into an edge-flipping algorithm for computing the Delaunay triangulation, and the Delaunay triangulation in $\mathbb{R}^2$ minimizes the maximum $h/R$. In fact, every triangulation that lexicographically minimizes the vector of decreasing $h/R$-values is a Delaunay triangulation [57, 21].

On the other hand, as we have already seen, in $\mathbb{R}^3$ the Delaunay triangulation does not necessarily minimize the maximum $h/R$. The reason is that retriangulating to get the Delaunay triangulation and improve the $h/R$ value at some specific facet $\tau^{n-1}$ may introduce some other (locally Delaunay) facet that has a larger $h/R$ value than the original $h/R$ value at $\tau^{n-1}$. In the triangulation of

Example 6.2.3 that is not Delaunay, the maximum $h/R$ value of approximately 0.707 occurs at the locally Delaunay facets on the boundary. Switching to the Delaunay triangulation reduces the $h/R$ value at these facets to about $-0.196$ but introduces three interior locally Delaunay facets that have $h/R$ values of about 0.721 in both halfspaces.

We claimed earlier that Proposition 6.2.4 and 6.2.7 do not extend $\mathbb{R}^n$ for $n \geq 4$. The following examples prove this for $\mathbb{R}^4$. It is not hard to generalize the examples to higher dimensions.

**Example.** Let V be the set of vertices in $\mathbb{R}^4$ given by

$$\begin{aligned}
\{v_0 &= (0, 0, -\sqrt{199/100}, -99/10),\\
v_1 &= (0, \sqrt{398/225}, \sqrt{199/900}, -99/10),\\
v_2 &= (-\sqrt{199/150}, \sqrt{199/450}, \sqrt{199/900}, -99/10),\\
v_3 &= (\sqrt{199/150}, \sqrt{199/450}, \sqrt{199/900}, -99/10),\\
v_4 &= (0, 0, 0, -10),\\
v_5 &= (0, 0, 0, 99/10)\}\,.
\end{aligned}$$

Vertices $v_0$, $v_1$, $v_2$, and $v_3$ are the vertices of a regular tetrahedron in the plane $x_4 = -99/10$. The triangulation $T$ of $V$ by the two 4-simplices $[v_0v_1v_2v_3v_4]$ and $[v_0v_1v_2v_5v_3]$ is not a Delaunay triangulation. For $T$ the minimum $h/R$ value is

$$h(v_4, [v_0v_1v_2v_3v_4])/\,R([v_0v_1v_2v_3v_4]) = -0.99\,,$$

and the maximum $h/R$ value is

$$h(v_5, [v_0v_1v_2v_5v_3])/\,R([v_0v_1v_2v_5v_3]) \approx 0.98989925\,.$$

Both the maximum and the minimum occur for vertices opposite facet $[v_0v_1v_3v_2]$, which is not locally Delaunay. Thus the maximum $h/R$ occurs at a facet that is not locally Delaunay, showing that Proposition 6.2.4 does not extend to $\mathbb{R}^4$, and in simplex $[v_0v_1v_2v_3v_4]$ the maximum $|h/R|$ value is $0.99 = |-0.99|$, showing that Proposition 6.2.7 does not extend to $\mathbb{R}^4$.

# Chapter 7

# Experimental Results

The mesh optimization algorithm introduced in Chapter 5 was described as a heuristic for obtaining well-centered meshes. In this chapter we present experimental results of applying that algorithm to a variety of meshes. We begin with a description of our implementation of the mesh optimization algorithm, followed by some general comments about the presentation of the results and the machine used to run the experiments. The rest of the chapter is divided into sections that discuss the experimental results for specific meshes. [1]

The algorithm described in Chapter 5 is focused on energy minimization for energies $E_\infty$ and $E_p$, but also includes a preprocessing method for updating the mesh connectivity of triangle meshes in the plane. We implemented the preprocessing algorithm by writing some MATLAB scripts. The MATLAB scripts are fairly slow, and it is clear that a faster, more robust implementation could be written in some other language, but the MATLAB code sufficed for preprocessing the triangle meshes presented in this chapter.

We argued in Chapter 5 that the preprocessing algorithm always produces a mesh without lonely vertices. Since this is known theoretically, there is little benefit in presenting experimental results for the preprocessing. Thus in many of the experimental results in this chapter, the so-called initial mesh is, in fact, the output mesh from MATLAB preprocessing code, and we do not show the mesh that preceded the preprocessing step. For the mesh of the disk in Fig. 7.2, the mesh that preceded the preprocessing step is shown in [63]. Although we noted earlier that it might not be possible to make a 2-dimensional triangle mesh in $\mathbb{R}^2$ 2-well-centered even if it has no lonely vertices, every initial mesh for the 2-dimensional experimental results in this chapter can be made 2-well-centered by relocating its interior vertices.

We implemented the energy minimization using the Mesquite library developed at Sandia National Laboratories [13]. The cost function $E_p$ is implemented on top of Mesquite as an element-based `QualityMetric` with a constructor accepting the argument $p$. The standard `LPtoPTemplate` objective function of Mesquite with power 1 sums the energy values over the different elements to complete the definition of $E_p$ as defined in Chapter 5.

The minimization of $E_p$ is performed using the `ConjugateGradient` class of Mesquite to relo-

[1] Portions of Figs. 7.2 and 7.8 are substantially similar to, but not exactly the same as portions of Figs. 10 and 12 of [63]. Material from that publication is reprinted here with kind permission of Springer Science+Business Media. The publication information and copyright notice for [63] appear in the footnote beginning on page 59.

Figures 7.1, 7.2, 7.3, 7.4, 7.5, 7.6, 7.7, 7.8, 7.9, 7.10, 7.11, and 7.12 are scheduled to appear as Figs. 7.1, 7.2, 7.3, 7.4, 7.5, 7.6, 7.7, 7.8, 7.9, 7.10, 7.11, and a portion of Fig. 7.12 in the article "Well-Centered Triangulation" in the SIAM Journal of Scientific Computing [64]. The article was written by the author Evan VanderZee and his coauthors Anil N. Hirani, Damrong Guoy, and Edgar A. Ramos. A significant portion of the text of this chapter is also based on that article. The copyright for that article belongs to the Society for Industrial and Applied Mathematics (SIAM). The copyrighted material that is used here is reprinted with kind permission of SIAM.

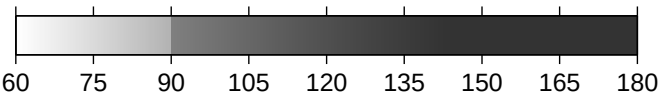


Figure 7.1: For two-dimensional meshes included in the experimental results, the shade of a triangle indicates the measure of its largest angle. This scale shows the relationship between the shade of the triangle and the angle measure.

cate interior vertices. The conjugate gradient method (CG) depends on a gradient computation. Rather than implement an analytical gradient for $E_p$, we chose to let Mesquite numerically estimate the necessary gradients. For the experiments in this chapter, optimization was terminated with a `TerminationCriterion` based on the number of iterations of CG. Thus where the phrase *number of iterations* appears in the experimental results, it refers to the number of CG iterations.

The experimental results for two-dimensional meshes include histograms showing the distribution of angle measures for all the angles in the mesh. The mean of each distribution is 60°, and the standard deviation $\sigma$ is reported near the histogram, along with the percentage $p$ and number $n$ of nonacute triangles in the mesh.

The results also include the running time of the optimization. The timings were obtained running experiments on a desktop machine with a dual 1.42 GHz PowerPC G4 processor and 2 GB of memory. As is often the case with mesh optimization algorithms, the method is quite slow. There are some opportunities for improving the running times. For instance, modifying the algorithm to optimize in the specific regions where improvement is necessary might significantly improve efficiency over the current implementation, which optimizes over the entire mesh at every iteration. In this study, however, efficiency was not a primary concern, and the current implementation was fast enough to complete an experiment in a reasonable amount of time for a mesh with more than 60000 triangles.

*Shading scheme.* For all the two-dimensional meshes shown in this chapter, we use the scale shown in Fig. 7.1 to determine the shade of each triangle. The shade of a triangle is determined by the measure of the largest angle of the triangle. The shade gets darker as the largest angle increases, with a noticeable jump at 90° so that 2-well-centered triangles can be distinguished from nonacute triangles. For example, the three small meshes in Fig. 6.1 on page 72 use this shading scheme, and it should be easy to identify which of the triangles are not 2-well-centered.

## 7.1 Mesh of a Disk

The mesh of the disk in Fig. 7.2 has 870 triangles. The triangles are all of similar size, and there are few enough triangles that the whole mesh can be visually inspected. Many of the triangles are already acute in the initial mesh, but 27 of them are not. The shading scheme makes it visually evident that the result mesh has no nonacute triangles. The angles histogram for the result mesh confirms this, showing that the maximum angle in the result is 82.55°. The minimum angle also improved in this experiment, increasing from 22.15° to 33.46°. Optimization of $E_4$ with Mesquite took 1.61 seconds over 30 iterations.

In this small example the initial mesh is fairly high quality, and it is easy to for the optimization to find a 2-well-centered mesh. The experiment demonstrates that the heuristic is successful for at least this simple problem. We also see that the result mesh is quite similar to the initial mesh.

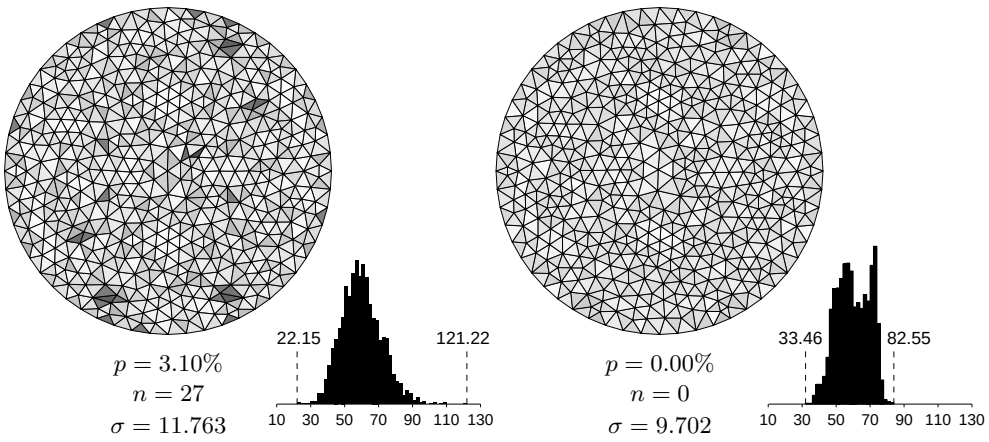


Figure 7.2: From the initial mesh shown at left, with 3.10% of its triangles nonacute, minimizing $E_4$ produces the 2-well-centered mesh shown at right in 30 iterations. Histograms of the angles in the mesh are included, with the minimum and maximum angles marked on each histogram. The optimization took 1.61 seconds.

Significant changes have occurred primarily in the specific places where change was necessary.

## 7.2 A Larger Mesh

Figure 7.3 displays results for a larger mesh, a mesh of a two-dimensional slice of the combustion chamber inside the Titan IV rocket. This mesh, which is based on a mesh that Damrong Guoy produced from his work for the Center for Simulation of Advanced Rockets, has 8966 triangles. The top portion of Fig. 7.3 has an overview of the experiment for the entire mesh, with the initial mesh at the very top and the result mesh (obtained by optimizing $E_{10}$ for 1000 iterations) just below it. These meshes are drawn without element edges because even very thin edges would entirely obscure some parts of the mesh. The background color helps visually define the boundary of the mesh by providing contrast with the light gray elements.

Below the mesh overview is a zoomed view of the top center portion of the mesh, which comes from a portion of a joint slot of the combustion chamber of the Titan IV rocket. Figure 7.3 also includes histograms of the angle distribution of the full mesh before and after the optimization. The angle histogram and zoomed portion for the initial mesh appear at left and for the optimized mesh are shown on the right.

In the initial mesh there are 1188 nonacute triangles ($\approx 13.25\%$ of the triangles), with a maximum angle around 155.89°. The result mesh has a maximum angle of 89.98°, and all but 143 triangles ($\approx 1.59\%$) have maximum angle below 85°. Of the 143 triangles that have angles above 85°, 14 have all three vertices on the boundary and are thus completely specified by the boundary. One such triangle is in the upper left nearly square corner of the zoomed portion of the mesh, where there is a triangle that looks much like an isosceles right triangle. Another 60 triangles are forced to have triangles larger than 85° because they are part of a pair of triangles along a part of the boundary with small but nonzero curvature. There are four such pairs along each curved boundary in the zoomed view in Fig. 7.3. In fact, all but four of the 143 largest angles occur in a triangle that has at least one vertex on the boundary of the mesh, and the remaining four angles larger than 85° each

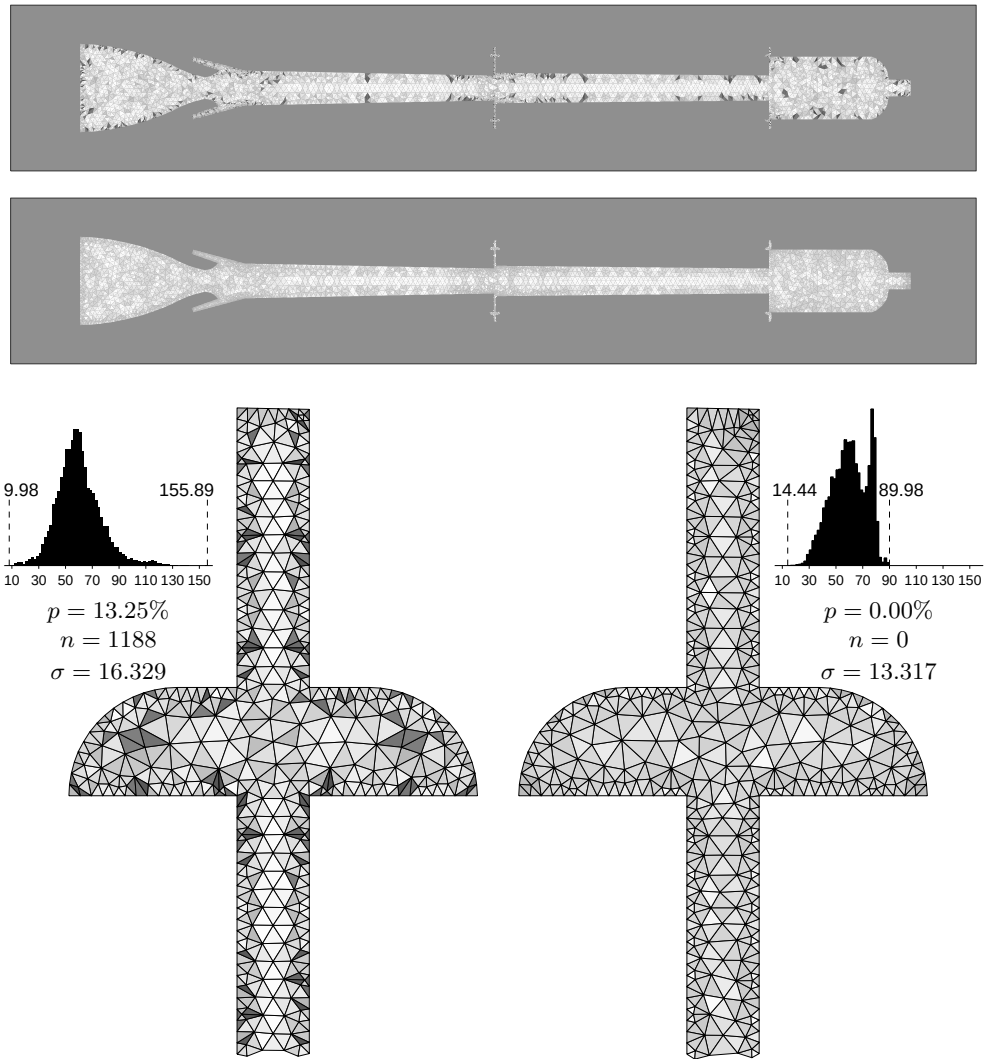


Figure 7.3: Results of an experiment with a mesh of a 2-dimensional slice of the combustion chamber inside the Titan IV rocket. The initial mesh is displayed at the very top. Below it is the result mesh, which was obtained by 1000 iterations minimizing $E_{10}$ on the mesh. Histograms show the distribution of angles in the full initial and final meshes. The zoomed-in views of the joint slot (at top center of the full mesh) show the level of mesh refinement in the regions of higher detail. For the histograms and the zoomed views, the original mesh is on the left, and the result mesh is on the right. The optimization took 805.35 seconds.

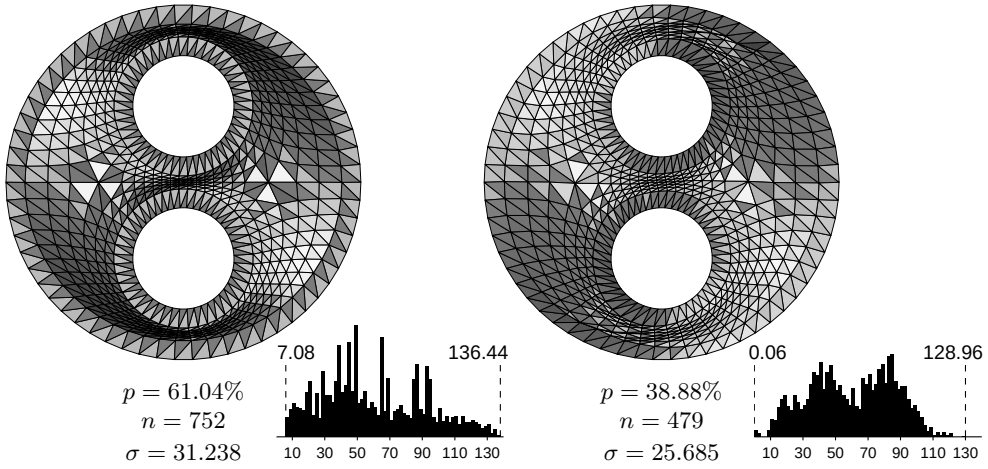


Figure 7.4: A first attempt at energy minimization applied to the two holes mesh on the left does not yield a well-centered mesh. Result after 500 iterations of $E_4$ minimization is shown on the right. The optimization took 88.70 seconds. The result mesh has some inverted triangles which are too thin to be seen. In subsequent figures we show several strategies for producing a well-centered configuration.

occur in a triangle that has a vertex at distance one from the boundary.

## 7.3 Some More Difficult Tests

Next we consider some meshes of a circular domain with two circular holes. The initial mesh in Fig. 7.4 was provided by Guoy. It was created by adding diagonals to a quadrilateral mesh generated with a method based on his work with Erickson in [32]. Because of the way the mesh was generated, it needed no preprocessing to remove lonely vertices; however, the initial mesh is geometrically far from being 2-well-centered, with 61.04% of its triangles nonacute and a standard deviation $\sigma \approx 31.238$ for the angle distribution.

An initial attempt to make the mesh 2-well-centered with the Mesquite-based optimization was unsuccessful, but two slightly different strategies, described later, do produce a 2-well-centered mesh. The initial mesh and its angle histogram are shown in Fig. 7.4 (left), along with the result of minimizing $E_4$ on the mesh for 500 iterations (right). In this case, the optimization took 88.70 seconds. Comparing the optimized mesh to the initial mesh, we see that the quality has improved; the percentage of nonacute triangles is reduced, the standard deviation is smaller, and many of the largest angles have been reduced.

Unfortunately, some of the smallest angles of the initial mesh have also gotten smaller in the optimized mesh. In fact, four angles got so small that their triangles became inverted in the optimized mesh. The inverted triangles are too thin to actually see, but they occur in two pairs. One pair is near the top right of the mesh, near some other triangles with noticeably small angles, and the other pair is near the bottom left. The energy value required to invert a triangle is quite high, but for meshes with a larger number of elements or a high percentage of bad triangles, improvements at other locations in the mesh may be significant enough to push a small number of triangles up to (and over) the energy of inversion. Thus using the basic mesh optimization energy $E_p$ can lead to

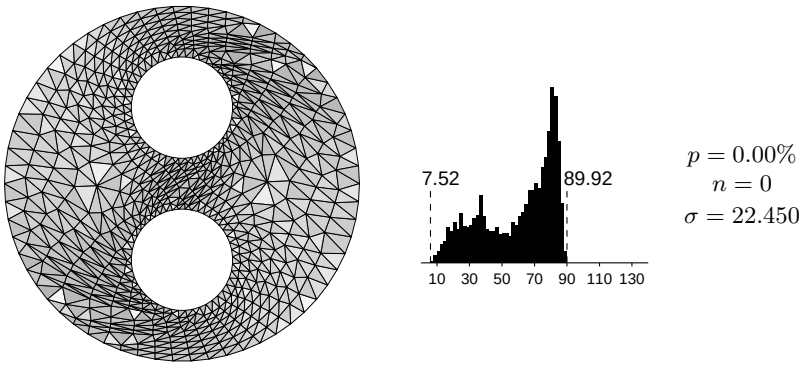


Figure 7.5: A 2-well-centered mesh of the two holes domain conforming to the mesh connectivity and boundary vertices of the original two holes mesh shown in Fig. 7.4. The mesh was obtained using cost functions $\widetilde{E}_p$ that are similar to cost functions $E_p$ but have a barrier against triangle inversion. The optimization procedure was 500 iterations of $\widetilde{E}_4$, followed by 500 iterations of $\widetilde{E}_6$, followed by 500 iterations of $\widetilde{E}_{10}$. Total optimization time was 115.37 seconds.

inverted triangles.

**Energy combined with inversion barrier.** The triangle inversion that occurs when optimizing the basic $E_p$ can be prevented by introducing an explicit barrier to inversion in the cost function. That is, we modify the energy by adding a term that goes to infinity as a triangle moves towards becoming degenerate. This has the potential to adversely affect the primary goal of optimizing $E_p$, but it is an effective way to deal with the problem of triangles that would become inverted optimizing the basic $E_p$. The Mesquite library provides a `QualityMetric` called the `IdealWeightInverseMeanRatio` that has an implicit barrier against inversion [44]. Let $E_{\text{imr}}$ denote the cost function associated with the `IdealWeightInverseMeanRatio`. We define $\widetilde{E}_p := 100E_p + E_{\text{imr}}$ , a linear combination of the energy $E_p$ with $E_{\text{imr}}$. This new energy has a barrier against inversion and, because of the chosen coefficients, is still quite similar to the basic $E_p$ when there are no triangles with small angles. The particular coefficients chosen for the linear combination might not be best possible, and it might be better to optimize with a series of linear combinations approaching the basic $E_p$ rather than use any particular coefficients for the linear combination, but we have found that $\widetilde{E}_p$ is often effective in cases where the basic $E_p$ leads to inverted triangles.

For this particular mesh of a circular domain with two circular holes, optimizing $\widetilde{E}_p$ leads to a 2-well-centered result with no inverted triangles. Starting from the initial mesh and applying 500 iterations of $\widetilde{E}_4$, followed by 500 iterations of $\widetilde{E}_6$, followed by 500 iterations of $\widetilde{E}_{10}$ produced the 2-well-centered mesh of the original domain displayed in Fig. 7.5. The optimization took $37.37 + 36.79 + 41.21 = 115.37$ seconds.

**Improved boundary vertex locations.** Another way to get a well-centered mesh similar to the initial mesh in Fig. 7.4 is to change the location of the boundary vertices to make the optimization problem easier. The mesh on the left side of Fig. 7.6 has the same mesh connectivity as the initial mesh, but the vertices along the boundary have been relocated. In the initial mesh the vertices along each boundary were equally spaced, but in this mesh, the vertices on the outer boundary are more dense at the north and south and less dense at the east and west. The vertices along the inner boundary circles have also moved a bit. For this mesh optimizing the basic energy $E_6$ reaches a well-centered configuration by 200 iterations. The result, obtained in 18.03 seconds, appears on the

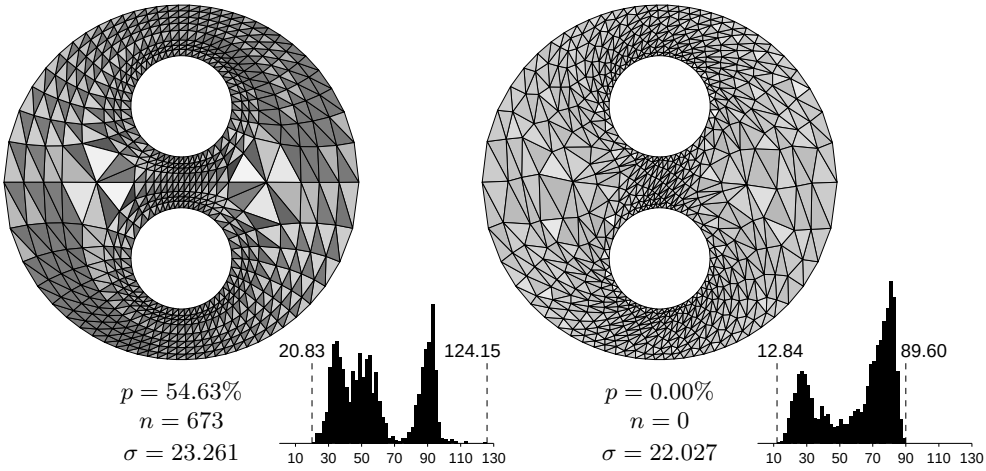


Figure 7.6: This mesh has the same mesh connectivity as the initial mesh in Fig. 7.4, but the vertices along the boundary have been relocated. The 2-well-centered mesh on the right was obtained from the mesh on the left in 18.03 seconds with 200 iterations of $E_6$ minimization.

right in Fig. 7.6.

**Different mesh of the same domain.** The difficulty of finding a 2-well-centered mesh is primarily due to the combined constraints of the mesh connectivity of the initial mesh and the locations of the boundary vertices. The shape of the domain or the fact that the domain is not simply connected are not inherent difficulties for the problem of finding a 2-well-centered triangulation. When separated from the mesh connectivity of the initial mesh, the location of the boundary vertices are not a problem either, at least for this mesh of this domain. We demonstrate this by an experiment on the same domain with a completely different mesh that has the same set of boundary vertices and the same boundary vertex locations as the meshes of Figs. 7.4 and 7.5. The experiment, shown in Fig. 7.7, produced a mesh of the domain with maximum angle around 79.50° by optimizing $E_8$ for 100 iterations. The optimization took 7.44 seconds.

## 7.4 A Graded Mesh

The two holes mesh of Fig. 7.4 and the mesh in Fig. 7.3 related to the Titan IV rocket are both graded meshes, i.e., they have triangles of different sizes in different regions of the mesh, and the size changes gradually between the different regions. The gradation of the meshes in Fig. 7.4 and Fig. 7.3 is controlled partly by the size of elements on the boundary and by the geometry of the mesh. For the initial mesh at left in Fig. 7.8, however, the size of the small triangles near the center of the mesh is not necessary to accurately represent the mesh geometry and is not controlled by elements on the boundary of the mesh. The nearly converged result produced by 30 iterations minimizing $E_4$ is displayed on the right side of Fig. 7.8. We see that the sizes of triangles in the result mesh are similar to sizes of triangles in the input mesh.

Mesh optimization with cost functions $E_p$ does not not always preserve the initial size of triangles in a mesh. We expect, however, that the energy will generally preserve the grading of an input mesh if the initial mesh is relatively high quality. This hypothesis stems from the observation that the energy is independent of triangle size, the idea that the mesh connectivity combined with the

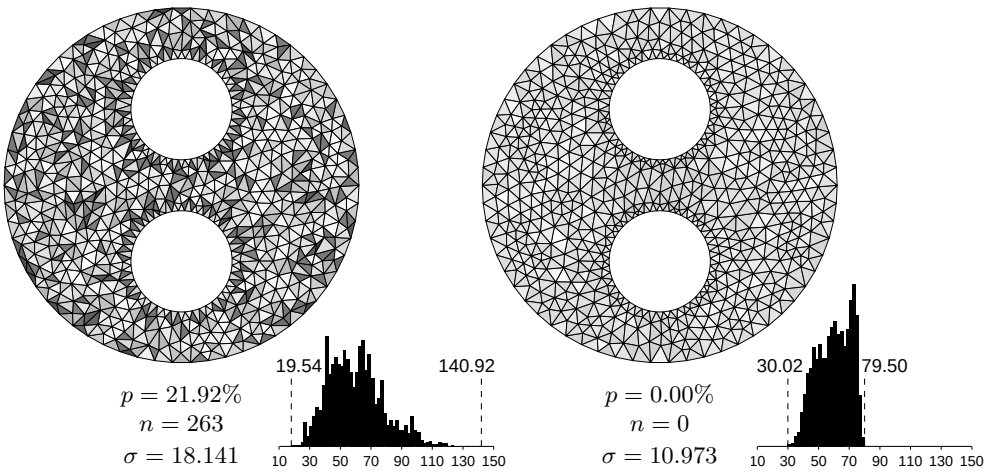


Figure 7.7: This is a mesh with the same domain and same boundary vertices as the mesh in Fig. 7.4. The 2-well-centered mesh on the right was obtained from the mesh on the left in 7.44 seconds by minimizing $E_8$ for 100 iterations. The high-quality result shows that the difficulty of getting a 2-well-centered mesh in Fig. 7.4 is not due solely to the domain or the boundary vertices. The initial mesh for this experiment was generated using the freely available software Triangle [55] and heuristics for improving the mesh connectivity.

property of 2-well-centeredness somehow controls the triangle size, and the supporting evidence of the experimental results presented in this chapter, especially this particular experiment.

Thus we expect that optimizing graded meshes to obtain 2-well-centered graded meshes may be a useful application of our algorithm. We have not proved that we preserve the grading, but there are no known algorithms proven to create graded acute-angled triangulations of planar domains. The recent algorithm of [28] has produced graded acute triangulations in a variety of experiments, but in all cases we have tried, we have been able to improve the quality of their triangulations. (See Sec. 7.5.) Moreover, their algorithm is not known to generalize to higher dimensions.

## 7.5 Mesh of Lake Superior

The Lake Superior domain, with its complicated shape, has appeared in many papers about quality meshing. We include an example optimizing a mesh of this well-known domain. The initial mesh is already 2-well-centered in this experiment, but we show that we can improve its quality by minimizing $E_p$ on the mesh. The results are represented graphically in Fig. 7.9.

The initial acute-angled mesh is from the work of Erten and Üngör [28] on generating acute 2-D triangulations with a variant of Delaunay refinement. The initial mesh has a maximum angle of 89.00° with 174 triangles having angles larger than 88.00°. Directly optimizing $E_{10}$ on the initial mesh, Mesquite finds a local minimum of $E_{10}$ after 6.63 seconds (21 iterations). The local minimum has exactly one nonacute triangle (maximum angle 91.03°) and only 40 triangles having angles larger than 88.00°. The angle histogram for this result is included in Fig. 7.9 at top center. The mesh is visually very similar to the initial mesh and does not appear here.

If we start by optimizing $E_4$ and follow that by optimizing $E_{10}$, we obtain a local (perhaps also global) minimum of $E_{10}$ with much lower energy than the result obtained by directly optimizing

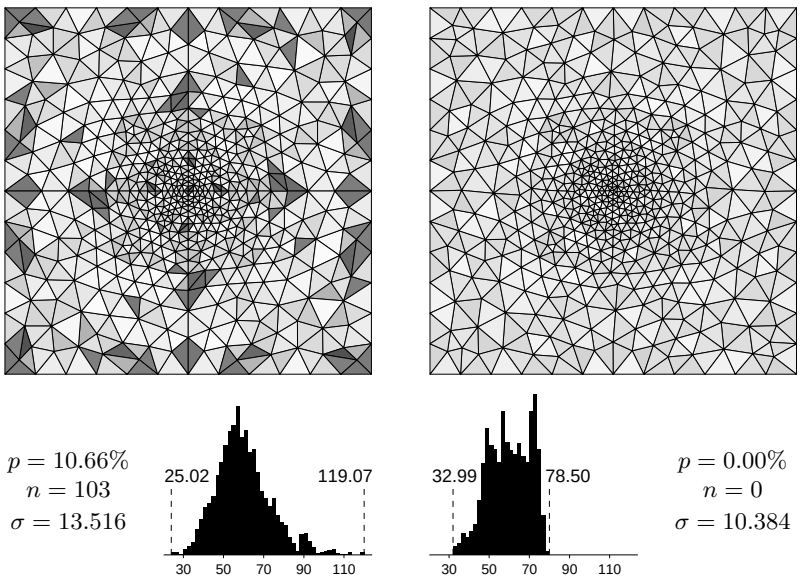


Figure 7.8: For this graded mesh of the square, minimizing $E_4$ on the initial mesh (left) produces a 2-well-centered mesh (right) that has grading similar to the initial mesh. The optimization ran for 30 iterations, completing in 2.16 seconds.

$E_{10}$. The result of this optimization process is shown on the right in Fig. 7.9. The optimization took 131.48 seconds total; Mesquite spent 102.81 seconds (453 iterations) finding a minimum of $E_4$ and 28.67 seconds (125 iterations) finding a minimum of $E_{10}$. For these experiments the optimization was run until Mesquite's implementation of CG stopped improving the $E_p$ energy of the mesh, and the number of iterations was not chosen a priori.

Laplacian smoothing is a popular mesh optimization technique that was first used for structured meshes with quadrilateral elements and later generalized to triangle meshes [67]. A brief description of Laplacian smoothing is given in [29]. We compare our mesh optimization technique with Laplacian smoothing, using the implementation of Laplacian smoothing provided by the Mesquite library. The result of Laplacian smoothing on the Lake Superior mesh is shown in Fig. 7.10. The optimization was terminated after 100 iterations, which is near convergence. The run time was 1.31 seconds. The maximum angle in the result is 109.27°, and more than 4% of the triangles are nonacute.

The result of optimizing the Lake Superior mesh with Laplacian smoothing is typical of the results obtained with Laplacian smoothing. We performed experiments with Laplacian smoothing on all of the 2-D meshes presented in this chapter, and no mesh became 2-well-centered except for the mesh of the square in Fig. 7.8, where Laplacian smoothing produced a mesh with maximum angle 87.54° compared to the maximum angle of 78.50° obtained by our method. In most cases the percentage of nonacute triangles after Laplacian smoothing was between 1% and 5%, but for the meshes in Figs. 7.4, 7.5, and 7.6, the percentage of nonacute triangles was much higher, getting as high as 48.70% for the mesh in Fig. 7.6. Clearly the traditional Laplacian smoothing is not an appropriate tool for finding acute triangulations.

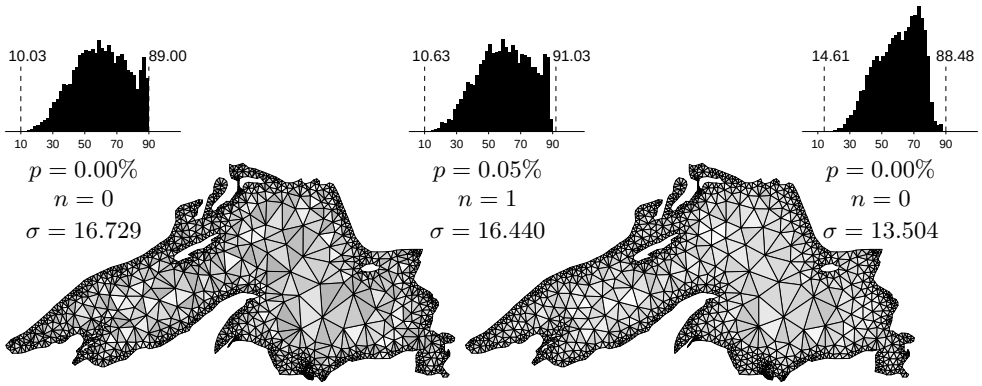


Figure 7.9: Result for a mesh of Lake Superior. The initial mesh shown on the left is a 2-well-centered mesh from [28]. The improved mesh shown on the right was obtained by first optimizing $E_4$ and then optimizing $E_{10}$. The angle histogram at top center shows the result of optimizing $E_{10}$ directly on the initial mesh.

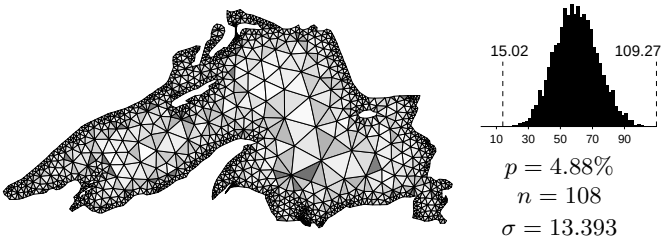


Figure 7.10: Result of applying Laplacian smoothing to the initial acute mesh of Lake Superior (left side of Fig. 7.9). More than 4% of the triangles become nonacute, and the maximum angle increases to 109.27°.

## 7.6 Colombia, India, and Thailand

We end our 2-D experimental results with a collection of three large meshes of complicated geographical domains. The experiments are summarized in Fig. 7.11. For each of these meshes the optimization started by minimizing $\widetilde{E}_8$ for 500 iterations and then proceeded by minimizing $E_8$, running 500 iterations at a time until the mesh became well-centered. After the mesh became well-centered, we used one more round of 500 iterations minimizing $E_8$ to get some additional improvement in the angle distribution.

The total number of iterations for the meshes was 2000 iterations for Colombia, 3500 iterations for India, and 3000 iterations for Thailand, with total optimization times of 5284.01 seconds, 16162.20 seconds, and 8263.82 seconds, respectively. The meshes are quite large, with 38233 triangles, 62370 triangles, and 34562 triangles, respectively. In each case, more than 19% of the triangles are nonacute in the initial mesh, and the maximum angle is larger than 160°, yet the optimization finds a well-centered result. It is also clear that the optimization preserves the gradual change in element size from the tiny triangles needed to resolve the boundaries to the much larger triangles in the interiors of the meshes.

## 7.7 A 3-D Mesh

For tetrahedral meshes, the question of whether the mesh connectivity permits a well-centered mesh is more difficult than its two-dimensional analogue. (See Chapter 4 and [65].) In part because we do not have an effective preprocessing algorithm for tetrahedral meshes, many of our optimization experiments in three dimensions have been limited to meshes with carefully designed mesh connectivity. The mesh shown in Fig. 7.12 is one of these meshes. The shading of the tetrahedral elements in Fig. 7.12 represents the shadows that would result from viewing the faceted object under a light source; it has nothing to do with the quality of the elements of the mesh. The full mesh is a mesh of the three-dimensional cube with 430 tetrahedra, but Fig. 7.12 uses a cutaway view, so some of the elements in the interior of the mesh are visible.

Although the initial mesh was carefully designed to have good mesh connectivity (e.g., each vertex has at least 10 incident edges) and a high-quality surface mesh, it is not 3-well-centered. In fact, 22.33% of the tetrahedra are not 3-well-centered. Optimizing $E_{3,16}$ for 3.92 seconds (20 iterations) produced a 3-well-centered mesh. Recall that $E_{3,16}$ is a cost function designed to seek 3-well-centered meshes. The energy does not explicitly seek a 2-well-centered mesh, and the result mesh is not 2-well-centered.

Even though the initial mesh was carefully designed to have good mesh connectivity, this optimization result is nontrivial. We compared optimization of $E_{3,16}$ to the Mesquite implementation of Laplacian smoothing, applying Laplacian smoothing to the initial mesh and running it until it converged after 60 iterations (0.14 seconds). The result of Laplacian smoothing is a mesh in which 22.33% of the tetrahedra are not 3-well-centered. Figure 7.12 includes the $h(v, \sigma^3)/\,R(\sigma^3)$ distributions for the initial mesh, the mesh obtained by optimizing $E_{3,16}$, and the mesh resulting from Laplacian smoothing. Near each histogram we show the percentage $p$ and number $n$ of tetrahedra (not $h/R$ values) that are not 3-well-centered, and we report the mean $\mu$ and standard deviation $\sigma$ of the distribution of $h/R$ values.

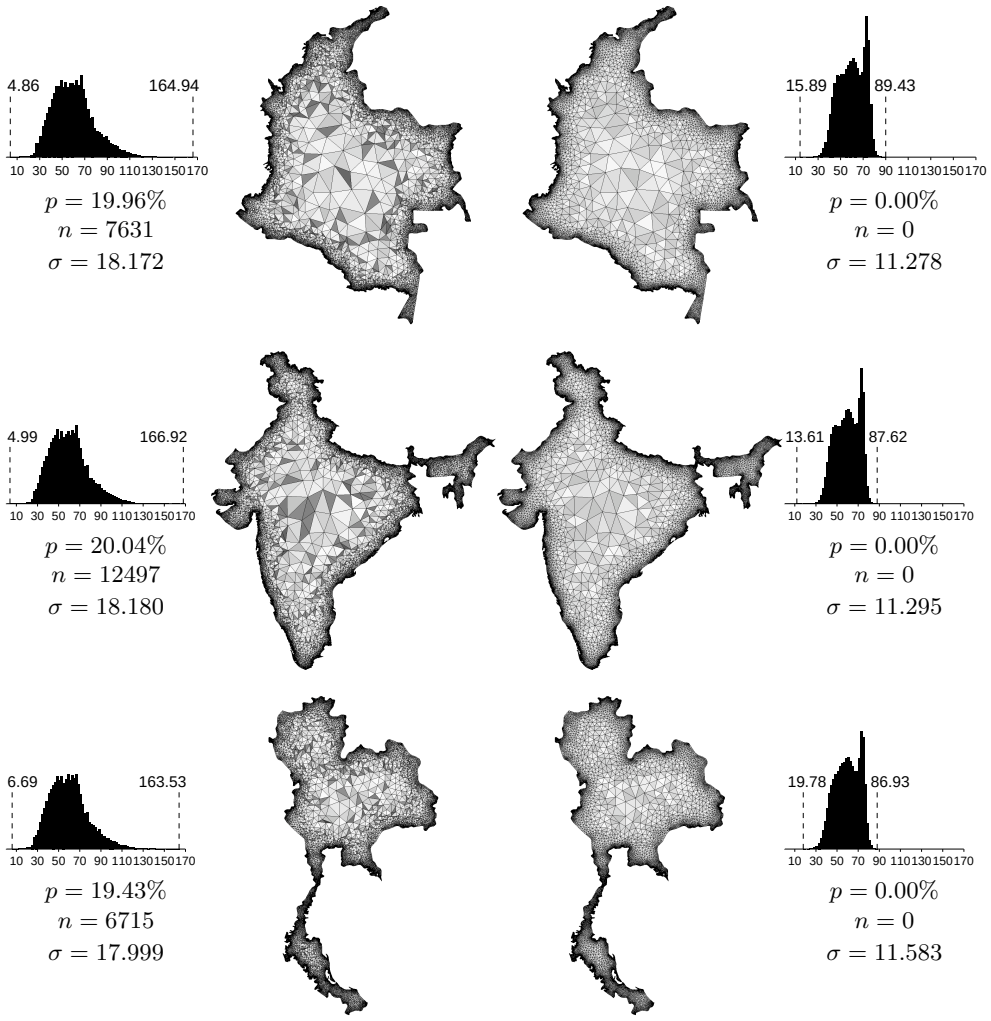


Figure 7.11: These meshes of complicated geographical boundaries were optimized with an initial 500 iterations of CG minimizing $\widetilde{E}_8$, followed by successive rounds of 500 iterations of CG minimizing the basic $E_8$. The optimization produces well-centered meshes that preserve the grading of the input meshes. (The dark regions near the boundaries of the meshes come from the agglomeration of the edges of triangles that are too small to be seen.) The data for the geographical boundaries was produced using the `CountryData` command of Mathematica. Initial meshes were constructed from the input polygons using Triangle [55] and heuristics for improving the mesh connectivity.

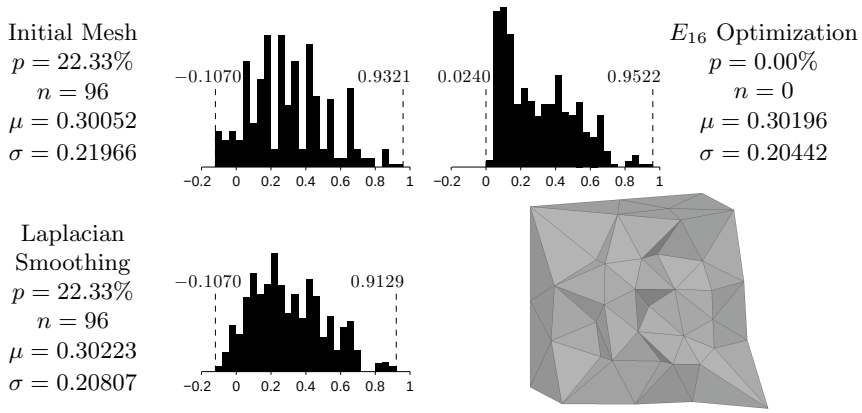


Figure 7.12: A cutout view showing the interior of a 3-well-centered mesh of the cube. The mesh is the result of 3.92 seconds (20 iterations) of optimizing $E_{16}$ on an initial mesh in which 22.33% of the tetrahedra were not 3-well-centered. Recall that a tetrahedron $\sigma^3$ is 3-well-centered if and only if $h(v, \sigma^3)/R(\sigma^3) > 0$ for each vertex $v$ of $\sigma^3$. For a regular tetrahedron, $h/R = 1/3$. The $h/R$ distributions for the initial mesh, the result of optimizing $E_{16}$, and the result of Laplacian smoothing show the superiority of our method for finding 3-well-centered meshes.

It is worth noting that, because of its difficulty, obtaining well-centered triangulations and/or acute triangulations of 3-dimensional objects is significant no matter how they are obtained. As discussed in the next chapter and in our other work, we have made use of the optimization techniques developed in this paper to construct well-centered triangulations of several simple three-dimensional shapes [62] and to constructively prove the existence of an acute triangulation of the 3-dimensional cube [66].

# Chapter 8

# Quality Meshes of Particular Domains

Chapter 7 closes with an example of optimizing a tetrahedral mesh in $\mathbb{R}^3$. The initial mesh in that example was constructed to have a high-quality surface mesh and good mesh connectivity. Many of the well-centered meshes presented in this chapter are tetrahedral meshes in $\mathbb{R}^3$ that continue the theme of that closing example of Chapter 7, combining a hand construction of combinatorics with mesh optimization. Some of the meshes, however, are directly constructed, such as those in Sec. 8.1.

The meshes presented here are by no means exhaustive of the well-centered meshes constructed in the author's research, but most of them are of particular interest for one reason or another. For some the interest is related to the analogous problem for acute triangulations in $\mathbb{R}^3$. Others are included to establish claims from Chapter 4 about the existence of certain well-centered tetrahedral meshes. The chapter closes with a variety of acute triangulations of the square, continuing the discussion of a problem that has fascinated mathematicians for years. [1]

## 8.1 3-Space, Slabs, and Infinite Rectangular Prisms

Eppstein, Sullivan, and Üngör showed in 2004 that it is possible to fill $\mathbb{R}^3$ with acute tetrahedra and possible to triangulate an infinite slab $\mathbb{R}^2 \times [0, a]$ for $a \in \mathbb{R}$ with acute tetrahedra [26]. They suggest several different ways to fill space with acute tetrahedra, each using copies of at least two different tetrahedra, and they suggest that it is unlikely that there is a tiling of space with copies of any single tetrahedron. Their acute triangulation of the slab appears to use copies of seven distinct tetrahedra.

As we shall see later in this section, there are simpler tilings of 3-space and infinite slabs with completely well-centered tetrahedra. Indeed, the same construction used for these domains extends to triangulate any infinite rectangular prism $\mathbb{R}\times[0, a]\times[0, b]$ with completely well-centered tetrahedra.

We start by describing the vertex set of one of these triangulations, and later discuss the mesh connectivity that produces a triangulation with the given vertex set. Consider first the set of vertices $\{(i, 0, 0) : i \in \mathbb{Z}\}$. Choose a parameter $a > 0$ and make copies of the initial set of vertices translated by integer multiples of the vector $(1/2, a, 0)$. This produces a set of vertices in the $xy$-plane $P$. Then choose a parameter $b > 0$ and duplicate the vertices from the plane $P$ displaced by integer multiples

[1] The constructions presented in Secs. 8.1, 8.2.1, and 8.3 appeared previously in a paper by the author and his coauthors [62]. The bounds on the number of tetrahedra in a well-centered triangulation of the cube, discussed in Sec. 8.2.2, are similar to a discussion of those bounds in [62]. Versions of Figs. 8.1, 8.3, 8.2, 8.4, 8.7, 8.8, 8.9, and 8.10 appeared as Figs. 9, 10, 8, 11, 12, 13, 14, and 15 in [62]. The picture portions of Figs. 8.4, 8.9, and 8.10 were created by Damrong Guoy for [62]. 

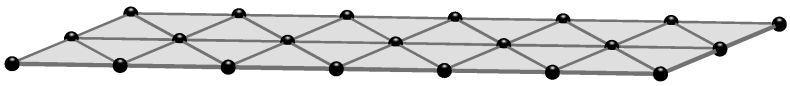

Figure 8.1: We define a triangulation of $\mathbb{R}^3$ whose vertices are the points of a lattice with basis vectors $u_1 = (1, 0, 0)$, $u_2 = (1/2, a, 0)$, and $u_3 = (1/2, 0, b)$. In each plane $z = kb$ for $k \in \mathbb{Z}$, the lattice points are triangulated as shown.

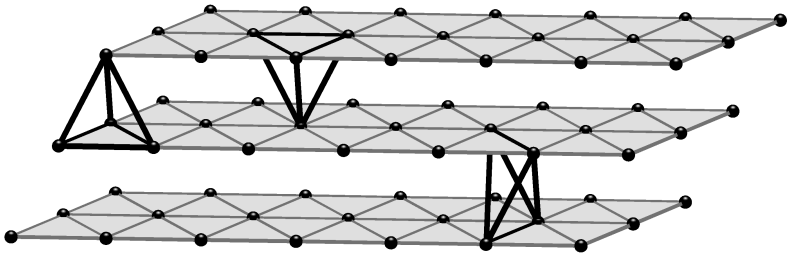

Figure 8.2: After defining the triangulation of each plane $z = kb$ for $k \in \mathbb{Z}$, we construct tetrahedra between each pair of planes $z = kb$ and $z = (k + 1)b$ as shown here. There are two distinct types of tetrahedra in the construction, one type that has three vertices in one plane and one vertex in the other plane (top two tetrahedra), and one type that has two vertices in each plane (bottom tetrahedron).

of translation vector $(1/2, 0, b)$. The resulting vertex set is

$$\{(i + j/2 + k/2, aj, bk) : i, j, k \in \mathbb{Z}\},$$

which can also be described as the points of the lattice $\Lambda = \{\sum_{i=1}^{3} c_i u_i : c_i \in \mathbb{Z}\}$ with basis vectors

$$u_1 = (1, 0, 0),\ u_2 = (1/2, a, 0), \text{ and } u_3 = (1/2, 0, b)\,.$$

The mesh connectivity for this vertex set is defined as follows. First we define the triangular facets in each plane $z = kb$ for $k \in \mathbb{Z}$. For each vertex $v$ there are six edges incident to $v$ in the plane $z = kb$. These edges connect $v$ to the vertices at positions $v \pm (1, 0, 0)$, $v \pm (1/2, a, 0)$, and $v \pm (1/2, -a, 0)$. (See Fig. 8.1.) For example, if $a = \sqrt{3}/2$, this produces a standard tiling of the plane with equilateral triangles.

Now we describe the mesh connectivity between planes $z = (k - 1)b$, $z = kb$ and $z = (k + 1)b$. Each triangle in $z = kb$ is incident to exactly one edge in the direction $(1, 0, 0)$. Let $v$ be the endpoint of this edge with smaller $x$-coordinate. There is a vertex directly above the midpoint of the edge at $v + (1/2, 0, b)$, and a vertex below the midpoint at $v + (1, 0, 0) - (1/2, 0, b)$. The first type of tetrahedron is the convex hull of a triangle in $z = kb$ with a vertex directly above or below the midpoint of the edge in direction $(1, 0, 0)$. (See Fig. 8.2.)

After creating all possible tetrahedra of the first type, the gaps that remain are, in fact, tetrahedra. An example of this second type of tetrahedron is the convex hull of the points $(0, 0, 0)$, $(1/2, a, 0)$, $(1/2, 0, b)$, and $(0, a, b)$. For this second type of tetrahedron there are two vertices in a plane $z = kb$ and two vertices in a plane $z = (k+1)b$. The midpoint of the edge in the plane $z = kb$ is directly below the midpoint of the edge in the plane $z = (k + 1)b$.

**Proposition 8.1.1.** *A triangulation in the two-parameter family of triangulations just discussed is*

*completely well-centered if and only if both $a > 1/2$ and $b > 1/2$.*

*Proof.* We work with a canonical tetrahedron of each type. For a tetrahedron of the first type we analyze the tetrahedron with vertices $u_0 = (0, 0, 0)$, $u_1 = (1, 0, 0)$, $u_2 = (1/2, a, 0)$, and $u_3 = (1/2, 0, b)$, and for the tetrahedron of the second type we analyze the tetrahedron with vertices $v_0 = (0, 0, 0)$, $v_1 = (1/2, a, 0)$, $v_2 = (1/2, 0, b)$, and $v_3 = (0, a, b)$.

The faces $u_0u_1u_2$ and $u_0u_1u_3$ of the tetrahedron of the first type are isosceles triangles with apices at $u_2$ and $u_3$ respectively. The angles at the apices are $2\,\mathrm{atan}(1/2a)$ and $2\,\mathrm{atan}(1/2b)$ respectively. Since $\mathrm{atan}(1) = \pi/4$, these angles and the associated isosceles triangles will be acute if and only if both $a > 1/2$ and $b > 1/2$.

The remaining two faces of the type one tetrahedron meet along the edge $u_2u_3$ and are congruent to each other. The length of edge $u_2u_3$ is $\sqrt{a^2 + b^2}$, and the other two edges have length $\sqrt{1/4 + a^2}$ and $\sqrt{1/4 + b^2}$. We compare the squared length of each edge to the sum of the squared length of the other two edges and find that for any $a \neq 0$, $b \neq 0$ the inequalities

$$\begin{aligned} a^2 + b^2 &< a^2 + b^2 + \frac{1}{2} \\ a^2 + \frac{1}{4} &< a^2 + 2b^2 + \frac{1}{4} \\ b^2 + \frac{1}{4} &< 2a^2 + b^2 + \frac{1}{4} \end{aligned}$$

hold. Thus by the law of cosines we conclude that these triangles are acute triangles. This shows that the type one tetrahedron is 2-well-centered if $a > 1/2$ and $b > 1/2$.

To show that the type one tetrahedron is 3-well-centered we explicitly compute its circumcenter. The coordinates of the circumcenter are

$$\left(\frac{1}{2}, \frac{a}{2} - \frac{1}{8a}, \frac{b}{2} - \frac{1}{8b}\right),$$

and the circumradius is $(a^2+b^2)/4+1/(64a^2)+1/(64b^2)$. The intersection of the plane $x = 1/2$ with the canonical tetrahedron of the first type is a triangle with vertices at $(1/2, 0, 0)$, $(1/2, a, 0)$, and $(1/2, 0, b)$. It suffices to show that the circumcenter of the tetrahedron is in the interior of this triangle of intersection. We will show this by proving that the circumcenter lies in the three halfspaces whose intersection defines the triangle. These three halfspaces are defined by the inequalities $y > 0$, $z > 0$ and $z < b - (b/a)y$.

For $a > 1/2$ the inequality $a/2 - 1/(8a) > 0$ is satisfied, showing that $y > 0$, and for $b > 1/2$ the inequality $b/2 - 1/(8b) > 0$ is satisfied, showing that $z > 0$. For the third inequality we note that

$$\frac{b}{2} - \frac{1}{8b} < \frac{b}{2} + \frac{b}{8a^2} = b - \frac{b}{a}\left(\frac{a}{2} - \frac{1}{8a}\right),$$

for any positive $a$ and $b$. Thus the type one tetrahedron is 3-well-centered (hence completely well-centered) if $a > 1/2$ and $b > 1/2$.

The proof for the type two tetrahedron is easier. We already know that the type two tetrahedron is 2-well-centered, because each facet of the type two tetrahedron is also a face of some type one tetrahedron and is congruent to to the faces that meet at edge $u_2u_3$. Thus the type two tetrahedron is 2-well-centered for any $a > 0$, $b > 0$.

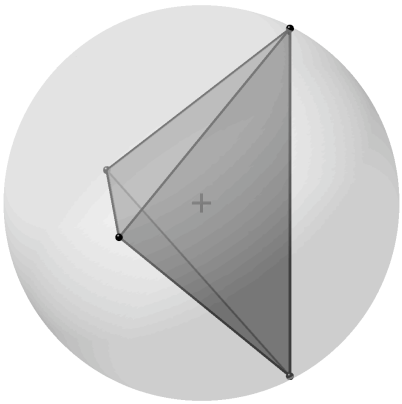

| Vertex Coordinates | | |
|---|---|---|
| $x$ | $y$ | $z$ |
| $-1$ | $-2$ | 0 |
| 1 | 0 | $-2$ |
| $-1$ | 2 | 0 |
| 1 | 0 | 2 |

| Quality Statistics | | |
|---|---|---|
| Quantity | Min | Max |
| $h/R$ | 0.316 | 0.316 |
| Face Angle | 54.74° | 70.53° |
| Dihedral Angle | 60.00° | 90.00° |
| $R/\ell$ | 0.645 | 0.645 |

Figure 8.3: The second Sommerville tetrahedron, shown here, is a completely well-centered tetrahedron that tiles 3-space. The tiling of 3-space with this tetrahedron is a special case of the two-parameter family of completely well-centered tilings.

The circumcenter of the canonical type two tetrahedron is $(1/4, a/2, b/2)$, and its circumradius is $1/16+(a^2+b^2)/4$. The circumcenter is also the barycenter, i.e., it is the point $(1/4)(v_0+v_1+v_2+v_3)$, which is a convex combination of the vertices. Thus the type two tetrahedron is 3-well-centered (and completely well-centered) for any positive parameters $a$ and $b$. □

Proposition 8.1.1 shows that there is a large family of fairly simple completely well-centered triangulations of 3-space. An important member of this family is the triangulation obtained for parameters $a = b = \sqrt{2}/2$. In this case the type one tetrahedron is congruent to the type two tetrahedron, and we obtain a tiling of 3-space with copies of a single complete well-centered tetrahedron. This tetrahedron, shown in Fig. 8.3, is the second tetrahedron of four tetrahedra discovered by Sommerville [58, 26] that tile space. The other three tetrahedra Sommerville described are neither 3-well-centered nor 2-well-centered, though one of them has a maximum face angle of $\pi/2$ and is dihedral nonobtuse. It is interesting to note that an algorithm of Fuchs for meshing a spatial domain based on a high-quality spatial tiling had "good performance ... when he used the second Sommerville construction," [26, 30].

It is also worth noting that when $a = b = \sqrt{2}/2$ the vertices of the lattice are the vertices of a body-centered cubic (BCC) lattice. It is not so hard to see that the vertices of the second Sommerville tetrahedron in Fig. 8.3 come from a BCC lattice, with the horizontal edge coming from a cube and the other two vertices taken from cube centers. It is more difficult to visualize this in the original description of the completely well-centered family of triangulations of 3-space, since the cubes of the BCC lattice are not fully axis-aligned in that description. Barnes and Sloane proved that the optimal lattice for quantizing uniformly distributed data in $\mathbb{R}^3$ is the BCC lattice [4]. Since this is related to centroidal Voronoi tesselations (CVTs) [19], and methods motivated by CVTs have been used for high-quality meshing of 3-dimensional domains (see [1]), it is not surprising that a Delaunay triangulation of the vertices of the BCC lattice gives rise to a high quality triangulation of space. (Proposition 6.2.1 shows that our triangulation of the BCC lattice is the Delaunay triangulation because it is 3-well-centered.)

One nice property of the two-parameter family of completely well-centered triangulations is that

it provides an elegant solution to the problems of tiling an infinite slab in $\mathbb{R}^3$ and tiling infinite rectangular prisms in $\mathbb{R}^3$. To tile the slab one merely restricts to the tetrahedra between the planes $z = k_1 b$ and $z = k_2 b$ for some $k_1, k_2 \in \mathbb{Z}$, limiting the vertex set to a finite interval of $|k_2 - k_1| + 1$ translates along the vector $(1/2, 0, b)$. A triangulation of a slab of one particular thickness can be scaled to get a triangulation of a slab of any other thickness, and choosing $a = b = \sqrt{2}/2$ shows that any slab in $\mathbb{R}^3$ can be triangulated with copies of a single appropriately scaled version of the second Sommerville tetrahedron. Triangulating infinite rectangular prisms is also easy. If we use a finite interval of translates along the vector $(1/2, a, 0)$ as well as a finite interval of translates along vector $(1/2, 0, b)$, the result will be a triangulation of an infinite rectangular prism. If the ratio of side lengths of the rectangle is a rational number $p/q$, then this triangulation can also be done with copies of the second Sommerville tetrahedron by choosing $a = b = \sqrt{2}/2$, using $p + 1$ translates of vector $(1/2, a, 0)$ and $q + 1$ translates of vector $(1/2, 0, b)$, and scaling the result appropriately.

## 8.2 The Cube

The 3-D experimental result of Chapter 7 showed that, given a sufficiently nice input mesh, mesh optimization with the energy $E_{3,p}$ can find a 3-well-centered mesh of a bounded domain. In fact, the result of that experiment may be the first mesh of the cube that was known to be 3-well-centered. Creating a completely well-centered mesh of the cube is somewhat more difficult than making a 3-well-centered mesh of the cube, but it can be accomplished by optimizing an appropriate input mesh with a linear combination of energy $E_{3,p}$ and $E_{2,p}$. This section discusses a completely well-centered mesh of the cube created by this method.

### 8.2.1 A Completely Well-Centered Triangulation

The completely well-centered mesh of the cube we describe has 194 tetrahedra. We first published a description of this mesh in [62], where we also mention that, as far as we know, the first completely well-centered mesh of the cube in $\mathbb{R}^3$ is a mesh with 224 tetrahedra that we generated in a similar fashion. Figure 8.4, courtesy of Damrong Guoy, gives a visual overview of our completely well-centered mesh of the cube with 194 tetrahedra.

The bottom left quarter of Fig. 8.4 shows a set of six tetrahedra that are incident to a corner vertex of the cube. The bottom right quarter of Fig. 8.4 shows the same corner with an additional layer of tetrahedra built on top of the six tetrahedra incident to the corner vertex. This triangulation that fits into a corner of the cube extends exactly to a diagonal of each of three faces of the cube. In constructing a triangulation of the cube as a whole, we use in each of four corners a triangulation that is combinatorially the same and geometrically similar to the triangulation in this corner. Bold lines in the top left quarter of Fig. 8.4 indicate the visible boundaries of the four corner triangulations, showing how the corner triangulations fit together and complete a triangulation of the surface of the cube. Given the triangulations in theses four corners, the triangulation of the cube volume is completed by adding a vertex at the center of the cube and computing the Delaunay triangulation.

The mesh pictured in Fig. 8.4 does not have the best possible quality for meshes of the cube with the given combinatorics, but it is chosen because the surface triangulation has some desirable symmetries. In particular, every vertex on the surface of the cube is either at a corner of the cube,

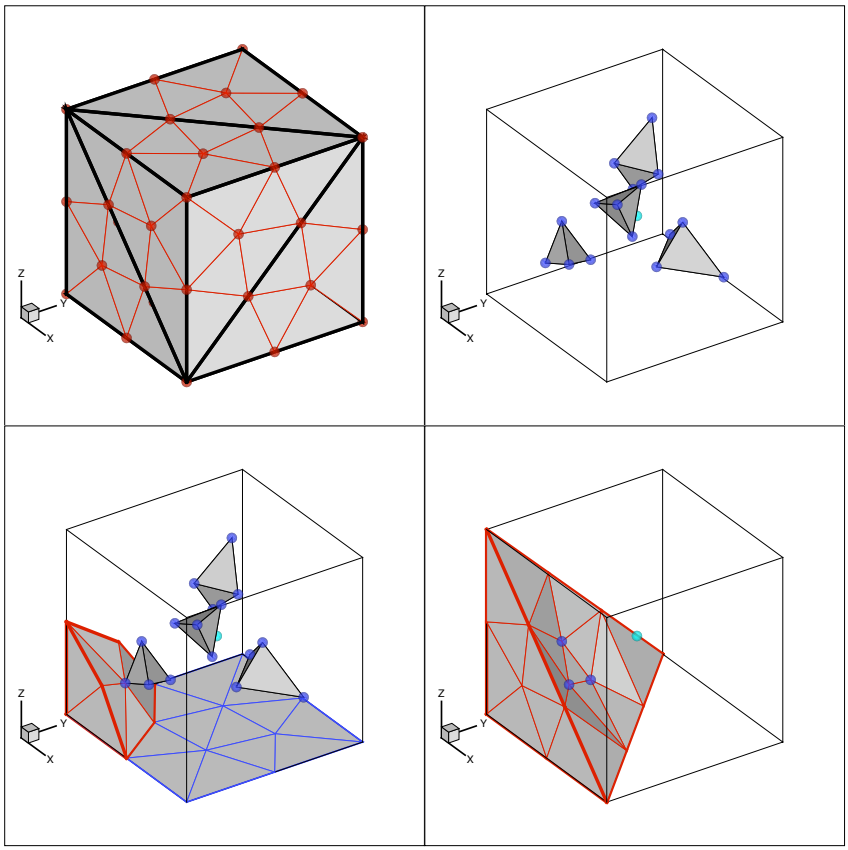


Figure 8.4: The mesh shown here is a completely well-centered mesh of the cube with 194 tetrahedra. The view at top left shows the surface triangulation and highlights the structure of the mesh. The other views show important parts of the interior of the mesh, as described more fully in the text.

| Cube Mesh Quality Statistics | | | | | | |
|---|---|---|---|---|---|---|
| Quantity | 224 Tets | | 194 Tets | | 146 Tets | |
| | Min | Max | Min | Max | Min | Max |
| $h/R$ | 0.041 | 0.850 | 0.005 | 0.790 | 0.016 | 0.854 |
| Face Angle | 21.01° | 87.49° | 26.93° | 89.61° | 17.09° | 112.60° |
| Dihedral Angle | 24.91° | 105.61° | 28.26° | 126.64° | 10.73° | 163.17° |
| $R/\ell$ | 0.618 | 1.569 | 0.612 | 1.134 | 0.711 | 1.835 |

Table 8.1: The quality of our meshes of the cube decreases with the number of tetrahedra in the mesh of the cube.

or at a midpoint of an edge of the cube, or on a diagonal of a face of the cube. Up to an appropriate symmetry of $\mathbb{R}^3$, the triangulation on each face of the cube exactly matches the triangulation on any other face of the cube. Thus it is easy to fit together copies of this triangulation of the cube to triangulate any three-dimensional object that can be tiled with cubes.

### 8.2.2 Bounds on Number of Tetrahedra

Cassidy and Lord showed that there is an acute triangulation of the square with $n$ triangles for $n = 8$ and for $n \geq 10, n \in \mathbb{Z}$. They also proved that for any other $n$, the square has no acute triangulation with $n$ triangles [16]. The research of Cassidy and Lord can be generalized to questions about the three-dimensional cube in a variety of ways. From a practical point of view, since it usually requires less computer time to solve a problem on a mesh with a smaller number of elements, one of the more interesting generalizations is the question of the minimum number of tetrahedra necessary for a well-centered triangulation of the cube.

We have just seen that there exists a completely well-centered triangulation of the cube with 194 tetrahedra. For completely well-centered and 2-well-centered meshes, this is the best known. The smallest known 3-well-centered mesh of the cube, on the other hand, is a mesh with 146 tetrahedra, which we constructed with the same general technique used to create the meshes with 194 and 224 tetrahedra. We do not describe in detail the meshes with 146 or 224 tetrahedra, but in Table 8.1 we compare their quality to the quality of the mesh of the cube with 194 tetrahedra.

An upper bound on the number of tetrahedra needed for a well-centered mesh can be proved by presenting an explicit construction. Lower bounds are necessarily more abstract. The observations in Chapter 3 and Chapter 4 about the geometry and combinatorics of well-centered meshes are helpful in both regards. In constructing a mesh, these observations guide decisions about what constitutes a good mesh. In proving lower bounds, the observations become useful theoretical tools. For example, no cube corner tetrahedron, e.g., the tetrahedron shown in Fig. 8.5, can be 3-well-centered; considering the bottom facet to be a given facet, we see that the fourth vertex of the tetrahedron projects onto (not inside) the circumcircle of the given facet, violating the necessary Cylinder Condition of Proposition 3.2.1.

It follows that in a 3-well-centered mesh of the cube there must be at least two tetrahedra incident to each corner of the cube. Indeed, there must be at least three tetrahedra incident to each corner of the cube in a 3-well-centered mesh. In the case of two tetrahedra incident to a corner vertex there must be exactly four edges incident to the corner vertex, of which three are in the directions of the coordinate axes. The fourth edge must lie in a face, and both tetrahedra are incident to the

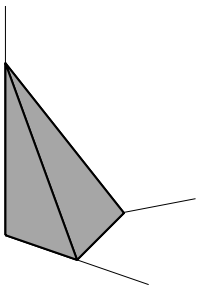

Figure 8.5: No 2-well-centered or 3-well-centered mesh of the solid cube has a tetrahedron with three of its facets lying in faces of the cube.

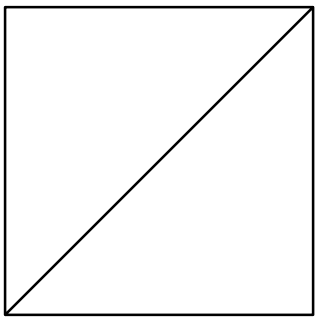

Figure 8.6: No 3-well-centered mesh of the cube has a face with this triangulation.

axis orthogonal to the face of the cube containing the fourth edge. The Cylinder Condition applies again, and we see that the mesh cannot be 3-well-centered.

Ad hoc arguments from basic Euclidean geometry provide more restrictions on well-centered triangulations of the solid cube. For instance, in any 3-well-centered mesh of the cube, no face of the cube is triangulated as shown in Fig. 8.6, with two right triangles meeting along the hypotenuse. The two right triangles have the same circumcenter, which lies at the midpoint of the common hypotenuse of the triangles—the center of the face of the cube. For either triangle, a tetrahedron having that triangle as a facet must have its circumcenter on a line $\ell$ perpendicular to the face of the cube that meets the cube face at its center. Considering two tetrahedra $\sigma_1$ and $\sigma_2$, each having one of the right triangles as a face, it can be shown that at most one of $\sigma_1, \sigma_2$ can be 3-well-centered. There is a plane that contains the hypotenuse of the right triangles and divides $\mathbb{R}^3$ into two open halfspaces $H_1$ and $H_2$ such that $\sigma_1$ is in the (topological) closure of $H_1$ and $\sigma_2$ is in the closure of $H_2$. If $\sigma_1$ and $\sigma_2$ share a common face, the plane must be $\text{aff}(\sigma_1 \cap \sigma_2)$. Otherwise there is some flexibility in the choice of the plane. The portion of $\ell$ interior to the cube is either in the boundary between $H_1$ and $H_2$ or without loss of generality can be assumed to lie entirely in $H_1$. In either case, the circumcenter of $\sigma_2$ is not strictly interior to $\sigma_2$, so $\sigma_2$ is not 3-well-centered.

In a triangulation of the cube, the number of tetrahedra incident to the surface of the cube is a lower bound on the total number of tetrahedra, so one can obtain a lower bound on the number of tetrahedra by counting the number of triangular facets in a surface triangulation. The number of surface facets is not a direct lower bound, since there may be a single tetrahedron with multiple facets in the surface of the cube. Because there are at least three distinct tetrahedra incident to a cube corner in a 3-well-centered triangulation of the cube, however, a tetrahedron cannot be counted more than twice in counting the number of surface facets of a 3-well-centered triangulation of the cube. We also know that a tetrahedron cannot be counted more than twice in counting the number of surface facets of a 2-well-centered triangulation of the cube, since three of the facets of a cube corner tetrahedron are right triangles.

Noting, then, that each face of the cube must contain at least 3 triangles in a 3-well-centered mesh of the cube and at least 8 triangles in a 2-well-centered mesh of the cube, we easily obtain a

lower bound of 9 tetrahedra for a 3-well-centered triangulation of the cube, and 24 tetrahedra for a 2-well-centered triangulation of the cube. In fact, every acute triangulation of the surface of the cube must have at least 56 surface facets, and any tetrahedron that is counted twice in counting the number of surface facets must have an edge coinciding with an edge of the cube. This implies a lower bound of 38 tetrahedra for a 2-well-centered triangulation of the cube. These relatively simple bounds count only tetrahedra with three or more vertices on the surface of the cube, and can hardly be considered more than a starting place for a more careful analysis.

### 8.2.3 Acute Triangulation

The question of obtaining well-centered triangulations of the cube is motivated in part by the similar but more difficult problem of constructing an acute triangulation of the cube. One of the motivations for acute triangulations in $\mathbb{R}^3$ is that a finite element solution of a reaction-diffusion problem is guaranteed to satisfy a discrete maximum principle if the mesh satisfies some geometric conditions. In particular, the mesh must be an acute triangulation [17, 12].

A review article published in 2009 on the subject of nonobtuse and acute triangulations shows that the topic is of current interest [11]. The specific problem of construction an acute triangulation of the cube is posed by Eppstein, Sullivan, and Üngör in [26], where they solve the acute triangulation of 3-space and slabs in $\mathbb{R}^3$. The problem is also mentioned in [49].

We solved the problem in [66], using essentially the same method that we used to construct well-centered triangulations of the cube. Every edge in the interior of an acute triangulation in $\mathbb{R}^3$ must be incident to at least five tetrahedra. It is an easy exercise to show that this implies every interior vertex must be incident to at least 12 edges (20 tetrahedra). Thus the combinatorial requirements of an acute triangulation are more restrictive than the requirements for a completely well-centered triangulation. To meet these combinatorial requirements, we constructed a mesh of the cube with 1370 tetrahedra. In other respects, our solution to the problem was similar to the well-centered case, and it is worth noting that our mesh of the cube with 1370 tetrahedra is completely well-centered as well as dihedral acute.

The problem of acute triangulation of the cube was independently solved at about the same time as our solution by Kopczyński, Pak, and Przytycki, who give a construction using 2715 tetrahedra [37]. Kopczyński et al. also solve some other important problems related to acute triangulation in dimensions higher than 2. In particular, they show that the cube in $\mathbb{R}^4$ (and higher dimensions) cannot be triangulated with dihedral acute simplices. In $\mathbb{R}^5$ and higher there is no tiling of Euclidean space with dihedral acute simplices. (This result was stated by Křížek in [38], but his proof is incorrect [37].) For $\mathbb{R}^3$ Kopczyński et al. show that all the Platonic solids can be triangulated with acute tetrahedra.

Although the subject of acute triangulation is somewhat related to well-centered triangulation, a more detailed discussion of the acute triangulation of the cube or other Platonic solids is outside the scope of this dissertation.

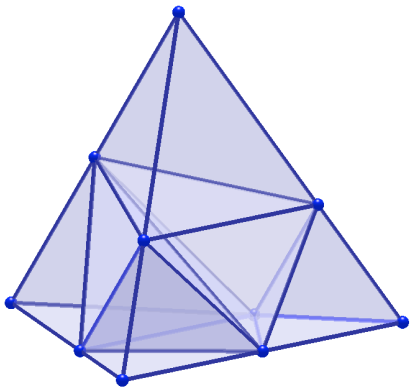

| Quality Statistics | | |
|---|---|---|
| Quantity | Min | Max |
| $h/R$ | 0.0345 | 0.712 |
| Face Angle | 38.87° | 86.76° |
| Dihedral Angle | 38.44° | 121.37° |
| $R/\ell$ | 0.702 | 0.934 |

Figure 8.7: The triangulation shown here is a triangulation of the regular tetrahedron with eight smaller completely well-centered tetrahedra.

## 8.3 The Standard Tetrahedron and the Regular Tetrahedron

We have seen that the cube in $\mathbb{R}^3$ has a triangulation with completely well-centered tetrahedra. A natural follow-up question concerns tetrahedra. Does the regular tetrahedron have a nontrivial triangulation into completely well-centered tetrahedra? What about other tetrahedra?

We begin by observing that the standard tetrahedron, or cube corner tetrahedron, does have a subdivision into completely well-centered tetrahedra. The bottom right quarter of Fig. 8.4 shows a triangulation of a region in $\mathbb{R}^3$ that fits into the corner of a cube. The region shown in Fig. 8.4 is not a tetrahedron, but the three visible vertices in the interior of the cube can be moved onto the boundary of a standard tetrahedron, and one can obtain a completely well-centered triangulation of the standard tetrahedron with 34 tetrahedra.

Subdividing the regular tetrahedron into smaller well-centered tetrahedra might seem relatively simple, but the problem is not so easy as it might initially seem. For instance, it is know that the regular tetrahedron can be triangulation with 543 smaller acute tetrahedra, but no smaller nontrivial acute triangulation of the regular tetrahedron is known. In two dimensions the Loop subdivision, which refines a triangle by connecting the midpoints of each edge of the triangle, produces four smaller triangles. Each of these smaller triangles is similar to the original triangle, so the Loop subdivision of an acute triangle is an acute triangulation of the triangle with four smaller triangles. Thus there is an easy way to triangulate a 2-dimensional regular simplex into smaller completely well-centered (and acute) regular simplices. In three dimensions, however, there is no obvious analog of the Loop subdivision.

Connecting the midpoints of the edges of a tetrahedron cuts out four corner tetrahedra that are similar to the original tetrahedron. The shape that remains in the center after removing these four tetrahedra is an octahedron. In the case of the regular tetrahedron, it is a regular octahedron, and it can be triangulated with four tetrahedra by adding an edge between a pair of opposite vertices of the octahedron. The result is not well-centered; the center of the octahedron is the circumcenter of all four tetrahedra, so the tetrahedra are not 3-well-centered. In addition, the facets incident to the new edge are right triangles, so the tetrahedra are not 2-well-centered.

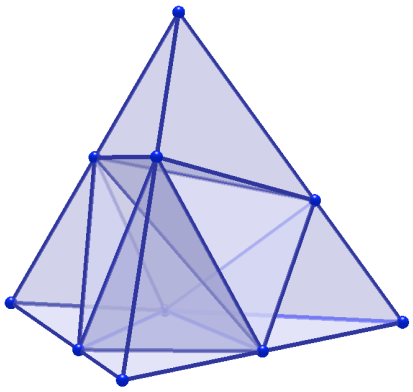

| Quality Statistics | | |
|---|---|---|
| Quantity | Min | Max |
| $h/R$ | 0.0448 | 0.584 |
| Face Angle | 39.63° | 87.43° |
| Dihedral Angle | 46.72° | 105.95° |
| $R/\ell$ | 0.777 | 0.826 |

Figure 8.8: The triangulation of the regular tetrahedron shown here is another triangulation of the regular tetrahedron into eight completely well-centered tetrahedra. It has the same combinatorics as the mesh in Fig. 8.7, but the geometry is quite different.

We can find a combinatorially equivalent triangulation of the regular tetrahedron into well-centered tetrahedra, however. By sliding some of the new vertices along the edges of the regular tetrahedron, moving them away from the edge midpoints, one can make the four center tetrahedra well-centered without destroying the well-centeredness of the four corner tetrahedra. Figures 8.7 and 8.8 illustrate two different successful ways we can slide the vertices along edges of the tetrahedra. In both cases, the midpoint vertices that are adjacent to the central edge remain stationary, to keep the central edge as short as possible. In Fig. 8.7, the four free midpoints all slide towards the same edge of the regular tetrahedron. In Fig. 8.8, the free midpoints slide along a directed four-cycle through the vertices of the regular tetrahedron.

There are also more complicated ways to divide the regular tetrahedron into smaller well-centered tetrahedra. Figure 8.9 shows the basic structure of a subdivision of the regular tetrahedron into 49 tetrahedra. A smaller regular tetrahedron is placed in the center of the large tetrahedron with the same orientation as the original. Each face of the smaller tetrahedron is connected to the center of a face of the larger tetrahedron. At each corner of the large tetrahedron, a small regular tetrahedron is cut off of the corner, and the resulting face is connected to a vertex of the central regular tetrahedron. After filling in a few more tetrahedral faces, six more edges need to be added to subdivide octahedral gaps into tetrahedra. The mesh shown in Fig. 8.10 is the completely well-centered mesh that results from optimizing the mesh shown in Fig. 8.9. This subdivision of the regular tetrahedron is interesting partly because all of the surface triangulations match and have three-fold radial symmetry. It is also possible that this type of subdivision will be easier to use in mesh refinement than the other two subdivisions.

It is not clear whether either of these constructions would be useful for refining a completely well-centered mesh into a completely well-centered mesh with a larger number of smaller elements. In particular, we it is not clear whether the constructions can be extended create a well-centered triangulation of an arbitrary well-centered tetrahedron. It is clear that neither construction can be extended to create a well-centered subdivision of an arbitrary (not well-centered) tetrahedron, since both constructions cut off corners of the tetrahedron to create smaller tetrahedra that are nearly similar to the original tetrahedron.

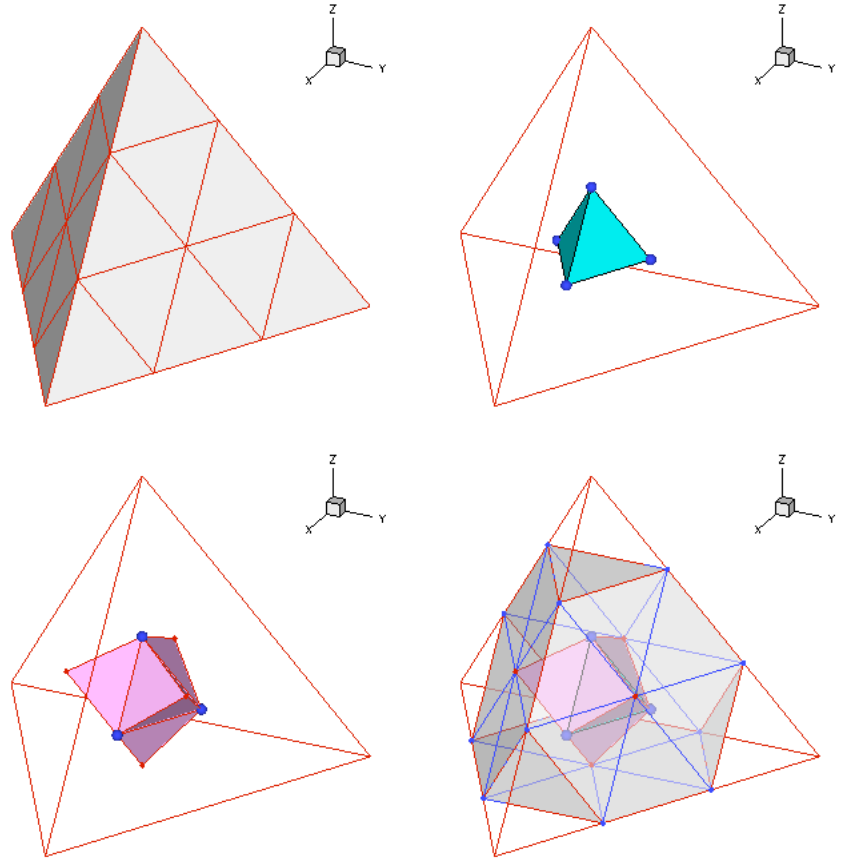

Figure 8.9: This is a subdivision of the regular tetrahedron that can be made completely well-centered through optimization.

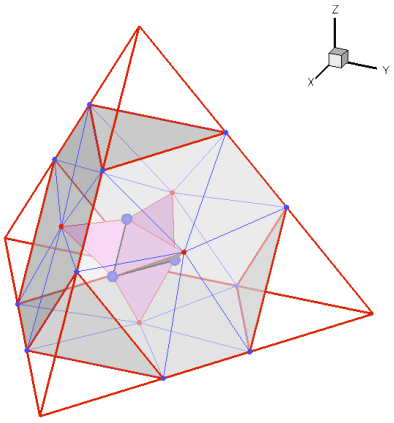

| Quality Statistics | | |
|---|---|---|
| Quantity | Min | Max |
| $h/R$ | 0.0146 | 0.845 |
| Face Angle | 23.36° | 89.07° |
| Dihedral Angle | 29.93° | 107.73° |
| $R/\ell$ | 0.612 | 1.305 |

Figure 8.10: This is the completely well-centered subdivision of the regular tetrahedron that results from optimizing the mesh shown in Fig. 8.9.

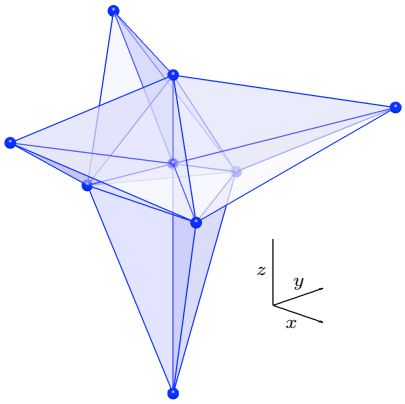


| $x$ | $y$ | $z$ |
|---|---|---|
| 0 | 0 | 0 |
| 0 | 0 | 1 |
| 0 | 0.9428 | −0.3333 |
| −0.8165 | −0.4714 | −0.3333 |
| 0.8165 | −0.4714 | −0.3333 |
| 0 | 0 | −2.5941 |
| 0 | −2.4457 | 0.8647 |
| −2.1181 | 1.2229 | 0.8647 |
| 2.1181 | 1.2229 | 0.8647 |

Figure 8.11: This is a 3-well-centered tetrahedral mesh with a single interior vertex $u$ such that Lk $u$ is isomorphic to polyhedron 8–1 from the catalog of Britton and Dunitz [14]. Vertex $u$ is at the origin. For each face $uv_iv_j$ incident to vertex $u$, the angles $\measuredangle uv_iv_j$ and $\measuredangle uv_jv_i$ are acute.

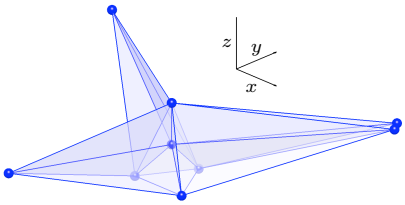


| $x$ | $y$ | $z$ |
|---|---|---|
| 0 | 0 | 0 |
| 0 | 0 | 1 |
| 0 | 0.8334 | −0.86 |
| −0.7217 | −0.4167 | −0.86 |
| 0.7217 | −0.4167 | −0.86 |
| 0 | −5.0494 | 0.97 |
| 4.3729 | 2.5247 | 0.97 |
| −4.3729 | 2.5247 | 0.97 |
| 4.2265 | 2.7475 | 0.9981 |

Figure 8.12: This is a 3-well-centered tetrahedral mesh with a single interior vertex $u$ such that Lk $u$ is isomorphic to polyhedron 8–2 from the catalog of Britton and Dunitz [14]. Vertex $u$ is at the origin. For each face $uv_iv_j$ incident to vertex $u$, the angles $\measuredangle uv_iv_j$ and $\measuredangle uv_jv_i$ are acute.

## 8.4 Tetrahedral One-Ring Neighborhoods

In Chapter 4 we proved that polyhedra 8–4, 8–5, 8–6, 8–7, and 8–13 from the catalog of Britton and Dunitz [14] cannot appear as the link of a vertex in a 3-well-centered tetrahedral mesh in $\mathbb{R}^3$. We claimed that any other triangulation of $S^2$ with 8 vertices can appear as the link of a vertex in a 3-well-centered tetrahedral mesh in $\mathbb{R}^3$. Figures 8.11 through 8.19 are 3-well-centered tetrahedral meshes in $\mathbb{R}^3$ that verify this claim. Each mesh has exactly one interior vertex $u$ with Lk $u$ isomorphic to one of the triangulations of $S^2$ on 8 vertices. In each mesh, the angles $\measuredangle uv_iv_j$ and $\measuredangle uv_jv_i$ in faces incident to the interior vertex $u$ are acute angles. Thus by Proposition 4.3.7, a degree 3 vertex can be inserted in any face on Lk $u$ to create a triangulation of $S^2$ with 9 vertices that can appear as the link of a vertex in a 3-well-centered tetrahedral mesh in $\mathbb{R}^3$.

Many of the 3-well-centered meshes shown here were, in fact, constructed using the method discussed in Proposition 4.3.7. The 3-well-centered tetrahedral mesh in Fig. 4.8 can be modified slightly to satisfy the acute face angle conditions of Proposition 4.3.7, and it is plain to the eye that modified versions of the mesh were used to construct the 3-well-centered meshes in Figs. 8.12 and 8.13. Similarly, modified versions of the mesh shown in Fig. 4.7 were used with Proposition 4.3.7 to construct the meshes in Figs. 8.15, 8.16, and 8.17.

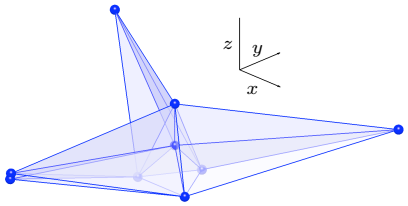


| $x$ | $y$ | $z$ |
|---|---|---|
| 0 | 0 | 0 |
| 0 | 0 | 1 |
| 0 | 0.8334 | −0.8588 |
| −0.7217 | −0.4167 | −0.8588 |
| 0.7217 | −0.4167 | −0.8588 |
| 0 | −5.0494 | 0.99 |
| 4.3729 | 2.5247 | 0.99 |
| −4.3729 | 2.5247 | 0.99 |
| 0 | −5.0747 | 0.8609 |

Figure 8.13: This is a 3-well-centered tetrahedral mesh with a single interior vertex $u$ such that Lk $u$ is isomorphic to polyhedron 8–3 from the catalog of Britton and Dunitz [14]. Vertex $u$ is at the origin. For each face $uv_iv_j$ incident to vertex $u$, the angles $\measuredangle uv_iv_j$ and $\measuredangle uv_jv_i$ are acute.

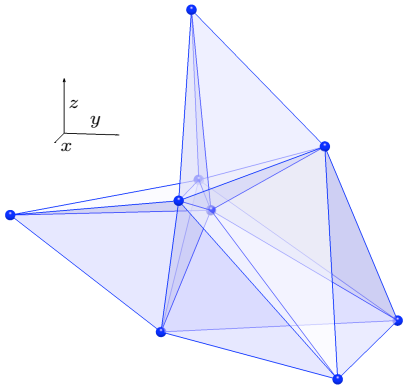


| $x$ | $y$ | $z$ |
|---|---|---|
| 0 | 0 | 0 |
| −1.1093 | −0.4179 | 0.3486 |
| 1.0908 | −0.3956 | 0.3507 |
| −0.0141 | 2.0729 | 1.2221 |
| 0.0195 | −0.9073 | −2.2409 |
| 3.1552 | 2.8663 | −2.4441 |
| −3.2107 | 2.8365 | −2.4802 |
| −0.0248 | −0.3602 | 3.6381 |
| 0.0123 | −3.6572 | −0.1974 |

Figure 8.14: This is a 3-well-centered tetrahedral mesh with a single interior vertex $u$ such that Lk $u$ is isomorphic to polyhedron 8–8 from the catalog of Britton and Dunitz [14]. Vertex $u$ is at the origin. For each face $uv_iv_j$ incident to vertex $u$, the angles $\measuredangle uv_iv_j$ and $\measuredangle uv_jv_i$ are acute.

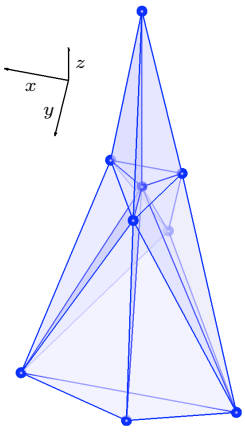


| $x$ | $y$ | $z$ |
|---|---|---|
| 0 | 0 | 0 |
| 0 | 0 | 1 |
| −0.1041 | −0.0601 | 0.0117 |
| 0.1041 | −0.0601 | 0.0117 |
| 0 | 0.1202 | 0.0117 |
| 0 | −0.3622 | −0.8656 |
| 0.3137 | 0.1811 | −0.8656 |
| −0.3137 | 0.1811 | −0.8656 |
| 0 | 0.2118 | −0.9728 |

Figure 8.15: This is a 3-well-centered tetrahedral mesh with a single interior vertex $u$ such that Lk $u$ is isomorphic to polyhedron 8–9 from the catalog of Britton and Dunitz [14]. Vertex $u$ is at the origin. For each face $uv_iv_j$ incident to vertex $u$, the angles $\measuredangle uv_iv_j$ and $\measuredangle uv_jv_i$ are acute.

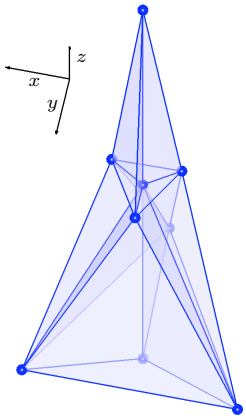


| $x$ | $y$ | $z$ |
|---|---|---|
| 0 | 0 | 0 |
| 0 | 0 | 4.3459 |
| −0.4386 | −0.2641 | 0.0516 |
| 0.4480 | −0.2478 | 0.0516 |
| −0.0094 | 0.5119 | 0.0516 |
| 0.0007 | −1.5813 | −3.7527 |
| 1.3691 | 0.7912 | −3.7527 |
| −1.3698 | 0.7901 | −3.7527 |
| 0 | 0 | −4.3200 |

Figure 8.16: This is a 3-well-centered tetrahedral mesh with a single interior vertex $u$ such that Lk $u$ is isomorphic to polyhedron 8–10 from the catalog of Britton and Dunitz [14]. Vertex $u$ is at the origin. For each face $uv_iv_j$ incident to vertex $u$, the angles $\measuredangle uv_iv_j$ and $\measuredangle uv_jv_i$ are acute.

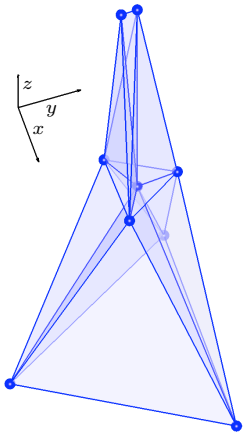


| $x$ | $y$ | $z$ |
|---|---|---|
| 0 | 0 | 0 |
| −0.4357 | −0.2700 | 0.0511 |
| 0.4413 | −0.2397 | 0.0497 |
| −0.0165 | 0.5001 | 0.0492 |
| −0.0104 | −1.5697 | −3.8206 |
| 1.3646 | 0.7829 | −3.8055 |
| −1.3665 | 0.7723 | −3.8162 |
| 0 | 0 | 4.1500 |
| 0.0012 | −0.1996 | 4.1432 |

Figure 8.17: This is a 3-well-centered tetrahedral mesh with a single interior vertex $u$ such that Lk $u$ is isomorphic to polyhedron 8–11 from the catalog of Britton and Dunitz [14]. Vertex $u$ is at the origin. For each face $uv_iv_j$ incident to vertex $u$, the angles $\measuredangle uv_iv_j$ and $\measuredangle uv_jv_i$ are acute.

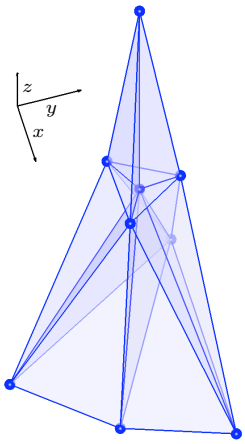


| $x$ | $y$ | $z$ |
|---|---|---|
| 0 | 0 | 0 |
| −0.4357 | −0.2700 | 0.0511 |
| 0.4413 | −0.2397 | 0.0497 |
| −0.0165 | 0.5001 | 0.0492 |
| −0.0104 | −1.5697 | −3.8206 |
| 1.3646 | 0.7829 | −3.8055 |
| −1.3665 | 0.7723 | −3.8162 |
| 0 | 0 | 4.1500 |
| 0.7290 | −0.4424 | −4.1518 |

Figure 8.18: This is a 3-well-centered tetrahedral mesh with a single interior vertex $u$ such that Lk $u$ is isomorphic to polyhedron 8–12 from the catalog of Britton and Dunitz [14]. Vertex $u$ is at the origin. For each face $uv_iv_j$ incident to vertex $u$, the angles $\measuredangle uv_iv_j$ and $\measuredangle uv_jv_i$ are acute.

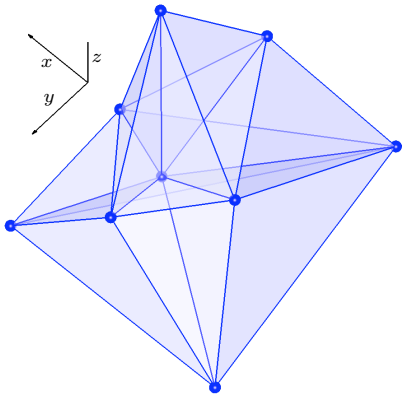


| $x$ | $y$ | $z$ |
|---|---|---|
| 0 | 0 | 0 |
| −0.8918 | −0.2777 | 0.1629 |
| 0.8968 | −0.2584 | 0.1610 |
| −0.0091 | 0.8720 | 0.1750 |
| −0.0383 | −3.9987 | −4.4176 |
| 1.5828 | 0.8552 | −1.9216 |
| −1.6059 | 0.8227 | −1.9221 |
| 0.0030 | 0.0161 | 3.8461 |
| 0.0197 | −1.8007 | 0.9312 |

Figure 8.19: This is a 3-well-centered tetrahedral mesh with a single interior vertex $u$ such that Lk $u$ is isomorphic to polyhedron 8–14 from the catalog of Britton and Dunitz [14]. Vertex $u$ is at the origin. For each face $uv_iv_j$ incident to vertex $u$, the angles $\measuredangle uv_iv_j$ and $\measuredangle uv_jv_i$ are acute.

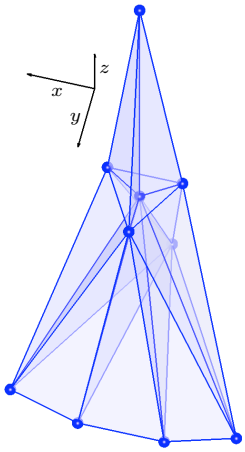


| $x$ | $y$ | $z$ |
|---|---|---|
| 0 | 0 | 0 |
| 0 | 0 | 1 |
| −0.1041 | −0.0601 | 0.0117 |
| 0.1041 | −0.0601 | 0.0117 |
| 0 | 0.1202 | 0.0117 |
| 0 | −0.3622 | −0.8656 |
| −0.3137 | 0.1811 | −0.8656 |
| 0.3137 | 0.1811 | −0.8656 |
| −0.1200 | 0.2080 | −0.9200 |
| 0.1200 | 0.2080 | −0.9200 |

Figure 8.20: This is a 3-well-centered tetrahedral mesh with a single interior vertex $u$ such that vertex $u$ is at the origin and for each face $uv_iv_j$ incident to vertex $u$, the angles $\measuredangle uv_iv_j$ and $\measuredangle uv_jv_i$ are acute. The triangulation Lk $u$ has degree list $(7, 6, 5, 5, 4, 4, 4, 4, 3)$ and is one of 5 triangulations of $S^2$ that cannot be analyzed either by Theorem 4.3.2 or by using Proposition 4.3.7 to add a degree 3 vertex to some triangulation of $S^2$ with 8 vertices.

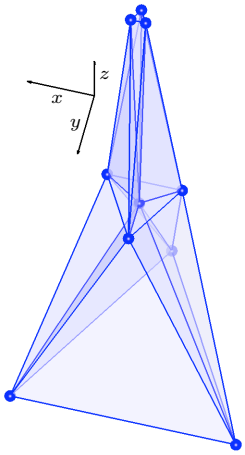


| $x$ | $y$ | $z$ |
|---|---|---|
| 0 | 0 | 0 |
| −0.1041 | −0.0601 | 0.0117 |
| 0.1041 | −0.0601 | 0.0117 |
| 0 | 0.1202 | 0.0117 |
| 0 | −0.3622 | −0.8656 |
| −0.3137 | 0.1811 | −0.8656 |
| 0.3137 | 0.1811 | −0.8656 |
| 0 | −0.0240 | 1 |
| −0.0208 | 0.0120 | 1 |
| 0.0208 | 0.0120 | 1 |

Figure 8.21: This is a 3-well-centered tetrahedral mesh with a single interior vertex $u$ such that vertex $u$ is at the origin and for each face $uv_iv_j$ incident to vertex $u$, the angles $\measuredangle uv_iv_j$ and $\measuredangle uv_jv_i$ are acute. The triangulation Lk $u$ is the unique triangulation of $S^2$ with degree list $(6, 6, 6, 4, 4, 4, 4, 4, 4)$ and is one of 5 triangulations of $S^2$ that cannot be analyzed either by Theorem 4.3.2 or by using Proposition 4.3.7 to add a degree 3 vertex to some triangulation of $S^2$ with 8 vertices.

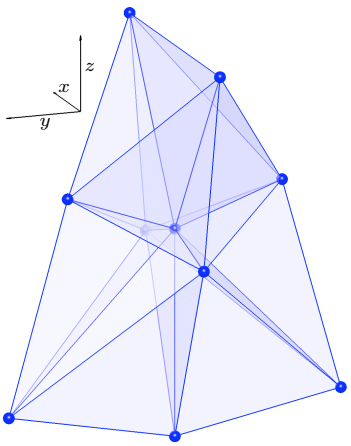


| $x$ | $y$ | $z$ |
|---|---|---|
| 0 | 0 | 0 |
| −0.5237 | 0 | 0.7543 |
| 0.5237 | 0 | 0.7543 |
| −0.3367 | 0 | −0.0911 |
| 0.3367 | 0 | −0.0911 |
| 0 | −0.4518 | 0.1623 |
| 0 | 0.4518 | 0.1623 |
| 0 | 0 | −0.8516 |
| 0 | −0.7000 | −0.7140 |
| 0 | 0.7000 | −0.7140 |

Figure 8.22: This is a 3-well-centered tetrahedral mesh with a single interior vertex $u$ such that vertex $u$ is at the origin and for each face $uv_iv_j$ incident to vertex $u$, the angles $\measuredangle uv_iv_j$ and $\measuredangle uv_jv_i$ are acute. The triangulation Lk $u$ is the unique triangulation of $S^2$ with degree list $(6, 6, 5, 5, 4, 4, 4, 4)$ and is one of 5 triangulations of $S^2$ that cannot be analyzed either by Theorem 4.3.2 or by using Proposition 4.3.7 to add a degree 3 vertex to some triangulation of $S^2$ with 8 vertices.

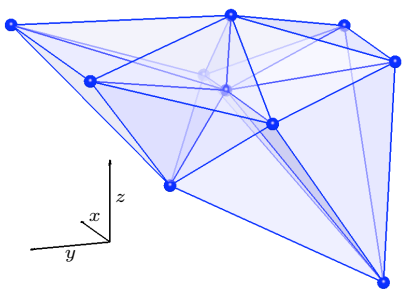


| $x$ | $y$ | $z$ |
|---|---|---|
| 0 | 0 | 0 |
| 0 | −0.0190 | 0.2832 |
| −0.3701 | −0.0472 | −0.0396 |
| 0.3701 | −0.0472 | −0.0396 |
| −0.4256 | 0.6868 | 0.2040 |
| 0.4256 | 0.6868 | 0.2040 |
| −0.2735 | −0.5617 | 0.1254 |
| 0.2735 | −0.5617 | 0.1254 |
| 0 | −0.6160 | −0.7877 |
| 0 | 0.2195 | −0.3422 |

Figure 8.23: This is a 3-well-centered tetrahedral mesh with a single interior vertex $u$ such that vertex $u$ is at the origin and for each face $uv_iv_j$ incident to vertex $u$, the angles $\measuredangle uv_iv_j$ and $\measuredangle uv_jv_i$ are acute. The triangulation Lk $u$ is the unique triangulation of $S^2$ with degree list $(6, 5, 5, 5, 5, 4, 4, 4, 4)$ and is one of 5 triangulations of $S^2$ that cannot be analyzed either by Theorem 4.3.2 or by using Proposition 4.3.7 to add a degree 3 vertex to some triangulation of $S^2$ with 8 vertices.

There are 50 nonisomorphic triangulations of $S^2$ with 9 vertices [42]. Although we do not show or list them here, 34 of these triangulations are triangulations $G$ with some vertex $v_1$ of degree 3 such that $G - v_1$ is one of the triangulations of $S^2$ shown as Lk $u$ in Figs. 8.11 through 8.19. Thus by Proposition 4.3.7, each of these 34 triangulations of $S^2$ can appear as the link of a vertex in a 3-well-centered tetrahedral mesh. Moreover, we can continue to insert vertices of degree 3 into any face of these 34 triangulations of $S^2$ to create more triangulations of $S^2$ that can appear as the link of a vertex in a 3-well-centered tetrahedral mesh.

There are 11 triangulations of $S^2$ with 9 vertices that cannot appear as the link of a vertex in a 3-well-centered mesh. For those 11 triangulations, Theorem 4.3.2 applies, and each has a corresponding tetrahedral complex that can be constructed by gluing tetrahedra together as described in Chapter 4.

There are 5 other triangulations of $S^2$ with 9 vertices. One of these is Lk $u$ in Fig. 4.18. As shown in that figure, it can appear as the link of a vertex in a completely well-centered mesh. The other 4 of these triangulations appear in Figs. 8.20 through 8.23, which are 3-well-centered tetrahedral meshes in $\mathbb{R}^3$ that certify that each of these triangulations of $S^2$ can appear as the link of a vertex in a 3-well-centered tetrahedral mesh in $\mathbb{R}^3$. Moreover, in each mesh every face incident to the central vertex $u$ satisfies the angle conditions specified in Proposition 4.3.7.

There are 233 nonisomorphic triangulations of $S^2$ with 10 vertices, and all but 12 of them have at least one vertex of degree 3. One can show that most of them can appear as the link of a vertex in a 3-well-centered mesh by removing a vertex of degree 3 and applying Proposition 4.3.7.

For triangulations of $S^2$ with 10 vertices, it is interesting to determine whether they can appear as the link of a vertex in a 2-well-centered or completely well-centered tetrahedral mesh in $\mathbb{R}^3$. Since Proposition 4.4.6 is an if and only if statement, we can use the proposition to determine whether any triangulation of $S^2$ with 10 vertices and a vertex of degree 3 permits a 2-well-centered neighborhood. There are only 3 such triangulations that do permit a 2-well-centered neighborhood, and each of them can appear as the link of a vertex in a completely well-centered tetrahedral mesh in $\mathbb{R}^3$. (See Figs. 8.24, 8.25, and 8.26.)

For the 12 triangulations of $S^2$ with 10 vertices and minimum degree 4, Theorem 4.4.4 shows that 5 of them do not permit a 2-well-centered neighborhood. Inserting a degree 4 vertex into the trian-

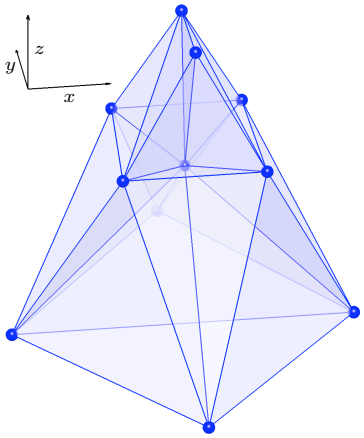


| $x$ | $y$ | $z$ |
|---|---|---|
| 0 | 0 | 0 |
| 0 | 0.0879 | 0.6059 |
| −0.2716 | −0.2745 | 0.0985 |
| 0.2716 | −0.2745 | 0.0985 |
| −0.2447 | 0.2214 | 0.1415 |
| 0.2447 | 0.2214 | 0.1415 |
| 0 | −0.6452 | −0.7640 |
| 0 | 0.7375 | −0.5788 |
| −0.6430 | 0.0514 | −0.6924 |
| 0.6430 | 0.0514 | −0.6924 |
| 0 | −0.2884 | 0.6280 |

Figure 8.24: This is a completely well-centered tetrahedral mesh with a single interior vertex $u$ such that Lk $u$ is a triangulation of $S^2$ with 10 vertices. The triangulation of $S^2$ can be obtained by adding a vertex of degree three to the only triangulation of $S^2$ with 9 vertices that can appear as the link of a vertex in a completely well-centered mesh.

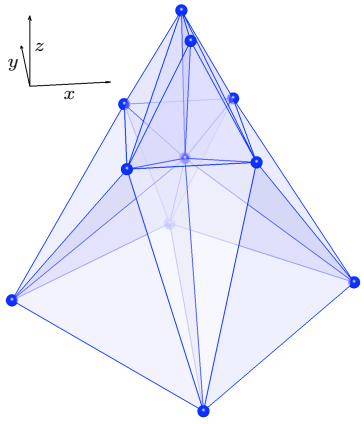


| $x$ | $y$ | $z$ |
|---|---|---|
| 0 | 0 | 0 |
| 0 | 0.13 | 0.58 |
| −0.25 | −0.25 | 0.11 |
| 0.25 | −0.25 | 0.11 |
| −0.21 | 0.23 | 0.12 |
| 0.21 | 0.23 | 0.12 |
| 0 | −0.68 | −0.73 |
| 0 | 0.56 | −0.61 |
| −0.66 | 0.07 | −0.63 |
| 0.66 | 0.07 | −0.63 |
| 0 | −0.21 | 0.64 |

Figure 8.25: This is a completely well-centered tetrahedral mesh with a single interior vertex $u$ such that Lk $u$ is a triangulation of $S^2$ with 10 vertices. The triangulation of $S^2$ can be obtained by adding a vertex of degree three to the only triangulation of $S^2$ with 9 vertices that can appear as the link of a vertex in a completely well-centered mesh.

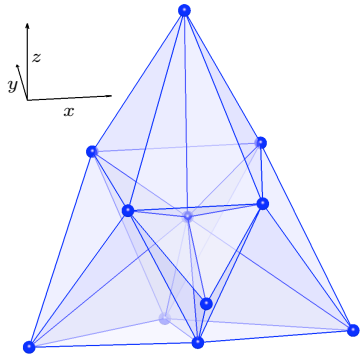


| $x$ | $y$ | $z$ |
|---|---|---|
| 0 | 0 | 0 |
| 0 | 0.095 | 0.794 |
| −0.25 | −0.236 | 0.149 |
| 0.25 | −0.236 | 0.149 |
| −0.312 | 0.334 | 0.128 |
| 0.312 | 0.334 | 0.128 |
| 0 | −0.312 | −0.365 |
| 0 | 0.685 | −0.729 |
| −0.601 | −0.109 | −0.444 |
| 0.601 | −0.109 | −0.444 |
| 0 | −0.569 | −0.089 |

Figure 8.26: This is a completely well-centered tetrahedral mesh with a single interior vertex $u$ such that Lk $u$ is a triangulation of $S^2$ with 10 vertices. The triangulation of $S^2$ can be obtained by adding a vertex of degree three to the only triangulation of $S^2$ with 9 vertices that can appear as the link of a vertex in a completely well-centered mesh.

gulation of $S^2$ with 9 vertices that permits a 2-well-centered neighborhood creates 3 triangulations of $S^2$ with 10 vertices that have minimum degree 4 and do permit a 2-well-centered neighborhood (by Proposition 4.4.7). Each of these three can also appear as the link of a vertex in a completely well-centered tetrahedral mesh in $\mathbb{R}^3$. (See Figs. 8.27, 8.28, and 8.29.)

The author believes that the other 4 triangulations of $S^2$ with 10 vertices and minimum degree 4 do not permit a 2-well-centered neighborhood, even though Theorem 4.4.4 does not directly apply.

## 8.5 The Square

In 1960 Gardner found a dissection of the square into 8 acute triangles and claimed that this was the minimum number of triangles possible for an acute dissection of the square [31]. Later Lindgren gave an easy proof that dissecting the square into acute triangles requires at least 8 triangles and showed that the dissection into 8 triangles is unique [40]. The dissection into 8 acute triangles happens to be a triangulation, and since triangulations are dissections, it is the smallest triangulation of the square into acute triangles. Cassidy and Lord proved that the square has a triangulation into $n$ acute triangles for $n = 8$ and $n \geq 10$, but not for $n = 9$ [16]. (There is a dissection into 9 acute triangles [16].)

The problem of finding acute triangulations of the square, though perhaps primarily a recreational problem, has sparked the interest of a number of mathematicians over the years, and the author of this dissertation also finds the problem interesting. Since any acute or 2-well-centered triangulation of the cube in $\mathbb{R}^3$ must include an acute triangulation of the surface of the cube, acute triangulations of the square may also contribute to the problem of finding acute or 2-well-centered triangulations of the cube with a small number of tetrahedra.

We say that two triangulations of the square are isomorphic if they are isomorphic as simplicial complexes and there is an isomorphism mapping every corner (edge, interior) vertex of one triangulation of the square onto a corner (edge, interior) vertex of the other triangulation of the square. The isomorphism need not preserve the orientation of the simplicial complex. The 8-triangle acute triangulation of the square is unique up to this definition of isomorphism.

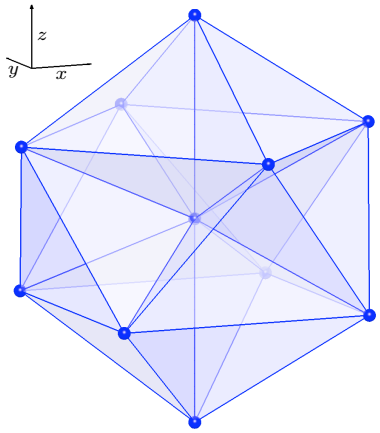


| $x$ | $y$ | $z$ |
|---|---|---|
| 0 | 0 | 0 |
| 0 | 0 | −1 |
| 0 | 0 | 1 |
| −0.9101 | 0 | 0.4144 |
| 0 | −0.9101 | 0.4144 |
| 0.9101 | 0 | 0.4144 |
| 0 | 0.9101 | 0.4144 |
| −0.6435 | 0.6435 | −0.4144 |
| −0.6435 | −0.6435 | −0.4144 |
| 0.6435 | −0.6435 | −0.4144 |
| 0.6435 | 0.6435 | −0.4144 |

Figure 8.27: This is a completely well-centered tetrahedral mesh with a single interior vertex $u$ such that Lk $u$ is a triangulation of $S^2$ with 10 vertices. The triangulation of $S^2$ can be obtained by adding a vertex of degree four to the only triangulation of $S^2$ with 9 vertices that can appear as the link of a vertex in a completely well-centered mesh. This is also an example of a construction of a completely well-centered mesh that uses a triangulation of a unit sphere $S^2$ based on two out-of-phase regular polygons. (See Fig. 4.11 and the discussion of Proposition 4.3.6.)

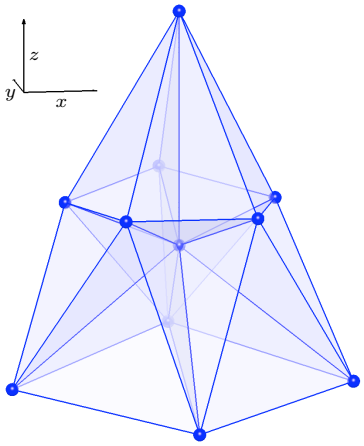


| $x$ | $y$ | $z$ |
|---|---|---|
| 0 | 0 | 0 |
| 0 | 0 | 1 |
| −0.28 | −0.388 | 0.175 |
| 0.28 | −0.388 | 0.175 |
| −0.446 | 0.274 | 0.146 |
| 0.446 | 0.274 | 0.146 |
| −0.725 | −0.112 | −0.578 |
| 0.725 | −0.112 | −0.578 |
| 0 | 0.337 | −0.383 |
| 0 | −0.622 | −0.7 |
| 0 | 0.614 | 0.232 |

Figure 8.28: This is a completely well-centered tetrahedral mesh with a single interior vertex $u$ such that Lk $u$ is a triangulation of $S^2$ with 10 vertices. The triangulation of $S^2$ can be obtained by adding a vertex of degree four to the only triangulation of $S^2$ with 9 vertices that can appear as the link of a vertex in a completely well-centered mesh.

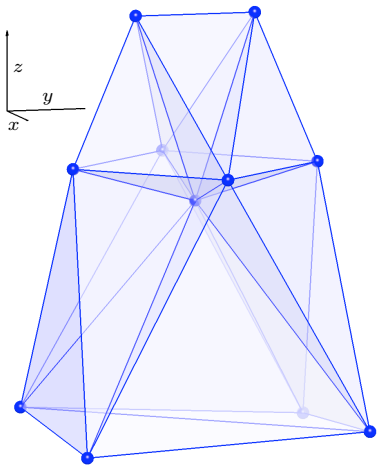


| $x$ | $y$ | $z$ |
|---|---|---|
| 0 | 0 | 0 |
| 0 | −0.19 | 0.58 |
| 0 | 0.19 | 0.58 |
| 0 | −0.39 | 0.11 |
| −0.39 | 0 | 0.11 |
| 0 | 0.39 | 0.11 |
| 0.39 | 0 | 0.11 |
| −0.44 | −0.44 | −0.68 |
| 0.44 | 0.44 | −0.68 |
| −0.47 | 0.47 | −0.73 |
| 0.47 | −0.47 | −0.73 |

Figure 8.29: This is a completely well-centered tetrahedral mesh with a single interior vertex $u$ such that Lk $u$ is a triangulation of $S^2$ with 10 vertices. The triangulation of $S^2$ can be obtained by adding a vertex of degree four to the only triangulation of $S^2$ with 9 vertices that can appear as the link of a vertex in a completely well-centered mesh.

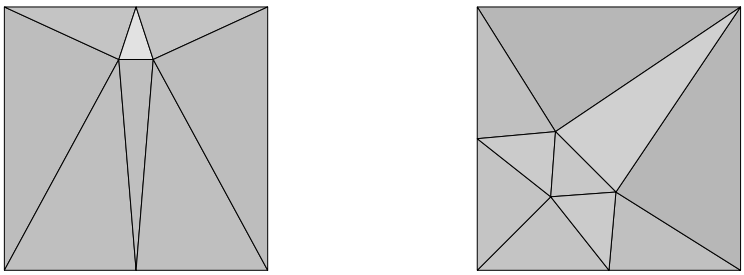

Figure 8.30: There is an triangulation of the square with 8 triangles (left) and an acute triangulation of the square with 10 triangles (right).

We present 25 nonisomorphic triangulations of the square in Figs. 8.30 through 8.34. Each triangulation uses at most 14 triangles, and the triangulations are divided according to the number of triangles. Fig. 8.30 shows the acute triangulation with 8 triangles and a triangulation with 10 triangles. Fig. 8.31 shows two triangulations with 11 triangles, Fig. 8.32 shows four triangulations with 12 triangles, Fig. 8.33 shows five triangulations with 13 triangles, and Fig. 8.34 shows twelve triangulations with 14 triangles. We conjecture that up to isomorphism these are the only acute triangulations of the square with at most 14 triangles.

A proof by case analysis could probably be assembled. If we consider a particular number of interior vertices and specify the triangulation of the interior vertices, this forces a particular interaction with the boundary. For example, if there are three interior vertices and the triangulation restricted to these three vertices is a path, then we are forced to use at least three vertices on the edges of the square, and there must be exactly two triangles incident to each corner of the square. Up to isomorphism, there are exactly two options for acute triangulation that have three interior vertices in a path; these are the rightmost triangulations in Figs. 8.31 and 8.32. Within each of the figures, the triangulations are arranged so that in left to right, top to bottom order, all triangulations that have the same triangulation on the interior vertices are next to each other.

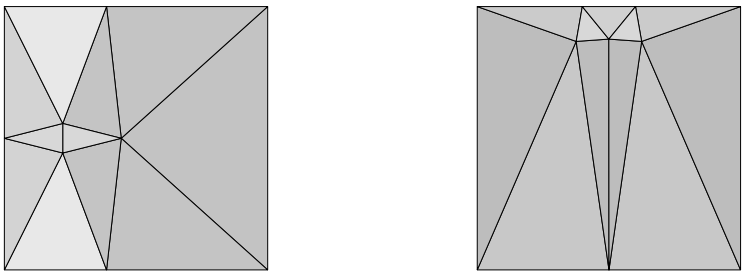

Figure 8.31: There are two acute triangulations of the square with 11 triangles.

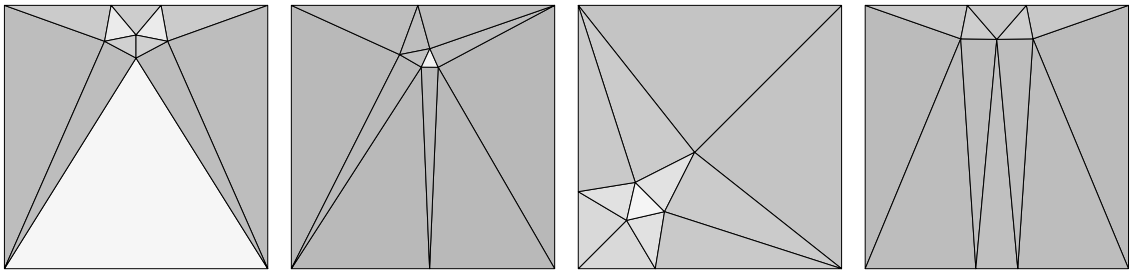

Figure 8.32: There are four acute triangulations of the square with 12 triangles.

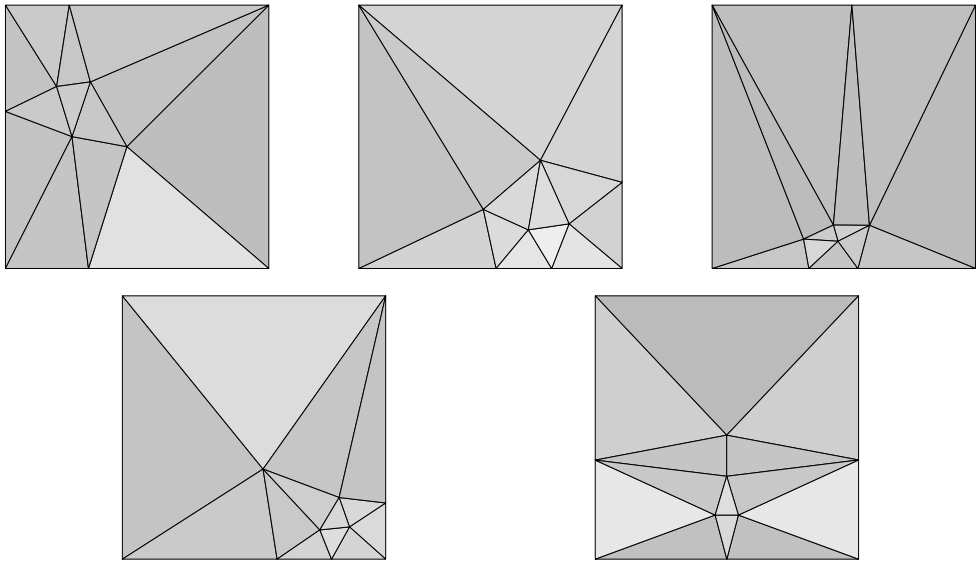

Figure 8.33: There are five acute triangulations of the square with 13 triangles.

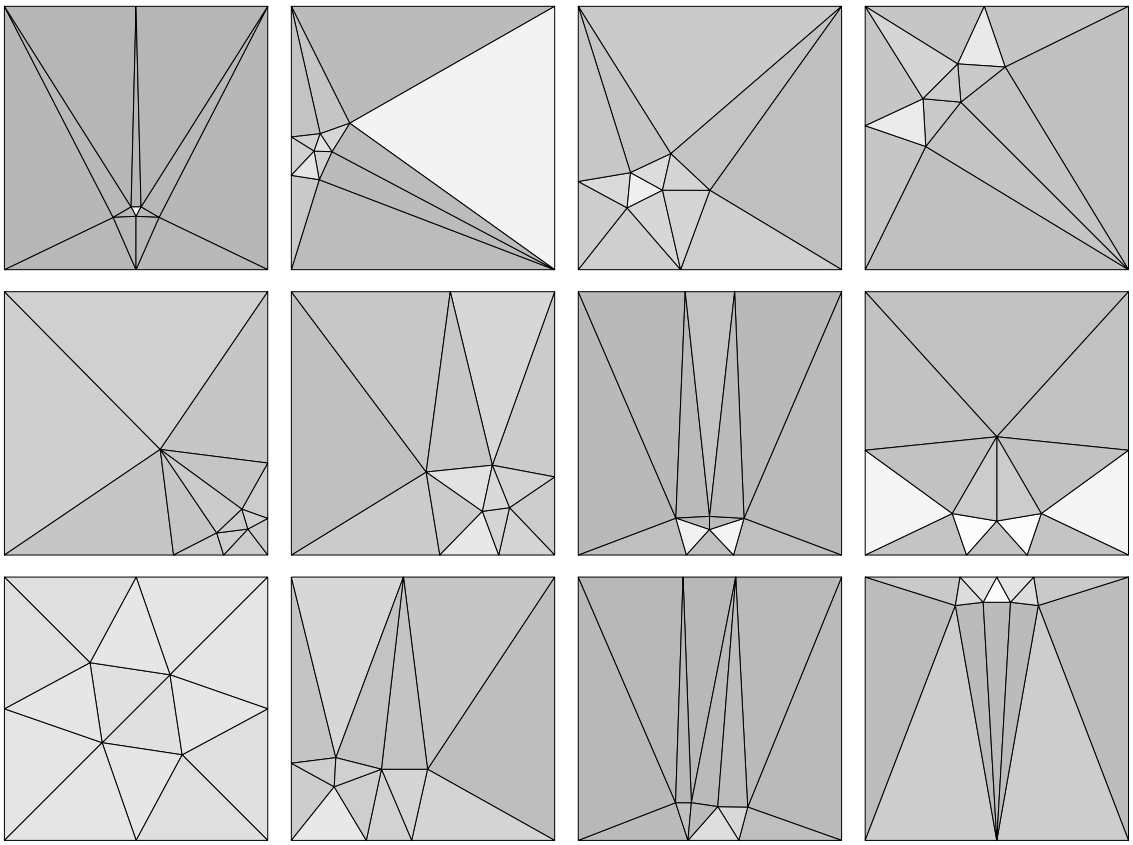

Figure 8.34: There are twelve acute triangulations of the square with 14 triangles.

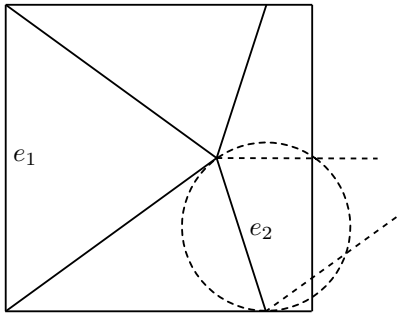


Figure 8.35: A triangulation of the square with some edge $e_1$ of the square not subdivided by a boundary must have maximum angle larger than $2\pi/5$. Assuming a maximum angle of $2\pi/5$ forces the three triangles incident to $e_1$, and it is impossible to construct a second triangle incident to $e_2$ that has maximum angle at most $2\pi/5$.

One interesting thing to note about these triangulations of the square is that, except for the triangulation at the bottom left corner of Fig. 8.34, every triangulation includes at least one edge of the square that contains no boundary vertices except its two endpoints. If this listing of triangulations of the square with at most 14 triangles is complete, this property can be used to prove that no triangulation of the square with fewer than 14 triangles can have a maximum angle of $2\pi/5$. (This question was posed by Eppstein on the web in the Geometry Junkyard [25]. Euler's formula shows that a maximum angle smaller than $2\pi/5$ is not achievable.)

**Lemma 8.5.1.** *Any triangulation of the square with* 3 *or more triangles incident to a corner has maximum angle at least* $5\pi/12 > 2\pi/5$.

*Proof.* Suppose there are $k \geq 3$ triangles incident to the corner. The sum of angle measures in the triangles is $k\pi$, and the angles incident to the corner take up $\pi/2$. This leaves $(2k-1)\pi/2$ angle measure distributed among the remaining $2k$ angles, implying a maximum angle of at least $\pi/2 - \pi/(4k) \geq 5\pi/12$. □

**Lemma 8.5.2.** *Any triangulation of the square including an edge that contains no boundary vertices except its endpoints has maximum angle strictly larger than* $2\pi/5$.

*Proof.* Let $e_1$ be the edge of the square that is not subdivided by a boundary vertex. If there are 3 or more triangles incident to either endpoint of $e$, then Lemma 8.5.1 applies. If there is only one triangle incident to an endpoint of $e$, then the maximum angle is at least $\pi/2$. So we assume that there are exactly two triangles incident to each endpoint of $e$.

This produces 3 triangles incident to $e$, as shown in Fig. 8.35. The edge at left is edge $e$. The three triangles incident to $e$ form a pentagon, with total angle sum of $3\pi$. Four of the angles are incident to corners of the square and use $\pi$ angle measure. This leaves exactly $2\pi$ angle measure to distribute among the remaining five angles. Thus the maximum angle is at least $2\pi/5$, and $2\pi/5$ can be achieved if and only if each of these five angles has measure exactly $2\pi/5$.

This restriction forces three isosceles triangles with the geometry shown in Fig. 8.35. Completing this partial construction to a triangulation of the square requires adding a second triangle along edge $e_2$. In order to construct a triangle with maximum angle at most $2\pi/5$, the third vertex of this triangle would have to lie outside the indicated circle and in between the dotted rays. As shown in the figure,

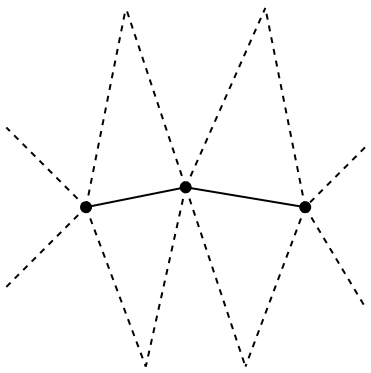

Figure 8.36: There is only one way to construct a triangulation of the square with fewer than four interior vertices and at least four distinct triangles that have one vertex on the boundary of the square and two vertices interior to the square. This figure is a sketch of the structure of that triangulation. The interior vertices are filled circles, edges with both endpoints interior are solid lines, and edges with exactly one endpoint interior are dashed lines.

such a vertex would be outside the square. (In a square with side length 1 and lower left corner at $(0, 0)$, the intersection of ray and circle along $y = 1/2$ is at $x = \tan(\pi/10)+(1/2)\tan(3\pi/10) \approx 1.013$, so although it's a little hard to tell from the figure, this intersection point is outside the square.) □

Even without proving the completeness of this listing of acute triangulations of the square with at most 14 triangles, it is possible to use Lemma 8.5.1 and Lemma 8.5.2 to prove that no triangulation of the square with fewer than 14 triangles achieves a maximum angle of $2\pi/5$. Lemma 8.5.2 implies that any triangulation of the square with maximum angle $2\pi/5$ must have at least eight vertices on the boundary of the square (four corners and at least four on the edges). Each vertex along an edge of the square must be incident to at least three triangles and must form a triangle with two vertices interior to the square.

It follows that there must be at least four distinct triangles that have one vertex on the boundary of the square and two vertices interior to the square. The only way to satisfy this condition with fewer than four interior vertices is shown in Fig. 8.36. With interior edges specified as shown in Fig. 8.36, there is essentially no choice about which edges will contain the four edge vertices, and any acute triangulation of the square with this structure in its interior will be isomorphic to the rightmost triangulation in Fig. 8.32, which by Lemma 8.5.2 cannot achieve maximum angle $2\pi/5$.

We conclude that any triangulation of the square with maximum angle $2\pi/5$ must have at least four vertices along edges of the square and at least four interior vertices. A triangulation of the square with $i$ interior vertices and $j$ vertices along the edges has $2i + j + 2$ triangles. (See, e.g., [40].) Thus we have proved the following.

**Proposition 8.5.3.** *Any triangulation of the square with maximum angle* $2\pi/5$ *must have at least* 14 *triangles.*

This proposition leads to the following question. For which $n$ does there exist a triangulation of the square with $n$ triangles and maximum angle $2\pi/5$? To be more precise, we define the following function $f : \mathbb{Z} \to \mathbb{Z}$. For given $n$, $f(n)$ is the number of nonisomorphic triangulations of the square

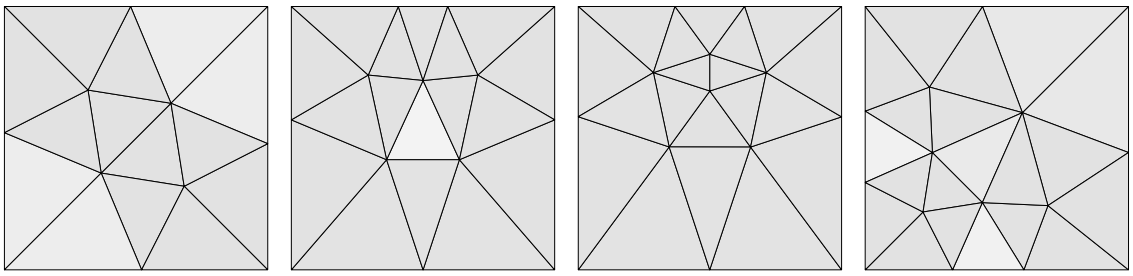

Figure 8.37: For each of $n = 14$, $n = 17$, $n = 19$, and $n = 20$, there is at least one triangulation of the square with $n$ triangles and maximum angle $2\pi/5$.

with $n$ triangles and maximum angle $2\pi/5$. We have seen that $f(n) = 0$ for $n < 14$ and $f(14) \geq 1$. If the listing of acute triangulations with at most 14 triangles is complete, then $f(14) = 1$. But what can be said about $f(n)$ for $n > 14$?

Not much is known, but the author suspects that $f(15) = f(16) = f(18) = 0$. It can be shown that $f(17) \geq 1$, $f(19) \geq 1$, and $f(20) \geq 1$. The meshes in Fig. 8.37 show (approximate) constructions for these cases and for the $n = 14$ case. (The mesh in Fig. 8.34 does not achieve maximum angle $2\pi/5$.) It seems likely that for each $k$ there exists some $n_k$ such that $n > n_k$ implies $f(n) \geq k$, but the existence of $n_1$ has not yet been shown.

# Chapter 9

# Conclusions

It has been said that one of the marks of good research is that it not only answers questions but also generates new questions. A few of the questions generated by this research on well-centered meshes have been mentioned earlier in the thesis, but many have not been explicitly posed. Here we review many of the questions that have been answered and explicitly point out some important questions that remain. [1]

In Chapter 2 we saw that an acute tetrahedron might not be well-centered and a well-centered tetrahedron might not be acute. Indeed, we exhibited a family of completely well-centered tetrahedra with dihedral angle approaching $\pi$. We proved a bound on the solid angle of a 3-well-centered tetrahedron and a bound on the solid angle of a 2-well-centered tetrahedron. We also showed that no upper bound on the solid angle can guarantee that a tetrahedron is well-centered. We closed asking whether some lower bound on the solid angle can guarantee that a tetrahedron is well-centered. Now that we have seen the importance of the quantity $h/R$ in this research on well-centered meshing, we also pose the following question. Does a lower bound $h/R \geq \alpha > 0$ for some $\alpha$ imply a better bound on the solid angle of a tetrahedron? Does such a lower bound on $h/R$ imply any nontrivial bound on the dihedral angle of a tetrahedron? We also note that in both families of tetrahedra that showed the sharpness of the bounds on the solid angle, there is some vertex for which $h/R$ approaches 1. Perhaps an upper bound on $h/R$ or a simultaneous upper and lower bound on $h/R$, e.g., a bound on $E_\infty$, would imply quality in terms of solid or dihedral angles.

Chapter 3 discussed geometric properties of the $n$-well-centered $n$-simplex, introducing the concept of equatorial balls and proving the Cylinder Condition and Prism Condition. It also proved a characterization of the $n$-well-centered $n$-simplex in terms of cubic polynomial inequalities. The Cylinder Condition and Prism Condition were both used later in the thesis, but the characterization in terms of polynomial inequalities, which seems to be a more powerful result, is not used elsewhere. Can any of the other results in this dissertation be strengthened with a more algebraic argument where the Cylinder Condition or Prism Condition has been used for a geometric argument?

The combinatorial properties of well-centered meshes proved in Chapter 4 are arguably the most interesting and powerful results in the dissertation, but leave much unanswered. For $\mathbb{R}^2$, we developed a global combinatorial condition; no 2-well-centered triangle mesh in $\mathbb{R}^2$ has an enclosing cycle of length less than 5. We asked for a triangle mesh homeomorphic to a disk, whether this condition is sufficient to show that the mesh has an embedding in $\mathbb{R}^2$. This question is intriguing

[1] This chapter contains many questions. Some of the questions in this chapter have been asked in previous publications of the author and his coauthors [63, 62, 64]. The organization of these questions is new, and for all prior publications where these questions may appear, permission has been granted by the copyright owner to reprint the material. For [63], the copyright information appears in the footnote beginning on page 59, and for [62] the copyright information appears in the footnote beginning on page 9.

from a theoretical point of view, and an answer could be interesting for a variety of reasons. On the other hand, most practical meshing problems work with a specific domain, and from that viewpoint a more important problem is determining the constraints on a well-centered mesh relative to a fixed boundary. On the surface, at least, this looks like a difficult problem either with input boundary vertices with fixed locations or for boundary vertices constrained to some piecewise smooth boundary curve. We have encountered a number of triangle meshes in $\mathbb{R}^2$ where insufficient mesh refinement or other sometimes complicated combinatorial constraints of creating a 2-well-centered mesh near a fixed boundary have made it impossible to get a 2-well-centered mesh conforming to fixed boundary vertex locations and the input mesh connectivity table.

We also considered the local combinatorial properties of well-centered tetrahedral meshes in $\mathbb{R}^3$. We proved that there are infinitely many triangulations of $S^2$ that can appear as the link of a vertex in a completely well-centered tetrahedral mesh in $\mathbb{R}^3$ and infinitely many triangulations of $S^2$ that cannot appear as the link of a vertex in a 3-well-centered or 2-well-centered tetrahedral mesh in $\mathbb{R}^3$. We constructed large families of triangulations of $S^2$ and expanded them by showing that one can add or delete vertices of specific low degree. All of this work so far, however, falls short of a complete characterization of whether an arbitrarily chosen triangulation of $S^2$ can appear as the link of a vertex in a 2-well-centered, 3-well-centered, or completely well-centered tetrahedral mesh in $\mathbb{R}^3$.

There are at least two other important unanswered questions related to the specific work in Chapter 4 on local combinatorial neighborhoods in well-centered meshes. First, it is not clear whether a triangulation of $S^2$ that permits a 2-well-centered neighborhood of a vertex as defined in Chapter 4, can appear as the link of a vertex in a 2-well-centered mesh. Second, it is not clear whether a triangulation of $S^2$ that can appear in both a 2-well-centered tetrahedral mesh and a 3-well-centered tetrahedral mesh can appear as the link of a vertex in a completely well-centered tetrahedral mesh in $\mathbb{R}^3$. It seems likely that completely well-centered meshes will be the most important for applications, so this may be an important question to answer.

A broader question arising from the work in Chapter 4 concerns the relationship between theory and practice. Can this knowledge about triangulations of $S^2$ that can or cannot appear in well-centered meshes be turned into an algorithm to improve the mesh connectivity of tetrahedral meshes, perhaps one like the local preprocessing algorithm of Chapter 5 for triangle meshes in $\mathbb{R}^2$? In developing a practical algorithm like this another question must arise. Is a triangulation of $S^2$ that in theory can appear as the link of an interior vertex in a well-centered tetrahedral mesh in $\mathbb{R}^3$ actually good in a practical setting? For instance, in a triangle mesh in $\mathbb{R}^2$ a vertex with 100 neighbors can theoretically appear in a 2-well-centered triangles mesh in $\mathbb{R}^2$, but a mesh with such a vertex would be considered poor quality in almost any application. It seems likely to the author that a triangulation of $S^2$ with 7 vertices would usually be poor quality as the link of a vertex in a tetrahedral mesh, and even if the triangulation can appear in a 3-well-centered mesh, it may make it practically very difficult (or even impossible) to find a 3-well-centered mesh by relocating interior vertices of the mesh.

Another important practical question for well-centered tetrahedral meshes is the neighborhood of a boundary vertex in a well-centered tetrahedral mesh. In $\mathbb{R}^2$ many of the worst quality elements in a triangle mesh appear near the boundary, constrained by the requirements of the fixed geometry of the domain. Intuition and preliminary experiments suggest that a similar statement may hold

for tetrahedral meshes in $\mathbb{R}^3$. Thus improving mesh connectivity near the boundary may be crucial, but the work on characterizing the neighborhood of an interior vertex in a well-centered tetrahedral mesh does not immediately generalize to boundary vertices.

Clearly our understanding of the combinatorics of well-centered tetrahedral meshes in $\mathbb{R}^3$ is still quite limited. Similar questions for acute tetrahedral meshes may also be posed. Since every edge in an acute tetrahedral mesh must have five incident tetrahedra, it is not hard to show that any interior vertex in an acute tetrahedral mesh must have at least twelve incident edges. But it is not clear whether every triangulation of $S^2$ with minimum degree 5 can appear as the link of a vertex in an acute tetrahedral mesh, and questions near the boundary, though probably more approachable than such questions for well-centered meshes, are more complicated than the interior vertex case.

In Chapter 5 the focus shifted to a mesh optimization method designed to find well-centered meshes by relocating interior vertices of a given input mesh. The optimization algorithm was designed with some of the observations from earlier chapters in mind, and Chapter 7 suggests that the method gives reasonably good results, but it is possible that the method could be improved. The local preprocessing algorithm increases the valence of lonely vertices effectively, but always refines the mesh, i.e., adds vertices, and might be improved by allowing vertex removal or other coarsening operations in certain circumstances. A potential improvement to the optimization method would be to allow vertices to move along the boundary of a mesh. Finally, optimizing over smaller regions than the entire mesh could be a significant improvement. Preliminary experiments suggest that optimizing $E_p$ by relocating a single vertex at a time is not a good idea, but optimizing the 3-ring neighborhood of each vertex may be effective. Limiting optimization to subregions of the mesh like this is almost essential to parallelizing the method, and it might also help in designing an adaptive method focused on improving the lowest quality parts of a mesh.

One of the reasons that relocating a single vertex at a time has not been an effective means for optimizing $E_p$ may be that a single vertex can easily get stuck in a local minimum of $E_p$. Is there an efficient way to calculate the global optimum of $E_\infty$ (or $E_p$) in the one-ring neighborhood of a vertex? This question is interesting in its own right, and for $E_\infty$ involves determining the locus of points where two different angles have equal measure or equal $E_\infty$ value. This problem appears to have connections to algebraic geometry. Recent work on angular Voronoi diagrams is related, and proves that the edges of an angular Voronoi diagram in $\mathbb{R}^2$ are curves of degree three [2, 45].

We saw in Chapter 6 that for a set of points in $\mathbb{R}^2$ a triangulation that optimizes $E_\infty$ is a triangulation that minimizes the maximum angle. We argued, however, that using the local preprocessing algorithm of Chapter 5 is better than computing a triangulation that minimizes the maximum angle, since a minmax triangulation may have lonely vertices. We posed the question of whether there is a reasonable way to compute the minmax triangulation subject to the constraint that the mesh have no lonely vertices.

We also saw in Chapter 6 that the Delaunay triangulation does not necessarily optimize $h/R$ in $\mathbb{R}^n$ for $n \geq 4$ and might not globally optimize $h/R$ in $\mathbb{R}^3$. Our examples showing that the Delaunay triangulation does not minimize the maximum $h/R$ were all for point sets that had no well-centered triangulation. The question of whether an $n$-well-centered or completely well-centered triangulation has a double optimality in $\mathbb{R}^n$ for $n \geq 3$ remains unanswered.

The experimental results of Chapter 7 leave some questions unanswered as well. In addition to questions about limiting optimization to subregions of the mesh, there are questions about which

$E_p$ to use. Many of the earlier experiments of the research used $E_4$ as a default and moved to higher $p$ if $E_4$ was unsuccessful. Later experiments used $E_8$ or $\widetilde{E}_8$ as default. But as the experiment with the Lake Superior mesh shows, starting with a high power $p$ is not always effective. In any case, it is clear that the Mesquite implementation does not always find a global minimum of the cost function, and we see that finding global or near global minima for nonconvex functions is an important, though difficult, problem in optimization.

In Chapter 8 we saw that it is not hard to triangulate a variety of regions in $\mathbb{R}^3$ with completely well-centered tetrahedra. The meshes of some of these regions, such as the completely well-centered mesh of the cube, can be assembled face to face to create meshes of complicated shapes in $\mathbb{R}^3$. By showing that a large number of well-centered meshes exist, the example meshes also encourage continued work towards efficient automatic generation of well-centered tetrahedral meshes.

One possible direction for future research based on Chapter 8 is a method for meshing based on an octree refinement and the second Sommerville tetrahedron. This type of method is used in [39] along with rules for warping vertices to the mesh boundary to generate high-quality tetrahedral meshes of complicated domains. In addition to work on the mesh boundary, some work would be needed to construct completely well-centered meshes conforming to an octree, since elements proposed in [39] to transition between different levels of refinement are not completely well-centered.

Another question raised by Chapter 8 is that of higher dimensions than three. We have seen that there is no acute triangulation of the 4-cube [37], but it is not known whether there is a well-centered triangulation of the 4-cube. Can the simple construction of a tiling of $\mathbb{R}^3$ with completely well-centered tetrahedra be extended to a tiling of $\mathbb{R}^4$ with well-centered 4-simplices? These and similar questions are of interest in comparing and contrasting acute and well-centered simplices.

In closing, we comment that the initial research goal of efficient methods for obtaining well-centered meshes is only partially met. It is clear that methods presented here and elsewhere provide reasonably efficient heuristics for obtaining well-centered meshes of domains in $\mathbb{R}^2$, but efficient methods for generating well-centered meshes of domains in $\mathbb{R}^3$ are still largely lacking. The results of this dissertation, however, represent a significant increase in our understanding of well-centered simplices and well-centered meshes, and it seems that through some combination of the optimization presented in Chapter 5, the propositions about the combinatorics of well-centered meshes proved in Chapter 4, and the constructions of well-centered meshes in Chapter 8, it may be possible to develop methods for creating well-centered meshes of domains in $\mathbb{R}^3$. Moreover, the topic of well-centered meshing is at an exciting intersection of different fields of research, and this work has generated many interesting questions that remain unanswered.

# References


[1] Alliez, P., Cohen-Steiner, D., Yvinec, M., and Desbrun, M. Variational tetrahedral meshing. *ACM Transactions on Graphics 24*, 3 (2005), 617–625. doi:10.1145/1073204.1073238.

[2] Asano, T., Tamaki, H., Katoh, N., and Tokuyama, T. Angular Voronoi diagram with applications. In *Voronoi Diagrams in Science and Engineering, 2006. ISVD '06. 3rd International Symposium on* (July 2006), pp. 18–24. doi:10.1109/ISVD.2006.9.

[3] Babuška, I., and Aziz, A. K. On the angle condition in the finite element method. *SIAM Journal on Numerical Analysis 13*, 2 (1976), 214–226. URL http://link.aip.org/link/?SNA/13/214/1, doi:10.1137/0713021.

[4] Barnes, E. S., and Sloane, N. J. A. The optimal lattice quantizer in three dimensions. *SIAM Journal on Algebraic and Discrete Methods 4*, 1 (1983), 30–41. doi:10.1137/0604005.

[5] Bell, W. N., and Hirani, A. N. PyDEC: Algorithms and software for Discrete Exterior Calculus. In preparation, 2009.

[6] Bern, M., Chew, P., Eppstein, D., and Ruppert, J. Dihedral bounds for mesh generation in high dimensions. In *SODA '95: Proceedings of the sixth annual ACM-SIAM symposium on discrete algorithms* (Philadelphia, PA, USA, 1995), Society for Industrial and Applied Mathematics, pp. 189–196.

[7] Bern, M., Mitchell, S., and Ruppert, J. Linear-size nonobtuse triangulation of polygons. In *Proceedings of the Tenth Annual ACM Symposium on Computational Geometry* (New York, 1994), ACM Press, pp. 221–230.

[8] Bern, M. W., and Eppstein, D. Mesh generation and optimal triangulation. In *Computing in Euclidean Geometry*, D.-Z. Du and F. K.-M. Hwang, Eds., second ed., no. 4 in Lecture Notes Series on Computing. World Scientific, River Edge, NJ, 1995, pp. 47–123. URL http://www.ics.uci.edu/~eppstein/pubs/BerEpp-CEG-95.pdf.

[9] Bern, M. W., Eppstein, D., and Gilbert, J. Provably good mesh generation. *J. Computer and System Sciences 48*, 3 (June 1994), 384–409. Special issue for 31st FOCS.

[10] Brandts, J., Korotov, S., and Křížek, M. Dissection of the path-simplex in $\mathbb{R}^n$ into $n$ path-subsimplices. *Linear Algebra and its Applications 421*, 2–3 (March 2007), 382–393. doi:10.1016/j.laa.2006.10.010.

[11] Brandts, J., Korotov, S., Křížek, M., and Šolc, J. On nonobtuse simplicial partitions. *SIAM Review 51*, 2 (2009), 317–335. URL http://link.aip.org/link/?SIR/51/317/1, doi:10.1137/060669073.

[12] Brandts, J. H., Korotov, S., and Křížek, M. The discrete maximum principle for linear simplicial finite element approximations of a reaction-diffusion problem. *Linear Algebra and its Applications 429*, 10 (2008), 2344 – 2357. Special Issue in honor of Richard

S. Varga. URL http://www.sciencedirect.com/science/article/B6V0R-4T2S02T-2/2/40a03300493ca05268aaf67c2f963a43, doi:10.1016/j.laa.2008.06.011.

[13] Brewer, M., Diachin, L., Knupp, P., Leurent, T., and Melander, D. The Mesquite mesh quality improvement toolkit. In *Proceedings of the 12th International Meshing Roundtable* (2003), pp. 239–250. URL http://www.imr.sandia.gov/papers/imr12/brewer03.pdf.

[14] Britton, D., and Dunitz, J. D. A complete catalogue of polyhedra with eight or fewer vertices. *Acta Crystallographica Section A 29*, 4 (July 1973), 362–371. URL http://dx.doi.org/10.1107/S0567739473000963, doi:10.1107/S0567739473000963.

[15] Burago, J. D., and Zalgaller, V. A. Polyhedral embedding of a net. *Vestnik Leningrad. Univ. 15*, 7 (1960), 66–80.

[16] Cassidy, C., and Lord, G. A square acutely triangulated. *J. Recreational Math 13* (1980/81), 263–268.

[17] Ciarlet, P. G., and Raviart, P.-A. Maximum principle and uniform convergence for the finite element method. *Computer Methods in Applied Mechanics and Engineering 2*, 1 (February 1973), 17–31. URL http://dx.doi.org/10.1016/0045-7825(73)90019-4, doi:10.1016/0045-7825(73)90019-4.

[18] Desbrun, M., Hirani, A. N., Leok, M., and Marsden, J. E. Discrete exterior calculus. *arXiv:math.DG/0508341* (August 2005). URL http://arxiv.org/abs/math.DG/0508341.

[19] Du, Q., Faber, V., and Gunzburger, M. Centroidal Voronoi tessellations: applications and algorithms. *SIAM Review 41*, 4 (1999), 637–676. doi:10.1137/S0036144599352836.

[20] Du, Q., and Gunzburger, M. Grid generation and optimization based on centroidal Voronoi tessellations. *Applied Mathematics and Computation 133*, 2-3 (December 2002), 591–607. doi:10.1016/S0096-3003(01)00260-0.

[21] Edelsbrunner, H. *Algorithms in Combinatorial Geometry*. Springer–Verlag, 1987.

[22] Edelsbrunner, H., and Shah, N. R. Incremental topological flipping works for regular triangulations. *Algorithmica 15*, 3 (March 1996), 223–241. doi:10.1007/BF01975867.

[23] Edelsbrunner, H., Tan, T. S., and Waupotitsch, R. An $O(n^2 \log n)$ time algorithm for the minmax angle triangulation. In *SCG90: Proceedings of the sixth annual ACM Symposium on Computational Geometry* (New York, 1990), ACM Press, pp. 44–52.

[24] Edelsbrunner, H., Tan, T. S., and Waupotitsch, R. An $O(n^2 \log n)$ time algorithm for the minmax angle triangulation. *SIAM Journal on Scientific and Statistical Computing 13*, 4 (July 1992), 994–1008. doi:10.1137/0913058.

[25] Eppstein, D. Acute square triangulation [online]. February 2009. URL http://www.ics.uci.edu/~eppstein/junkyard/acute-square/ [cited November 12, 2009].

[26] Eppstein, D., Sullivan, J. M., and Üngör, A. Tiling space and slabs with acute tetrahedra. *Computational Geometry: Theory and Applications 27*, 3 (2004), 237–255. doi:10.1016/j.comgeo.2003.11.003.

[27] Erickson, J., Guoy, D., Sullivan, J., and Üngör, A. Building spacetime meshes over arbitrary spatial domains. In *Proceedings of the 11th International Meshing Roundtable* (2002), Sandia National Laboratories, pp. 391–402.

[28] Erten, H., and Üngör, A. Computing acute and non-obtuse triangulations. In *Proceedings of the 19th Canadian Conference on Computational Geometry (CCCG2007)* (August 20–22 2007).

[29] Field, D. A. Laplacian smoothing and Delaunay triangulations. *Communications in Applied Numerical Methods 4*, 6 (1988), 709–712.

[30] Fuchs, A. Automatic grid generation with almost regular Delaunay tetrahedra. In *Proceedings of the 7th International Meshing Roundtable* (Dearborn, Michigan, October 26–28 1998), Sandia National Laboratories, pp. 133–147.

[31] Gardner, M. Mathematical games. *Scientific American 202* (March 1960), 177–178.

[32] Guoy, D., and Erickson, J. Automatic blocking scheme for structured meshing in 2D multiphase flow simulation. In *Proceedings of the 13th International Meshing Roundtable* (2004), pp. 121–132.

[33] Hirani, A. N. *Discrete Exterior Calculus*. PhD thesis, California Institute of Technology, Pasadena, CA, May 2003. URL `http://resolver.caltech.edu/CaltechETD:etd-05202003-095403`.

[34] Hirani, A. N., Nakshatrala, K. B., and Chaudhry, J. H. Numerical method for Darcy flow derived using Discrete Exterior Calculus. Tech. Rep. UIUCDCS-R-2008-2937, Department of Computer Science, University of Illinois at Urbana-Champaign, February (Revised October) 2008. Also available as preprint arXiv:0810.3434v1 [math.NA] on arxiv.org. URL `http://arxiv.org/abs/0810.3434`.

[35] Kimmel, R., and Sethian, J. Computing geodesic paths on manifolds. *Proc. Nat. Acad. Sci. 95* (1998), 8341–8435. `doi:10.1073/pnas.95.15.8431`.

[36] Klamkin, M. S., and Tsintsifas, G. A. The circumradius-inradius inequality for a simplex. *Mathematics Magazine 52*, 1 (January 1979), 20–22. URL `http://www.jstor.org/stable/2689968`.

[37] Kopczyński, E., Pak, I., and Przytycki, P. Acute triangulations of polyhedra and $\mathbb{R}^n$. Available as preprint arXiv:0909.3706v1 [math.MG] on arxiv.org, 2009.

[38] Křížek, M. There is no face-to-face partition of $\mathbb{R}^5$ into acute simplices. *Discrete and Computational Geometry 36*, 2 (September 2006), 381–390. `doi:10.1007/s00454-006-1244-0`.

[39] Labelle, F., and Shewchuk, J. R. Isosurface stuffing: Fast tetrahedral meshes with good dihedral angles. *ACM Transactions on Graphics 26*, 3 (2007), 57. `doi:10.1145/1276377.1276448`.

[40] Lindgren, H. Dividing a square into acute-angled triangles. *The Australian Mathematics Teacher 18*, 1 (April 1962), 14–15.

[41] Maehara, H. Acute triangulations of polygons. *European Journal of Combinatorics 23*, 1 (2002), 45–55.

[42] McKay, B. D., and Brinkmann, G. Fast generation of planar graphs. *MATCH Communications in Mathematical and Computer Chemistry 58*, 2 (February 2007), 323–357.

[43] Munkres, J. R. *Elements of Algebraic Topology*. Addison–Wesley Publishing Company, Menlo Park, 1984.

[44] Munson, T. Mesh shape-quality optimization using the inverse mean-ratio metric. *Math. Program. 110*, 3 (2007), 561–590. `doi:10.1007/s10107-006-0014-3`.

[45] Muta, H., and Kato, K. Degeneracy of angular Voronoi diagram. In *Voronoi Diagrams in Science and Engineering, 2007. ISVD '07. 4th International Symposium on* (July 2007), pp. 288–293. `doi:10.1109/ISVD.2007.14`.

[46] Nicolaides, R. A. Direct discretization of planar div-curl problems. *SIAM Journal on Numerical Analysis 29*, 1 (1992), 32–56. doi:10.1137/0729003.

[47] Rajan, V. Optimality of the Delaunay triangulation in $\mathbb{R}^d$. *Discrete and Computational Geometry 12*, 1 (December 1994), 189–202. doi:10.1007/BF02574375.

[48] Rajan, V. T. Optimality of the Delaunay triangulation in $\mathbb{R}^d$. In *SCG '91: Proceedings of the seventh annual symposium on computational geometry* (New York, NY, USA, 1991), ACM, pp. 357–363. doi:10.1145/109648.109688.

[49] Saraf, S. Acute and nonobtuse triangulations of polyhedral surfaces. *European Journal of Combinatorics 30*, 4 (2009), 833–840. doi:10.1016/j.ejc.2008.08.004.

[50] Sazonov, I., Hassan, O., Morgan, K., and Weatherill, N. P. Smooth Delaunay–Voronoi dual meshes for co-volume integration schemes. In *Proceedings of the 15th International Meshing Roundtable* (Birmingham, Alabama, September 17–20 2006), Sandia National Laboratories.

[51] Sazonov, I., Hassan, O., Morgan, K., and Weatherill, N. P. Yee's scheme for the integration of Maxwell's equation on unstructured meshes. In *Proceedings of the European Conference on Computational Fluid Dynamics (ECCOMAS CFD 2006)* (2006), P. Wesseling, E. Oñate, and J. Périaux, Eds.

[52] Sazonov, I., Hassan, O., Morgan, K., and Weatherill, N. P. Generating the Voronoi-Delaunay dual diagram for co-volume integration schemes. In *Proceedings of the 4th International Symposium on Voronoi Diagrams in Science and Engineering (ISVD 2007)* (2007).

[53] Sazonov, I., Wang, D., Hassan, O., Morgan, K., and Weatherill, N. P. A stitching method for the generation of unstructured meshes for use with co-volume solution techniques. *Computer Methods in Applied Mechanics and Engineering 195*, 13-16 (February 2006), 1826–1845. URL http://dx.doi.org/10.1016/j.cma.2005.05.037, doi:10.1016/j.cma.2005.05.037.

[54] Schmitt, D., and Spehner, J.-C. Angular properties of Delaunay diagrams in any dimension. *Discrete and Computational Geometry 21*, 1 (January 1999), 17–36. doi:10.1007/PL00009407.

[55] Shewchuk, J. R. Triangle: Engineering a 2D quality mesh generator and Delaunay triangulator. In *Applied Computational Geometry: Towards Geometric Engineering*, M. C. Lin and D. Manocha, Eds., vol. 1148 of *Lecture Notes in Computer Science*. Springer, Berlin, May 1996, pp. 203–222. From the First ACM Workshop on Applied Computational Geometry. doi:10.1007/BFb0014497.

[56] Shewchuk, J. R. What is a good linear element? interpolation, conditioning, and quality measures. In *Proceedings of the 11th International Meshing Roundtable* (2002), Sandia National Laboratories, pp. 115–126.

[57] Sibson, R. Locally equiangular triangulations. *The Computer Journal 21*, 3 (March 1978), 243–245. URL http://dx.doi.org/10.1093/comjnl/21.3.243, doi:10.1093/comjnl/21.3.243.

[58] Sommerville, D. M. Y. Space-filling tetrahedra in euclidean space. *Proceedings of the Edinburgh Mathematical Society 41* (1923), 49–57.

[59] Springborn, B. A. *Variational principles for circle patterns*. PhD thesis, Technische Universität Berlin, 2003.

[60] Üngör, A. Premium quality triangulations. University of Illinois at Urbana-Champaign CSE Seminar, May 19 2009.

[61] Üngör, A., and Sheffer, A. Pitching tents in space-time: Mesh generation for discontinuous Galerkin method. *International Journal of Foundations of Computer Science 13*, 2 (2002), 201–221. doi:10.1142/S0129054102001059.

[62] VanderZee, E., Hirani, A. N., and Guoy, D. Triangulation of simple 3D shapes with well-centered tetrahedra. In *Proceedings of the 17th International Meshing Roundtable*, R. V. Garimella, Ed. Springer Berlin Heidelberg, Pittsburgh, Pennsylvania, October 12–15 2008, pp. 19–35. Also available as a preprint arXiv:0806.2332v2 [cs.CG] on arxiv.org. doi:10.1007/978-3-540-87921-3_2.

[63] VanderZee, E., Hirani, A. N., Guoy, D., and Ramos, E. Well-centered planar triangulation — an iterative approach. In *Proceedings of the 16th International Meshing Roundtable* (Seattle, Washington, October 14–17 2007), M. L. Brewer and D. Marcum, Eds., Springer Berlin, pp. 121–138. doi:10.1007/978-3-540-75103-8_7.

[64] VanderZee, E., Hirani, A. N., Guoy, D., and Ramos, E. Well-centered triangulation. *SIAM Journal on Scientific Computing (Accepted)* (2009). Available as preprint arXiv:0802.2108v3 [cs.CG] on arxiv.org. URL http://arxiv.org/abs/0802.2108.

[65] VanderZee, E., Hirani, A. N., Guoy, D., Zharnitsky, V., and Ramos, E. Geometric and combinatorial properties of well-centered triangulations in three and higher dimensions. In preparation, 2009.

[66] VanderZee, E., Hirani, A. N., Zharnitsky, V., and Guoy, D. A dihedral acute triangulation of the cube. *Computational Geometry: Theory and Applications (Accepted, and available online)* (2009). Also available as preprint arXiv:0905.3715v3 [cs.CG] on arxiv.org. URL http://arxiv.org/abs/0905.3715, doi:10.1016/j.comgeo.2009.09.001.

[67] Winslow, A. M. An irregular triangle mesh generator. Tech. Rep. UCRL-7880, National Technical Information Service, Springfield, VA, 1964.

[68] Yuan, L. Acute triangulations of polygons. *Discrete and Computational Geometry 34*, 4 (2005), 697–706.

[69] Yuan, L. *Acute Triangulations*. PhD thesis, Dortmund University, April 2006.

# Index


acute, 6
affine hull, 4
angle
    associated to a facet, 9, 13, 63
    dihedral, 5
    face, 6
    solid, 6, 9, 15
    vertex, 9, 13, 63

barycentric coordinates, 6, 16, 17, 31
boundary of a simplex, 35

circumball, 5
circumcenter, 4
circumradius, 4
circumsphere, 4
closure, 35
cone, 35
Cylinder Condition, 25

dihedral acute, 5
dihedral angle, *see* angle, dihedral

$E_\infty$, 62, 69, 81
$E_p$, 62, 81
$\widetilde{E}_p$, 86
edge, 5
enclosing cycle, 36
energy, 59
equatorial ball, 21

face angle, *see* angle, face
face of a simplex, 5
facet, 5

geometric realization, 35

inradius, 61
interior of a simplex, 35
interior vertex, 35
isosceles simplex, 47

link, 35, 66
locally Delaunay, 75

lonely vertex, 36, 59, 64

manifold complex, 35
minmax triangulation, 69

One-Facet Equatorial Ball Condition, 23

permit a 2-well-centered neighborhood, 51
planar triangulation, 39
Prism Condition, 28

self-centered, 5
simplex, 4
simplicial complex, 34
solid angle, *see* angle, solid
star, 35

underlying space, 35

vertex, 4
vertex angle, *see* angle, vertex

well-centered, 5